

**MODELLING OF TRENCH EFFECT ON FATIGUE
PERFORMANCE OF STEEL CATENARY RISER**

by

© Rahim Shoghi

A Thesis Submitted to the
School of Graduate Studies

in partial fulfillment of the requirements for the degree of

Doctor of Philosophy

Faculty of Engineering and Applied Science

Memorial University of Newfoundland

Oct 2020

St. John's

Newfoundland

Canada

ABSTRACT

The riser-seabed interaction resulting in a trench formed in the touchdown zone (TDZ) of steel catenary risers (SCR) has a significant influence on accumulated fatigue damage. Several studies have used different trench modeling approaches to investigate the trench effect on fatigue performance of SCR. However, contradictory observations have been reported with no coherent agreement on the beneficial or detrimental effect of the trench on fatigue. In this study, the significance of trench geometry in fatigue damage evaluation was investigated. Using boundary-layer methods (BLM) and numerical approaches, a meaningful relationship was observed between the trench geometry in different zones and the peak fatigue damage. A new set of rules was proposed for the qualitative assessment of the overall trend of the trench effect on the variation of fatigue damage. The proposed assessment rules were validated by performing comprehensive numerical fatigue analysis. A comparison with samples of published experimental and numerical studies was also conducted. The developed geometrical model and the set of rules for qualitative assessment of the trench effect on fatigue were used to re-assess the majority of the key published studies. The proposed methodology resulted in a more coherent agreement between the published studies. It was observed that for the near, far, or out of the plane direction of the vessel excursions, the ultimate fatigue damage might be slightly increased or decreased depending on the probability of occurrence in different geographical locations. Instead, the trench effect appeared in the form of significant shifting of the peak damage point towards the opposite direction of the low-frequency vessel excursions. This implied that the case dependency of the trench effect on fatigue response in different geographical locations with various environmental loads was a potential source for the contradictory results reported

in previously published studies. Moreover, the study revealed the significance of riser flexural rigidity and its relation with TDP oscillation on the trench surface and the fatigue damage accumulation, consequently. The peak fatigue damage depending on the trench profile was analytically obtained and showed a good agreement with numerical models. The effect of seabed soil stiffness on the fatigue performance of SCR was compared with the contribution of the trench profile in the touchdown zone. The conducted research revealed several significant trench effect on the fatigue performance of SCR and provided an in-depth insight into this challenging problem.

STATEMENT OF AUTHORSHIP

I have been the first author and the main contributor to the conducted work, including mathematical works, numerical modeling, post-processing, and preparation of the paper draft. Dr. Hodjat Shiri was my supervisor providing the research topic, overall approach, checking the results and providing advice, reviewing and editing the paper drafts, etc. Also, I visited the Offshore Mechanics Laboratory (LMO) at the University of São Paulo for collaborative research work under the supervision of Prof. Celso Pupo Pesce. The visit was financially supported by the Mitacs Globalink program. During my visit to USP, I was preparing weekly progress reports and receiving significant support on theoretical and numerical works by both my home and host supervisors, Dr. Hodjat Shiri at Memorial University and Prof. Celso Pesce in LMO. Besides, I had the chance to take some excellent courses and workshops in USP, such as the “Advanced Analytical Mechanics,” “Design of Ocean Systems,” and “Advanced Science on Nonlinear Dynamics.” These courses were held by Prof. Celso Pesce, Prof. Clóvis A. Martins, Dr. Renato M. M. Orsino, and Prof. Kazuo Nishimoto.

ACKNOWLEDGMENT

First and foremost, I would like to express my very great appreciation to my supervisor, Dr. Hodjat Shiri, who provided me excellent opportunity to join his research team and involved me in a challenging research topic. I am grateful for his unconditional supports, keen supervision, and guidance thorough out this study, and especially for his confidence in me. I would like to express my heartfelt gratefulness to Prof. Celso Pupo Pesce for his explicit instructions and supervision during my visit to the University of São Paulo. Professional guidance given by Prof. Pesce has been a great help, and I learned from his insight a lot. I would like to offer my sincere gratitude to Dr. Bruce Quinton and Dr. Ashutosh Dhar, the members of my supervisory committee, for their supportive advice. Prof. Clóvis Martins and Dr. Renato Orsino provided me with precious insight; I appreciate.

I gratefully acknowledge the financial support of this research by the Research and Development Corporation (RDC) (now TCII) through the Ignite funding program, the Memorial University of Newfoundland through VP start-up funding support, and Mitacs through “Globalink” program for funding this project. Special thanks are extended to the School of Graduate Studies (SGS) and Faculty of Engineering and Applied Science at Memorial University for providing financial supports and excellent resources to conduct this research project.

Also, I would like to offer my special thanks to the Engineering Graduate Studies Office staff for their patience and willingness to help. My friends and my colleagues, I appreciate all your supports, especially Xiaoyu Dong and Mohammad Javad Moharrami, for scientific discussions.

I am very much thankful to my lovely sisters for their love, understanding, encouragement, prayers and continuing support to complete this research work. Last but not least, I am incredibly grateful to my amazing parents for their unconditional love, prayers, caring, and sacrifices for educating and preparing me for my future. I could not have accomplished this without their supports and blessings.

"Always take the path that makes you can learn the most!"

Theodore Wu

Contents

ABSTRACT.....	1
STATEMENT OF AUTHORSHIP	3
ACKNOWLEDGMENT.....	4
List of Figures	10
List of Tables	13
List of Abbreviations and Symbols.....	14
1. Chapter 1	10
Introduction.....	10
1.1. Overview	10
1.2. Key objectives	12
1.3. Organization of the Thesis	14
1.4. Thesis outcomes	16
References.....	16
2. Chapter 2.....	19
Literature Review.....	19
2.1. Overview	19
2.2. Introduction	19
2.2.1. Riser-Seabed Interaction.....	20
2.2.2. Steel Catenary Riser (SCR) Mechanics.....	25
2.2.3. Trench Geometry	28
2.2.4. SCR Analysis Software	33
2.2.5. SCR Design Guidelines and Fatigue Analysis	34
References.....	37
3. Chapter 3.....	43
Modeling Touchdown Point Oscillation and Its Relationship with Fatigue Response of Steel Catenary Risers	43
Abstract.....	44
3.1. Introduction	45
3.2. Conceptual Basis and Motivation	48

3.3.	Mathematical Dependence of Fatigue Damage on TDP Oscillation and Average Shear Force	50
3.4.	Analytical TDP Oscillation on Curved Trenches.....	57
3.4.1.	Geometrical Idealization of the Curved Trench	60
3.4.2.	Analytical Case Study	65
3.4.3.	Qualitative Fatigue Assessment Rules	71
3.5.	Numerical Fatigue Analysis	72
3.6.	Conclusions	79
3.7.	Acknowledgments	80
	References	81
4.	Chapter 4.....	84
	Re-assessment of Trench Effect on Fatigue Performance of Steel Catenary Risers in the Touchdown Zone	84
	Abstract	85
4.1.	Introduction	86
4.2.	The analytical Framework Proposed by Shoghi and Shiri (2019)	89
4.3.	Outlined Rules for Re-assessing the Published Studies	95
4.4.	Re-assessment of Previous Studies	96
4.4.1.	Effect of “Cyclic Embedment” on Fatigue Damage	97
4.4.2.	Effect of a “Trench” on Fatigue Damage	109
4.4.2.1.	Discussion	118
4.5.	Conclusions	120
4.6.	Acknowledgments	123
	References	123
5.	Chapter 5.....	127
	Influence of Trench Geometry on Fatigue Response of Steel Catenary Risers by Using a Boundary Layer Solution on a Sloped Seabed	127
	Abstract	128
5.1.	Introduction	129
5.2.	Developing a Boundary Layer Model	130
5.2.1.	Sloped Rigid Seabed.....	131
5.2.2.	Sloped Elastic Seabed.....	136

5.3.	Perturbation of the TDP on the sloped seabed	140
5.3.1.	Effect of Seabed Geometry and Soil Stiffness	141
5.3.2.	Discussion on TDP Relocation on Sloped Seabed	149
5.3.3.	Discussion on TDP Oscillation Amplitude	152
5.4.	Numerical Fatigue Analysis and the Trench Effect	154
5.5.	Re-assessing of a Case Study	156
5.6.	Conclusions	164
5.7.	Appendix – some basics on the planar static problem at TDZ on horizontal and rigid seabed	165
5.8.	Acknowledgments	168
	References	168
Chapter 6	170
Dynamic Curvature of a Steel Catenary Riser on Elastic Seabed Considering Trench Shoulder Effects: an Analytical Model.....		170
	Abstract	171
6.1.	Introduction	172
6.2.	Boundary-Layer Solution in TDZ.....	174
6.2.1.	Planar Dynamic Equations for the Suspended Part of the SCR	175
6.2.2.	Dynamic Equations for the Supported Part of the SCR on the Seabed	184
6.2.3.	Matching Solutions at TDP	187
6.3.	Dynamic Curvature of SCR in TDZ	188
6.4.	Fatigue Response of SCR.....	198
6.5.	Conclusions	202
6.6.	APPENDIX – Dynamic equilibrium equations for the planar problem of a catenary riser	203
6.7.	Acknowledgments	209
	References	209
7.	Chapter 7.....	212
Conclusions and Recommendations		212
7.1.	Conclusions	212
7.2.	Recommendations for Future Study.....	215
Bibliography		217

APPENDIX.....	225
Appendix A.....	226
The Geometrical Significance of Seabed Trench in Fatigue Performance of Steel Catenary Risers in the Touchdown Zone.....	226
Abstract.....	227
A.1. Introduction.....	228
A.2. Conceptual Basis.....	230
A.3. Re-assessment of Previous Studies.....	235
A.4. Conclusions.....	241
A.5. Acknowledgments.....	244
References.....	244

List of Figures

Figure 1-1. Schematic view of SCR and the trench formation in the TDZ	11
Figure 2-1. Schematic view of SCR connected to a floating system.....	19
Figure 2-2. Comparison of bending moment along SCR, $k = 100 \text{ kPa}$, Shiri (2010b)..	27
Figure 2-3. Shear force distribution in TDZ, $k = 100 \text{ kPa}$, Shiri (2010b).....	27
Figure 2-4. Trench shape definitions in profile view, Bridge and Howells (2007)	28
Figure 2-5. Schematic trench profile, Shiri (2014a)	30
Figure 2-6. Mathematical approximation of non-linear seabed trench, Shiri (2014a)	30
Figure 2-7. Stepped trench model proposed by Randolph et al. (2013).....	31
Figure 2-8. Comparison of different trench models in Randolph et al. (2013).....	32
Figure 2-9. Sketch of the proposed trench by Wang and Low (2016).....	33
Figure 3-1. Cyclic trench development in the TDZ of SCR.....	45
Figure 3-2. SCR-soil-seawater interaction mechanisms and the relation with TDP oscillation.....	49
Figure 3-3. Schematic view of near and far SCR configuration.....	51
Figure 3-4. SCR schematic configuration in the trenched seabed	58
Figure 3-5. Quadratic exponential trench (Shiri 2014).....	58
Figure 3-6. Idealization of the curved trench with linear sloped lines.....	60
Figure 3-7. Different scenarios of TDP oscillation on sloped ((b), (c), (d)) and flat seabed (a)	62
Figure 3-8. SCR Configuration for analytical investigations	66
Figure 3-9. Variation trends of key parameters in FOZ and NOZ.....	69
Figure 3-10. Schematic TDP trajectory toward the anchored end by increasing seabed slope	69
Figure 3-11. Variation trends of key parameters in MPZ.....	70
Figure 3-12. SCR configuration in numerical simulation.....	72
Figure 3-13. Generic Spar RAO, Head sea, Gulf of Mexico (Bridge and Howells 2007)	74
Figure 3-14. Comparison of different trench types for numerical analysis	74
Figure 3-15. Fatigue damage distribution over various trenches.....	76
Figure 3-16. Assessment of sample published numerical and experimental studies (Zargar 2017, Hodder 2009)	78
Figure 4-1. Trench formation in the TDZ under riser-seabed-seawater interaction	86
Figure 4-2. Riser-seabed-seawater interaction mechanisms and the relation with TDP migration	90
Figure 4-3. Fatigue damage distribution over various trenches (Shoghi and Shiri 2019)	94
Figure 4-4. Effect of cyclic penetration on fatigue damage in different studies.....	99
Figure 4-5. The overall shape of the riser embedment profile in the literature compared with Elliott et al. (2013).....	102

Figure 4-6. Assessment of penetration profile vs. bending moment obtained by Elliott et al. (2013)	104
Figure 4-7. Experimental stress range variation over positive and negative sloped faces of SCR profile (Elliott et al. 2013).....	104
Figure 4-8. Assessment of test results published by Nakhaee and Zhang (2008)	106
Figure 4-9. Assessment of test results published by Hodder and Byrne (2009).....	108
Figure 4-10. Assessment of test results published by Randolph et al. (2013).....	114
Figure 4-11. Potential fatigue distortion in Sharma and Aubeny (2011).....	117
Figure 5-1. Schematic view of TDZ and trench slopes beneath the SCR.....	132
Figure 5-2. SCR configuration in numerical simulation.....	140
Figure 5-3. Non-dimensional BLM solutions around TDP for different seabed slopes, (a) horizontal seabed; (b) positive slope seabed (2 degrees), (c) negative slopes (2 degrees)	143
Figure 5-4. TDP relocation trend on the elastic seabed, obtained via BLM.....	144
Figure 5-5. Inclination angle, curvature and shear force distribution. Non-dimensional results for a riser configuration close to the TDP on the horizontal seabed. Left: BLM; right: FEA	145
Figure 5-6. Inclination angle, curvature and shear force distribution. Non-dimensional results of riser configuration close to the TDP on NOZ shoulder (positive slope seabed). Left: BLM; right: FEA.....	147
Figure 5-7. Inclination angle, curvature and shear force distribution. Non-dimensional results of riser configuration close to the TDP on FOZ shoulder (negative slope seabed). Left: BLM; right: FEA.....	148
Figure 5-8. Comparison of different mathematical seabed geometry (Shoghi and Shiri, 2019)	150
Figure 5-9. The magnitude of TDP relocation ratio	151
Figure 5-10. Schematic view of created FOZ shoulder respect to vessel positions	152
Figure 5-11. Schematic view of created NOZ shoulder respect to vessel positions.....	152
Figure 5-12. Incorporated seabed for NOZ and FOZ	155
Figure 5-13. Fatigue damage distribution on SCR for different seabed configuration; (a) represents FOZ shoulder, (b) represents NOZ shoulder	155
Figure 5-14. Different considered trench profiles, (Randolph et al., 2013).....	157
Figure 5-15. The slope of trench profile	157
Figure 5-16. Fatigue life distribution over various trenches, (Randolph et al., 2013)....	158
Figure 6-1. Dynamic curvature of SCR in TDZ (analytical results Schematic view of the simplified trench with linear sloped lines, Shoghi and Shiri (2019).....	172
Figure 6-2. Schematic view of trench and vessel configuration.....	175
Figure 6-3. Schematic view of SCR configuration.....	176
Figure 6-4. Static and dynamic configuration of SCR in the TDZ.....	177
Figure 6-5. Considered seabeds, Flat: $\theta_{sb} = 0^\circ$, NOZ: $\theta_{sb} = +2^\circ$, and FOZ: $\theta_{sb} = -1^\circ$	189
Figure 6-6. The SCR configuration in numerical simulation	190

Figure 6-7. Schematic view of the critical zone of the SCR.....	191
Figure 6-8. Nondimensional dynamic curvature of SCR in TDZ.....	193
Figure 6-9. Nondimensional dynamic curvature of SCR in TDZ.....	194
Figure 6-10. Nodal curvature sensitivity of SCR to seabed stiffness in TDZ. (a-i): analytical solution for small TDP oscillation, $\tau_0/T_0 = 0.01$; (j-r): analytical solution for mild TDP oscillation, $\tau_0/T_0 = 0.03$	195
Figure 6-11. Nondimensional dynamic curvature of SCR in TDZ.....	197
Figure 6-12. Fatigue damage distribution on SCR in TDZ	200
Figure 6-13. Nondimensional dynamic curvature of SCR in TDZ.....	201
Figure 6-14. The planar problem; Pesce (1997)	204
Figure A-1. Cyclic trench development in the TDZ of SCR	228
Figure A-2. Different scenarios of TDP oscillation on the seabed (Shoghi and Shiri 2019)	232
Figure A-3. Assessment of test results published by Hodder and Byrne (2009).....	235
Figure A-4. Assessment of profile vs. bending moment obtained by Elliott et al. (2013)	238
Figure A-5. Assessment of test results published by Randolph et al. (2013).....	239

List of Tables

Table 3-1. Geometrical compatibility equations for TDP oscillation on different trench zones.	63
Table 3-2. Analytical equations for TDP oscillation amplitude in different trench zones.	64
Table 3-3. SCR parameters for the analytical case study.	65
Table 3-4. Analytically obtained key parameters in different idealized trenches.....	68
Table 3-5. Variation trends of key parameters relative to the non-trenched virgin seabed.	70
Table 3-6. Manipulated wave scatter diagram for a 30-year operational life (Gulf of Mexico).	75
Table 4-1. Variation trends of key parameters relative to the non-trenched virgin seabed (Shoghi and Shiri 2019).	93
Table 4-2. Re-assessment of the published studies for the effect of “cyclic embedment” on fatigue	98
Table 4-3. Re-assessment of the published studies for the effect of “trench” on fatigue.	110
Table 5-1. Geometrical properties of rigid seabed.	134
Table 5-2. Typical SCR data (Pesce et al., 2006).	141
Table 5-3. Normalized TDP relocation on the sloped seabed.	150
Table 5-4. Fatigue damage peak coordination for GoM location, (Randolph et al., 2013).	160
Table 5-5. Fatigue damage peak coordination for WA location, (Randolph et al., 2013).	160
Table 5-6. Fatigue damage peak relocation of each trench respect to the horizontal seabed, (Randolph et al., 2013).	160
Table 5-7. Normalized ratio of the peak damage relocation in Langner’s trench to the Stepped seabed, (Randolph et al., 2013).	161
Table 5-8. Normalized fatigue lives of the trench shoulder, for GoM.	163
Table 5-9. Normalized fatigue lives of the trench shoulder, for WA.	163
Table 6-1. Typical SCR data, Pesce et al., (2006).	190
Table A-1. Variation trends of key parameters relative to the non-trenched virgin seabed.	234

List of Abbreviations and Symbols

Abbreviations

API	American petroleum institute
BLM	Boundary layer method
DISP	User-defined boundary condition subroutine in ABAQUS
DNV	Det Norske Veritas
FEA	Finite element analysis
FE	Finite element
FOZ	Far offset zone of trench
FSHR	Free-standing hybrid riser
GoM	Gulf of Mexico
ISO	International organization for standardization
LF	Low-frequency
LSD	Limit state design
MPZ	Mean position zone
NOZ	Near offset zone of trench
$P_{1,2}$	Intervals of horizontal displacements from vessel position from 1 to 2
PDF	Probability density function
RAO	Response amplitude operator
RMS	Root mean square
ROV	Remote operation vehicle

RQ model	Randolph and Quiggin model
SCR	Steel catenary riser
TBP	Trench beginning point
TDP	Touchdown point
TDZ	Touchdown zone
TEP	Trench endpoint
TF	Transfer function
TLP	Tension leg platform
TMP	Maximum depth point
TTR	Top tensioned riser
UEL	User-defined element subroutine in ABAQUS
VIV	Vortex-induced vibrations
WA	Western Australia
WF	Wave-frequency
WSD	Working stress design
ZSP	Zero slope point

Symbols

Chapter 1

Chapter 2

q	immersed weight of SCR per unit length
λ	Flexural length parameter
k	Soil stiffness
y	Trench position in the vertical direction
x	Trench position in the horizontal direction
h	Maximum depth of trench (Langner's trench)
a, b, c, d, e	Coefficient of trench equation (Langner's trench)
L	Pipeline side segment length of the trench (Langner's trench)
X	Catenary side segment length (Langner's trench)
k_1	Curvature facture (Langner's trench)
k_2	Length facture (Langner's trench)
R	Radius of curvature (Langner's trench)
T_0	Horizontal tension in SCR (Langner's trench)
W	Submerged weight of SCR (Langner's trench)
$c_1, \bar{c}_1, c_2, \bar{c}_2$	Coefficient of trench equations (Shiri's trenches)
Z_{max}	Trench depth (Shiri's trenches)
X_{z-max}	Distance from a bottom point to the trench (Shiri's trenches)
$C_1, C_2, C_3, \lambda, L_{max}$	Coefficient of trench equations (Wang and Low)

d_{max}	Maximum penetration depths (Wang and Low)
\bar{x}	Relative position to beginning of the trench (Wang and Low)
L_T	Trench length (Wang and Low)
σ_{RMS}	Root mean square of stress
S	Amplitude of cyclic stress
N	Number of cyclic stress

Chapters 3,4

Δ_{TDP}	TDP oscillation amplitude
\tilde{V}	Average shear force distribution
$\Delta\sigma$	von Mises stress range
T	Tension force
M	Bending moment
A	Cross-section area
S	Section modulus
T_0	Tension force at TDP
x	Horizontal coordinate
m_s	Mass per unit length of SCR
g	Graviational acceleration
E	Young's modulus
C	Distance to the neutral axis
I	Second moment of area

λ	Boundary layer length
K	Non-dimensional soil rigidity
k	Soil stiffness
χ_0	Curvature at TDP
q	Immersed weight of SCR per unit length
ξ	Non-dimensional length parameter
ξ_f	Actual TDP position
L_{rest}	Lengths of SCR resting portions on the seabed
S	Length of the catenary part
X_{TDP}	Length horizontal projection of SCR
z	Vertical coordinate
θ_f	Hang-off angles for far vessel offset by horizontal
θ_n	Hang-off angles for near vessel offset by horizontal
b	Horizontal vessel excursion
y	Vertical coordinates of trench
ξ	Horizontal discretization of trench
y_{max}	Trench depth
ξ_{z-max}	Distance from a bottom point to the trench mouth
ω	Set of Horizontal discretization of trench
θ_{seabed}	Seabed slope (trench slope)
D	Outer diameter

L_{total}	Riser length
Z_0	SCR top height from the seabed
EI	Bending stiffness
β	TDP corresponding to different mean vessel position
H_s	Wave height in Scatter diagram
T_z	Wave period in Scatter diagram
n	Number of applied wave in scatter diagram
fd_{max}	Peak fatigue damage
LF_{far}	Low-frequency vessel excursion toward far offset
LF_{near}	Low-frequency vessel excursion toward near offset
$\Theta_{Polynomial}$	Average slope of the polynomial trench
$\Theta_{Quadratic\ exponential}$	Average slope of the quadratic trench
$\Theta_{Linear\ exponential}$	Average slope of the linear trench
Δm	Bending moment variation

Chapter 5

fd_{max}	Fatigue damage peak
λ	Flexural length parameter
s	Curvilinear coordination
χ	Curvature
χ_{TDP}	Curvature of TDP
ρ_0	Radius of curvature at TDP
ρ_{sb}	Radius of curvature of seabed
χ_{sb}	Seabed curvature

χ_0	Curvature at TDP
T_0	Tension force at TDP
q	Immersed weight of SCR per unit length
θ	Angle respect to horizon
θ_{sb}	Seabed angle
$\tan \theta_{sb}$	Seabed slope
R_χ	perturbation parameter respect to seabed curvature
R_θ	perturbation parameter respect to seabed slope
s_f	Ideal position of TDP (position of the contact)
Q	Shear force
Q_0	TDP shear force
y	Riser configuration
y_{sb}	Seabed configuration
y_{SCR}	SCR configuration
y_{st}	Static riser penetration to soil on supported side
x	Horizontal coordination (Cartesian system)
ξ	Dimensionless form of x
η	Dimensionless form of y
η_{sb}	Dimensionless form of y_{sb}
ξ_f	Dimensionless form of s_f
r	Characteristic equation root

m	Seabed slope
k	Soil stiffness
K	Non-dimensional soil stiffness
Δ_{TDP}	TDP oscillation
\hat{s}	Dimensionless form of s
\hat{q}	Dimensionless form of q
\hat{Q}_0	Dimensionless form of Q_0
f_t	Hydrodynamic forces component in tangential direction
f_n	Hydrodynamic forces component in normal direction
r_1 and r_2	Determined parameter related to boundary conditions

Chapter 6

$u(s, t)$	Displacement in tangent direction around the static configuration
$v(s, t)$	Displacement in normal direction around the static configuration
s	Curvilinear coordination
t	Time
q	Immersed weight of SCR per unit length
Θ	Dynamic angle of SCR with respect to the horizontal
θ	Static angle of the SCR with respect to the horizontal
θ_{sb}	Seabed angle
$\tan \theta_{sb}$	Seabed slope
R_θ	Normalized seabed slope

γ	Instantaneous angle of SCR with respect to the horizontal
T	Dynamic tension of SCR
T	Static tension of SCR
τ	Perturbed value of tension
T_0	Static tension of SCR at TDP
Q	Dynamic shear force of SCR
Q	Static shear force of SCR
ϑ	Perturbed value of shear force
h_u	Hydrodynamic force in tangential direction
h_u	Static parcel of hydrodynamic force in tangential direction
ϖ_u	Perturbed parcel of hydrodynamic force in tangential direction
h_v	Hydrodynamic force in normal direction
h_v	Static parcel of hydrodynamic force in normal direction
ϖ_v	Perturbed parcel of hydrodynamic force in normal direction
EI	Bending stiffness of the SCR
EA	Axial stiffness of the SCR
λ	Flexural length parameter
m	Distributed mass along SCR
m_a	Distributed added mass along SCR
L	Total suspended length of SCR
ω_u	Frequency scale for the axial vibration of the riser considering a total suspended length

x	Horizontal coordination (Cartesian system)
$x_0(t)$	TDP oscillation function
ξ	Dimensionless form of x
$\xi_0(t)$	Non-dimensional TDP oscillation
$\xi_K(t)$	Non-dimensional ideal TDP relocation
y	Riser configuration
η	Dimensionless form of y
y_{sb}	Seabed configuration
η_{sb}	Non-dimensional seabed configuration
u_0	axial displacement amplitude
v_0	Non-dimensional axial displacement amplitude
$s_K(t)$	Actual TDP position
χ	Total curvature of the SCR
χ_0	Curvature of the SCR at TDP
χ_{sb}	Seabed curvature
$\Delta\chi$	Curvature variation
Δs	Small segment of riser
V_0	Speed of the TDP (a non-material point)
c_0	Transversal wave celerity of a cable
M	Dynamic bending moment of SCR
M	Static bending of the SCR

$\mu(s, t)$	Dynamic parcel of the bending
\mathcal{M}	Normalized speed of the TDP to transversal wave celerity of a cable
$f(t)$	Non-dimensional dynamic tension at TDZ
a_0	TDP oscillation amplitude
T_s	Period of vessel motion
φ	Phase angle
k	Soil stiffness
K	Non-dimensional soil rigidity
χ_{max}	Maximum curvature

Chapter 1

Introduction

1.1. Overview

Deep offshore oil and gas production, which involves extracting oil and gas from beneath the sea, has significantly increased in the last two decades. This is due to the reduction in available hydrocarbon resources of onshore and nearshore that no longer meet industrial demand. On the other hand, the opportunity of extracting hydrocarbon from deep offshore fields, which are about 8 to 20 times bigger than the onshore and shallow water reservoirs has confirmed by advanced technologies in the oil and gas industry (Hatton et al. 2004). Production and transmission of hydrocarbon in the deep offshore field require the use of sophisticated technology and ever-greater attention to the related engineering capability and environmental impacts. Risers are one of the vital components in the deep offshore field development. Different types of risers are categorized as Conventional steel risers, Flexible risers, Free-standing hybrid risers (FSHRs), Top tensioned risers (TTRs) and Steel catenary risers (SCRs); and are used for production, export and service phase in the offshore field (Lim and Gauld 2003).

Steel catenary risers (SCRs) are amongst the most attractive riser families that are made of welded series of steel pipes together and hung from platform to the seafloor. The first SCR was a 12-inch pipe installed to a Seastar mini TLP production vessel in the Auger field with 992 m water depth in 1994 (Howells 1995). Thereafter, the number of successful SCR installation has been dramatically increased in the offshore industry, and it seems it will continue in the future. Despite the sophisticated design procedure, manufacturing and

installation are easy to handle. Lower cost to fabrication, lower uncertainty in design, and applicability of using different diameters in SCR in various water depths have caused SCRs to be a preferable option compared to others (Maclure and Walters 2007). SCRs are fatigue-prone because of the dynamic and cyclic nature of the environmental and operational loads. The prediction of SCR fatigue life, particularly in the touchdown zone (TDZ) is one of the most challenging aspects of their design. This complexity in the TDZ is emerged by the continuous oscillation of the riser and its cyclic contact with the seabed that results in a gradual trench formation beneath the riser (see Figure 1-1). The cyclic seabed soil stiffness degradation, mobilization of suction force during the riser uplift, continuous changing of the trench profile and embedment depth, the seabed scour under the impact of seabed currents and riser oscillations, the contribution of riser dynamics because of multiphase flow and pressure oscillation inside the riser and many more are all contributing to a wide range of uncertainties that make the SCR fatigue life assessment challenging. (Clukey et al. 2008, Shiri and Randolph 2010).

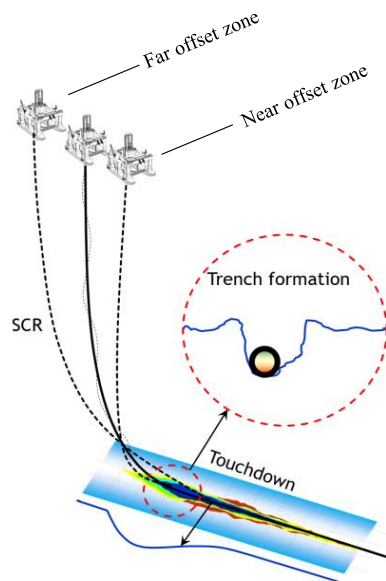


Figure 1-1. Schematic view of SCR and the trench formation in the TDZ

Over the past two decades, a challenging question has been whether the trench formation is for the benefit of the SCR fatigue life or to the detriment. Indeed, this is a significantly important question for the industry, both for making decisions on the continued operation of the existing brownfields that are approaching the end of their design life and for green fields that are under development. Several studies have been published in the literature to explore the trench effect on SCR fatigue. Some of these studies have concluded that the trench formation has a beneficial effect on fatigue life of SCR due to the gradual relaxation of the SCR by penetrating the seabed (Wang and Low 2016, Elliott et al. 2013, Randolph et al. 2013, Nakhaee and Zhang 2008, Clukey et al. 2007, Langner 2003). Some other studies have reported the detrimental effect of the trench on fatigue performance (Zargar 2017, Shiri 2014, Shiri 2014, Rezazadeh et al. 2012, Sharma and Aubeny 2011, Shiri and Randolph 2010, Nakhaee and Zhang 2008, Leira et al. 2004, Giertsen et al. 2004). However, there remains no coherent agreement amongst the researchers. The current research project aimed to fill this knowledge gap by obtaining an answer for this challenging question by developing mathematical, analytical, and numerical models and validation through the published data. To achieve the primary goal of the research project, a set of research objectives were defined.

1.2. Key objectives

The main objectives of this research were as follows:

- Perform a screening analysis to show that all of the complex mechanisms affecting the SCR fatigue in the TDZ can be simply expressed in terms of the seabed soil stiffness and the trench geometry.

- Perform a comparative study to prove the significance of trench geometry versus the seabed stiffness in terms of fatigue damage accumulation in the touchdown zone.
- Identify a simple relationship between the average shear force, TDP oscillation on the trench surface, and the resultant axial stress range that can mimic the fatigue damage variation trends.
- Examine the significance of low-frequency vessel excursions against the wave-frequency oscillations in terms of TDP relocation on the trench surface and the accumulated fatigue damage in the TDZ.
- Investigate the effect of different trench geometries on TDP oscillation and peak damage point location.
- Develop a model and set a series of simplified rules that can support identifying the trench effect on riser fatigue in the touchdown zone.
- Apply the developed framework and the proposed rules to re-assess the key published papers with a contradictory prediction of the trench effect on fatigue and improve the coherence amongst the existing predictions.
- Extend the developed model by incorporation the nonlinear riser dynamics and flexural rigidity effects around the TDP.
- Extract the dynamic equations of SCR in the touchdown zone and obtain the SCR curvature fluctuation on the sloped elastic seabed.

All of these objectives were successfully achieved and disseminated through developing novel methodologies and models that are shortly explained in the next section.

1.3. Organization of the Thesis

This is a paper-based thesis which includes 7 chapters (including four journal papers, two published and two journal manuscripts) and 1 Appendix (including one conference paper accepted).

Chapter 1 presents an introduction to the topic along with the significance, novelty, and the motivation of conducted research work. Chapter 2 includes an overall review of the literature covering different aspects of the riser-seabed interaction and the trench effect on fatigue performance in the touchdown zone. A more specific literature review was included in each chapter to facilitate transferring the paper message as needed. Chapter 3 presents a journal paper published in *Applied Ocean Research* (Elsevier), where the significance of trench geometry in fatigue damage evaluation was investigated. Analytical and numerical modellings were used to obtain a meaningful relationship between the peak fatigue damage and the seabed slope in different zones of the trench. A popular boundary layer model (BLM) developed for SCR interaction with the flat seabed was combined with conventional catenary equations to model the touchdown zone. By using the developed model and running a series of analyses, a new set of rules was proposed for the qualitative assessment of the overall trend of the trench effect on the variation of fatigue damage. The proposed rules were validated through a few case studies. Chapter 4 presents a journal paper published by *Applied Ocean Research* (Elsevier). In this chapter, a set of rules were proposed based on the outcome of Chapter 3 to re-assess the majority of the key published

studies. The proposed methodology resulted in a more coherent agreement between the published studies and proved the validity of the proposed method on a broader perspective. Chapter 5 was submitted as a journal paper to Ocean Engineering (Elsevier). In this chapter, the boundary layer model (BLM) used in chapter 3 that has been initially developed for the flat seabed was expanded to incorporate the sloped seabed effect with no stress discontinuity within the riser to the seabed transition zone. In this chapter, the significance of the touchdown point (TDP) oscillation was explored in terms of peak fatigue damage migration in the TDZ. The improved BLM model extended the validity of the findings and the proposed methodologies in chapters 3 and 4. Chapter 6 was submitted as a journal paper to Engineering Structures (Elsevier). In this chapter, the Newtonian frame was used to obtain the SCR's dynamic curvature oscillation in the sloped seabed and to investigate the significance of seabed soil stiffness relative to the trench profile. This was achieved by mathematical modeling of SCR's dynamic curvature around the TDP. The soil stiffness and the TDP oscillation amplitude were found to be the primary sources of dynamic curvature oscillation. It was observed that the fatigue performance of SCR, which is affected by curvature oscillation in the TDZ, is directly related to the soil stiffness and the TDP oscillation amplitude. The study conducted in chapter 6 completed project's objectives. Chapter 7 summarizes the key findings of the study and the recommendations for future studies. Appendix A includes a conference paper accepted in the 4th International Symposium on Frontiers in Offshore Geotechnics (ISFOG) 2020, Houston, Texas, USA. The paper presents a summary of Chapter 3 and Chapter 4. The research outcome prepared the ground for proposing new methodologies to incorporate the trench effect in SCR fatigue analysis.

1.4. Thesis outcomes

The outcomes of this research work have been disseminated as follows:

Shoghi R, Shiri H. “Modelling Touchdown Point Oscillation and Its Relationship with Fatigue Response of Steel Catenary Risers”. *Applied Ocean Research*, 2019 March, 87 (2019) 142–154.

Shoghi R, Shiri H. “Re-assessment of Trench Effect on Fatigue Performance of Steel Catenary Risers in the Touchdown Zone”. *Applied Ocean Research*, 2020 January, 94 (2020) 1–16.

Shoghi R, Pesce C. P., Shiri H. “Trench Geometry Effect on Fatigue Performance of Steel Catenary Risers”, *Ocean Engineering* (under review).

Shoghi R, Pesce C. P., Shiri H. “Dynamic Curvature of Steel Catenary Riser on Elastic Seabed”, *Engineering Structures* (under review).

Shiri H., Shoghi R. “The geometrical significance of seabed trench in fatigue performance of steel catenary risers in the touchdown zone.” 4th *International Symposium on Frontiers in Offshore Geotechnics*, Austin, Texas, August 2020 (accepted for oral presentation).

References

- Clukey EC, Ghosh R, Mokalala P, Dixon M. Steel catenary riser (SCR) design issues at touchdown area. Proceedings of The 17th International Offshore and Polar Engineering Conference ISOPE-I-07-388; 2007 July 1-6; Lisbon, Portugal. <https://doi.org/10.4043/22557-MS>.
- Clukey E, Jacobs P, Sharma PP. (2008) “Investigation of riser seafloor interaction using explicit finite element methods”, *Offshore Technology Conference*, Houston, Texas, OTC19432-MS.
- Dixon M (2009). "Modelling advances enhance riser fatigue prediction accuracy." *Online Oil & Gas Engineer Magazine-Exploration Drilling*, London, UK.
- Elliott BJ, Zakeri A, Barrett J, Hawlader B, Li G, Clukey EC. Centrifuge modeling of steel catenary risers at touchdown zone Part II: assessment of centrifuge test results using kaolin clay. *Ocean Engineering*. 2013 March 1; 60, 208-218. <https://doi.org/10.1016/j.oceaneng.2012.11.013>.
- Giertsen E, Varley R, Schroder K. CARISIMA: a catenary riser/soil interaction model for global riser analysis. Proceedings of the 23rd International Conference on Offshore Mechanics and Arctic Engineering OMAE 2004-51345; 2004 June 20-25; Vancouver, Canada. doi:10.1115/OMAE2004-51345.

- Hatton S, An P., Eyles T. (2004). Steel Catenary Risers (SCR'S) System Design and Experience. *2H OffShore Engineering Ltd*, Surrey.
- Howells H. (1995). Advances in Steel Catenary Riser Design. *2H OffShore Engineering Ltd*, Surrey.
- Langner C. Fatigue life improvement of steel catenary risers due to self- trenching at the touchdown point. Proceedings of the Offshore Technology Conference OTC 15104; 2003 May 5-8; Texas, USA.
- Leira BJ, Passano E, Karunakaran D, Farnes KA, Giertsen E. Analysis guidelines and application of a riser–soil interaction model including trench effects. Proceedings of the 23rd International Conference on Offshore Mechanics and Arctic Engineering OMAE 2004-51527; 2004 June 20-25; Vancouver, Canada. pp. 955-962, doi:10.1115/OMAE2004-5152.
- Lim F, Gauld S. (2003). Riser Solutions for Ultra-Deep Water Developments. *Proceedings of 10th Annual India Oil & Gas Symposium*, Mumbai, India.
- Maclure D, Walters D. (2007). Freestanding Risers in the Gulf Of Mexico — A Unique Solution For Challenging Field Development Configurations. *2H Offshore Engineering Ltd*, Surrey.
- Nakhaee A, Zhang J. Effects of the interaction with the seafloor on the fatigue life of a SCR. Proceedings of the 18th International Society of Offshore and Polar Engineers Conference ISOPE-I-08-397; 2008 July 6-11; Vancouver, Canada. pp 87-93.
- Randolph MF, Bhat S, Mekha B. Modeling the touchdown zone trench and its impact on SCR fatigue life. Proceedings of the Offshore Technology Conference OTC-23975-MS; 2013 May 6-9; Texas, USA. <https://doi.org/10.4043/23975-MS>.
- Rezazadeh K, Shiri H, Zhang L, Bai Y. Fatigue generation mechanism in touchdown area of steel catenary risers in non-linear hysteretic seabed. *Research Journal of Applied Sciences, Engineering and Technology*. 2012; 4(24):5591-5601.
- Shiri H. Response of steel catenary risers on hysteretic non-linear seabed. *Applied Ocean Research*, 2014 January; 44:20-28. <https://doi.org/10.1016/j.apor.2013.10.006>.
- Shiri H. Influence of seabed trench formation on fatigue performance of steel catenary risers in touchdown zone. *Marine Structures*. 2014 April; 36:1-20. <https://doi.org/10.1016/j.marstruc.2013.12.003>.
- Shiri H., Randolph MF. Influence of seabed response on fatigue performance of steel catenary risers in touchdown zone. Proceeding of the 29th International Conference on Ocean, Offshore and Arctic Engineering OMAE 2010-20051; 2010 June 6-11; Shanghai, China. pp. 63-72; doi:10.1115/OMAE2010-20051.

Wang K, Low YM. Study of seabed trench induced by steel catenary riser and seabed interaction. Proceedings of the 35th International Conference on Ocean, Offshore and Arctic Engineering OMAE2016-54236; 2016 June 19-24; Busan: South Korea. [doi:10.1115/OMAE2016-54236](https://doi.org/10.1115/OMAE2016-54236).

Zargar, E. A new hysteretic seabed model for riser-soil interaction. PhD Thesis; 2017; University of Western Australia.

Chapter 2

Literature Review

2.1. Overview

Since the thesis is paper-based, each chapter has its independent literature review. However, a summary of the literature review was integrated into this chapter to facilitate reading the thesis.

2.2. Introduction

Steel catenary risers (SCRs) are widely used in offshore field development to transfer hydrocarbons from the seabed to the floating facilities. These popular risers are made of thin-wall steel pipes and connected to floating facilities using a special flexible joint at the hanging point called “flexjoint” (API-RP-2RD 1997). The SCR, which is suspended in the form of a catenary, rests on the seabed at the lower end (see Figure 2-1).

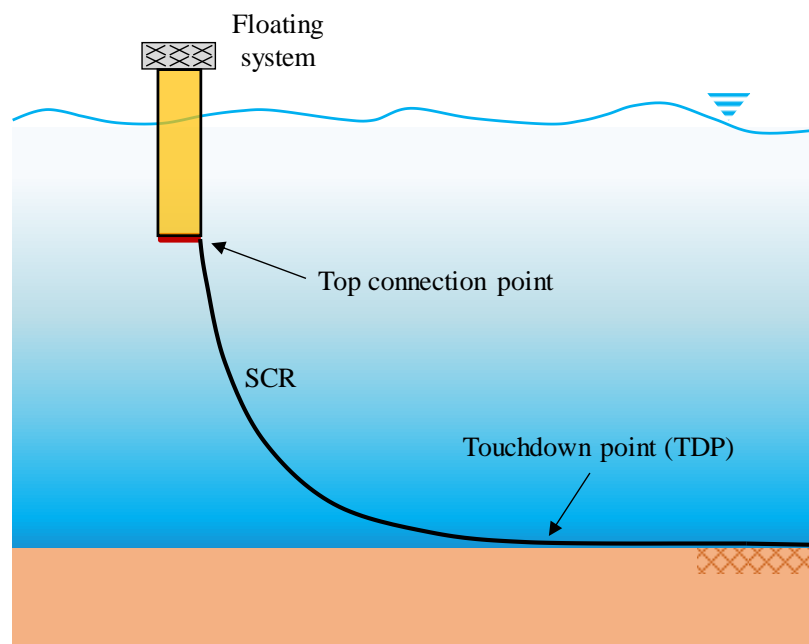


Figure 2-1. Schematic view of SCR connected to a floating system

The first application of a steel catenary, the Auger export pipeline supported by Shell's tension leg platform (TLP), installed in the Gulf of Mexico (Phifer et al. 1994). There are several advantages for SCRs such as compatibility with different floating systems in different water depths and geographical zone, harsh operating environments ability, no need to have compensation for heave motion, and no need to have special subsea connections. These advantages have made them a popular solution in developing the deepwater offshore fields.

The complex riser-seabed interaction affects the global integrity and the design conditions of the SCR both through ultimate and fatigue limit states. The ultimate limit state is related to the response of the SCR to the extreme environmental loads, mooring system failure, and the out-of-plane motions. In this case, the lateral soil resistance acting on the riser imposes excessive bending and tensile stresses on the SCR, from both partial embedment and created trench due to the riser oscillations. The fatigue limit state is related to the cyclic bending stress in the SCR, especially in touchdown zone. The magnitude of the bending stress variations is closely associated with the shear force distribution throughout the touchdown zone. The latter is the area that was explored in the current study.

In this study, the trench effect on fatigue performance of the SCR in the touchdown zone was investigated by modeling the touchdown point oscillation on a range of rigid flat, sloped, linear elastic, and non-linear hysteretic seabed through mathematical, analytical and numerical approaches.

2.2.1. Riser-Seabed Interaction

The touchdown zone of SCR, where there is exposure to riser-seabed interaction, is one of the crucial parts of steel catenary riser for fatigue study. It continuously experiences cyclic

contact with the seabed around the touchdown point (Campbell M. 1999, Larsen and Halse 1997).

Riser-seabed interaction is important from different perspectives such as static embedment, lateral and axial friction mobilization, on-bottom stability, self-burial, liquefaction around the pipeline, sediment transport, heat transfer, response to submarine slides, ploughing and trenching. All of these events affect the riser design and its performance. However, the vertical riser-seabed interaction, which results in cyclic seabed soil stiffness degradation and the gradual trench formation, is the most critical factor in terms of the ultimate fatigue life (Cathie et al. 2005, Randolph and White 2008). The amount of embedment has an impact on the fatigue life of SCR through changing stress range variation in the TDZ (Clukey et al. 2007, Fontaine 2006, Langner 2003).

The riser-seabed interaction can be incorporated into the design by appropriate riser-seabed interaction models. Therefore, these models can have a significant effect on the predicted fatigue life of risers. Bridge and Willis (2002) studied a steel catenary riser, 110m long, and 168.3 mm diameter, with the soil parameter similar to the Gulf of Mexico to capture riser-soil interaction behaviour (STRID JIP (joint industry project)). They used an actuator in a harbour area to model the vessel motions. The study resulted in developing a riser-soil interaction model. Also, Bridge et al. (2004) presented state-of-the-art models related to vertical riser-seabed interaction using published and experimental data via STRIDE and CARISIMA JIPs.

Aubeny et al. (2005) investigate the collapse load of a cylinder embedded in cohesive soil to propose simplified equations modelling the trench effect in the fatigue analysis. They performed plane-strain finite element analysis, including shear strength variation in depth

to calculate collapse load in different trench depths. Using classic plasticity, the authors modeled the soil resistance versus riser embedment. The study showed that the model well simulates the small pipe penetrations, but overestimate the penetrations greater than the half-riser diameter.

Clukey et al. (2008) conducted coupled Eulerian-Lagrangian analysis using LS-DYNA software to model fluid-riser-soil interaction and the trench formation around the riser in TDZ. The Eulerian domain was used to define soil and water, and the Lagrangian domain was used to model the riser with monotonic loading. The numerical results showed good agreement with the published experimental results.

Nakhaee and Zhang (2008) conducted numerical modeling with the incorporation of gradual seabed soil stiffness degradation and cyclic riser embedment through two different riser configurations. They captured stiffness degradation due to cyclic loading by improving a numerical code. The authors considered only the wave-frequency vessel motions and achieved a maximum penetration depth of about $0.4D$ and $0.8D$. The authors observed a cyclic reduction of maximum variation of the bending moment and concluded that trench formation improves the fatigue life near the TDZ.

Hodder and Byrne (2009) conducted a series of large-scale 3D flume tests in silica sand at Oxford University to investigate the cyclic embedment of the oscillating SCR into the seabed. The truncated model of the instrumented riser (7.65 m length, and 110 mm diameter) made of PVC material was pin connected to an actuator applying monotonic and cyclic excitations. The experimental results for clay soil showed good agreement with the result of the numerical analysis.

Randolph and Quiggin (2009) developed a non-linear hysteric riser-seabed interaction model (R-Q model) that could automatically simulate the gradual embedment of the riser into the seabed. The model was validated by centrifuge tests and found to be able to simulate the main non-linear features of the riser seabed interaction, including the initial embedment, uplift, suction generation and decay, breakout, and re-penetration. The proposed model became a popular tool and incorporated into OrcaFlex software that is used for riser design worldwide. Dong and Shiri (2018 and 2019) conducted a study to evaluate the nodal and global performance of the R-Q model. The authors showed that the model is not able to explicitly model a realistic trench but still is a strong tool for non-linear seabed simulation. Shiri and Randolph (2010a) incorporated the non-linear hysteretic riser-seabed interaction model proposed by Randolph and Quiggin into comprehensive fatigue analysis. The authors developed a methodology to incorporate the trenching effect in fatigue analysis automatically. The study concluded that fatigue damage increases in deeper trenches. Also, with gradual trench formation, the peak fatigue damage location is shifted toward the vessel.

Nakhaee and Zhang (2010) studied the dynamic behaviour of the SCRs. The authors captured the riser penetration into the seabed due to cyclic loading using the model developed by Aubeny and Biscontin (2008, 2009). The study showed that riser embedment could improve fatigue life of SCR around the TDP.

Elliot et al. (2013a) developed an apparatus for modelling the riser-soil interaction in the centrifuge test. The performance of the designed apparatus was validated through a series of tests on an elastic seabed and numerical analysis. Elliot et al. (2013b) used the developed apparatus to study the effect of gradual trench formation under cyclic riser motions and its

impact on fatigue life in the TDZ. The study provided the time-domain variation of bending moment in several spots on a truncated riser. The authors concluded that the trench formation would improve the fatigue life of SCR.

Wang et al. (2013) conducted a 3D large-scale 1g flume test in clay to calibrate a numerical model capturing the effect of trench shape and the mobilization and release of the soil suction on fatigue. The rain-flow cycle counting was used for fatigue damage calculation. The result of numerical and experimental case studies showed a good agreement. The authors extended the study to capture the soil parameters affecting the riser-seabed interaction mechanisms. The study showed that the modal shape of riser changes near the TDP, but the natural frequency remains constant for different seabed parameters. Also, the area between the TDP and maximum trench depth was found to be a critical zone.

Shiri (2014a) conducted an analysis by coding the R-Q model into the ABAQUS. The gradual trench development through the touchdown zone was captured by simulation of the cyclic seabed stiffness degradation. The author examined the artificial insertion of the trench in the TDZ and showed that this approach is highly risky due to incompatibilities between the SCR natural catenary profile and the inserted trench profile, particularly in the trench mouth. The author concluded that this approach that has been undertaken by several researchers might easily lead to contact pressure hot spots and distort the fatigue results.

Shiri (2014b) conducted riser fatigue analysis with incorporated non-linear riser-seabed interaction to investigate the effect of trench geometry on fatigue damage accumulation. Under cyclic loading and non-linear seabed, the riser stress profile was investigated. The author proposed two linear and quadratic-exponential equations to simulate the trench profile in the TDZ. The study showed that the quasi-static analysis results in conservative

fatigue damage predictions and the riser dynamic improve fatigue life by 14% in a non-trenched system and 9% in the pre-trenched seabed.

Clukey et al. (2017) conducted a state-of-the-art review of the riser-seabed interaction and concluded that the modelling of the riser-seabed interaction is of crucial importance and may significantly improve the riser fatigue life in the TDZ. Zargar et al. (2019) developed and improved version of the R-Q model and incorporated the secondary non-linear mechanism into the original model developed by Randolph and Quiggin (2009). The new model uses a unified mathematical approach for different modes of the soil-riser interaction and incorporates an explicit degradation model for soil behaviour. The model can also incorporate variable parameters depending on riser penetration rates and depth. The new model was calibrated against existing data from model tests and found to provide good agreement for a range of test conditions.

2.2.2. Steel Catenary Riser (SCR) Mechanics

The catenary elements, such as hanging cables, chains, and risers, have been widely used in a variety of engineering disciplines. Leibniz (1691) proposed the first historical mathematical solution for catenary shape. This equation is still used for the hanging section of the risers between the attachment points and TDP. There are several studies on developing analytical predictions for the non-linear behaviour of SCRs using the boundary layer effects. Most of these studies have focused on the top boundaries (Plunkett 1967, Dixon and Rutledge 1968, Palmer et al. 1974, Konuk 1980, Champneys et al. 1997, Guarracino and Mallardo 1999, Karayaka and Xu 2003). There are a limited number of studies tackling the transition zone in the touchdown area.

Aranha et al. (1995) studied the dynamic catenary configuration of the riser resting on a rigid seabed in a planar condition. The suspended part of SCR was formulated for small fluctuations around the static configuration. The boundary layer technique was used to obtain the curvature of riser around TDP through an asymptotic analytical solution. The curvature of the riser was found to be a function of dynamic tension and TDP displacement.

Pesce et al. (1997) conducted an experiment to capture the dynamic results of a riser around TDP. The results of the experimental study showed a good agreement with the boundary layer solution in terms of time histories, root mean square (RMS), peak-to-peak, and average values. The findings of the study supported previously obtained analytical solutions for SCR dynamics by Aranha et al. (1995).

Aranha et al. (1997) investigated the static and dynamic curvature of SCR around the TDP. An asymptotic boundary layer type approximation of the bending moment in the TDZ was proposed using the quasi-linear frequency domain response of a cable. The viscous drag as the only source of nonlinearity, and the motion of the TDP was considered as important factors in the fatigue analysis. For all of the regular and extreme sea states, an agreement was observed between the analytical and numerical results from nonlinear time-domain models.

Pesce et al. (1998) developed the static boundary layer solution considering a linear elastic seabed by introducing a non-dimensional soil rigidity comprising the seabed stiffness, k , the submerge weight per unit length of SCR (q), and the flexural length parameter, (λ). The parameter λ represents the distance between the actual and ideal (pure catenary) TDP on the infinitely rigid seabed (Aranha et al. 1997). Pesce et al. (1998) modified parameter λ , to consider linear elastic seabed. They matched the catenary solution for the suspended part

of the SCR with riser laid on the soil part. The study resulted in a reasonably accurate curvature oscillation in the TDZ with continuity in both shear force and bending moment at the TDP. The authors concluded that the maximum curvature is located somewhere close to the TDP in the suspended part, and its location is not influenced by the seabed stiffness. Shiri (2010b) compared the result of FEA and developed a boundary layer solution by Pesce et al. (1998) (Figure 2-2 and Figure 2-3). The results showed an exceptionally great correlation between proposed boundary layer solution and FEA results, which makes it a robust method for expression of the SCR in the touchdown zone using the analytical method, for a range of linear soil property.

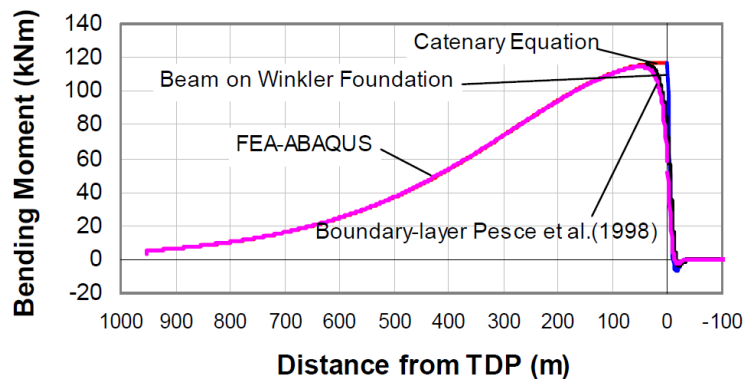


Figure 2-2. Comparison of bending moment along SCR, $k = 100 \text{ kPa}$, Shiri (2010b)

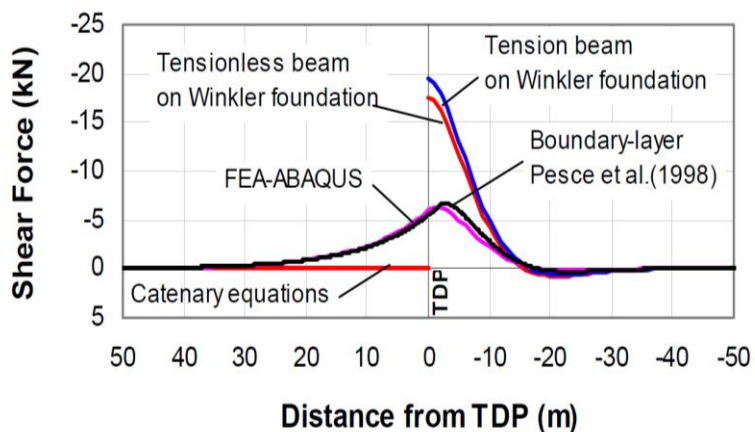


Figure 2-3. Shear force distribution in TDZ, $k = 100 \text{ kPa}$, Shiri (2010b)

All of these studies are limited to the flat seabed and do not consider the sloped seabed that are encountered when a trench is formed beneath the SCR. In the current study, the conventional catenary equations were first combined with a boundary layer solution on the flat seabed to capture the curvature on the sloped seabed. Then the boundary layer equations were further developed directly for the sloped seabed, and the combining process was repeated to compare the results with the flat seabed.

2.2.3. Trench Geometry

There are only a few real trench assessments via reviewing the video recorded by remote operation vehicles (ROVs) from the touchdown zone of the existing SCRs. Researchers have tried to propose mathematical equations for trenches based on the ROV observations. This can be an option to insert a mathematically defined trench in the TDZ to incorporate the trench effect on fatigue analysis. Although, Dong and Shiri (2018 and 2019) showed that this may not be a safe methodology and may result in fatigue hot spots due to the incompatibility of the mathematical trench profile and the natural catenary shape of the riser.

Bridge and Howells (2007) studied sample seabed trenches in the Gulf of Mexico to outline the common features of a generic trench. They divided the trench profile into three different zones with different slopes as a catenary, buried, and surface zones (see Figure 2-4).

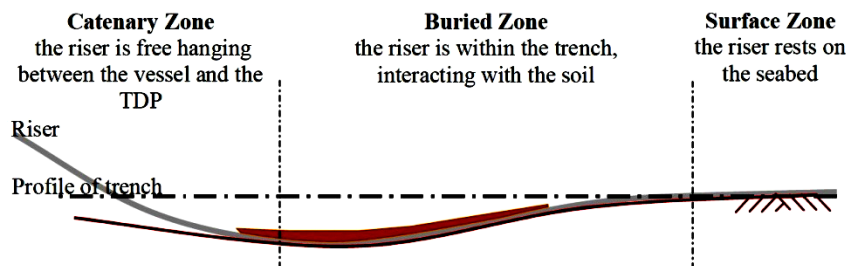


Figure 2-4. Trench shape definitions in profile view, Bridge and Howells (2007)

The authors noticed that the trench has a ladle shape in the longitudinal direction with the deepest portion around the TDP. A few mathematical expressions have been proposed by researchers during the last two decades to represent the trench profile.

Langner (2003) proposed a mathematical trench profile in the form of a circular arc for the catenary side (catenary zone in Bridge and Howells study) and a seventh-order polynomial for the pipeline side (buried zone in Bridge and Howells study). The Langner's trench profile (y) was fit to the boundary conditions on the pipeline side of the trench and parameters are detailed as follows:

$$\begin{cases} y = ax^2 - h & ; \quad 0 \leq x \leq X \\ y = ax^2 + bx^4 + cx^5 + dx^6 + ex^7 - h & ; \quad -L \leq x \leq 0 \end{cases} \quad (1)$$

where the coefficients are defined as a function of catenary radius (defined as the ratio of horizontal tension to the submerged weight of SCR per unit length), a curvature factor, and a length factor.

Shiri (2014a) proposed two sets of linear and quadratic-exponential equations that were compared with the finite element analysis results containing a non-linear hysteretic riser-seabed interaction (see Figure 2-5). These trenches profiles are expressed by the following equations:

$$\begin{cases} y = -c_1 x e^{-c_2 x} & ; \text{Linear exponential} \\ y = -\bar{c}_1 x^2 e^{-\bar{c}_2 x} & ; \text{Quadratic exponential} \end{cases} \quad (2)$$

where $c_1 = Z_{max} e / X_{z-max}$, $c_2 = 1 / X_{z-max}$, $\bar{c}_1 = Z_{max} e^2 / X_{z-max}^2$, and $\bar{c}_2 = 2 / X_{z-max}$. The parameters y and x are the vertical and horizontal coordinates positive upward and toward the pipeline, and Z_{max} is the trench depth, X_{z-max} is the distance from a bottom point to the trench mouth (see Figure 2-5).

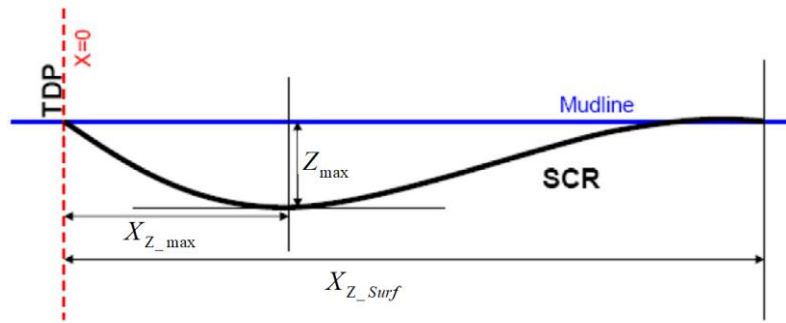


Figure 2-5. Schematic trench profile, Shiri (2014a)

The author considered a seabed trench formation using the proposed equations and investigated the fatigue damage near TDP. The ABAQUS software was used and a coded a nonlinear soil hysteretic model (Randolph and Quiggin in 2009) was incorporated for seabed soil stiffness degradation. The obtained trench via FEA was approximated more precisely compared with the other methods when the trench depth is increased. Trench results after 5 and 1000 load cycles are shown in Figure 2-6 (a) and Figure 2-6 (b).

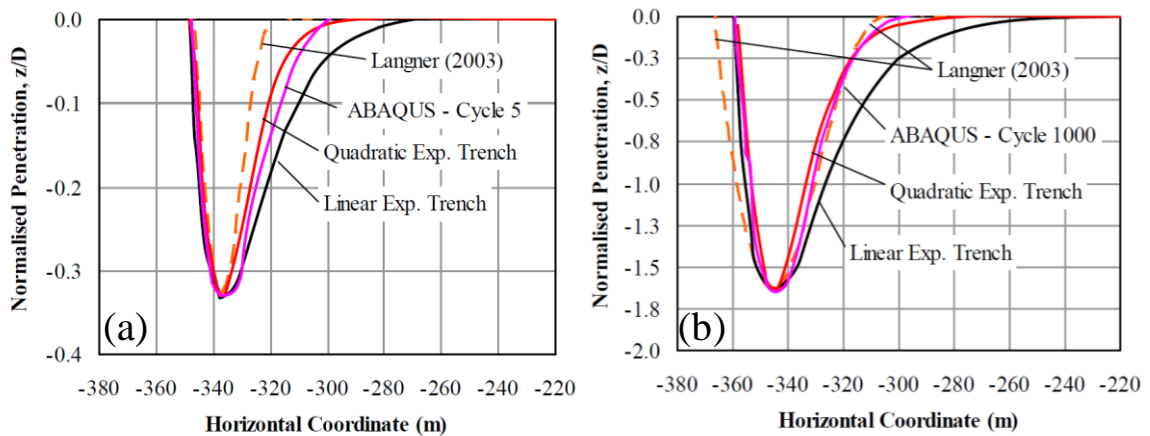


Figure 2-6. Mathematical approximation of non-linear seabed trench, Shiri (2014a)

Randolph et al. (2013) proposed the stepped seabed model, including three different zone (see Figure 2-7). The flowline side surface (zone 1, buried zone in Bridge and Howells 2007) was obtained from the riser profile. The riser side surface (zone 2, catenary zone in Bridge

and Howells 2007) was obtained by mirroring the first zone from the trench bottom point to the inflection point (for the second zone) and linear extrapolation beyond inflection point to virgin seabed surface (for the third zone).

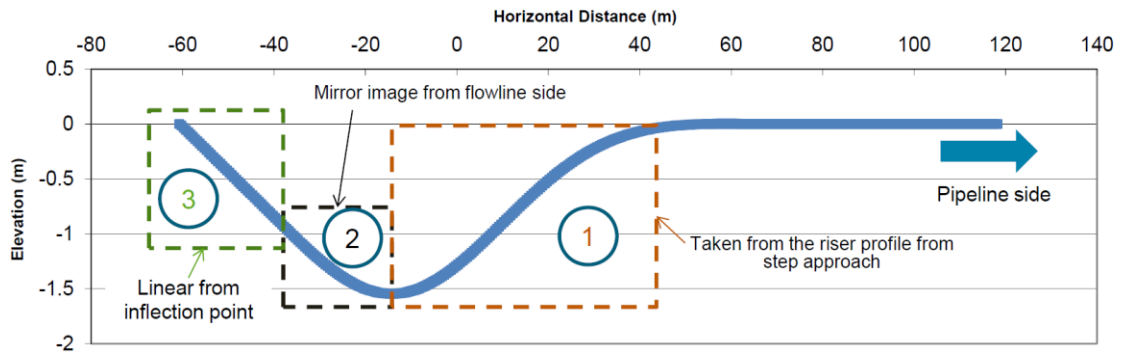


Figure 2-7. Stepped trench model proposed by Randolph et al. (2013)

Randolph et al. (2013) examined three different approaches for modeling the trench and evaluating its impact on the fatigue performance of SCR. The authors considered the trenches proposed by Langner (2003), the cyclically created trench proposed by Shiri and Randolph (2010a), and their new approach known as the “Stepped method.” Figure 2-8 shows the different approaches for modeling the trench by the authors. The analyses were conducted by assuming different low-frequency vessel motions towards far, near, cross offsets to assess the fatigue performance of the riser on the Linear and nonlinear soil properties were examined. The study showed that in the majority of cases, the trench has a beneficial effect on fatigue life in the TDZ. However, some exceptional cases were also observed with increased fatigue damage due to the trench formation.

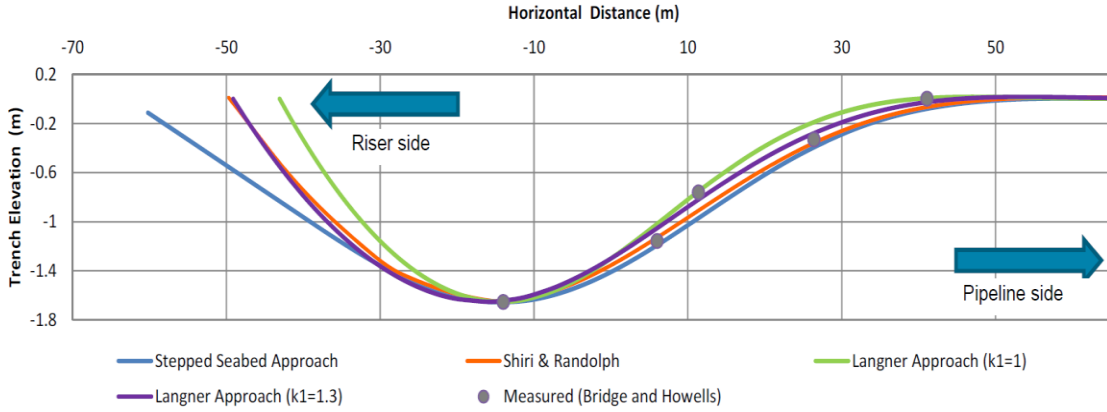


Figure 2-8. Comparison of different trench models in Randolph et al. (2013)

Wang and Low (2016) proposed a simplified parametric model for the trench profile (y) based on iterative static analysis of the catenary riser. The problem was optimized to match the catenary riser and the seabed trench profile. The model was based on a polynomial function, including three dimensionless variables that were achieved by approximating the trench parameters.

$$y = d_{max} \left[C_1 \left(\frac{\bar{x}}{L_T} \right)^3 + C_2 \left(\frac{\bar{x}}{L_T} \right)^2 + C_3 \left(\frac{\bar{x}}{L_T} \right)^1 \right] \quad (3)$$

where \bar{x} is the relative position to the trench beginning point (TBP), d_{max} is the maximum penetration depths, L_{max} is the horizontal distance between TBP to trench maximum depth point (TMP), L_T is the trench length, and $\lambda = L_{max}/L_T$. The coefficients are described as: $C_1 = -(2\lambda - 1)/[\lambda(\lambda - 1)]^2$, $C_2 = (3\lambda^2 - 1)/[\lambda(\lambda - 1)]^2$, $C_3 = -(3\lambda^2 - 2\lambda)/[\lambda(\lambda - 1)]^2$, where L_{max} is calculated as $L_T/3$ under the hypothesis of the null slope at the trench endpoint (TEP). The proposed trench by Wang and Low (2016) is shown in Figure 2-9.

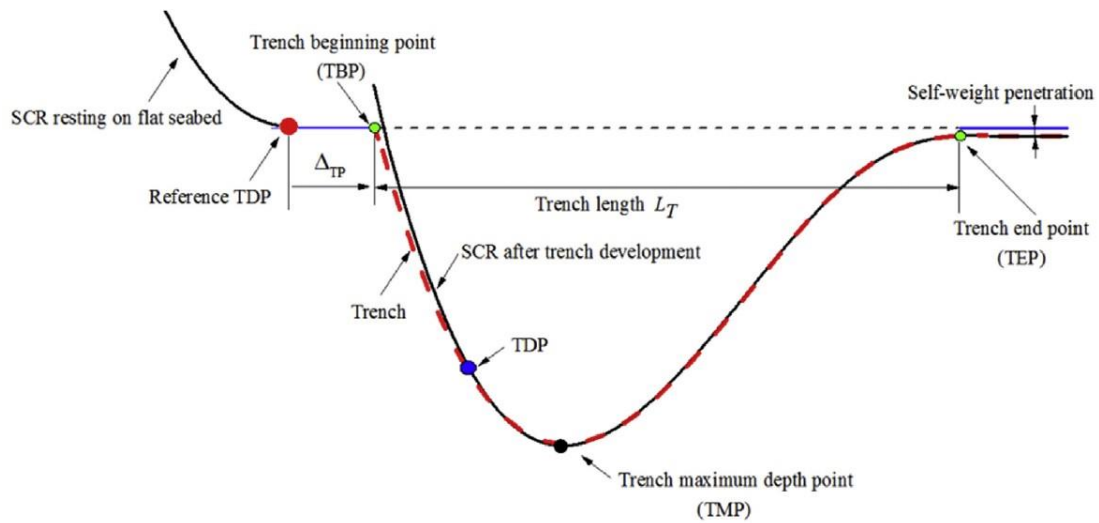


Figure 2-9. Sketch of the proposed trench by Wang and Low (2016)

It should be mentioned that the riser penetration due to static analysis was not considered in the proposed trench profile by Wang and Low.

2.2.4. SCR Analysis Software

There are various finite element software packages such as FLEXCOM3D (MCS, 1994), RIFLEX (SINTEF, 1998), and ORCAFLEX (ORCINA, 1986), which are used in the offshore industry for riser analysis. These software are typically able to model the motions of floating structures, riser system, and simulate VIV, fatigue analysis, and line interference using either explicit or implicit time-integration approaches. These commercial software packages are developed for specific applications in order to minimize the computation time and provide a user-friendly interface for the user to model even a relatively complex model. Although general finite element software, such as ABAQUS and ANSYS are not developed for specific applications in the offshore industry, they provide more capability for the user to develop new material and interface models that are limited in commercial tailor-made software.

2.2.5. SCR Design Guidelines and Fatigue Analysis

There are a few steel catenary riser design guidelines such as API-STD-2RD (2013), API-RP-16Q (2017), 17A (2017), 17B (2014), and 17C (2002); and DNV (DNV-OS-C101 (2018)) which are recommended by classification societies. These guidelines may use different approaches, such as working stress design (WSD) and limit state design (LSD). The DNV and ISO guidelines are based on limit state design (LSD), and API series of guidelines are usually based on working stress design (WSD). In recommended industry approaches, a combination of various guidelines is sometimes used. As an example, STRIDE (Hatton and Willis 1998) for pipe sizing for burst and collapse has recommended using DNV (1996) while for extreme storm response (Hatton and Willis 1998) API-STD-2RD (2013) is recommended to use. For fatigue design of steel catenary riser, three sources of fatigue damage have to be considered based on API-STD-2RD, 2013:

- first-order fatigue as a result of first-order wave frequency vessel excursion due to wave action
- second-order fatigue as a result of second-order low frequency and slow drift motion of the vessel due to action of swell and light winds
- vortex-induced vibration (VIV) fatigue due to current action on SCR

It worth noting that there are other sources of fatigue which need to need to be considered in design in addition to the mentioned sources above, such as installation and shut-down and start-up effects.

In order to calculate first and second-order fatigue damage, two methodologies are used:

- deterministic methodology
- stochastic methodology

In deterministic fatigue analysis, the relation between fatigue life in cycles (N) to failure to the cyclic stress amplitude (S) is provided simply by a constant-amplitude S-N diagram. For the deterministic fatigue analysis method, a wave scatters diagram, including wave heights, wave periods, and the number of each wave applied during a given period, is used to define the environmental loads. In this method, usually wave scatter diagram is manipulated; first, the wave package is divided into several windows, then, a single wave (sea state) that represents the range from each window is selected. This manipulation provides cost-effective computations in order to calculate the damages from all sea states and all directions of loading. For each sea state, by analyzing the system, the response transfer function or stress RAO along the riser is calculated. Assuming riser response is proportional to wave height and constant throughout the window, the linearized riser response for other sea states in the window is obtained. The dividing the scatter diagram into several windows requires identifying the sea states, including the significant contribution to the total fatigue damage, for this purpose, a preliminary assessment is necessary (Bai 2001). By appropriate vessel offsets within the linearization, the effect of the second-order motions, due to low-frequency and slow drift motions, can be considered as part of the first-order fatigue (API-STD-2RD 2013). Each sea state in the windowed wave scatters diagram provides the relative damage. Using Miner's rule, which is linear summation of all relative damages, total fatigue damage is obtained (Miner 1945, Palmgren 1924).

In stochastic fatigue analysis, the system behaviour probabilities, as well as nonlinearities, are considered. This method is more accurate and requires a wave spectrum and a probability density function (PDF) for the environmental loads (SACS 2009, Vughts and

Kima 1976). For a range of common wave frequencies in analysis, the wave spectrum and the probability density function provide dimensionless spectral density and probability of occurrence of a given wave. Using observation data, either single peak spectra such as Pierson-Moskovitz (Pierson Jr and Moskowitz 1964) and JONSWAP (Hasselmann et al. 1973) or Bi-modal spectrum are selected to express wave spectrum.

In the stochastic method, after defining wave spectra, the transfer function (TF) –which is similar to the vessel motion RAO– is obtained in order to relate the wave period to the desired output, such as stress or even cyclic stress range of the system. The required waves for analysis in order to find TF are obtained after selecting a wave frequency band with an appropriate width. The system is analyzed for the selected waves around the peak point of the spectrum with unit wave height, in order to obtain the transfer function. Then, the spectrum of the desired output (e.g., von Mises stress) is obtained by plotting the output versus the frequency in the range of the chosen frequencies band. The system output can be obtained using this plot for any frequency by multiplying the obtained output with unit wave height into the actual wave height at the given frequency, exactly like motion in RAO. Using the number of applied waves obtained from the probability density function (PDF) combining with either the stress RAO or transfer function, the root mean square of stress (σ_{RMS}), and the mean period is calculated. Applying Miner's rule in the form of an integral over the specified frequency range, the fatigue damage is calculated. For the environmental loads in the form of the time history of random waves, the Fourier transform functions from time trace are used to generate the wave spectrum. It should be mentioned that the time trace taken in the Fourier transform functions of this case is commonly 3 hours based on API-STD-2RD 2013. Also, there is another technique which is known as the rain-flow

half-cycle counting method. This method is applied to a time history of wave heights, to extract the number of applied waves and wave periods directly.

Although the stochastic method is more accurate compared to the deterministic method, the deterministic method has always been demanding in the industry because of its simplicity. Because the absolute accuracy of the total fatigue damage of riser is not the main focus in this study and since the research is considered to investigating the influence of the seabed interaction model on fatigue in the touchdown zone, the deterministic method has been chosen for fatigue analysis. The results of deterministic and stochastic approaches for different cases of flexible risers were compared by Sheehan et al. (2005). They obtained that if the wave scatters diagram is described with an appropriate number of wave blocks, the deterministic method is sufficiently accurate.

References

- API-STD-2RD. (2013). "Standard for riser systems that are part of a floating production system (FPS)." American Petroleum Institute, Washington, DC, USA.
- API-RP-16Q. (2017). "Recommended practice for design, selection, operation and maintenance of drilling riser system." American Petroleum Institute, Washington, DC, USA.
- API-RP-17A. (2017). "Design and operation of subsea production systems." American Petroleum Institute, Washington, DC, USA.
- API-RP-17B. (2014). "Design and operation of subsea production systems." American Petroleum Institute, Washington, DC, USA.
- API-RP-17C. (2003). "Recommended practice for TFL (Through Flowline) systems." American Petroleum Institute, Washington, DC, USA.
- DNV-OS-C101 (2018). "Design of offshore steel structures, general- LRFD method." Det Norske Veritas, DNV GL group, classification, certification and technical assurance and advisory company.

- Aranha, J., Martins, C., and Pesce, C. (1997) "Analytical Approximation for the Dynamic Bending Moment at the Touchdown Point of a Catenary Riser." *Int. Journal of Offshore and Polar Engineering*, 293-300.
- Aubeny, C., and Biscontin, G., 2008. Interaction model for Steel Compliant Riser on Soft Seabed. OTC194193, Houston, TX.
- Aubeny, C., and Biscontin, G., 2009. Seafloor-Riser Interaction Model. *International Journal of Geomechanics* 9(3), 133–141.
- Aubeny, C. P., Shi, H., and Murff, J. D. (2005). "Collapse loads for a cylinder embedded in trench in cohesive soil." *International Journal of Geomechanics, ASCE*, 5(4),320–325.
- Bai, Y. (2001). *Pipelines and risers*, Elsevier Science.
- Bridge, C., and Howells, H. (2007) "Observations and modeling of steel catenary riser trenches." *The Seventeenth International Offshore and Polar Engineering Conference, ISOPE2007*, Lisbon, Portugal, 803-813.
- Bridge, C., Laver, K., Clukey, E., and Evans, T. (2004), "Steel Catenary Riser Touchdown Point Vertical Interaction Models." *Offshore Technology Conference*, Houston, Texas, USA, OTC16628.
- Bridge, C., and Willis, N. (2002), "Steel Catenary Risers—Results and Conclusions from Large Scale Simulations of Seabed Interaction". *14th Annual Conference Deep Offshore Technology*, Cape Town, South Africa, 40-60.
- Bruton, D., Carr, M., & White, D. J. (2007, January 1). The Influence Of Pipe-Soil Interaction On Lateral Buckling And Walking of Pipelines- *The SAFEBUCK JIP. Society of Underwater Technology*.
- Campbell, M. (1999), "The Complexities of Fatigue Analysis for Deepwater Risers." *Deepwater Pipeline Conference*, New Orleans, USA.
- Cathie, D. N., Jaeck, C., Ballard, J. C., and Wintgens, J. F. (2005), "Pipeline geotechnics—State of the Art." *Proceedings of the international symposium on frontiers in offshore geotechnics*, Perth, Australia, 95–114.
- Champneys, A. R., Van der Heijden, G. H. M., and Thompson, J. M. T. (1997). "Spatially complex localization after one-twist-per-wave equilibria in twisted circular rods with initial curvature." *Philosophical Transactions: Mathematical, Physical and Engineering Sciences*, 2151-2174.
- Cheuk, C. Y., and White, D. J. (2008), "Centrifuge modelling of pipe penetration due to dynamic lay effects." *Proceedings of the 27th International Conference on Offshore Mechanics and Arctic Engineering*, Estoril, Portugal, 15–20.

- Clukey, E., Ghosh, R., Mokarala, P., and Dixon, M. (2007), "Steel Catenary Riser (SCR) design issues at touchdown area." *International Offshore and Polar Engineering Conference*, Lisbon, Portugal, 814-819.
- Clukey, E. C., Young, A. G., Dobias, J. R., and Garmon, G. R. (2008), "Soil response and stiffness laboratory measurements of SCR pipe/soil interaction." *Offshore Technology Conference*, Houston, USA, OTC 19303.
- Dixon, D. A., and Rutledge, D. R. (1968). "Stiffened catenary calculations in pipeline laying problem." *ASME J. Engng. Indust.*, 90, 153–160.
- DNV-OS-C101. (2008). "Design of Offshore Steel Structure." Det Norske Veritas, Hovik, Norway.
- DNV. (1996). "Rules for submarine pipeline systems." Det Norske Veritas, Hovik, Norway.
- Dong X, Shiri H. Performance of non-linear seabed interaction models for steel catenary riser, Part 1: nodal response. *Ocean Engineering*. 2018; (154) 153-166
- Dong X, Shiri H. Performance of non-linear seabed interaction models for steel catenary riser, Part 1: global response. *Ocean Engineering*. 2019; (82) 158-174
- Elliott BJ, Zakeri A, Barrett J, Macneill A, Phillips R, Clukey EC, and Li G. Centrifuge modeling of steel catenary risers at touchdown zone Part I: Development of novel centrifuge experimental apparatus. *Ocean Engineering*. 2013 March 1; 60, 200-207. <https://doi.org/10.1016/j.oceaneng.2012.11.012>.
- Elliott BJ, Zakeri A, Barrett J, Hawlader B, Li G, Clukey EC. Centrifuge modeling of steel catenary risers at touchdown zone Part II: Assessment of centrifuge test results using kaolin clay. *Ocean Engineering*. 2013 March 1; 60, 208-218. <https://doi.org/10.1016/j.oceaneng.2012.11.013>.
- Fontaine, E. "SCR-Soil Interaction: Effect on Fatigue Life and Trenching. (2006), "Proceedings of the Sixteenth (2006) International Offshore and Polar Engineering Conference, San Francisco, CA, USA, 2.
- Guarracino, F., and Mallardo, V. (1999). "A refined analytical analysis of submerged pipelines in seabed laying." *Applied Ocean Research*, 21(6), 281-293.
- Hasselmann, K., Barnett, T. P., Bouws, E., Carlson, H., Cartwright, D. E., Enke, K., Ewing, J. A., Gienapp, H., Hasselmann, D. E., and Kruseman, P. (1973). "Measurements of wind-wave growth and swell decay during the Joint North Sea Wave Project (JONSWAP)." *Dtsch. Hydrogr. Z. Suppl. A*, 8(12), 289–300.
- Hatton, S. A., and Willis, N. (1998), "Steel catenary risers for deepwater environments." *Offshore Technology Conference*, Houston, TX, USA, OTC8607.

- Hodder, M.S. and Byrne, B.W. (2009) "3D experiments investigating the interaction of a model SCR with the seabed", *Applied Ocean Research*, 32:145-157.
- Karayaka, M., and Xu, L. "Catenary Equations for Top Tension Riser Systems." *Proceedings of the International Offshore and Polar Engineering Conference 2003*, Honolulu, HI, United States, 638-644.
- Konuk, I. (1980). "Higher-order approximations in stress analysis of submarine pipelines." *J. Energy Resour. Technol*, 102(4), 190-196.
- Langner, C. G. (2003), "Fatigue Life Improvement of Steel Catenary Risers due to Self-Trenching at the Touchdown Point." *Offshore Technology Conference*, Houston, Texas, USA, OTC15104.
- Larsen CM, Halse KH. Comparison of models for vortex-induced vibrations of slender marine structures. *Marine Structures 1997 July*; 10(6):413-441. [https://doi.org/10.1016/S0951-8339\(97\)00011-7](https://doi.org/10.1016/S0951-8339(97)00011-7).
- Leibniz. (1691). "Solutions to the Problem of the Catenary, or Funicular Curve, Proposed by M. Jacques Bernoulli in the Acta of June 1691." *Acta Eruditorum, Leipzig, Germany*.
- MCS. (1994). *User Manual for FLEXCOM3D, a tailor-made finite element programme for non-linear time domain analysis of offshore structures*, MCS Advanced Subsea Engineering, Galway, Ireland.
- Miner, M. A. (1945). "Cumulative damage in fatigue." *Journal of applied mechanics*, 12(3), 159-164.
- Nakhaee A, Zhang J. Effects of the interaction with the seafloor on the fatigue life of a SCR. *Proceedings of the 18th International Society of Offshore and Polar Engineers Conference ISOPE-I-08-397*; 2008 July 6-11; Vancouver, Canada. pp 87-93.
- Nakhaee, A., and Zhang, J., (2010). Trenching effects on dynamic behavior of a steel catenary riser. *Ocean Engineering*. 37. 277–288.
- Orcina Ltd. (1986). "Orcaflex User Manual." Cumbria, UK.
- Palmer, A., Hutchinson, G., and Ells, J. (1974). "Configuration of Submarine Pipelines during Laying Operation." *ASME J. Engng. Industry* (96), 1112-1118.
- Palmgren, A. G. (1924). "Die Lebensdauer von Kugellagern (Life Length of Roller Bearings. In German)." *Zeitschrift des Vereines Deutscher Ingenieure (VDI Zeitschrift)*, 68(14), 339-341.
- Pesce, C. P., Aranha, J. A. P., and Martins, C. A. (1998), "The Soil Rigidity Effect in the Touchdown Boundary-Layer of a Catenary Riser: Static Problem." *Eighth*

- International Offshore and Polar Engineering Conference*, Montreal, Canada, 207-213.
- Pesce, C. P., Aranha, J. A. P., Martins, G. A., Ricardo, O. G. S., and Silva, S. (1997), "Dynamic curvature in catenary risers at the touchdown point: An experimental study and the analytical boundary-layer solution." ISOPE, Honolulu, HI, USA, 656-665.
- Phifer, E. H., Frans, K., Swanson, R. C., Allen, D. W., and Langner, C. G. (1994), "Design And Installation Of Auger Steel Catenary Risers." *Offshore Technology Conference*, Houston, Texas, USA, OTC7620.
- Pierson Jr, W. J., and Moskowitz, L. (1964). "A proposed spectral form for fully developed wind seas based on the similarity theory of SA Kitaigorodskii." *Journal of Geophysical Research*, 69(24), 5181–5190.
- Plunkett, R. (1967). "Static bending stresses in catenaries and drill strings." *Journal of Engineering for Industry, Transactions of the ASME*, 89(1), 31–36.
- Randolph MF, Bhat S, Mekha B. Modeling the touchdown zone trench and its impact on SCR fatigue life. *Proceedings of the Offshore Technology Conference OTC-23975-MS*; 2013 May 6-9; Texas, USA. <https://doi.org/10.4043/23975-MS>.
- Randolph, M. F., and Quiggin, P. (2009), "Non-linear hysteretic seabed model for catenary pipeline contact" *28th International Conference on Ocean, Offshore and Arctic Engineering OMAE 2009*, Honolulu, Hawaii, USA, 79259.
- Randolph, M. F., and White, D. J. (2008) "Pipeline embedment in deep water: processes and quantitative assessment." *Offshore Technology Conf.*, Houston, USA, OTC 19128.
- SACS. (2009). "The manual of Structural Analysis Computer system program (SACS)." *Engineering Dynamic Inc*, Release 5, Rev 3.
- Sheehan, J. M., Grealish, F. W., Smith, R. J., and Harte, A. M. (2005). "Characterization of the Wave Environment in the Fatigue Analysis of Flexible Risers." *Proceedings of OMAE2005, Paper*, 67507.
- Shiri H., Randolph MF. Influence of seabed response on fatigue performance of steel catenary risers in touchdown zone. *Proceeding of the 29th International Conference on Ocean, Offshore and Arctic Engineering OMAE 2010-20051*; (2010a) June 6-11; Shanghai, China. pp. 63-72; doi: 10.1115/OMAE2010-20051.
- Shiri H., *Influence of seabed response on fatigue performance of steel catenary risers in touchdown zone*. PhD Thesis; (2010b); University of Western Australia
- Shiri H. Influence of seabed trench formation on fatigue performance of steel catenary risers in touchdown zone. *Marine Structures*. (2014a) April; 36:1-20.

<https://doi.org/10.1016/j.marstruc.2013.12.003>.

- Shiri H. Response of steel catenary risers on hysteretic non-linear seabed. *Applied Ocean Research*, (2014b) January; 44:20-28. <https://doi.org/10.1016/j.apor.2013.10.006>.
- Vughts, J. H., and Kinra, R. K. (1976), "Probabilistic fatigue analysis of fixed offshore structures." *Offshore Technology Conference*, Dallas, Texas, OTC2608.
- Wang K., Xue H., and Tang W., Time domain prediction approach for cross-flow VIV induced fatigue damage of steel catenary riser near touchdown point. *Applied Ocean Research*, (2013) October, Vol 43, Pages 166-174.
- Wang K, Low YM. Study of seabed trench induced by steel catenary riser and seabed interaction. *Proceedings of the 35th International Conference on Ocean, Offshore and Arctic Engineering OMAE2016-54236*; 2016 June 19-24; Busan: South Korea. doi:10.1115/OMAE2016-54236.

Chapter 3

Modeling Touchdown Point Oscillation and Its Relationship with Fatigue Response of Steel Catenary Risers

Rahim Shoghi¹, Hodjat Shiri²

1: Department of Civil Engineering
Memorial University of Newfoundland
e-mail: rshoghi@mun.ca

2: Department of Civil Engineering
Memorial University of Newfoundland
e-mail: hshiri@mun.ca

This chapter was published as a journal paper in Applied Ocean Research (Elsevier).

Abstract

The riser-seabed interaction resulting in a trench formed in the touchdown zone (TDZ) of steel catenary risers (SCR) has a significant influence on accumulated fatigue damage. Several studies have used different trench modeling approaches to investigate the trench effect on fatigue. However, contradictory observations have been reported with no coherent agreement on the beneficial or detrimental effect of the trench on fatigue. In this study, the significance of trench geometry in fatigue damage evaluation was investigated. Using analytical and numerical approaches, a meaningful relationship was observed between the trench slope in different zones and the peak fatigue damage. A new set of rules was proposed for the qualitative assessment of the overall trend of the trench effect on the variation of fatigue damage. The proposed assessment rules were validated by performing comprehensive numerical fatigue analysis. A comparison with samples of published experimental and numerical studies was also completed. It was observed that depending on the direction of the low-frequency vessel excursions, the peak fatigue damage may increase towards the near offsets and decrease towards the far vessel offset. This implied that the case dependency of the trench effect on fatigue response in different geographical locations with various environmental loads was a potential source for the contradictory results reported in previously published studies.

Keywords: Steel catenary risers; Riser-seabed interaction; Touchdown point; Trench profile; Fatigue response

3.1. Introduction

Steel catenary risers (SCRs) are made of thin-wall steel pipes suspended from floating facilities to the seabed in the form of a catenary. These popular elements are usually used in offshore field developments for transferring hydrocarbon from the seabed to the floating systems. SCRs are subjected to dynamic and cyclic loads and are vulnerable to fatigue loads. One of the most fatigue prone parts of the SCR is the touchdown zone (TDZ), where it continuously experiences cyclic contact with the seabed around the touchdown point (TDP) (Campbell 1999, Larsen and Halse 1997).

Subsea surveys have proven a trench formation under the SCR several diameters deep (see Figure 3-1) (Zargar 2017). The trench is created by the contribution of several complicated mechanisms including the cyclic soil stiffness degradation, suction force mobilization in uplift movement, and soil scour due to riser-soil-seawater interaction. These mechanisms result in the gradual cyclic embedment of the SCR into the seabed and eventually an ultimate trench formation in the TDZ that is believed to have a significant influence on fatigue performance.

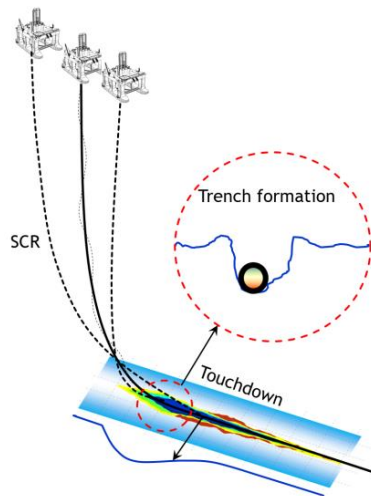


Figure 3-1. Cyclic trench development in the TDZ of SCR

Previous studies that have investigated the influence of trench formation on fatigue life have reported contradictory observations (e.g., Zargar 2017, Wang and Low 2016, Elliott et al. 2013, Shiri 2014ab, Randolph et al. 2013, Rezazadeh et al. 2012, Sharma and Aubeny 2011, Shiri and Randolph 2010, Nakhaee and Zhang 2008, Clukey and Gosh 2007, Leira et al. 2004, Giertsen et al. 2004, Langner 2003). Some of the studies have concluded that the trench formation benefits fatigue life because of the gradual relaxation of the SCR by penetrating into the seabed (e.g., Wang and Low 2016, Elliott et al. 2013, Randolph et al. 2013, Nakhaee and Zhang 2008, Clukey and Gosh 2007, Langner 2003). Other studies have observed the detrimental effect of the trench on fatigue performance (e.g., 3, Shiri 2014, Shiri 2014, Rezazadeh et al. 2012, Sharma and Aubeny 2011, Shiri and Randolph 2010, Nakhaee and Zhang 2008, Leira et al. 2004, Giertsen et al. 2004). Different methodologies have been used to incorporate the trench in the TDZ, such as the artificial insertion of mathematically expressed trenches (Wang and Low 2016, Randolph et al. 2013, Clukey and Gosh 2007, Langner 2003) or the automatic development of trenches using advanced non-linear hysteretic riser-seabed interaction models (Shiri 2014, Shiri 2014, Rezazadeh et al. 2012, Sharma and Aubeny 2011, Nakhaee and Zhang 2008). However, there remains no coherent agreement amongst researchers on the trench effect on fatigue. Obtaining a robust answer for this question is significant for developing a reliable and cost-effective design of SCRs.

In this study, a mathematical basis accompanied with a set of geometrical rules was proposed to facilitate the qualitative prediction of the trench effect on fatigue performance of SCR in the TDZ. The proposed basis was developed using the existing mathematical solutions and validated through performing advanced numerical analysis and comparing

with published experimental and numerical studies. Wave-frequency (WF) vessel motions and its combination with low-frequency (LF) vessel excursions towards different directions were considered. Meaningful relationships were observed between the seabed slope in different zones of the trench and peak fatigue damage. The direct product of the TDP oscillation amplitude (Δ_{TDP}) and average shear force distribution (\tilde{V}) was found to have an overall variation trend similar to von Mises stress range ($\Delta\sigma$) (or fatigue damage). This product ($\tilde{V} \times \Delta_{\text{TDP}}$) is neither equal to nor an approximation of von Mises stress range or fatigue, and there seems to be a complex relationship between them. However, it is a sensible parameter that mimics the von Mises stress variation and facilitates the evaluation of the overall trench effect on fatigue.

These observations led to the development of a set of rules used for qualitative assessment of the overall trend of the trench effect on fatigue. The proposed rules were validated by conducting a series of comprehensive fatigue analyses and comparing the results with samples of published numerical and experimental studies.

It was observed that the direction of predominant fatigue sea states and the LF vessel excursions in a given geographical location influenced the peak fatigue damage, which might be increased towards the near offset zone (NOZ) or decreased towards the far offset zone (FOZ) of the trench. This could explain the contradictions in the previously published studies. The observation implied that the fatigue damage variation due to trench effect is case dependent. Also, the results obtained from studies with purely WF oscillations cannot be generalized to the real SCR response.

3.2. Conceptual Basis and Motivation

Several complex and interactive mechanisms may contribute to trench formation underneath the SCR and fatigue performance. This has made challenges against achieving a coherent agreement about the trench effect on fatigue, and identifying the sources of contradiction in the published results. However, a qualitative assessment of various mechanisms in Figure 3-2 shows that regardless of the source of the contribution, it may ultimately affect only the soil stiffness degradation and/or the variation of TDP oscillation path on the sea bottom.

As illustrated in Figure 3-2, SCRs may be subjected to a range of environmental (wave, wind, and current; Figure 3-2 – C1) and operational (e.g., slugging; Figure 3-2 – C2) loads. These loads contribute to SCR oscillations in the TDZ both by the vessel motions (e.g., wave frequency (WF) and low frequency (LF) motions) and by the riser vibrations (e.g., vortex-induced vibrations (VIV), and slugging). The riser oscillation causes cyclic contact with the seabed in the forms of repetitive penetration and uplift. This process, in turn, results in gradual soil stiffness degradation (Figure 3-2 – C4), mobilization of suction force underneath the riser within uplift movements, cyclic embedment of the SCR into the seabed and eventually the formation of a trench under the SCR (Elliott et al. 2013, Clukey and Gosh 2007, Giertsen et al. 2004, Bridge and Howells 2007). The trench development process is accelerated by the sea-bottom currents and the water entrapped between the oscillating SCR and the trench bottom (Figure 3-2 – C3) (Clukey et al. 2017, Clukey et al. 2008, Fouzder 2012, Draper et al. 2016).

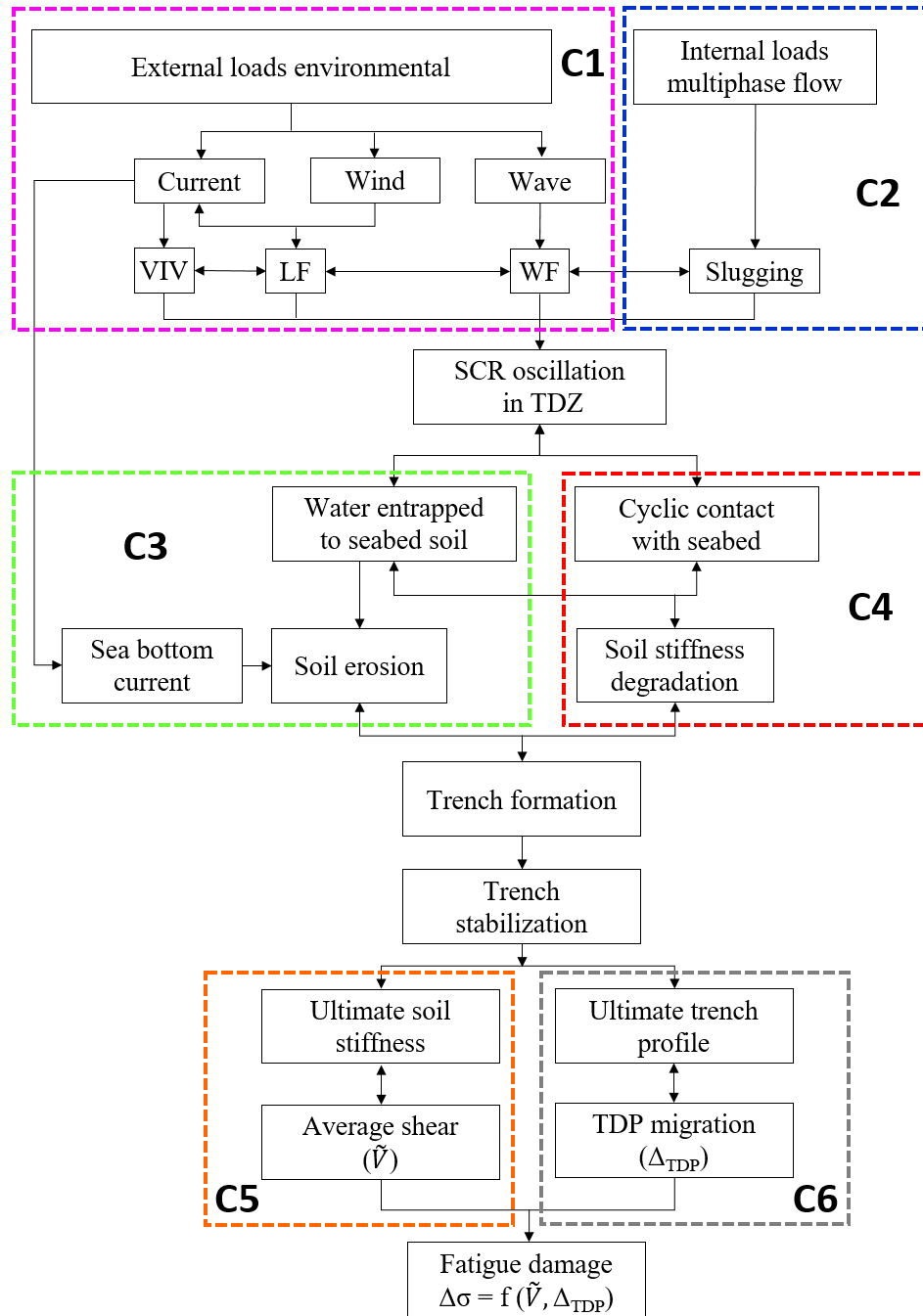


Figure 3-2. SCR-soil-seawater interaction mechanisms and the relation with TDP oscillation

Field observations have shown that the trench is mostly developed during the early stages of the riser production life (first 2 to 3 years). The natural trench infill is mostly washed

out in a fully developed trench (Giertsen et al. 2004, Bridge and Howells 2007) and the magnitude of suction force mobilization is reduced to a low level of importance (Randolph et al. 2013). Therefore, as shown in Figure 3-2, the cross-sectional stress oscillation or fatigue damage in a fully developed trench (assumed to be the ultimate version of cyclic embedment) is mainly affected by the softened trench bed (Figure 3-2 – C5) and the trench geometry (Figure 3-2 – C6). This will be mathematically shown in the next section.

It is worth mentioning that the mechanisms of seabed softening have been widely investigated through the development of a non-linear hysteretic seabed model (Randolph and Quiggin 2009, Hodder 2009, Aubeny et al. 2008, Aubeny and Biscontin 2006, CARISIMA 1999). However, since these models are unable to explicitly simulate the trench (because of premature stabilization), they couldn't be effectively used to assess the influence of ultimate trench geometry on fatigue (Dong X and Shiri 2018, Zargar and Kimiaei 2015).

3.3. Mathematical Dependence of Fatigue Damage on TDP Oscillation and Average Shear Force

In order to mathematically prove the qualitative outcome of Figure 3-2, i.e., the dependency of the fatigue damage on average shear force (\tilde{V}) and TDP oscillation amplitude (Δ_{TDP}), the boundary layer solution (BLM) proposed by Pesce et al. (2006) and the catenary equations solved by Leibniz (1691) were adopted (Pesce et al. 2006, Leibniz 1961). The BLM model is a further developed version of an earlier study conducted by the authors in 1998, Pesce et al. 1998). The model predicts the oscillatory behavior of the curvature in the TDZ, smoothly matching the riser catenary with continuous and reasonably accurate shear force distribution at the TDP. For an arbitrary SCR configuration (see Figure 3-3),

the circular cross-sectional von Mises stress can be written as follows for a given vessel position:

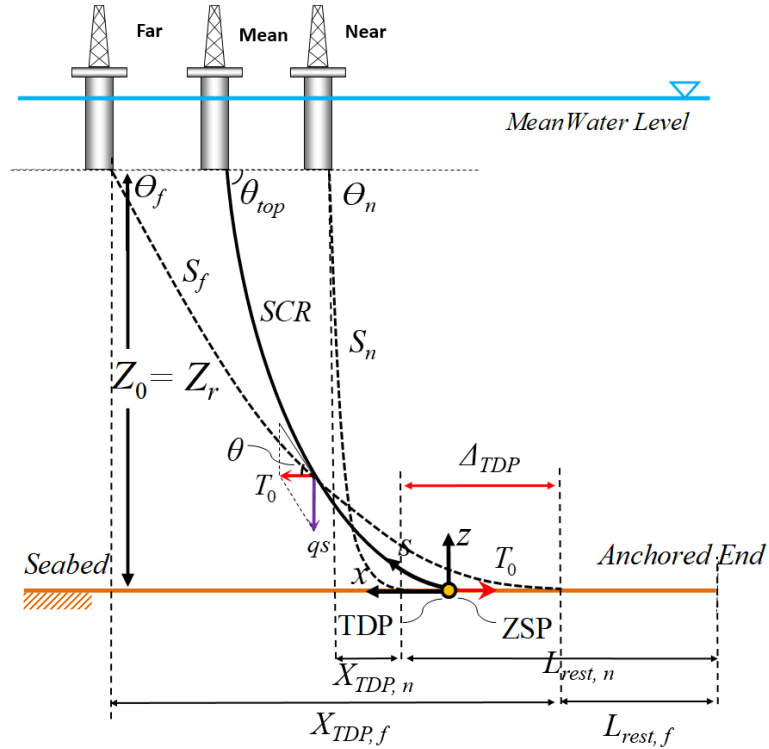


Figure 3-3. Schematic view of near and far SCR configuration

$$\sigma_{von\ Mises} = \frac{T}{A} + \frac{M}{S} \quad (1)$$

where T , M , A , and S are tension force, bending moment, cross-section area, and the section modulus of the riser, respectively. Fatigue damage in SCR is accumulated by cyclic oscillation of the stress defined in equation (1) through the far and near vessel offsets. Using the equation (1), the cyclic stress change which is the governing factor in the calculation of fatigue damage could be written as follows:

$$\begin{aligned}\Delta\sigma_{von Mises} &= \sigma_{v-far} - \sigma_{v-near} = \frac{\Delta T}{A} + \frac{\Delta M \times C}{I} \\ &= \frac{1}{A}(T_{x,f} - T_{x,n}) + \frac{C}{I}(M_{x,f} - M_{x,n})\end{aligned}\quad (2)$$

The subscripts n and f correspond to the near and far vessel offsets. From conventional catenary equations (Leibniz 1961) the tension can be written as:

$$T = T_0 \cosh(xm_s g / T_0) \quad (3)$$

where T_0 , x , and $m_s g$ are tension at TDP, horizontal coordinate, and submerged weight of SCR per unit length. Substituting the equation (3) into the (2) gives:

$$\begin{aligned}\Delta\sigma_{von Mises} &= \frac{1}{A}[T_{0,f} \cosh(xm_s g / T_{0,f}) - T_{0,n} \cosh(xm_s g / T_{0,n})] \\ &\quad + \frac{C}{I}(M_{x,f} - M_{x,n})\end{aligned}\quad (4)$$

Writing the bending moment in the form of curvature, κ gives:

$$\begin{aligned}\Delta\sigma_{von Mises} &= \frac{1}{A}[T_{0,f} \cosh(xm_s g / T_{0,f}) - T_{0,n} \cosh(xm_s g / T_{0,n})] + EC(\kappa_{x,f} \\ &\quad - \kappa_{x,n})\end{aligned}\quad (5)$$

where E , C , and I are Young's modulus, distance to the neutral axis, and the second moment of area, respectively. Pesce et al. (2006) define the parameter λ as boundary layer length, which denotes the difference between the actual and ideal position of the TDP (Fouzder 2012). The authors defined a non-dimensional soil rigidity parameter, K , as follow:

$$K = \frac{k\lambda^4}{EI} = \frac{k\lambda^2}{T_0} = \frac{kEI}{T_0^2} = \chi_0 \lambda \frac{k\lambda}{q} \quad (6)$$

where k , T_0 , χ_0 and q are soil stiffness, riser tension at the TDP, maximum curvature in suspended part, and the immersed weight of SCR per unit length. To facilitate tracking the functional dependency of the parameters, the key equations addressed above and the basic catenary equations could be abridged with the following sets of functions:

$$K = f_1(\chi_0, k, \xi, \xi_f) \quad (7)$$

where ξ and ξ_f are the non-dimensional length parameter, and the actual TDP, respectively. The BLM proposed by Pesce et al. (2006) shows that these parameters are functions of λ , K , and T_0 :

$$\xi = f_2(\lambda) = f_2(T_0) \quad (8)$$

$$\xi_f = f_3(K) = f_3(k, T_0) \quad (9)$$

$$\chi_0 = f_4(T_0) = \frac{q}{T_0} \quad (10)$$

Substituting these equations into equation (7) gives:

$$K = f_5(k, T_0) \quad (11)$$

Therefore, the curvature is a function of soil stiffness and the tension at the TDP:

$$\kappa = f_6(k, T_0) \quad (12)$$

Substituting the equation (12) to equation (5):

$$\Delta\sigma = f_7(k, T_{0,f}, T_{0,n}) \quad (13)$$

Using the conventional catenary equations, it can be shown that the touchdown tension in the near and far configurations are related to the migration of the TDP or Δ_{TDP} . For this

purpose, the TDP shifting can be obtained from the difference between the lengths of SCR resting portions on the seabed, L_{rest} , in far and near positions as follow (see Figure 3-3):

$$\Delta_{TDP} = L_{rest,n} - L_{rest,f} \quad (14)$$

Since the total length of the riser does not change, the compatibility equations for the curved and projected lengths of SCR in the near and far positions on a virgin seabed can be written as follows:

$$S_n + L_{rest,n} = S_f + L_{rest,f} \quad (15)$$

$$X_{TDP,n} + L_{rest,n} + b = X_{TDP,f} + L_{rest,f} \quad (16)$$

$$Z_0 = Z_r \quad (17)$$

where S and X_{TDP} are the length of the catenary part and its horizontal projection. Rearranging the equations (15) and (16) in the form of equation (14), the TDP relocation under given surge can be written as:

$$\Delta_{TDP} = S_f - S_n = X_{TDP,f} - X_{TDP,n} - b \quad (18)$$

The governing catenary equation for the hanging part of the SCR proposed by Leibniz (1691), is as follows:

$$T_0 \frac{d^2 z}{dx^2} = q \sqrt{1 + \left(\frac{dz}{dx}\right)^2} \quad (19)$$

where, z and x are the vertical and horizontal coordinates with origin at the seabed and the TDP, respectively. A simplified solution of equation (19) is given by Timoshenko (Timoshenko and Young 1968) (see Figure 3-3):

$$z = \frac{T_0}{q} \left(\cosh\left(\frac{q}{T_0}x\right) - 1 \right) \quad (20)$$

$$T_0 = zq \frac{\cos\theta_{top}}{1 - \cos\theta_{top}} \quad (21)$$

$$x = \frac{T_0}{q} \operatorname{asinh}(\tan\theta) \quad (22)$$

$$s = \frac{T_0}{q} \sinh\left(\frac{q}{T_0}x\right) \quad (23)$$

The slope of any given point on the SCR, “ θ ”, is given by:

$$\tan\theta = \frac{dz}{dx} = \sinh\left(\frac{q}{T_0}x\right) \quad (24)$$

Substituting the equations (22) to (24) into the equation (18), the TDP relocation can be written as follows:

$$\Delta_{TDP} = Z_0 \left(\frac{\cos\theta_f}{1 - \cos\theta_f} \tan\theta_f - \frac{\cos\theta_n}{1 - \cos\theta_n} \tan\theta_n \right) \quad (25)$$

Rearranging the equation (21) for the SCR attachment point, the equation (26) can be obtained:

$$\frac{T_0}{q} = Z_0 \frac{\cos\theta_{top}}{1 - \cos\theta_{top}} \quad (26)$$

Substituting the equation (26) into equation (25), the TDP migration can be obtained as follow:

$$\Delta_{\text{TDP}} = \frac{1}{q} (T_{0\text{-far}} \tan\theta_f - T_{0\text{-near}} \tan\theta_n) \quad (27)$$

where θ_f and θ_n are given hang-off angles for far and near vessel offset by horizontal excursion “ b .”

In conclusion, comparing the equations (13) and (27), the dependency of the cyclic cross-sectional stress on the two main parameters k and Δ_{TDP} can be concluded and written as:

$$\Delta\sigma = f_{10}(k, \Delta_{\text{TDP}}) \quad (28)$$

The seabed stiffness determines the contact pressure between the riser and the seabed. The contact pressure results in shear force distribution in the TDZ. Therefore, assuming an average shear force between far and near offsets (\tilde{V}), the equation (28) can be also written as:

$$\Delta\sigma \approx f_{11}(\tilde{V}, \Delta_{\text{TDP}}) \quad (29)$$

The equation (28) shows that the ultimate fatigue damage can be expressed in terms of the average shear force (\tilde{V}), and the TDP migration amplitude (Δ_{TDP}). It will be shown in the coming sections, through analytical and numerical investigation of \tilde{V} and Δ_{TDP} , that the product of these two key parameters ($\tilde{V} \times \Delta_{\text{TDP}}$) has the same variation trend as von Mises stress range ($\Delta\sigma$) or fatigue damage. Although, the mathematical relationship between the fatigue damage and these two key parameters can be a complicated explicit equation. However, the advantage of this dependency was used in this study to assess the overall trend of trench effect on fatigue life, i.e., the improvement or deterioration, without a quantitative assessment. It is noteworthy, that the product of the average shear force and the TDP migration amplitude ($\tilde{V} \times \Delta_{\text{TDP}}$) is neither equal to nor an approximation to von

Mises stress range or fatigue. However, as mentioned earlier, it is a sensible parameter that mimics the same variation trends in von Mises stress range. Also, it is neither proposed in this paper nor is it practical to physically monitor the TDP oscillations and assess the riser fatigue on that basis.

3.4. Analytical TDP Oscillation on Curved Trenches

While the vessel oscillates under the environmental loads, the TDP oscillates on the curved trench (see Figure 3-4) and moves opposite to the vessel motion. In a quasi-static system on a rigid seabed, the TDP oscillation amplitude, Δ_{TDP} , depends on the vessel oscillation amplitude and the trench profile. To find the analytical expression of Δ_{TDP} , first, the trench profile has to be mathematically defined. There are a couple of curves proposed for trench geometry in the literature (Wang and Low 2016, Shiri 2014, Langner 2003). The quadratic-exponential model proposed by Shiri (2014b) was selected to represent the trench profile because of its excellent correlation with numerical simulations (Shiri 2014). This trench is expressed by the following equations:

$$y = -\bar{c}_1 \xi^2 \cdot e^{-\bar{c}_2 \xi} \quad , \quad \bar{c}_1 = \frac{y_{max}}{\xi_{z-max}^2 \cdot e^2} \quad , \quad \bar{c}_2 = \frac{2}{\xi_{z-max}} \quad (30)$$

$$z_{max} = \frac{4\bar{c}_1}{\bar{c}_2^2} \cdot e^{-2} \quad , \quad \xi_{z-max} = \frac{2}{\bar{c}_2} \quad (31)$$

where y and ξ are the horizontal and vertical coordinates. y_{max} is the trench depth and ξ_{z-max} is the distance from a bottom point to the trench mouth (see Figure 3-5).

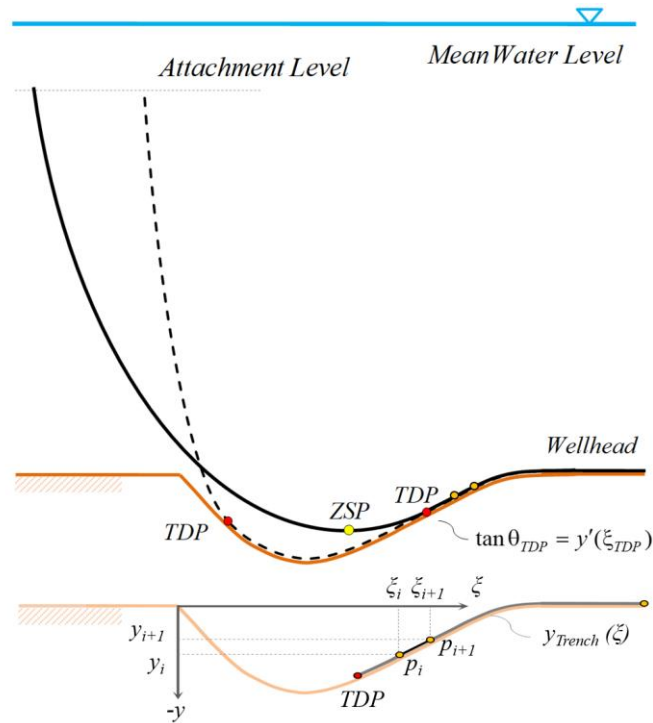


Figure 3-4. SCR schematic configuration in the trenched seabed

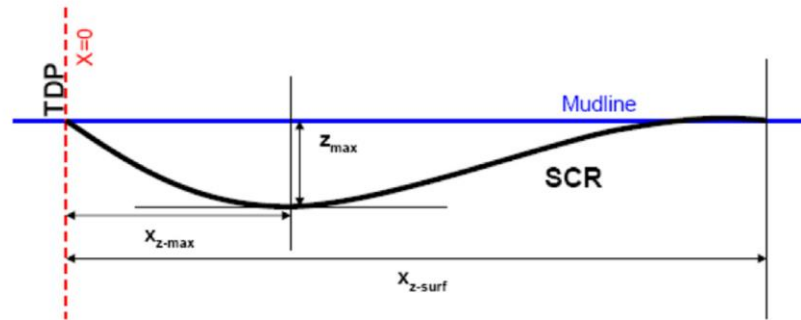


Figure 3-5. Quadratic exponential trench (Shiri 2014)

To construct the equation (14) for this case, the total length of the SCR, including the catenary part and the resting part on the trench, has to be calculated. To calculate the resting length on the trench, this portion was divided to a set of differential subsections, ω (see Figure 3-4):

$$\omega = \{\xi_{TDP}, \dots, \xi_i, \xi_{i+1}, \dots, \xi_{Wellhead}\} \quad (32)$$

The total length of the SCR resting on the trench can be simply obtained by integration over the domain:

$$\tilde{L}_{Q-Exp} = \int_{\xi_{TDP}}^{\xi_{Wellhead}} \sqrt{1 + y'(\xi)^2} d\xi = \int_{\xi_{TDP}}^{\xi_{Wellhead}} \sqrt{1 + c_1^2 \xi^2 e^{-2c_2 \xi} (c_2 \xi - 2)^2} d\xi \quad (33)$$

Using the catenary equations (22), (23), and (33), the equation (14) was reconstructed and an attempt was made to solve it by using the compatibility equations. However, no explicit solution was found for Δ_{TDP} to enable the analytical assessment of $\tilde{V} \times \Delta_{TDP}$. The complex form of the obtained corresponding shear force and bending moment distribution shows the implicit form of the equations that could not be used for assessing the TDP oscillation on the curved trench:

$$V(x) = 2A^2 \frac{\sinh(Ax)}{\cosh(Ax)^3} \quad (34)$$

$$M(x) = -\frac{AEI}{\cosh(Ax)^2} \quad (35)$$

$$A = \frac{(1 - \cos(\arctan(c_1 x_{TDP} e^{-c_2 x_{TDP}} (c_2 x_{TDP} - 2))))}{z \cos(\arctan(c_1 x_{TDP} e^{-c_2 x_{TDP}} (c_2 x_{TDP} - 2)))} \quad (36)$$

In order to resolve this issue and obtain an explicit expression for Δ_{TDP} , the curved profile of the trench was idealized by three linear sloped zones with positive, negative, and nil gradient (see Figure 3-6). It is important to note that this idealized approach may influence the “magnitude” of TDP oscillation amplitude but has no effect on TDP oscillation “trend”, while it enables proposing a mathematical basis for qualitative prediction of trench effect on fatigue, which has never been done in the past and is the main objective of the current study.

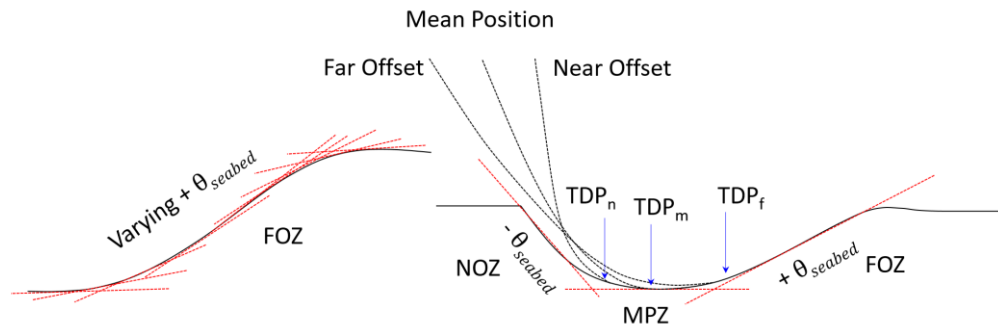


Figure 3-6. Idealization of the curved trench with linear sloped lines

As schematically shown in Figure 3-6, a curved surface is theoretically the union of the numerous straight lines with varying slopes. With no exception, every point on the curve has a tangential line with a positive, negative or zero slope. This results in an identical TDP oscillation trend between the curved and straight lines (but not the same oscillation magnitude). Therefore, the idealization of the curved trench with linear sloped surfaces does no harm to the main objective of this research work, which is a qualitative assessment of the trend of trench effect on fatigue, instead of quantitative calculation of the fatigue damage in the trenched seabed. This was numerically proven by the analysis of SCR oscillation on a curved trench that will be discussed later in this paper. The analytical oscillation of the TDP on idealized sloped trench is discussed in the next section.

3.4.1. Geometrical Idealization of the Curved Trench

As shown in Figure 3-6, in the WF vessel motions about the mean vessel position, the TDP oscillates around an area of the trench with nil gradient (called “mean position zone” (MPZ) from now on). While the trench is developed, the trench bottom point is shifted downward. Therefore, The MPZ area can be simply mimicked by the downward shifting of the flat seabed by a given maximum embedment depth. While the vessel oscillates about the mean position due to WF motions, depending on the type of vessel and the system

configuration, the LF excursions may also largely relocate the vessel (e.g., up to 5% of the water depth (Bridge and Howells 2007)). An LF excursion moving the vessel away from the anchored end (“far offset”) causes the TDP to relocate towards the right side of the trench with a positive slope ($+\theta_{\text{seabed}}$) (called “far offset zone” (FOZ)). This curved area can be simplified by a positive-sloped straight line (see Figure 3-6). Inversely, the “near offset” of the vessel due to the LF vessel excursions shifts the TDP towards the vessel side of the trench with a negative slope ($-\theta_{\text{seabed}}$) (called “near offset zone” (NOZ)). For simplification, this curved area can also be replaced by a negative-sloped strength line (see Figure 3-6).

As shown in Figure 3-7, the TDP may oscillate in one of these three different idealized zones depending on the combined effects of the WF vessel motions and the LF excursions. The TDP oscillation amplitude (Δ_{TDP}) can be analytically expressed for all of these scenarios only by developing the compatibility equations, the Timoshenko solutions for catenary equations (equations (22) and (23)), and the equation (14). Table 3-1 and Table 3-2 show the summary of compatibility equations and resultant Δ_{TDP} with the key parameters shown in Figure 3-7.

A case study was conducted in order to examine the performance of the obtained equations and investigate the variation trends of \tilde{V} , Δ_{TDP} , $\tilde{V} \times \Delta_{\text{TDP}}$, and $\Delta\sigma$.

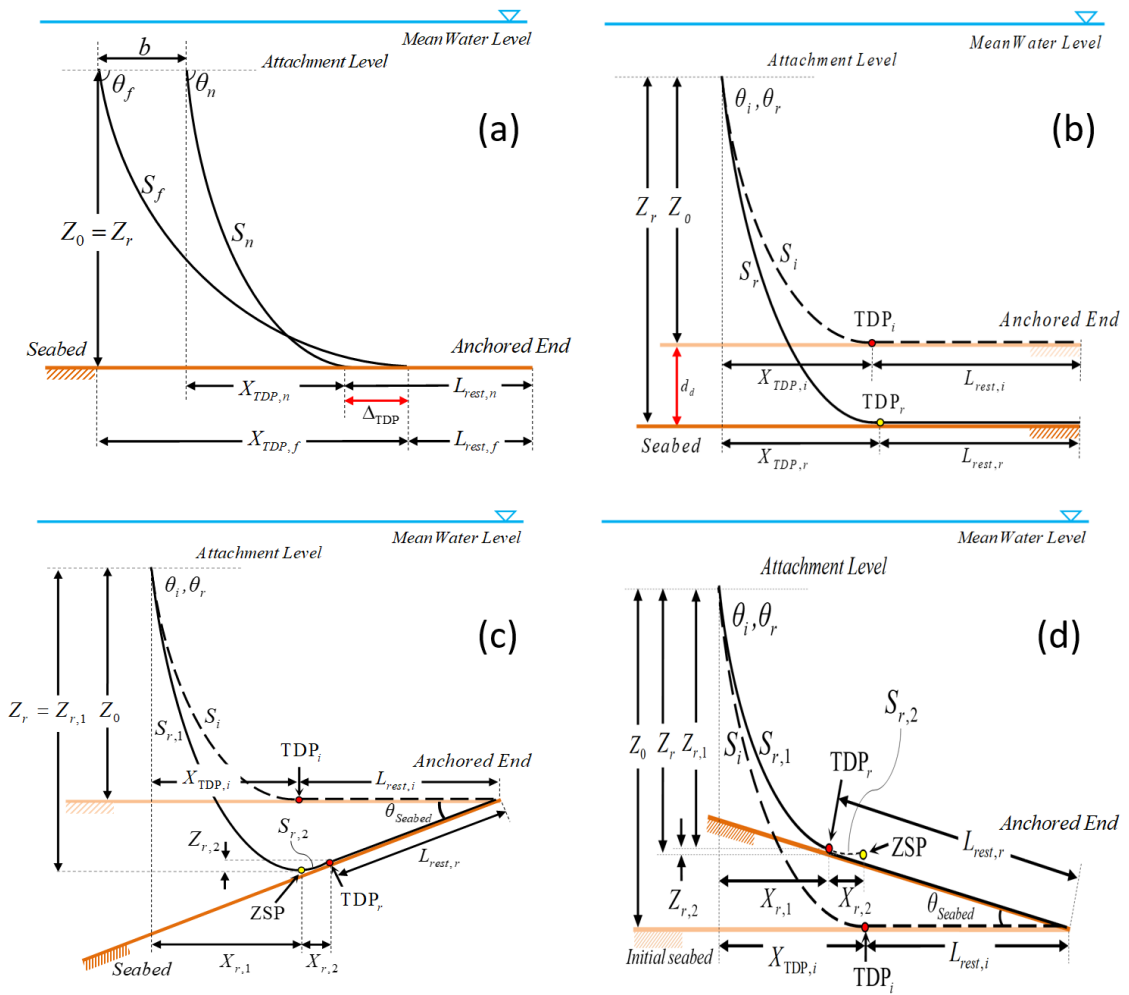


Figure 3-7. Different scenarios of TDP oscillation on sloped ((b), (c), (d)) and flat seabed (a)

Table 3-1. Geometrical compatibility equations for TDP oscillation on different trench zones.

Trench Zone	Geometrical Compatibility Equations	
Flat Figure 3-7 (a)	$S_n + L_{rest,n} = S_f + L_{rest,f}$ $X_{TDP,n} + L_{rest,n} + b = X_{TDP,f} + L_{rest,f}$ $Z_0 = Z_r$	(37)
	$S_f - S_n = X_{TDP,f} - X_{TDP,n} - b$	
MPZ Figure 3-7 (b)	$S_i + L_{rest,i} = S_r + L_{rest,r}$ $X_{TDP,i} + L_{rest,i} = X_{TDP,r} + L_{rest,r}$ $Z_0 + d_d = Z_r$	(38)
	$X_{TDP,r} - (X_{TDP,i} + (S_r - S_i)) = 0$	
FOZ Figure 3-7 (c)	$S_i + L_{rest,i} = S_{r,1} + S_{r,2} + L_{rest,r}$ $X_{TDP,i} + L_{rest,i} = X_{r,1} + X_{r,2} + L_{rest,r} \cos\theta_{seabed}$ $Z_0 + L_{rest,r} \sin\theta_{seabed} + Z_{r,2} = Z_r$	(39)
	$L_{rest,r} = S_i + L_{rest,i} - (S_{r,1} + S_{r,2}) = \frac{X_{TDP,i} + L_{rest,i} - (X_{r,1} + X_{r,2})}{\cos\theta_{seabed}}$ $= \frac{Z_r - (Z_0 + Z_{r,2})}{\sin\theta_{seabed}}$	
NOZ Figure 3-7 (d)	$S_i + L_{rest,i} = S_{r,1} + L_{rest,r}$ $X_{TDP,i} + L_{rest,i} = X_{r,1} + L_{rest,r} \cos\theta_{seabed}$ $Z_0 = Z_{r,1} + L_{rest,r} \sin\theta_{seabed} = (Z_r - Z_{r,2}) + L_{rest,r} \sin\theta_{seabed}$	(40)
	$L_{rest,r} = S_i + L_{rest,i} - S_{r,1} = \frac{X_{TDP,i} + L_{rest,i} - X_{r,1}}{\cos\theta_{seabed}}$ $= \frac{Z_0 - (Z_r - Z_{r,2})}{\sin\theta_{seabed}}$	

Table 3-2. Analytical equations for TDP oscillation amplitude in different trench zones.

Trench Zone	TDP Oscillation amplitude	
Flat Figure 3-7 (a)	$\Delta_{TDP} = Z_0 \left(\frac{\cos\theta_f}{1 - \cos\theta_f} \operatorname{asinh}(\tan\theta_f) - \frac{\cos\theta_n}{1 - \cos\theta_n} \operatorname{asinh}(\tan\theta_n) \right) - b$	
MPZ Figure 3-7 (b)	$\Delta_{TDP} = Z_0(1 + \delta) \left(\frac{\cos\theta_f}{1 - \cos\theta_f} \tan\theta_f - \frac{\cos\theta_n}{1 - \cos\theta_n} \tan\theta_n \right),$ $\delta = \frac{d_d}{z_i}$	
FOZ Figure 3-7 (c)	$\Delta_{TDP} = (S_i + L_{rest,i} - S_{r,1} - S_{r,2})_n - (S_i + L_{rest,i} - S_{r,1} - S_{r,2})_f$ $= \left(\frac{X_{TDP,i} + L_{rest,i} - X_{r,1} - X_{r,2}}{\cos\theta_{seabed}} \right)_n - \left(\frac{X_{TDP,i} + L_{rest,i} - X_{r,1} - X_{r,2}}{\cos\theta_{seabed}} \right)_f$ $= \left(\frac{Z_r - Z_0 - Z_{r,2}}{\sin\theta_{seabed}} \right)_n - \left(\frac{Z_r - Z_0 - Z_{r,2}}{\sin\theta_{seabed}} \right)_f$	
NOZ Figure 3-7 (d)	$\Delta_{TDP} = (S_i + L_{rest,i} - S_{r,1})_n - (S_i + L_{rest,i} - S_{r,1})_f$ $= \left(\frac{X_{TDP,i} + L_{rest,i} - X_{r,1}}{\cos\theta_{seabed}} \right)_n - \left(\frac{X_{TDP,i} + L_{rest,i} - X_{r,1}}{\cos\theta_{seabed}} \right)_f$ $= \left(\frac{Z_0 - (Z_r - Z_{r,2})}{\sin\theta_{seabed}} \right)_n - \left(\frac{Z_0 - (Z_r - Z_{r,2})}{\sin\theta_{seabed}} \right)_f$	

3.4.2. Analytical Case Study

An analytical case study was conducted by incorporating the extracted equations given in Table 3-1 and Table 3-2 into a Matlab code. A generic SCR configuration (from the Gulf of Mexico (Shiri 2014)) with the key parameters given in Table 3-3 was considered. The variation trends of \tilde{V} , Δ_{TDP} , $\tilde{V} \times \Delta_{TDP}$, and $\Delta\sigma$ were obtained using the catenary equations (Leibniz 1961), BLM solutions (Pesce et al. 2006), and the equations provided in Table 3-2 with the TDP oscillating in FOZ, MPZ, and NOZ of the three different idealized trenches (see Figure 3-8).

To configure the trenches 1, 2 and 3 the NOZ slopes of -1° , -2.5° , and -5° , the FOZ slopes of $+0.5^\circ$, $+1.5^\circ$, and the MPZ depths of 1.5D, 5.0D, and 10.0D were combined. These configurations are within the average range of subsea observations (Bridge and Howells 2007). As shown in Figure 3-8, LF excursions were applied to the vessel in 10m intervals of horizontal displacements from points $P_{1,2}$ to $P_{7,8}$. A single cycle of WF oscillation was applied by a surge amplitude of 5m at each mean position. Points P_1 to P_8 denote the far and near offsets of the vessel in the mean positions from $P_{1,2}$ to $P_{7,8}$. In other words, first, the vessel's mean position was set to $P_{1,2}$, and a surge amplitude of 5m was applied to oscillate the vessel between P_1 and P_2 (far and near offsets).

Table 3-3. SCR parameters for the analytical case study.

Parameter	Value
Outer diameter (D)	0.324 m
In service submerge weight (q)	100 kg/m
Riser length (L_{total})	2333 m
Water depth	1800 m
SCR top height from seabed (Z_0)	1600 m
Bending stiffness (EI)	4.67×10^7 N.m ²
Fatigue S-N Curve	DNV E Class, SCF = 1.15, m = 3, a = $1.05 \times 10^{+12}$

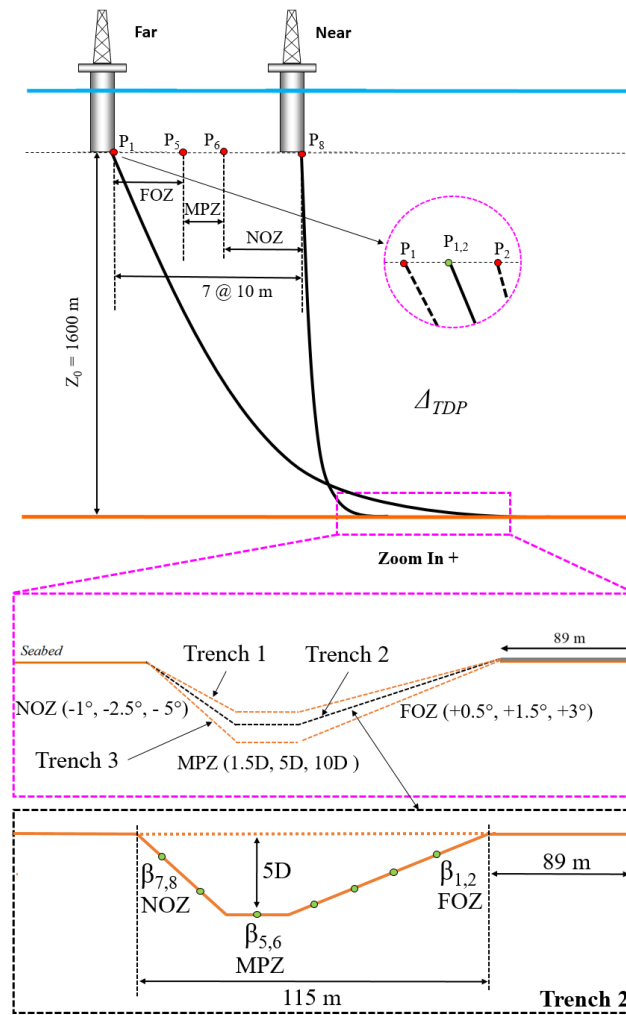


Figure 3-8. SCR Configuration for analytical investigations

Then, the vessel was relocated to the second mean position at $P_{2,3}$ and oscillated again with one surge cycle between P_2 and P_3 . This process was continued until the last oscillation at $P_{7,8}$.

The TDPs corresponding to different mean vessel positions is shown by β in Figure 3-8. The mean TDP positions $\beta_{1,2}$ to $\beta_{4,5}$ correspond to TDP oscillation on FOZ. For the NOZ and MPZ, the mean TDP positions are $\beta_{6,7}$ to $\beta_{7,8}$, and $\beta_{5,6}$, respectively. The magnitudes of average shear force (\tilde{V}), the TDP oscillation amplitude (Δ_{TDP}), and $\tilde{V} \times \Delta_{TDP}$ were obtained and compared with von Mises stress variation, $\Delta\sigma$, in Table 3-4. Figure 3-9 illustrates the main variation trends of these key

parameters. It also shows important trends in terms of the trench effect on fatigue in FOZ and NOZ. The average shear force, \tilde{V} , is decreased when increasing the absolute value of the trench slope on both sides. The deeper the trench, the less cyclic shear force oscillation amplitude was seen (see Figure 3-9 (a)). The Δ_{TDP} showed an inverse variation trend in FOZ and NOZ. In the positive sloped side of the trench (FOZ), deeper trenches resulted in less TDP oscillation amplitude. Inversely, the Δ_{TDP} was increased for deeper trenches or steeper negative slopes (see Figure 3-9 (b)). The geometrical mechanism of TDP oscillation on different slopes is illustrated in Figure 3-10. By increasing the slope of FOZ (positive slope), the TDP (point “A”) on the sloped seabed moves towards the anchored end. An inverse trend happens on the negative side (NOZ). The distance between the points A and B are theoretically decayed at an angle of $\theta = 90^\circ$. As shown in Figure 3-9 (c), the direct product of the \tilde{V} and Δ_{TDP} (i.e., $\tilde{V} \times \Delta_{TDP}$) was decreased in FOZ and increased in NOZ both for deeper trenches. This shows that Δ_{TDP} (or the trench geometry) is overriding the \tilde{V} (or the seabed stiffness in another word). Most importantly, the overall variation trend of the von Mises stress range, $\Delta\sigma$ (or fatigue damage), is similar to $\tilde{V} \times \Delta_{TDP}$, both decreasing in FOZ and increasing in NOZ for deeper trenches (see Figure 3-9 (d)).

Table 3-4. Analytically obtained key parameters in different idealized trenches.

Trench Zone	Vessel Mean Position	\tilde{V} (kN)				Δ_{TDP} (m)				$\tilde{V} \times \Delta_{TDP}$ (kNm)				$\Delta\sigma$ (MPa)			
		Flat seabed	Trench 1 (-1.0°, 1.5D, +0.5°)	Trench 2 (-2.5°, 5.0D, +1.5°)	Trench 3 (-5.0°, 10D, +3.0°)	Flat seabed	Trench 1 (-1.0°, 1.5D, +0.5°)	Trench 2 (-2.5°, 5.0D, +1.5°)	Trench 3 (-5.0°, 10D, +3.0°)	Flat seabed	Trench 1 (-1.0°, 1.5D, +0.5°)	Trench 2 (-2.5°, 5.0D, +1.5°)	Trench 3 (-5.0°, 10D, +3.0°)	Flat seabed	Trench 1 (-1.0°, 1.5D, +0.5°)	Trench 2 (-2.5°, 5.0D, +1.5°)	Trench 3 (-5.0°, 10D, +3.0°)
FOZ	P _{1,2}	8.76	8.75	8.72	8.63	14.20	14.14	14.01	13.85	124.39	123.76	122.25	119.48	3.44	3.40	3.33	3.24
	P _{2,3}	8.96	8.96	8.93	8.85	13.82	13.76	13.64	13.48	123.83	123.22	121.81	119.30	3.62	3.58	3.51	3.41
	P _{3,4}	9.16	9.15	9.13	9.05	13.51	13.45	13.33	13.17	123.75	123.12	121.70	119.19	3.90	3.86	3.78	3.67
	P _{4,5+}	9.36	9.36	9.34	9.28	13.14	13.08	12.97	12.81	122.92	122.37	121.12	118.89	4.10	4.06	3.97	3.86
MPZ	P _{-5,6+}	9.56	9.56	9.55	9.53	13.04	13.06	13.10	13.15	124.66	124.83	125.11	125.32	4.42	4.45	4.48	4.50
NOZ	P _{-6,7}	9.74	9.71	9.67	9.57	12.28	12.45	12.71	13.13	119.61	121.12	122.85	125.65	0.90	1.10	1.30	1.7
	P _{7,8}	9.95	9.92	9.87	9.77	12.18	12.36	12.60	13.04	121.19	122.61	124.36	127.40	1.30	1.40	1.60	2.00

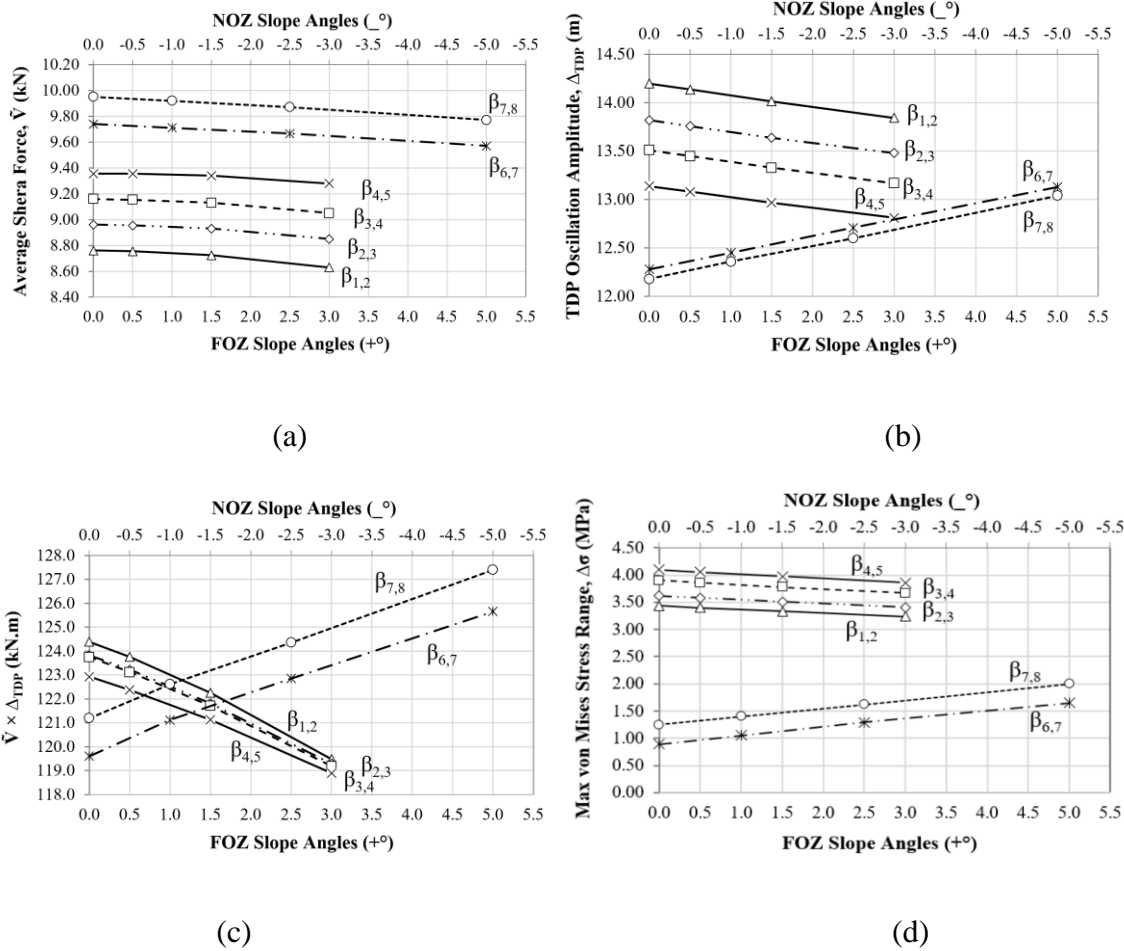


Figure 3-9. Variation trends of key parameters in FOZ and NOZ

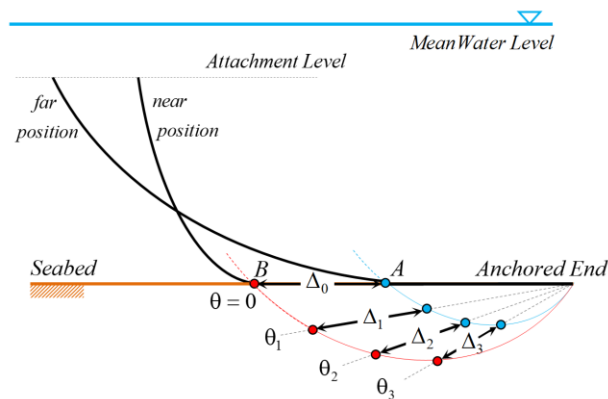


Figure 3-10. Schematic TDP trajectory toward the anchored end by increasing seabed slope

As shown in Figure 3-11, in MPZ (Horizontal trench bottom, nil sloped) the variation trend of these key parameters are similar to observations in NOZ, but less severe. Table 3-5 summarizes these important observations that could be potentially used to explain many of the aforementioned contradictory results published in the literature. In the next section, a set of geometrical rules will be proposed for the qualitative assessment of the trench effect on fatigue.

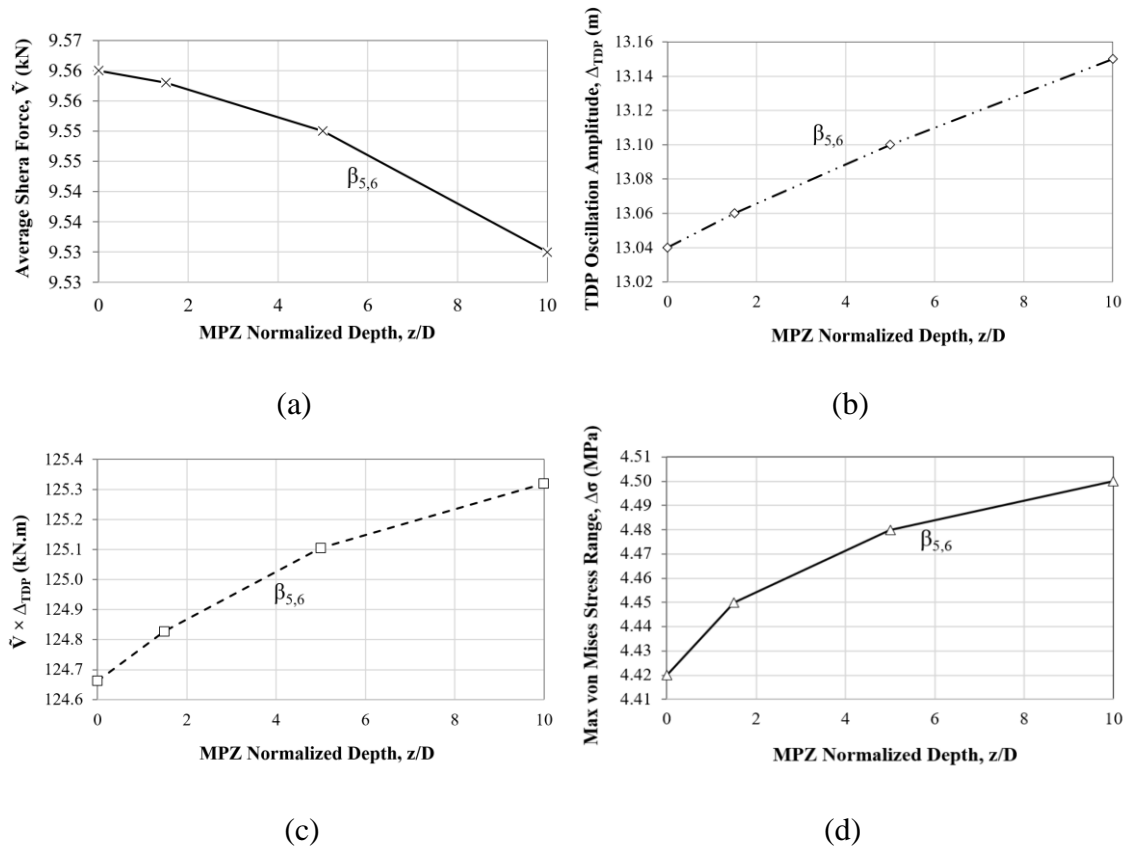


Figure 3-11. Variation trends of key parameters in MPZ

Table 3-5. Variation trends of key parameters relative to the non-trenched virgin seabed.

parameter	FOZ	MPZ	NOZ
\tilde{V}	Decrease	Decrease	Decrease
Δ_{TDP}	Decrease	Increase	Increase
$\tilde{V} \times \Delta_{TDP}$	Decrease	Slightly increase	Increase
$\Delta\sigma$	Decrease	Slightly increase	Increase

3.4.3. Qualitative Fatigue Assessment Rules

The observations summarized in Table 3-5 resulted in the following geometrical rules for qualitative assessment of the trench effect on SCR fatigue performance in the TDZ:

- i. If the SCR is cyclically penetrating into the seabed under the WF vessel oscillations, a trench is initiated in the TDZ, where its side slopes are gradually increased both in the FOZ and NOZ. In this case, the fatigue damage is slightly decreased in FOZ and increased in NOZ and MPZ. The same trends happens for WF motions on a developed trench.
- ii. Different results may be obtained if the SCR oscillates on a developed trench under the combined WF and LF motions, depending on the predominant direction of fatigue sea states. For far LF excursions, the TDP oscillates in FOZ resulting in reduced fatigue damage. Inversely, for the near LF excursions, the TDP will oscillate in NOZ resulting in increased fatigue damage.
- iii. The second rule above implies the case dependency. In reality, the pure WF motions never happen. Therefore, depending on the different dominant direction of fatigue sea states in different geographical locations, the TDP may migrate towards different zones of a developed trench under LF motions resulting in scattered conclusions. This means, there is probably no single response for the questions about the beneficial or detrimental influence of trench on fatigue.

These assessment rules were proposed based on simplified analytical models and needed to be further verified through more realistic fatigue analyses and experimental studies. This was accomplished by performing comprehensive fatigue analysis and comparisons with samples of published numerical and experimental studies.

3.5. Numerical Fatigue Analysis

A series of finite element fatigue analyses were conducted in ABAQUS to validate the mathematical and analytical observations presented in Table 3-5 and the proposed assessment rules. Three different patterns of vessel oscillations were investigated including pure WF motions, combined WF + LF motions (predominant “far” direction), and combined WF + LF motions (predominant “near” directions). The same SCR configuration with key parameters given in Table 3-3 was modeled with a total length of 2333 m using beam elements B21 (see Figure 3-12). The anchored end was set as the origin of the coordinates, and 829 nodes were defined along the riser as the axial nodes. From node 1 to node 450, a 1 m distance was set between the adjacent nodes to define the zone allocated by an in-house user-defined seabed interaction subroutine, UEL (Shiri and Randolph 2010).

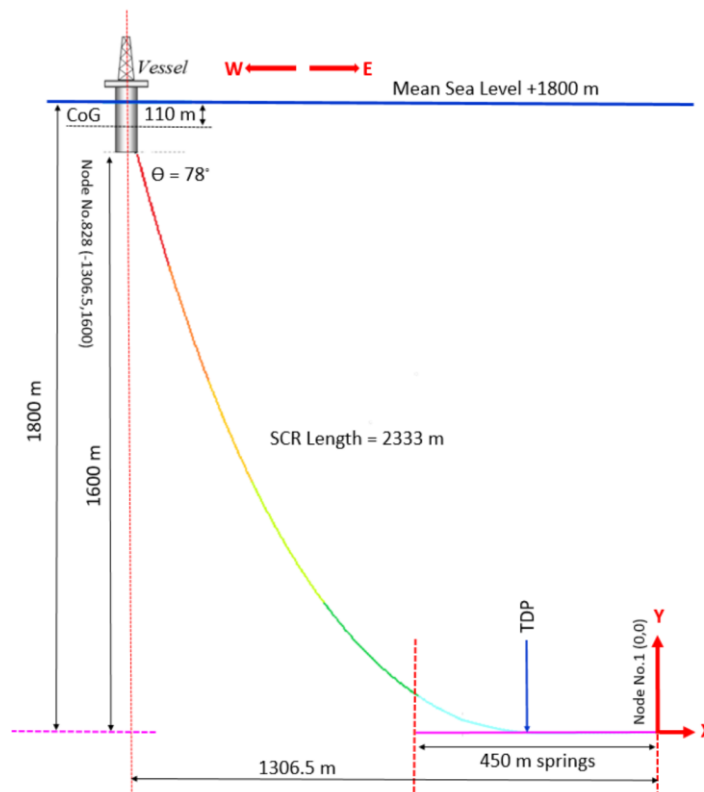


Figure 3-12. SCR configuration in numerical simulation

A linear elastic seabed stiffness of 300 kPa represented the real range of seabed sediments in the Gulf of Mexico (Randolph et al. 2013). For the hanging section of the SCR, a 5 m distance between nodes was established (except with the last element, 3 m in length). Simple hinge boundary conditions were defined both in the vessel attachment point and the anchored end. Planar displacement-controlled analyses were conducted in three steps. First, the submerged weight applied on the horizontal SCR, partly laid on the seabed springs and supported at both ends. In the second step, the vessel end was lifted by the height of the riser attachment point (1600 m) and transferred to the mean vessel position (about 856 m away from TDP). In the third step, the vessel was excited by the predefined oscillation patterns defined in an in-house user subroutine, DISP (Shiri and Randolph 2010). Table 3-6 shows the wave scatter diagram from the Gulf of Mexico used in fatigue analysis (Shiri 2014).

The response amplitude operator (RAO) of the spar vessel for the fatigue analysis is shown in Figure 3-13 (Bridge and Howells 2007). The AQUA module of ABAQUS was used to model the riser dynamics, including drag force, inertia and added mass. The hydrodynamic coefficients of the drag, inertia, and added mass were taken as 0.7, 1.5, and 1.0, respectively, based on recommendations provided by DNV-RP-H103. Further details of the UEL and DISP subroutines and construction of the SCR model can be found in earlier published studies (Shiri 2014ab, Shiri 2014, Shiri and Randolph 2010, Dong X and Shiri 2018).

Three different trench geometries were incorporated into the seabed in the TDZ using the in-house riser-seabed interaction interface (UEL). These trenches include linear and quadratic exponential trenches (Shiri 2014) and a polynomial trench (Langner 2003) that have different slopes in FOZ and NOZ. Figure 3-14 compares the seabed profiles defined by the selected trenches.

The pure WF vessel oscillations with TDP in MPZ, and combined WF+LF vessel motions towards the far and near directions with TDP oscillation in FOZ and NOZ, were investigated and compared with the flat seabed. The bottom point of the trenches were coincided and particular attention was taken to prevent the creation of contact pressure hotspots in NOZs and distortion of results (Shiri 2014, Langner 2003). An in-house post-processing macro was used to extract the cross-sectional stress oscillation and calculate the fatigue damage distributed throughout the TDZ.

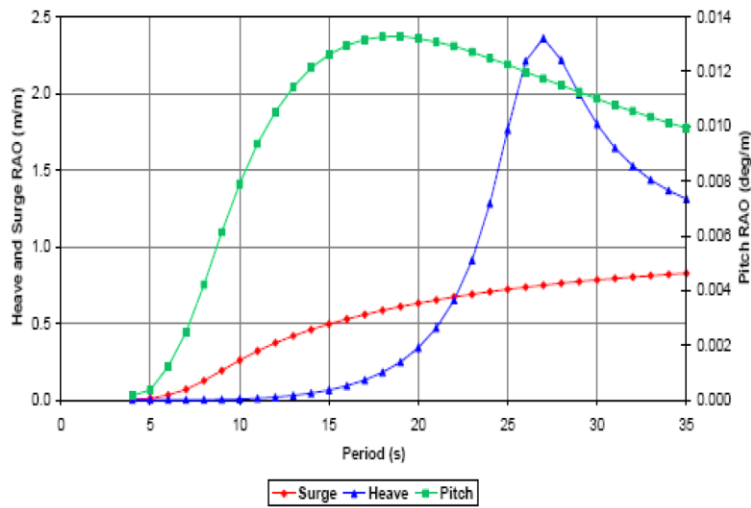


Figure 3-13. Generic Spar RAO, Head sea, Gulf of Mexico (Bridge and Howells 2007)

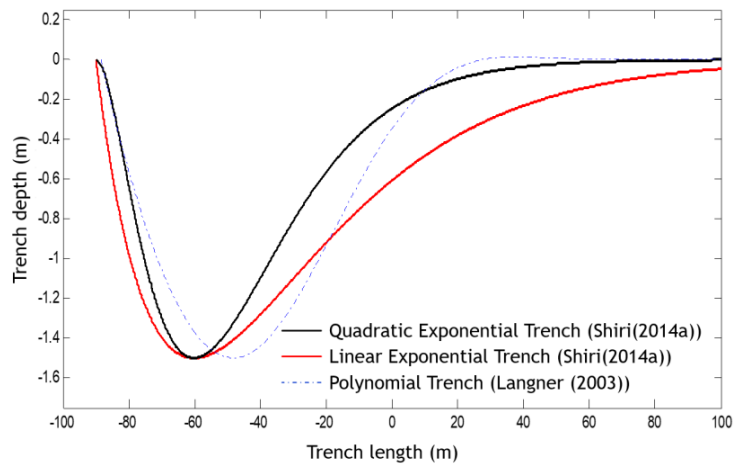


Figure 3-14. Comparison of different trench types for numerical analysis

Table 3-6. Manipulated wave scatter diagram for a 30-year operational life (Gulf of Mexico).

Sea State ID	H _s (m)	T _z (s)	n applied	Sea State ID	H _s (m)	T _z (s)	n applied
1	0.5	4.2	18011291	16	8	9.1	3389
2	1	4.6	71370445	17	8.5	9.3	3011
3	1.5	5	48449608	18	9	9.5	1822
4	2	5.4	25187856	19	9.5	9.7	1395
5	2.5	5.8	13529335	20	10	9.9	1070
6	3	6.1	7473660	21	10.5	10.1	1246
7	3.5	6.5	3080495	22	11	10.2	566
8	4	6.9	1631014	23	11.5	10.4	928
9	4.5	7.3	583770	24	12	10.6	544
10	5	7.7	363725	25	12.5	10.7	813
11	5.5	8	114700	26	13	10.9	712
12	6	8.4	33676	27	13.5	11	877
13	6.5	8.5	16907	28	14	11.2	262
14	7	8.7	10864	29	14.5	11.3	343
15	7.5	8.9	5421	30	15	11.5	420

The results of the conducted fatigue analyses are shown in Figure 3-15. The average slopes in various zones of the different trenches shown in Figure 3-14 could be expressed as follow:

$$\begin{cases} FOZ & \rightarrow \Theta_{Polynomial} > \Theta_{Quadratic\ exponential} > \Theta_{Linear\ exponential} \\ NOZ & \rightarrow \Theta_{Quadratic\ exponential} > \Theta_{Linear\ exponential} > \Theta_{Polynomial} \end{cases} \quad (45)$$

Using Table 3-5 and the resultant assessment rules proposed in the last section, the peak fatigue damage, fd_{max} , due to the trenching effects are expected to be as follows:

$$\begin{cases} WF + LF_{far} & \rightarrow fd_{max,Polynomial} < fd_{max,Quadratic\ exponential} < fd_{max,Linear\ exponential} \\ WF + LF_{near} & \rightarrow fd_{max,Quadratic\ exponential} > fd_{max,Linear\ exponential} > fd_{max,Polynomial} \end{cases} \quad (46)$$

The numerical fatigue analysis results presented in Figure 3-15 (a) and (b) are in perfect agreement with the equation (46), where the peak fatigue damage is less for the steeper trench slope in the FOZ, and higher for the steeper trench slope in the NOZ. As shown in Figure 3-

15 (c) and (d), for the pure WF oscillations corresponding to MPZ, the peak fatigue damage is slightly lower for the steeper trench slope towards the FOZ, and slightly higher for the steeper trench slope towards the NOZ. It was also observed that compared with the flat seabed, the peak fatigue damage is decreased for $WF + LF_{far}$ and increased for $WF + LF_{near}$. The increasing of the peak fatigue damage in MPZ for pure WF oscillations is quite limited (see Figure 3-15 (d)). Also, the location of peak fatigue damage is moved towards the FOZ in $WF + LF_{far}$ oscillations, towards the NOZ in $WF + LF_{near}$ oscillations, and slightly towards the NOZ in pure WF oscillations. These trends validated the mathematical and analytical findings presented in Table 3-5 and also the qualitative assessment rules proposed in the last section.

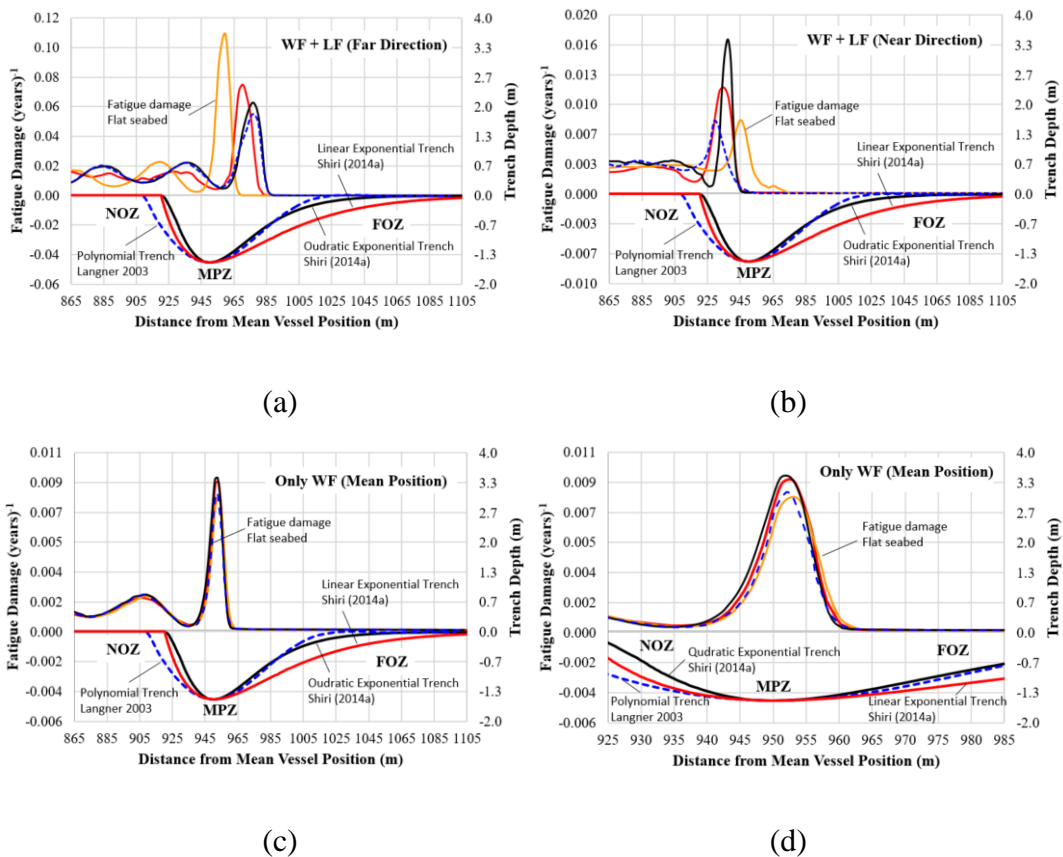


Figure 3-15. Fatigue damage distribution over various trenches

The proposed assessment rules were also used to evaluate two samples of the published numerical (Zargar 2017) and experimental (Hodder 2009) studies (see Figure 3-16). Both studies captured the cyclic penetration of the SCR into the seabed soil. In the numerical study conducted by Zargar (2017), a non-linear hysteretic seabed interaction model (Randolph and Quiggin 2009) has been used to simulate the gradual seabed soil stiffness degradation and consequently the cyclic penetration of SCR into the seabed. In the experimental study, a series of large-scale 3D flume tests in silica sand were conducted by Hodder and Byrne (2009) at Oxford University to investigate the cyclic embedment of the oscillating SCR into the seabed (Hodder 2009). Figure 3-16 shows the cyclic variation of the von Mises stress range throughout the TDZ for numerical study (Figure 3-16 (b) and (c)) and variation of the bending moment for two sample points from FOZ (BM4) and NOZ (BM1) in experimental study (Figure 3-16 (e) and (f)), both of which are representing the fatigue damage variation. All of the annotations in red colour were added in this study. As highlighted by annotations in Figure 3-16, in both of the studies, the fatigue damage is cyclically increased in NOZ and decreased in FOZ by the gradual increase of the slope of NOZ and FOZ, which is in perfect agreement with the findings of the current study in Table 3-5 and the resultant proposed assessment rules. The assessment methodology proposed in this study was used for a comprehensive review and re-assessment of all of the published studies in this challenging area of research, which is currently under publication as a second paper. It is worth noting that the current study targeted a qualitative assessment of the fatigue variation trend due to the creation of a trench underneath the SCR. The results showed that the peak fatigue damage may increase or decrease in different areas of TDZ depending on the predominant environmental loads relative to the riser configuration.

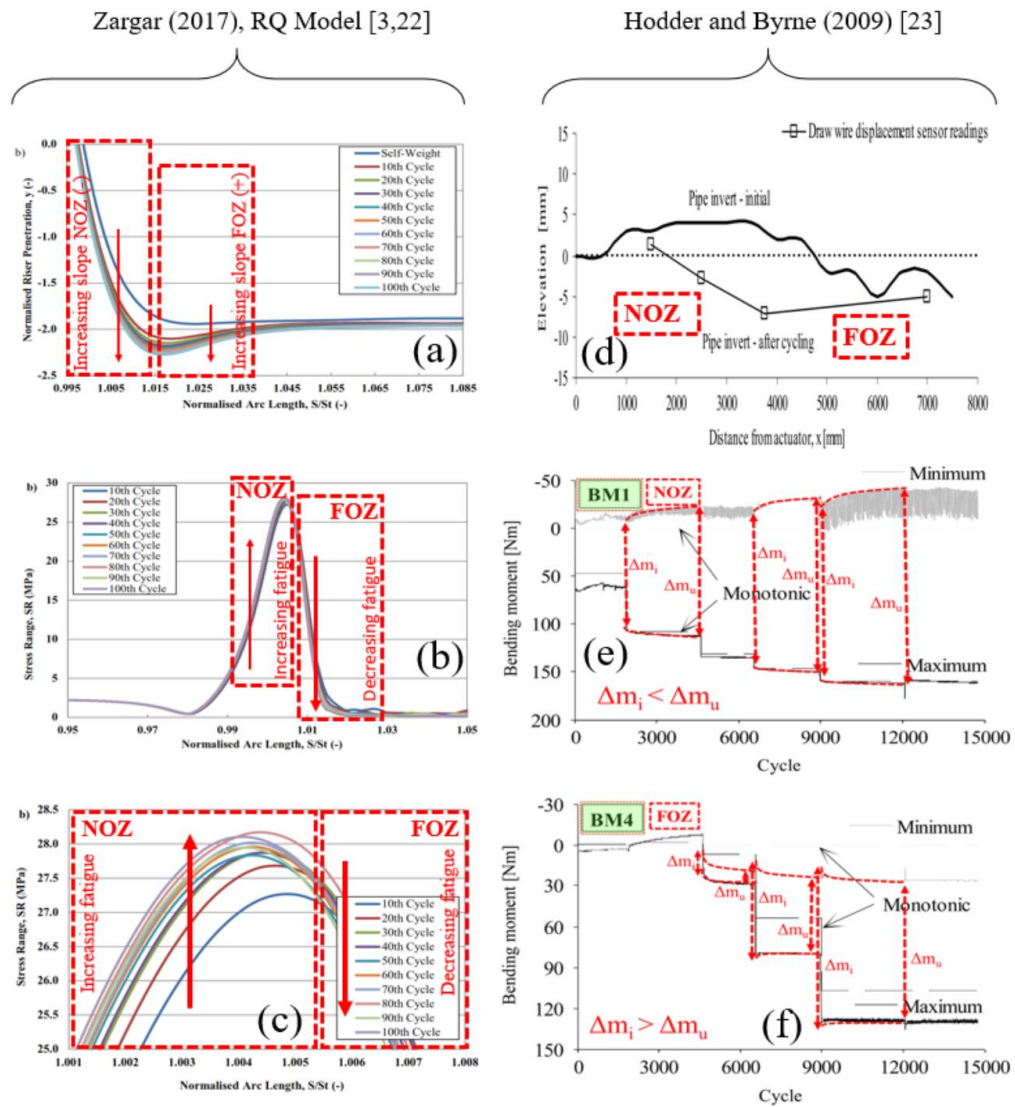


Figure 3-16. Assessment of sample published numerical and experimental studies (Zargar 2017, Hodder 2009)

The magnitude of this variation seems not to be significant, but it causes large shifting of peak fatigue damage location. This demonstrates the need for accurate and quantitative assessment of every individual project in a given geographical location with its specific environmental loads and seabed conditions. However, the ideal point might be the integrated modelling of all of the mechanisms contributing to the realistic riser-seabed

interaction, which still requires an extensive amount of advanced numerical and experimental research.

3.6. Conclusions

The significance of trench geometry was analytically investigated in fatigue response of SCR in the TDZ. A series of analyses were conducted on different trench profiles applying WF and LF vessel oscillations. A similar variation trend was observed between the von Mises stress range ($\Delta\sigma$) (or fatigue damage) and the direct product of the TDP oscillation amplitude (Δ_{TDP}) and average shear force distribution (\tilde{V}) with the dominance of Δ_{TDP} (or trench geometry in another view). The magnitude of this product ($\tilde{V} \times \Delta_{TDP}$) is neither equal to nor an approximation of the von Mises stress range or fatigue, but has a similar overall variation trend with dominance of the Δ_{TDP} . These observations facilitated developing a set of rules to qualitatively assess the overall trend of trench effect on variation of peak fatigue damage. The observations and proposed assessment rules were validated against comprehensive fatigue analyses using finite element simulations in ABAQUS and also samples of published experimental and numerical studies. The main findings and observations of the study can be summarized as follows:

- Disregarding the pure WF or combined WF + LF vessel oscillations, the peak fatigue damage is decreased in FOZ (far offset zone towards the vessel) and increased in NOZ (near offset zone towards the anchored end), when increasing the absolute value of the trench slope in these zones.
- The fatigue damage variation due to trench effect is case dependant. Depending on the direction of the predominant fatigue sea states and the LF vessel excursions in a given

geographical location, the peak fatigue damage might be increased towards the NOZ or decreased towards the FOZ. This may explain the contradictions in the studies published to date. It also implies that the fatigue results obtained from studies with purely WF oscillations cannot be generalized to the real SCR response.

- The fatigue damage variation due to trench effect is more significant in terms of peak point variation and less severe in terms of the magnitude of damage. The LF excursion cause the TDP and consequently the peak fatigue damage to largely relocate towards the NOZ or FOZ depending on the dominant direction.

The complex relationship between the $\Delta\sigma$ and $\tilde{V} \times \Delta_{TDP}$ needs further investigation to provide a solution for the quantitative assessment of the effect of trench geometry on peak fatigue damage variation. Developing new research programs with an extensive assessment of the real trench shapes accompanied by supporting field data such as vessel oscillations, SCR stress/strain oscillations, and seabed stiffness degradation histories can be beneficial for obtaining robust and reliable solutions for accurate evaluation of SCR fatigue on a real seabed.

3.7. Acknowledgments

The authors gratefully acknowledge the financial support of this research by the Research and Development Corporation (RDC) (now Innovate NL) through the Ignite funding program and the Memorial University of Newfoundland through VP start-up funding support.

References

- Aubeny CP, Gaudin C, Randolph MF. Cyclic tests of model pipe in kaolin. Proceedings of the Offshore Technology Conference OTC 2008-19494-MS; 2008 May 5-8; Texas, USA. <https://doi.org/10.4043/19494-MS>.
- Aubeny CP, Biscontin G. Seafloor interaction with steel catenary risers. Offshore Technology Research Center. Texas A&M University, College Station, Houston, Final Project Report to Minerals Management Service 2006, OTRC Library Number 9/06A173.
- Bridge CD, Howells HA. Observation and modeling of steel catenary riser trenches. Proceedings of the 17th International Society of Offshore and Polar Engineers Conference ISOPE-I-07-321; 2007 July 1-6; Lisbon, Portugal. pp 803-813.
- CARISIMA - Catenary Riser Soil Interaction Model for global riser Analysis - JIP Proposal T99-70.003 March 1999, Marintek. Trondheim, Norway.
- Campbell M. The complexities of fatigue analysis for deepwater risers. Proceedings of the Deepwater Pipeline Technology Conference; 1999 March; New Orleans, USA.
- Clukey EC, Aubeny CP, Zakeri A, Randolph MF, Sharma PP, White DJ, Sanico R, Cerkovnic M. A perspective on the state of knowledge regarding soil-pile interaction for SCR fatigue assessments. Proceedings of the Offshore Technology Conference OTC 27564-MS; 2017 May 1-4; Texas, USA
- Clukey, E., Jacobs, P., Sharma, P.P. (2008) "Investigation of riser seafloor interaction using explicit finite element methods", Offshore Technology Conference, Houston, Texas, OTC19432-MS.
- Clukey EC, Ghosh R, Mokalala P, Dixon M. Steel catenary riser (SCR) design issues at touchdown area. Proceedings of The 17th International Offshore and Polar Engineering Conference ISOPE-I-07-388; 2007 July 1-6; Lisbon, Portugal. <https://doi.org/10.4043/22557-MS>.
- Dong X, Shiri H. Performance of non-linear seabed interaction models for steel catenary riser, Part 1: nodal response. Ocean Engineering. 2018; (154) 153-166
- Draper S, Cheng L, White DJ. Scour and sedimentation of submarine pipelines: Closing the gap between laboratory experiments and field conditions. Journal Scour and Erosion: Proceedings of the 8th International Conference on Scour and Erosion. 2016 August. DOI: 10.1201/9781315375045-4.
- Elliott BJ, Zakeri A, Barrett J, Hawlader B, Li G, Clukey EC. Centrifuge modeling of steel catenary risers at touchdown zone Part II: assessment of centrifuge test results using

- kaolin clay. *Ocean Engineering*. 2013 March 1; 60, 208-218.
<https://doi.org/10.1016/j.oceaneng.2012.11.013>.
- Fouzder, A., Zakeri, A., and Hawlader, B. (2012) "Steel catenary risers at touchdown zone - A fluid dynamics approach to understanding the water-riser-soil interaction", 9th International Pipeline Conference, Calgary, V4, 31-36.
- Giertsen E, Varley R, Schroder K. CARISIMA: a catenary riser/soil interaction model for global riser analysis. Proceedings of the 23rd International Conference on Offshore Mechanics and Arctic Engineering OMAE 2004-51345; 2004 June 20-25; Vancouver, Canada. doi:10.1115/OMAE2004-51345.
- Hodder, M.S. and Byrne, B.W. (2009) "3D experiments investigating the interaction of a model SCR with the seabed", *Applied Ocean Research*, 32:145-157.
- Langner C. Fatigue life improvement of steel catenary risers due to self-trenching at the touchdown point. Proceedings of the Offshore Technology Conference OTC 15104; 2003 May 5-8; Texas, USA.
- Larsen CM, Halse KH. Comparison of models for vortex-induced vibrations of slender marine structures. *Marine Structures* 1997 July; 10(6):413-441.
[https://doi.org/10.1016/S0951-8339\(97\)00011-7](https://doi.org/10.1016/S0951-8339(97)00011-7).
- Leibniz. Solution to the problem of catenary, or funicular curve, proposed by M. Jacques Bernoulli in the Acta of June 1661. *Acta Eruditorum*. Leipzig, Germany.
- Leira BJ, Passano E, Karunakaran D, Farnes KA, Giertsen E. Analysis guidelines and application of a riser-soil interaction model including trench effects. Proceedings of the 23rd International Conference on Offshore Mechanics and Arctic Engineering OMAE 2004-51527; 2004 June 20-25; Vancouver, Canada. pp. 955-962, doi:10.1115/OMAE2004-5152.
- Nakhaee A, Zhang J. Effects of the interaction with the seafloor on the fatigue life of a SCR. Proceedings of the 18th International Society of Offshore and Polar Engineers Conference ISOPE-I-08-397; 2008 July 6-11; Vancouver, Canada. pp 87-93.
- Pesce CP, Martins C, Silveira LM. Riser-Soil Interaction: Local Dynamics at TDP and a Discussion on the Eigenvalue and the VIV Problems. *Journal of Offshore Mechanical and Arctic Engineering*; 2006; 128(1), 39-55
- Pesce CP, Aranha JAP, Martins CA. The soil rigidity effect in the touchdown boundary layer of a catenary riser: Static problem. Proceedings of the International Society of Offshore and Polar Engineers Conference ISOPE-I-98-130; 1998 May 24-29; Montreal, Canada.

- Randolph MF, Bhat S, Mekha B. Modeling the touchdown zone trench and its impact on SCR fatigue life. Proceedings of the Offshore Technology Conference OTC-23975-MS; 2013 May 6-9; Texas, USA. <https://doi.org/10.4043/23975-MS>.
- Randolph MF, Quiggin P. Non-linear hysteretic seabed model for catenary pipeline contact. Proceedings of the 28th International Conference on Ocean, Offshore and Arctic Engineering OMAE 2009-79259; 2009 May 31- June 5; Hawaii, USA.
- Rezazadeh K, Shiri H, Zhang L, Bai Y. Fatigue generation mechanism in touchdown area of steel catenary risers in non-linear hysteretic seabed. Research Journal of Applied Sciences, Engineering and Technology. 2012; 4(24):5591-5601.
- Sharma PP, Aubeny CP. Advances in pipe-soil interaction methodology and application for SCR fatigue design. Proceedings of the Offshore Technology Conference OTC-21179-MS; 2011 May 2-5; Texas, USA. <https://doi.org/10.4043/21179-MS>.
- Shiri H. Response of steel catenary risers on hysteretic non-linear seabed. Applied Ocean Research, 2014a January; 44:20-28. <https://doi.org/10.1016/j.apor.2013.10.006>.
- Shiri H. Influence of seabed trench formation on fatigue performance of steel catenary risers in touchdown zone. Marine Structures. 2014 April; 36:1-20. <https://doi.org/10.1016/j.marstruc.2013.12.003>.
- Shiri H., Randolph MF. Influence of seabed response on fatigue performance of steel catenary risers in touchdown zone. Proceeding of the 29th International Conference on Ocean, Offshore and Arctic Engineering OMAE 2010-20051; 2010b June 6-11; Shanghai, China. pp. 63-72; doi:10.1115/OMAE2010-20051.
- Timoshenko SP, Young DH. Theory of structures. McGraw-Hill Inc., US; 1968.
- Wang K, Low YM. Study of seabed trench induced by steel catenary riser and seabed interaction. Proceedings of the 35th International Conference on Ocean, Offshore and Arctic Engineering OMAE2016-54236; 2016 June 19-24; Busan: South Korea. doi:10.1115/OMAE2016-54236.
- Zargar, E. A new hysteretic seabed model for riser-soil interaction. PhD Thesis; 2017; University of Western Australia.
- Zargar E, Kimiaei M. An investigation on existing nonlinear seabed models for riser-fluid-soil interaction studies in steel catenary risers. Proceedings of the 3rd International Symposium on Frontiers in Offshore Geotechnics ISFOG; 2015 June; Oslo: Norway. DOI:10.1201/b18442-59.

Chapter 4

Re-assessment of Trench Effect on Fatigue Performance of Steel Catenary Risers in the Touchdown Zone

Rahim Shoghi¹, Hodjat Shiri²

1: Department of Civil Engineering
Memorial University of Newfoundland
e-mail: rshoghi@mun.ca

2: Department of Civil Engineering
Memorial University of Newfoundland
e-mail: hshiri@mun.ca

This chapter is a journal paper which has been published in Applied Ocean Research.

Abstract

Several studies have been published using different trench modeling approaches to investigate the trench effect on fatigue response of steel catenary risers (SCR) in the touchdown zone (TDZ). However, most of the conducted studies have come to contradictory observations and there remains no coherent agreement on the beneficial or detrimental effects of the trench. In this study, a recently developed geometrical model with a set of rules for qualitative assessment of the trench effect on fatigue was used to re-assess the majority of the key published studies. The proposed methodology resulted in a more coherent agreement between the published studies. It was observed that for the near, far, or out of plane direction of the vessel excursions, the ultimate fatigue damage might be slightly increased or decreased depending on the probability of occurrence in different geographical locations. Rather, the trench effect appeared in the form of significant shifting of the peak damage point towards the opposite direction of the low-frequency vessel excursions. The current study revealed several important trends in the trench effect on fatigue and provided an in-depth insight into this challenging problem.

Keywords: Steel catenary risers; Riser-seabed interaction; Touchdown point; Trench profile; Fatigue response

4.1. Introduction

Steel catenary risers (SCRs) are widely used in offshore field development to transfer gas and hydrocarbons from the seabed to the floating facilities. These popular risers are made of thin-wall steel pipes suspended from floating facilities to the seabed in the form of a catenary. The dynamic environmental and operational loads that are continuously applied to SCRs makes them vulnerable to fatigue. The SCR attachment point to the vessel and the touchdown area of the riser at the seabed are two fatigue hot spots that are considered for fatigue assessment in riser design practice. The latter one (touchdown zone (TDZ)) may be the most challenging area for fatigue analysis, whereby it continuously undergoes complex cyclic contact with the seabed around the touchdown point (TDP) (Campbell 19991, Larsen and Halse 1997). As soon as the SCR is installed, its cyclic oscillations around the TDZ result in progressive seabed soil stiffness degradation and consequently the gradual penetration of the riser into the seabed. The initiated cyclic embedment or the new-born young trench is further developed over the early years of its operating life resulting in a mature ultimate trench (see Figure 4-1).

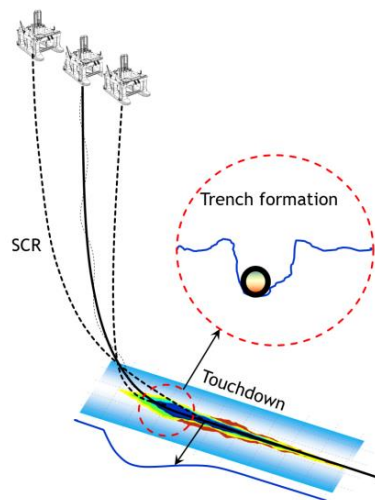


Figure 4-1. Trench formation in the TDZ under riser-seabed-seawater interaction

The measurements conducted by subsea surveys have proven a trench depth of several diameters underneath the SCR in the TDZ (Bridge and Howells 2007). Besides the cyclic soil stiffness degradation, there are several other complicated mechanisms that contribute to the development of the young trench. A sample of these less explored mechanisms includes trench erosion and bed softening due to the riser-soil-seawater interaction governed by sea bottom currents and water velocity fields generated by the water entrapped between the oscillating riser and the trench. This embedment process and the ultimate resultant trench is believed to have a significant influence on the fatigue performance of SCR in the TDZ.

The trench effect on fatigue has been widely investigated in the past fifteen years through a range of methodologies for modeling the trench (e.g., Zargar 2017, Wang and Low 2016, Elliott et al. 2013, Shiri 2014ab, Randolph et al. 2013, Rezazadeh et al. 2012, Sherma and Aubeny 2011, Shiri and Randolph 2010, Nakhaee and Zhang 2008, Clukey et al. 2007, Leira et al. 2004, Giertsen et al. 2004, Langner 2003). These methodologies mainly include an artificial insertion of mathematically expressed trenches (e.g., Wang and Low 2016, Randolph et al. 2013, Sherma and Aubeny 2011, Clukey et al. 2007, Langner 2003) or the automatic development of trenches using advanced non-linear hysteretic riser-seabed interaction models (e.g., Zargar 2017, Shiri 2014, Shiri and Randolph 2010, Nakhaee and Zhang 2008). However, contradictory results have been obtained by various researchers and there remains no coherent agreement about the trench effect on fatigue. Some of the studies have concluded that the trench formation is for the benefit of the fatigue life because of the gradual relaxation of the SCR by penetrating into the seabed (e.g., Wang and Low 2016, Elliott et al. 2013, Randolph et al. 2013, Nakhaee and Zhang 2008, Langner 2003).

Some other studies have observed the detrimental effect of the trench on fatigue performance (e.g., Zargar 2017, Shiri 2014ab, Rezazadeh et al. 2012, Sherma and Aubeny 2011, Shiri and Randolph 2010, Leira et al. 2004, Giertsen et al. 2004). Obtaining a robust answer for this important question is of significant importance for a reliable and cost-effective design of SCRs, but this needs first a robust answer to justify the observed contradictions. Researchers have compared their results with some other agreeing and disagreeing studies, but there is still no comprehensive study in the literature having assessed all of, or at least a majority of, the published works that have investigated the trench effect on fatigue.

In this study, a recently developed framework by Shoghi and Shiri (Shoghi and Shiri 2019) was used to comprehensively assess the published studies in this challenging field (Shoghi and Shiri 2019). The developed framework has been validated by mathematical, analytical, numerical, and experimental studies (Shoghi and Shiri 2019), and has incorporated both the wave-frequency (WF) vessel motions and low-frequency (LF) excursions on fatigue damage accumulation. The authors believe that the “cyclic embedment,” created by pure WF vessel motions, which is usually less than one riser diameter deep, is not necessarily same as a fully developed “trench,” several diameters deep (Bridge and Howells 2007) where several other mechanisms contribute to the trench formation. However, in the absence of sufficient field data and with the current status of knowledge, it can fairly be assumed, at least from a geometrical standpoint, that the overall profile of the ultimate trench is a non-linear scaled-up version of the cyclic embedment.

Some of the published studies do not provide sufficient details about the outputs or the rationale behind the undertaken methodologies. This lack of information makes challenges

in a consistent comparison of the results. A comprehensive review of the existing studies was conducted using the methodology proposed by Shoghi and Shiri (Shoghi and Shiri 2019) and care was taken in the assessment of the studies with a shortage of published information. The study resulted in a more coherent agreement between the published research works. The proposed methodology was found to be a simple but strongly promising approach for further developments towards more quantitative assessments. Recommendations were made on how to incorporate the trench effect on future fatigue studies.

4.2. The analytical Framework Proposed by Shoghi and Shiri (2019)

Shoghi and Shiri (2019) first classified various riser-soil-fluid interaction mechanisms contributing to the trench development to logically show the relevance and importance of TDP oscillation amplitude (Δ_{TDP}) as a key parameter for the assessment of SCR fatigue damage in the TDZ. As shown in Figure 4-2, the authors assumed that in a fully developed trench, the suction force mobilization is not significant (Randolph et al. 2013), therefore the fatigue damage was mainly dependent on trench geometry and seabed stiffness.

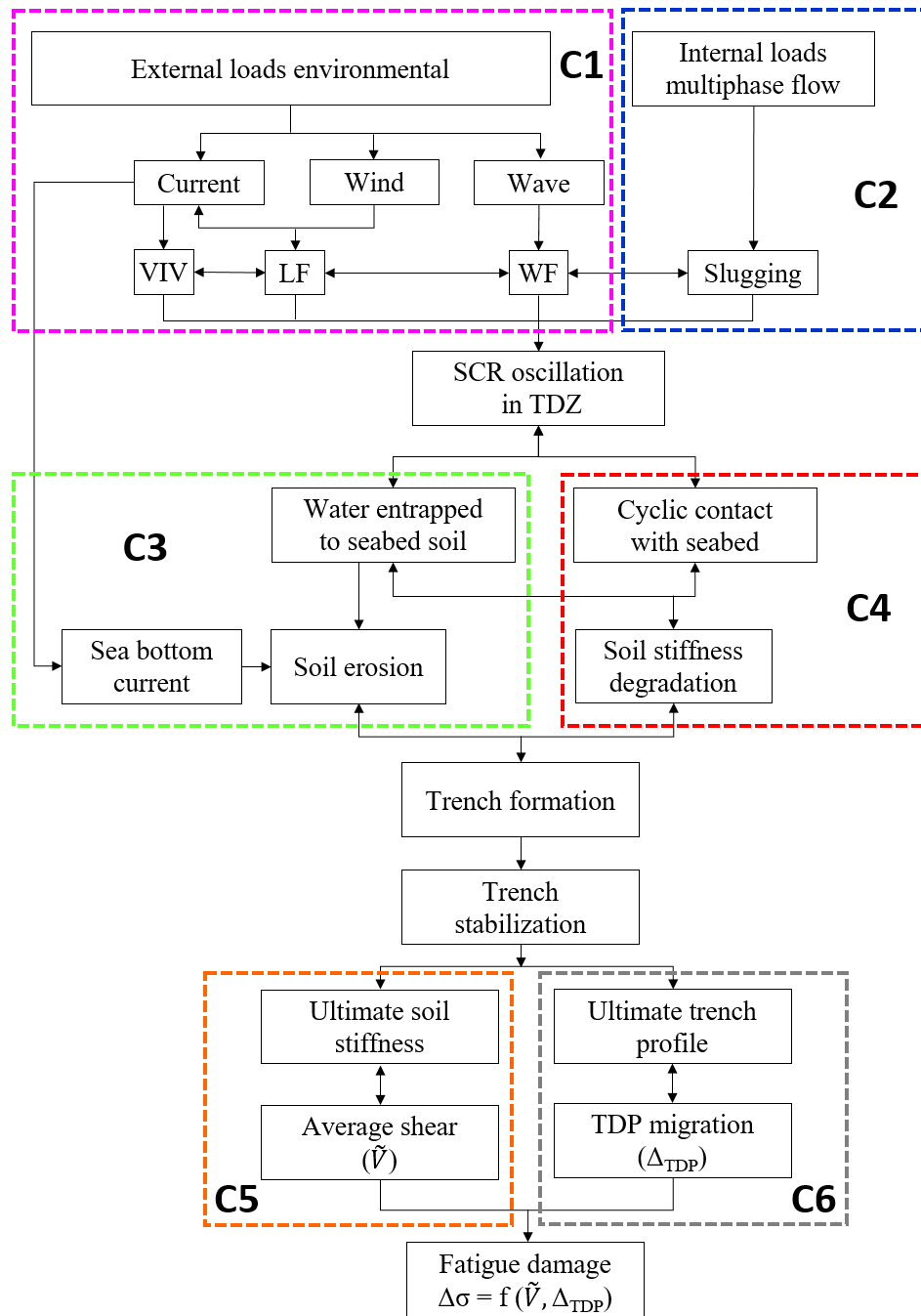


Figure 4-2. Riser-seabed-seawater interaction mechanisms and the relation with TDP migration

This assumption is supported by the field and experimental observations showing that the natural backfill inside the trench is largely washed out under the action of seabed current and the water velocity fields created by the water entrapped between the seabed and

oscillating SCR (Bridge and Howells 2007, Clukey et al. 2007, Fouzder et al. 2012, Draper et al. 2016). Using the boundary layer solution proposed by Pesce et al. (Pesce et al. 2006) for the SCR profile in the TDZ with a soil stiffness, k , Shoghi and Shiri (2019) showed that the non-dimensional soil rigidity parameter, K , introduced by Pesce et al. (2006) can be written as a function of four parameters as follows:

$$K = f(\chi_0, k, \xi, \xi_f) \quad (1)$$

Where χ_0 , ξ and ξ_f are the maximum curvature in the catenary part, the non-dimensional length parameter, and the actual TDP, respectively. The non-dimensional soil rigidity parameter, K , can be written as:

$$K = \frac{k\lambda^4}{EI} = \frac{k\lambda^2}{T_0} = \frac{kEI}{T_0^2} = \chi_0\lambda \frac{k\lambda}{q} \quad (2)$$

where T_0 , q , and λ are riser tension at the TDP, the immersed weight of SCR per unit length, and the boundary layer length, which denotes the difference between the actual and ideal position of the TDP (Pesce et al. 1998, 2006).

The cyclic stress change which is the governing factor in the calculation of fatigue damage was approximated by the authors in terms of bending and tensile stresses:

$$\Delta\sigma_{von Mises} = \frac{1}{A} [T_{0,f} \cosh(xm_s g/T_{0,f}) - T_{0,n} \cosh(xm_s g/T_{0,n})] + EC(\kappa_{x,f} - \kappa_{x,n}) \quad (3)$$

where E , C , A , and I are Young's modulus, distance to the neutral axis, cross section area, and second moment of area, respectively. T_0 , x , and $m_s g$ are tension at TDP, horizontal coordinate, and submerged weight of SCR. Also, κ is the curvature of the riser and the subscripts n and f are corresponding to the near and far offset of the riser.

Using the Leibnitz's catenary equations (Leibniz 1961) and Timoshenko's solution (Timoshenko 1968), Shoghi and Shiri (2019) showed that the cyclic cross-sectional axial stress range could be approximated as follows:

$$\Delta\sigma \approx f(\tilde{V}, \Delta_{\text{TDP}}) \quad (4)$$

where \tilde{V} is the average shear force between far and near offsets, and Δ_{TDP} is the TDP oscillation amplitude. This important equation shows that the ultimate fatigue damage can be expressed in terms of the average shear force (\tilde{V}), and the TDP migration amplitude (Δ_{TDP}). For a given vessel excitation, the \tilde{V} and Δ_{TDP} are governed by the seabed oil stiffness and the trench geometry, respectively. Further mathematical details of the developed framework can be found in (Shoghi and Shiri 2019).

Shoghi and Shiri (2019) defined three different zones of TDP oscillation corresponding to vessel excursions, i.e., the near offset zone (NOZ), the far offset zone (FOZ), and the mean position zone (MPZ) of the trench. Using analytical and numerical modeling of first, the simplified linear sloped trench, and then the realistic ladle-shape trenches, the authors showed that the direct product of these two key parameters ($\tilde{V} \times \Delta_{\text{TDP}}$) has the same variation trend as axial stress range ($\Delta\sigma$) or fatigue damage (see Table 4-1). Shoghi and Shiri (2019) highlighted that the mathematical relationship between the fatigue damage and these two key parameters can be quite complicated. However, the authors took the advantage of a similar trend between them to qualitatively assess the overall trend of trench effect on fatigue life, i.e., the improvement or deterioration, without a quantitative evaluation. The authors emphasized that the product of the average shear force and the TDP migration amplitude ($\tilde{V} \times \Delta_{\text{TDP}}$) is neither equal to nor an approximation to axial

stress range or fatigue. However, it is a sensible parameter that mimics the same variation trends in axial stress range.

Table 4-1 shows that Δ_{TDP} is the winner of the dominance competition between the Δ_{TDP} and \tilde{V} , wherein the cases of opposite trends between them, the trend of their product, $\tilde{V} \times \Delta_{TDP}$ or fatigue damage, follows the Δ_{TDP} . The authors validated the simplified analytical model by three different realistic ladle-shape trenches and observed that for any kind of vessel oscillations including wave-frequency (WF) and/or low-frequency vessel excursions, if the TDP moves towards the far vessel offset zone (FOZ) with a greater positive seabed gradient, the Δ_{TDP} , and consequently the fatigue damage is slightly decreased. Inversely, if the TDP moves towards the near vessel offset zone (NOZ) with a greater negative seabed gradient, the Δ_{TDP} , and consequently the fatigue damage, is slightly increased (see Figure 4-3).

Shoghi and Shiri (2019) concluded that disregarding the pure WF or combined WF + LF vessel oscillations, the peak fatigue damage is decreased in FOZ (far offset zone towards the vessel) and increased in NOZ (near offset zone towards the anchored end), by increasing the absolute value of the trench slope in these zones. The authors emphasized that the fatigue damage variation due to trench effect is case dependent.

Table 4-1. Variation trends of key parameters relative to the non-trenched virgin seabed (Shoghi and Shiri 2019).

parameter	FOZ	MPZ	NOZ
\tilde{V}	Decrease	Decrease	Decrease
Δ_{TDP}	Decrease	Increase	Increase
$\tilde{V} \times \Delta_{TDP}$	Decrease	Slightly increase	Increase
$\Delta\sigma$	Decrease	Slightly increase	Increase

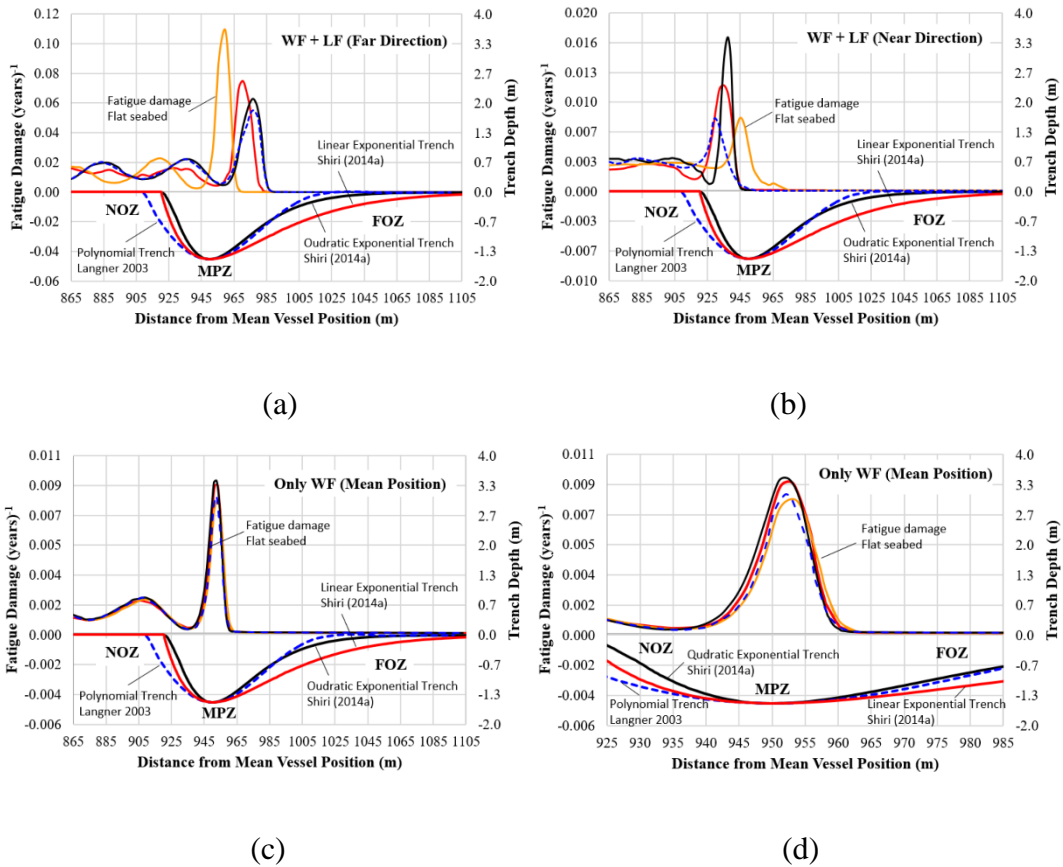


Figure 4-3. Fatigue damage distribution over various trenches (Shoghi and Shiri 2019)

Depending on the direction of the predominant fatigue sea states and the LF vessel excursions in a given geographical location, the peak fatigue damage might be increased towards the NOZ or decreased towards the FOZ.

This may explain some of the contradictions in the studies published to date. It also implies that the fatigue results obtained from studies with purely WF oscillations cannot be generalized to the real SCR response. Also, the fatigue damage variation due to trench effect was found to be more significant in terms of peak point variation and less severe in terms of the magnitude of damage. The LF excursion causes the TDP and consequently, the peak fatigue damage to largely relocate towards the NOZ or FOZ depending on the dominant direction.

4.3. Outlined Rules for Re-assessing the Published Studies

In the current study, to re-assess the trench effect on SCR fatigue in the TDZ, a qualitative assessment framework was proposed with four main rules (R-1 to R-4) based on the observations made by Shoghi and Shiri (2019):

R-1) The methodologies using an artificial insertion of a mathematically expressed trench profile underneath the SCR in the TDZ are highly suspicious to fatigue results distortion. This arises from the incompatibility of the natural SCR catenary profile and the assumed trench profile leading to the creation of contact pressure hot spots, particularly at the trench mouth. This has been reported in some of the previous studies (Shiri 2014b). The results obtained by this approach should be treated cautiously.

R-2) The “cyclic embedment” or “new-born young trench” is not necessarily equal to a fully developed “ultimate trench”. The “cyclic embedment” is usually less than one riser diameter deep. In the case of numerical simulations, this limited penetration happens due to the pre-mature stabilization of non-linear hysteretic models incorporated. Physical limitations in experimental studies may have a similar impact. However, a fully developed “trench” is several diameters deep ($3D \sim 5D$) and is developed by the contribution of many other mechanisms. Therefore, the studies with limited penetration ($<1D$) and missing explicate modeling of deep trenches, will be reviewed under the category of “cyclic embedment”.

R-3) Low-frequency vessel excursions leading to the migration of the TDP to different zones of a trench profile can have a significant impact on fatigue damage distribution. The fatigue results obtained from purely wave frequency (WF) vessel motions cannot

be simply generalized to real conditions. As per the findings of Shoghi and Shiri (2019) (see Table 4-1), it was hypothesized that a) any kind of WF, LF, or combined vessel motion resulting in TDP migration towards the FOZ of the trench slightly improves the fatigue life, b) if these oscillations move the TDP to the NOZ of the trench the fatigue life is slightly decreased, and c) if the TDP oscillates around the MPZ of the trench, the fatigue life does not change or is slightly decreased.

R-4) From a design perspective, the key question is the variation of the peak fatigue damage in the TDZ, not the damage in an individual point, e.g., TDP. The results of this study and many other published works show that the fatigue damage in different parts of the SCR in the TDZ varies in different directions, simultaneously. In other words, when the fatigue damage is increased at a given point on the riser, it may be decreased in other nodes in the vicinity, at the same time. This implies the shifting of fatigue damage distribution. Therefore, any conclusions made based on observations in a single node on the riser cannot be generalized to the riser's overall response.

These four rules (referred to R-1 to R-4 from now on) were used to analyze and re-assess most of the published papers in the area of trench effect on SCR fatigue in the TDZ.

4.4. Re-assessment of Previous Studies

The published research works were comprehensively reviewed and categorized using the outlined main rules (R-1 to R-4). The selected works were those that considered the effect of “cyclic embedment” and those that focused on the impact of “trench” on fatigue. There might be still other valuable publications related to this topic but not included in our study. However, for the sake of brevity, we eliminated the identical papers and selected only the

papers widely cited by researchers and those who provided relatively sufficient information to re-assess the obtained results.

4.4.1. Effect of “Cyclic Embedment” on Fatigue Damage

Table 4-2 summarizes the publications considering the effect of “cyclic embedment” on fatigue and their classification based on the proposed rules R-1 to R-4. Looking at columns 8 and 9 shows that there is a perfect agreement between the majorities of the published papers, where the cyclic penetration slightly increases the peak fatigue damage and decreases the damage near the TDP. Figure 4-4 shows the sample of coherent results obtained by studies number 1, 2, and 4 (Zargar 2017, Elliott et al. 2013, Elosta et al. 2014). These results are in perfect agreement with the findings of Shoghi and Shiri (2019) (Table 4-1), where the cyclic penetration increases the absolute gradient of the riser profile in FOZ and NOZ. In the absence of LF vessel excursions, the fatigue damage slightly increases in NOZ (or peak fatigue damage) and decreases in FOZ (or near the TDP).

Table 4-2. Re-assessment of the published studies for the effect of “cyclic embedment” on fatigue

ID	Study	R-1		R-2			R-3		R-4		
		Mathematical Trench	Trench type	Numerical Trench	Cyclic Penetration	Seabed model	WF motions	LF excursion	Fatigue damage near TDP	Peak Fatigue damage in TDZ	Peak damage relocation
		1	2	3	4	5	6	7	8	9	10
1	Zargar (2017)	*	NA.	*	✓	Non-linear hysteretic	✓	*	* Decreased	* Increased	Not moved
2	Elosta et al. (2016)	*	NA.	*	✓	Non-linear hysteretic	✓	✓	Decreased	Increased	Not moved
3	Wang (L) et al. (2013)	*	NA.	*	✓	NA.	✓	*	* Decreased	* Increased	No comment
4	Elliott et al. (2013b)	*	NA.	*	✓	NA.	✓	*	Decreased	** Decreased	Towards the anchored end
5	Shiri and Randolph (2010)	*	NA.	✓	✓	Non-linear hysteretic	✓	*	Decreased	Increased	Towards vessel
6	Hodder and Byrne (2009)	*	NA.	*	✓	NA.	✓	*	* Decreased	* Increased	No comment
7	Nakhaee and Zhang (2008)	*	NA.	*	✓	Non-linear hysteretic	✓	*	No comment	** Decreased	No comment
8	Bridge (2005)	*	NA.	*	✓	•Non-linear plastic •Linear elastic	✓	✓	* Decreased	* Increased	Towards vessel

* Observed in results but not directly commented by authors
 ** Technical issues were observed in results

In Table 4-2, cells with doubled borderline and a star sign refer to the studies that have made observations but have not directly commented on it. The results obtained by these studies are re-assessed in this section. Cells with a thick solid borderline refer to the studies that are not in agreement with others (e.g., Elliott et al. 2013, Nakhaee and Zhang 2008). These papers and the potential reasons for the opposite conclusion are further discussed later in this section.

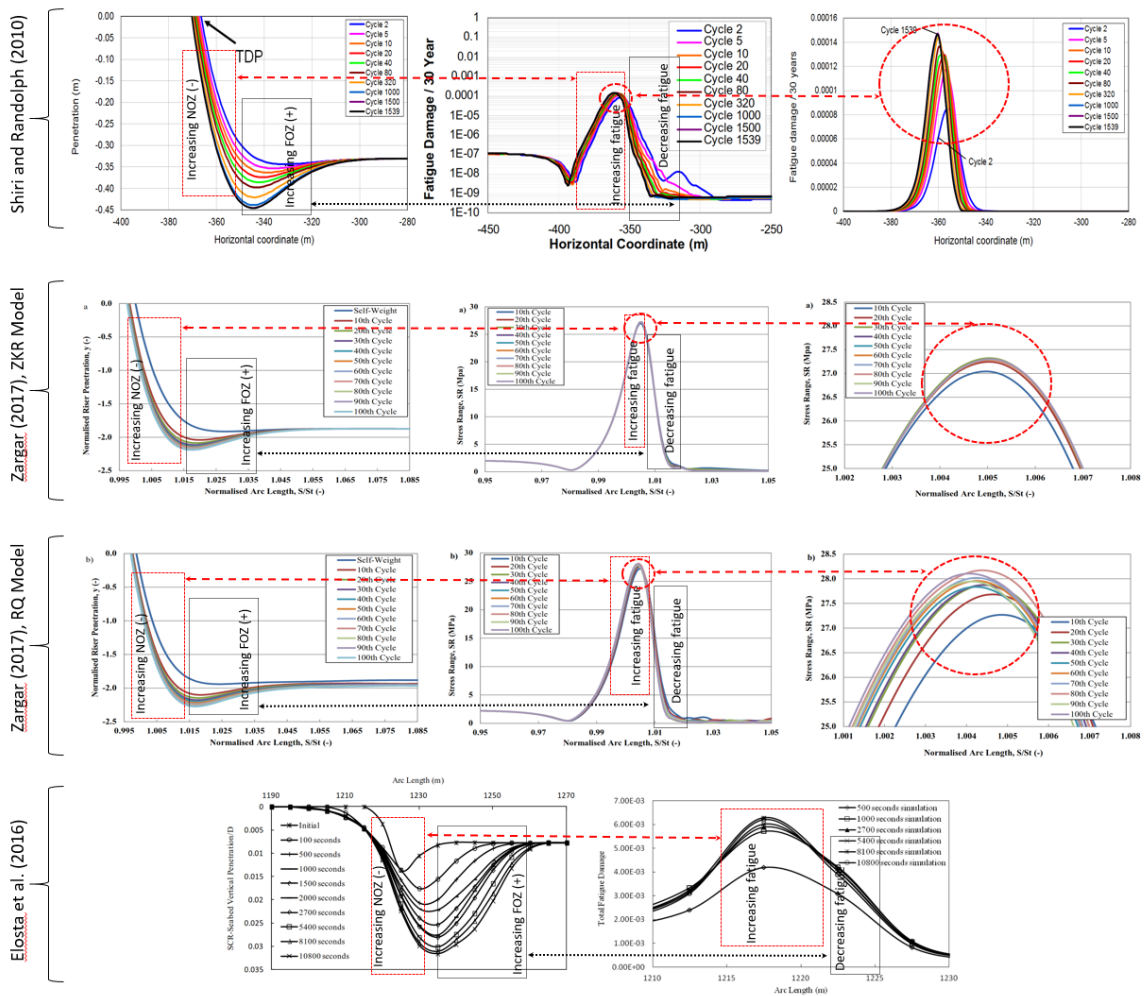


Figure 4-4. Effect of cyclic penetration on fatigue damage in different studies

- **Elliott et al. (2013)**

Elliott et al. (2013) published a series of centrifuge test results conducted at C-CORE (item No.4 in Table 4-2) with a total cyclic embedment of almost one riser diameter. The study was interesting and unique in its kind and provided the time-domain variation of bending moment in several spots on a truncated riser. The authors observed a cyclic reduction of peak bending moment variation near the TDP and concluded that the “trench” is for the benefit of fatigue life. This conclusion seems to disagree with the results obtained by other studies in Table 4-2 (except study No. 7). Figure 4-5 shows the comparison between the cyclic embedment profile of the SCR observed by Elliott et al. (2013) and some of the key experimental and numerical studies (Bridge and Howells 2007, Zargar 2017, Wang and Low 2016, Randolph et al. 2013, Shiri and Randolph 2010, Langner 2003, Wang et al. 2013, Hodder and Byrne 2009, Bridge 2005). The embedment profile observed by Elliott et al. is a ladle-shape profile with the mouth towards the anchored end. This embedment profile seems to be opposed to mathematical fundamentals, the published numerical and experimental studies (with no exception to our knowledge), and also the real subsea observations (Bridge and Howells 2007), where the mouth of ladle-shape embedment profile in the TDZ is inversely towards the vessel. Logically, and as observed in reality (Bridge and Howells 2007), the catenary riser enters into the seabed (NOZ) with a steeper slope and a shorter horizontal projection relative to the bottom point compared to the resting part on the seabed (FOZ).

A closer look at the test set up suggests that the potential reason behind the obtained unusual embedment profile in NOZ might be the using of pin-roller support in the actuator. The pin support may have caused the truncated riser model not to perfectly match the target

realistic catenary shape. By using the pin-roller support at the end of the riser, which is quite close to the TDP, the bending moment has been forced to be zero exactly in the location that SCR undergoes the highest bending moment oscillations (see Figure 4-6 and the dashed expected profiles in Figure 4-5).

In addition, it seems that the short length of the truncation (about $106D$ from the actuator to TDP, and $9.5D$ actuator height from seabed) combined with the high bending stiffness of the model riser and the low submerged weight have prevented the desired catenary shape to form resulting in a TDZ curvature that is much larger than expected. This enlarged curvature has interfered with the NOZ and imposed a straight line seabed profile instead of a steeply sloped curve. The lower bending moment variation and consequently less fatigue accumulation (see Figure 4-6) have caused the authors to conclude that the “trench” effect is beneficial for improving the fatigue life.

Technically, it is quite challenging to develop a semi-flexible truncated riser connection to the actuator in order to update the bending moment or the hang-off angle with riser oscillations. This usually causes the researchers to use the pin connection between the riser and the actuator. However, researchers usually combine three different remedial approaches to ensure that the truncation will not prevent the catenary action, which plays a significant role in the riser-seabed interaction. These remedial solutions may include a) lower SCR bending stiffness (e.g., using polyethylene pipes (Wang et al. 2013, Hodder and Byrne 2009)), b) heavier pipe weight (e.g., adding metal ballast wires inside the pipe (Hodder and Byrne 2009)), and/or c) selection of a far enough truncation point (e.g., $363D$ actuator to TDP, $57D$ actuator height from seabed (Bridge and Howells 2007)), all of which are seemed not to be well incorporated in the tests conducted by Elliott et al. (Elliott et al. 2013). The nodal results published by the authors

clearly shows the cyclic increase of the damage in NOZ (SG 10 to SG18), a proper trend that seems to be aborted midway by the unwanted interference of the catenary action.

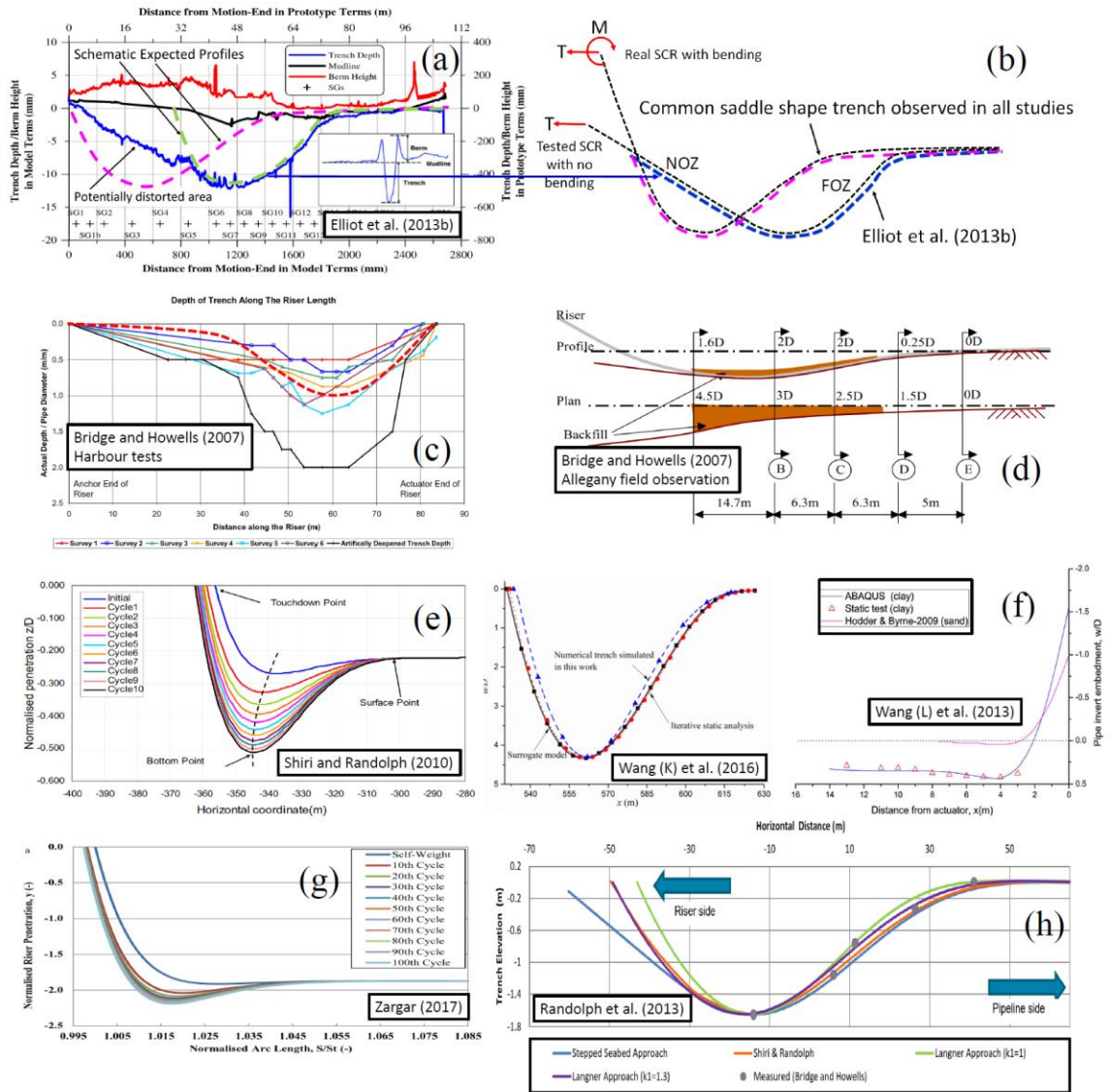


Figure 4-5. The overall shape of the riser embedment profile in the literature compared with Elliott et al. (2013)

The sample nodes presented in Figure 4-7 with bending moment variation through the first episode of vessel motions (M1) shows that the results produced by Elliott et al. could be potentially in agreement with the findings of the current study if the desired riser curvature

in the TDZ was properly achieved. Although, a similar trend was observed in later episodes of motions, but it should be noted that as the seabed goes under plastic deformations with different motion amplitudes, local profile variations may happen within the trench profile and this may affect the bending moment variation trend and consequently the fatigue damage (as earlier discussed by Bridge (Bridge 2005) and Shiri (Shiri 2014b)). This is more critical when the low-frequency vessel excursions are involved, and the ultimate fatigue damage will depend on the probabilistic distribution of TDP attendance in various zones of a trench. Unfortunately, Elliott et al. (2013) did not provide sufficient explanations about the rationale behind the assumed pin-roller connection, its impact on the curvature in the TDZ, and any comparison with ideal full-scale catenary configuration.

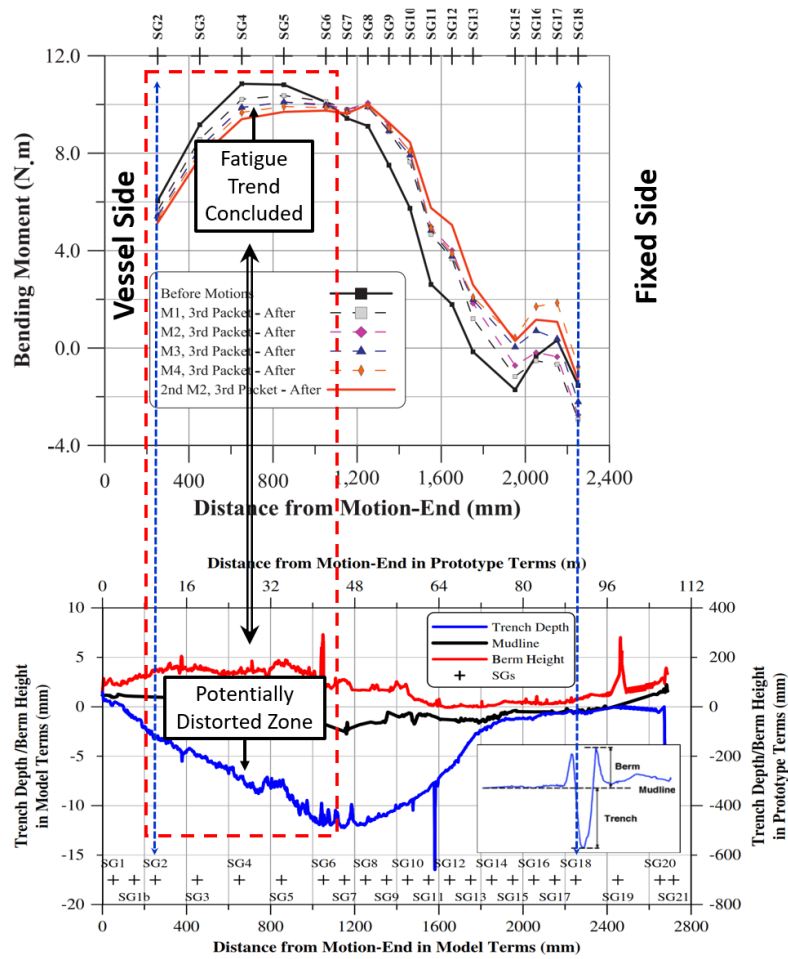


Figure 4-6. Assessment of penetration profile vs. bending moment obtained by Elliott et al.

(2013)

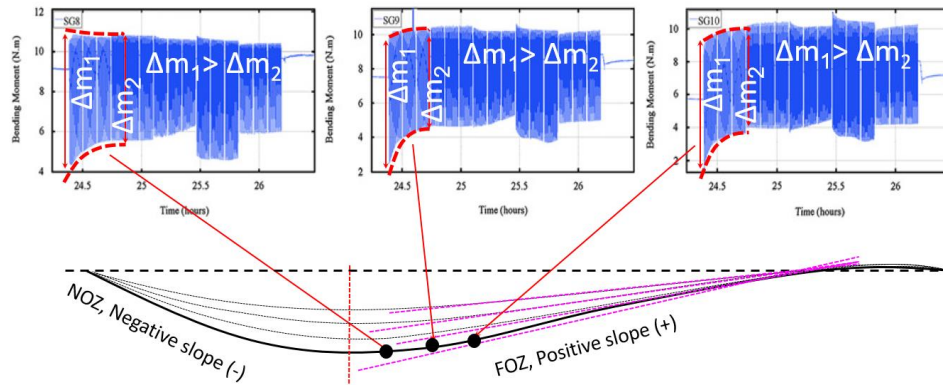


Figure 4-7. Experimental stress range variation over positive and negative sloped faces of

SCR profile (Elliott et al. 2013)

- **Nakhaee and Zhang (2008)**

Nakhaee and Zhang (2008) conducted an interesting numerical modeling with the incorporation of gradual seabed soil stiffness degradation and cyclic riser embedment through two different riser configurations (Riser 1 and 2). The authors considered only the wave-frequency vessel motions and achieved a maximum penetration depth of about $0.4D$ in Riser1 and $0.8D$ in Riser 2, over a 300 hours simulation time. The authors observed a cyclic reduction of maximum variation of the bending moment and concluded that trench formation improves the fatigue life near the TDZ (see Figure 4-8 (a)). As observed in almost all of the numerical (e.g., Figure 4-4) and experimental studies (e.g., Figure 4-6), the fatigue damage variation may be simultaneously decreased and increased in neighbor nodes throughout the TDZ, which is a relatively long area. Nakhaee and Zhang (2008) observed this diversity of trends in neighbor nodes as well (see Figure 4-8 (b)). A full profile of cyclic bending stress or fatigue damage distribution throughout the riser in the TDZ is mandatory to trace the overall effect of trench formation on fatigue in various zones of touchdown area and make a comparison with other studies. Nakhaee and Zhang (2008) presented valuable trends of dynamic stress variation in a couple of individual spots near the TDZ. However, the paper did not provide a full distribution of the fatigue damage or cyclic bending stress profile throughout the global riser configuration and this makes challenges to compare the results of this study with other published works presented in Table 4-2.

For instance, Figure 4-8 (a) shows that the magnitude of bending moment variation is decreased as the seabed soil becomes harder ($\Delta m_1 < \Delta m_2 < \Delta m_3$). Since the bending moment variation has the same trend as fatigue damage, Figure 4-8 (b) indicates less fatigue life in a softer seabed, which seems not to be in agreement with other published studies at the first

look. However, Nakhaee and Zhang (2008) did not mention the exact location of the observed nodes and only referred as to the nodes “near the TDZ,” and since the full distribution of the damage was not provided, these nodes may potentially belong to an area of the TDZ usually showing inverse variation trends. Therefore, there might be a potential agreement between the results observed by Nakhaee and Zhang (2008) and the other studies summarized in Table 4-2, but it couldn’t be verified due to having any access to a full damage distribution profile.

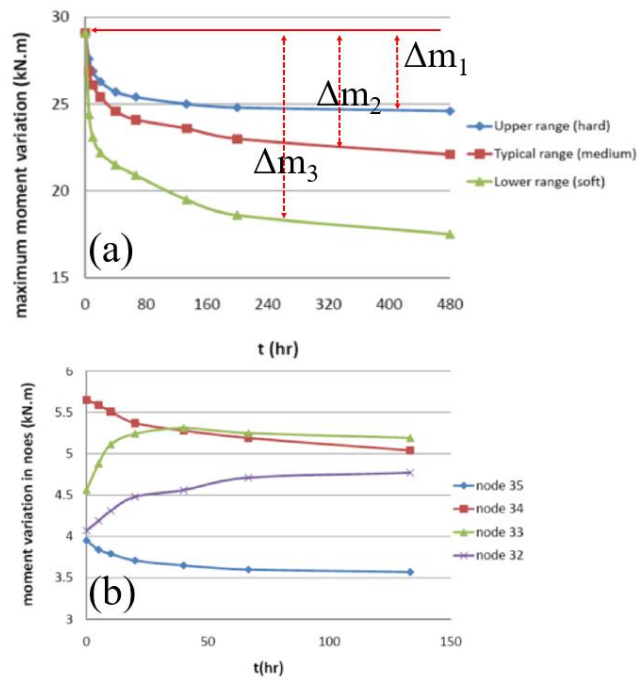


Figure 4-8. Assessment of test results published by Nakhaee and Zhang (2008)

- **Hodder and Byrne (2009)**

Hodder and Byrne (2009) conducted a series of large-scale 3D flume tests in silica sand at Oxford University to investigate the cyclic embedment of the oscillating SCR into the seabed. The results published by the authors are in agreement with the other studies in Table 4-2 and the findings of Shoghi and Shiri (2019) (Table 4-1). However, the authors did not make an explicit comment on

the effect of the cyclic embedment on fatigue damage accumulation. Figure 4-9 (a) and (b) shows the test's setup, where a water distribution and pumping system was used to fully liquefy the 350 mm deep soil bed with upward hydraulic gradients. The truncated model riser (7.65 m length, and 110 mm diameter) made of PVC material was pin connected to an actuator applying monotonic and cyclic excitations. Sufficiently low magnitudes of bending stiffness (Young modulus 2.6 GPa) and high amount of submerged weight (79.8 N/m) were adopted to ensure setting the target catenary curvature in the TDZ. A range of instrumentation including loads cells, displacement sensors, strain gauges, and pressure transducers was used to capture the vertical load, soil displacement, bending moment, and pore pressure in various locations, respectively. Figure 4-9 shows the variation of the bending moment (or fatigue) in three key locations selected from NOZ, NOZ near TDP, and FOZ (i.e., BM1, BM3, and BM4) to facilitate the comparison of the trends with the finding of the current study (colourful annotations were added in this study). The cyclic embedment profile in Figure 4-9 (c) coincided with an instrumentation sketch given in Figure 4-9 (b) at two points (1000 mm and 7000 mm far from the actuator) to identify the NOZ and FOZ of the trench. As annotated on Figure 4-9 (d), (e), and (f), the variation of the bending moment (or fatigue damage) shows a perfect agreement with findings of the current study (summarized in Table 4-1). Depending on the cyclic loading amplitude, the bending moment variation range in NOZ (BM1 and BM3) is gradually increased ($\Delta m_i < \Delta m_u$), while the riser cyclically penetrates into the seabed Figure 4-9 (d) and (e). The bending moment variation range in FOZ (BM4) is gradually decreased in an inverse trend Figure 4-9 (f) ($\Delta m_i > \Delta m_u$). The magnitude of the bending moment reduction in BM3 is less severe than BM1 because of its proximity with the TDP and a lower gradient compared with BM1.

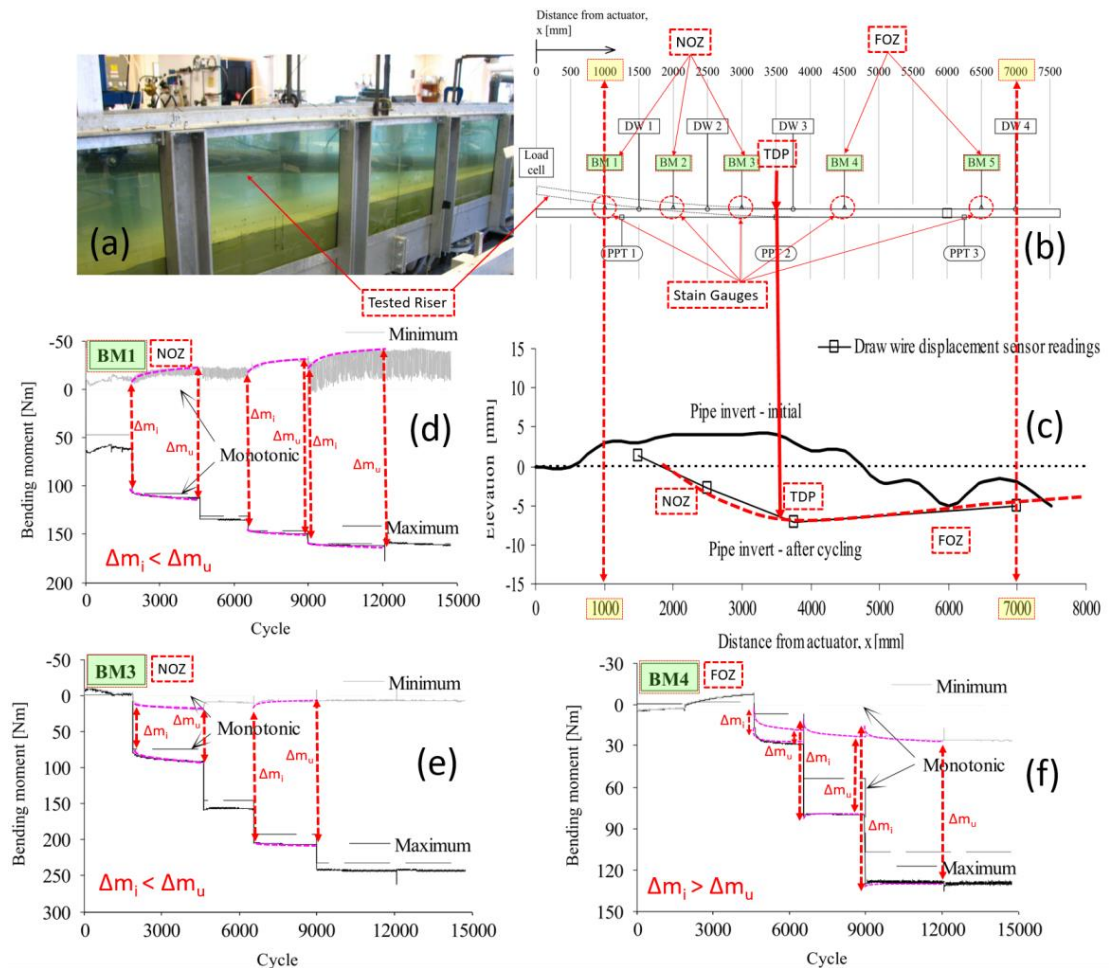


Figure 4-9. Assessment of test results published by Hodder and Byrne (2009)

The results published by the authors confirm the findings of Shoghi and Shiri (2019) (Table 4-1). Furthermore, the study conducted by Bridge (2005) has reported some results for fatigue damage variation in sloped seabed with positive and negative gradient, which are in perfect agreement with Shoghi and Shiri (2019) and other studies listed in Table 4-2. The results of these studies can be found in original papers and were not brought here in for the sake of conciseness.

Combining the observations reviewed above and considering the limitations in having access to some of the information needed for full involvement of the studies No. 4 and 7 in conducted comparison (Table 4-2), a coherent trend was observed in these series of

studies. The wave-frequency vessel oscillations cause the SCR resting on a non-linear hysteretic seabed to penetrate into the seabed gradually. This “cyclic embedment,” which is usually less than a pipe diameter deep, causes the peak fatigue damage to slightly increase towards the NOZ and slightly decrease around the FOZ. These variations lead to the peak fatigue damage location to either migrate towards the vessel slightly or to not move at all. The presence of low-frequency vessel motions does not change this overall trend. However, the large low-frequency vessel excursions are expected to largely relocate the peak damage point that will be further investigated later in this paper. In the next section, the studies conducted on understanding the “trench” effect or “deep embedment” effect on fatigue damage are re-assessed.

4.4.2. Effect of a “Trench” on Fatigue Damage

Table 4-3 summarizes and classifies the studies that have investigated the effect of a “trench” on fatigue response. To facilitate the review of results, the row numbers in Table 4-3 are continued from Table 4-2. Assuming that a deep trench is almost a developed version of shallow cyclic embedment, it does not seem logical to believe that the deep “trench” may have an effect on fatigue inverse to what was observed in the effect of shallow “cyclic embedment.” Therefore, to select the studies from Table 4-3 for re-assessment, it was assumed that the same trend observed for “cyclic embedment” would be valid for “trenches,” unless observing a convincing and coherent inverse trend, with no potential inconsistency issues in the studies. This assumption resulted in identifying some exceptions (Sherma and Aubeny 2011, Clukey et al. 2007, Langner 2003, Wang et al. 2013) that have been marked by thick solid borderlines in Table 4-3 that will be further reviewed. Study No. 11 (Randolph et al. 2013) was marked by a doubled borderline because it is in

agreement with some cases but remains mostly in disagreement with the findings of the last section and the results obtained by Shoghi and Shiri (2019). It is worth mentioning, almost all of the studies listed in Table 4-3 have inserted an artificial trench underneath the SCR to study the trench effect on fatigue. The inserted trench profiles have been defined by mathematical expressions or predicted by non-linear hysteretic seabed models. Shiri (2014b) is the only exception to this approach, who proposed a different methodology in which the trench was naturally created under the extreme wave-frequency vessel motions. Also, Shiri (2014b) examined the artificial insertion of the trench and showed that this approach is highly risky and could lead to contact pressure hot spots that distort the bending moment variation and consequently the fatigue damage distribution.

Table 4-3. Re-assessment of the published studies for the effect of “trench” on fatigue.

ID	Study	R-1		R-2			R-3		R-4		
		Mathematical Trench	Trench type	Numerical Trench	Cyclic Penetration	Seabed model	WF motions	LF excursion	Fatigue damage near TDP	Peak Fatigue damage in TDZ	Peak damage relocation
		1	2	3	4	5	6	7	8	9	10
9	Wang (K) and Low (2016)	✓	Cubic polynomial	✗	✓	Non-linear hysteretic	✓	✓	Decreased	*** Decreased	Towards vessel
10	Shiri (2014b)	✓	<ul style="list-style-type: none"> •Linear Exponential •Quadratic Exponential 	✓	✓	<ul style="list-style-type: none"> •Non-linear hysteretic •Linear elastic 	✓	✗	Decreased	Increased	Towards vessel

11	Randolph et al. (2013)	✓	•Stepped trench •Polynomial	✓	✓	•Non-linear hysteretic •Linear elastic	✓	✓	* Decreased in most of the cases * Increased in some cases	* Decreased in most of the cases * Increased in some cases	Towards the vessel and anchor (scattered)
12	Sharma and Aubeny (2011)	✓	Polynomial	✗	✓	•Non-linear hysteretic •Linear elastic	✓	✗	Decreased	** Decreased	Towards vessel
13	Clukey et al. (2007)	✓	No Comment	✗	✗	•Non-linear elastic •Linear elastic	✓	✓	Decreased	** Decreased	•Towards the vessel in linear seabed •Not moved in non-linear seabed
14	Fontaine et al. (2006)	✓	Polynomial	✗	✗	•Non-linear elastic •Linear elastic	✓	✗	Couldn't comment	Couldn't comment	No comment
15	Giertsen et al. (2004)	✓	Not Known Physical	✗	✓	Non-linear plastic, CARISIMA	✓	✗	No comment	Increased	No comment
16	Leira et al. (2004)	✓	Polynomial CARISIMA	✗	✓	Non-linear plastic, CARISIMA	✓	✗	No comment	Increased	No comment
17	Langner (2003)	✓	Polynomial	✗	✗	•Linear elastic •Rigid	✓	✗	Decreased	** Decreased	No comment
<p>* Observed in results but not directly commented by authors ** Technical issues were observed in results</p>											

The potential pressure hot spots are the result of incompatibilities between the SCR natural catenary profile and the inserted trench profile particularly in NOZ and the trench mouth (Shiri 2014). A real trench profile which is fully developed under a wide range of complex environmental loads should be able to accommodate the majority of SCR near, far, and cross configuration scenarios that may happen in its operation life without suffering from a contact pressure hotspot with the seabed. This important point was used to re-assess the aforementioned exceptions marked in Table 4-3 (i.e., studies No. 9, 11, 12, 13, and 17). Also, it should be noted that the existing riser-seabed interaction models are commonly based on purely vertical loading of riser under in-plane motions, whilst the SCR undergoes cyclic out-of-plane motions as well. There are some riser-seabed interaction studies that have considered the effects of out-of-plane motions (Oliphant et al. 2009, Martin and White 2012, Yuan et al. 2017). However, these motions are not directly contributing to fatigue, since the fatigue life is usually controlled by the top and bottom fibres of the riser pipe, which are loaded through in-plane motions. The out-of-plane motions may slightly affect the vertical riser-seabed stiffness and increase in the rate of embedment with cycles (Yuan et al. 2017). A closer look at columns 1 to 7 shows that the study conducted by Randolph et al. (2013) is maybe the most comprehensive study that has received a tick mark for all of the influential features. This study and the work published by Sharma and Aubeny (2011) were further discussed here, and comments were made on the results obtained by other marked studies (i.e., the study No. 9, 13, and 17).

- **Randolph et al. (2013)**

Randolph et al. (2013) examined three different approaches for modeling the trench and evaluating its impact on fatigue in two different geographical locations, the Gulf of Mexico and Offshore Western Australia. The authors considered low-frequency vessel excursions towards the far, cross, and near directions and investigated the analytical trench proposed by Langner (2003), the cyclically created trench proposed by Shiri and Randolph (2010), and a new approach called the “stepped method.” Randolph et al. (2013) concluded that in most of the cases, the trench is for the benefit of fatigue life in the TDZ. However, the authors also observed some exceptional cases with increased fatigue damage due to trench effect. Figure 4-10 shows some of the key results obtained by Randolph et al. (2013) that have been further annotated to highlight the findings of the current re-assessment study. For far and cross vessel excursions, Randolph et al. (2013) compared the fatigue lives on the flat and trenched seabed at points A₀, B₀, C₀, and D₀ (near the TDP, Figure 4-10 (a), (b), (c), and (d)) and concluded that the fatigue life is modestly improved near the TDP of trenched seabed (12% to 27% for far offset, and 7% to 14% for cross offset in case of Gulf of Mexico). This conclusion is completely true but it seems to be only a part of the scenario. A closer look at Figure 4-10 (a) to (d) shows that the insertion of the trench has not remarkably changed the fatigue life but shifted the life distribution towards the pipeline end (by Δ_1 , Δ_2 , Δ_3 , and Δ_4). Points A, B, C, and D on the flat seabed have been transferred to corresponding points A₀, B₀, C₀, and D₀ on the trenched seabed. In other words, while the fatigue life is increased at the point A₀, the point E₀ experiences an inverse trend or a decreased fatigue life. Therefore, a more consistent conclusion of the study can be improvement of the fatigue life in the TDP (e.g., point A₀) and reduction of the fatigue life

in the TDZ (e.g., point E_0), which is well in agreement with the findings of Shoghi and Shiri (2019) summarized in Table 4-1 and other studies listed in Table 4-3. This seems to be an appropriate approach since the industry is mainly looking for the effect of the trench on peak fatigue damage in the TDZ, not the TDP alone. In near offset analyses, Randolph et al. (2013) observed a significant improvement of the fatigue life in the case of Gulf of Mexico (40% to 144%, see Figure 4-10 (e) and (f)).

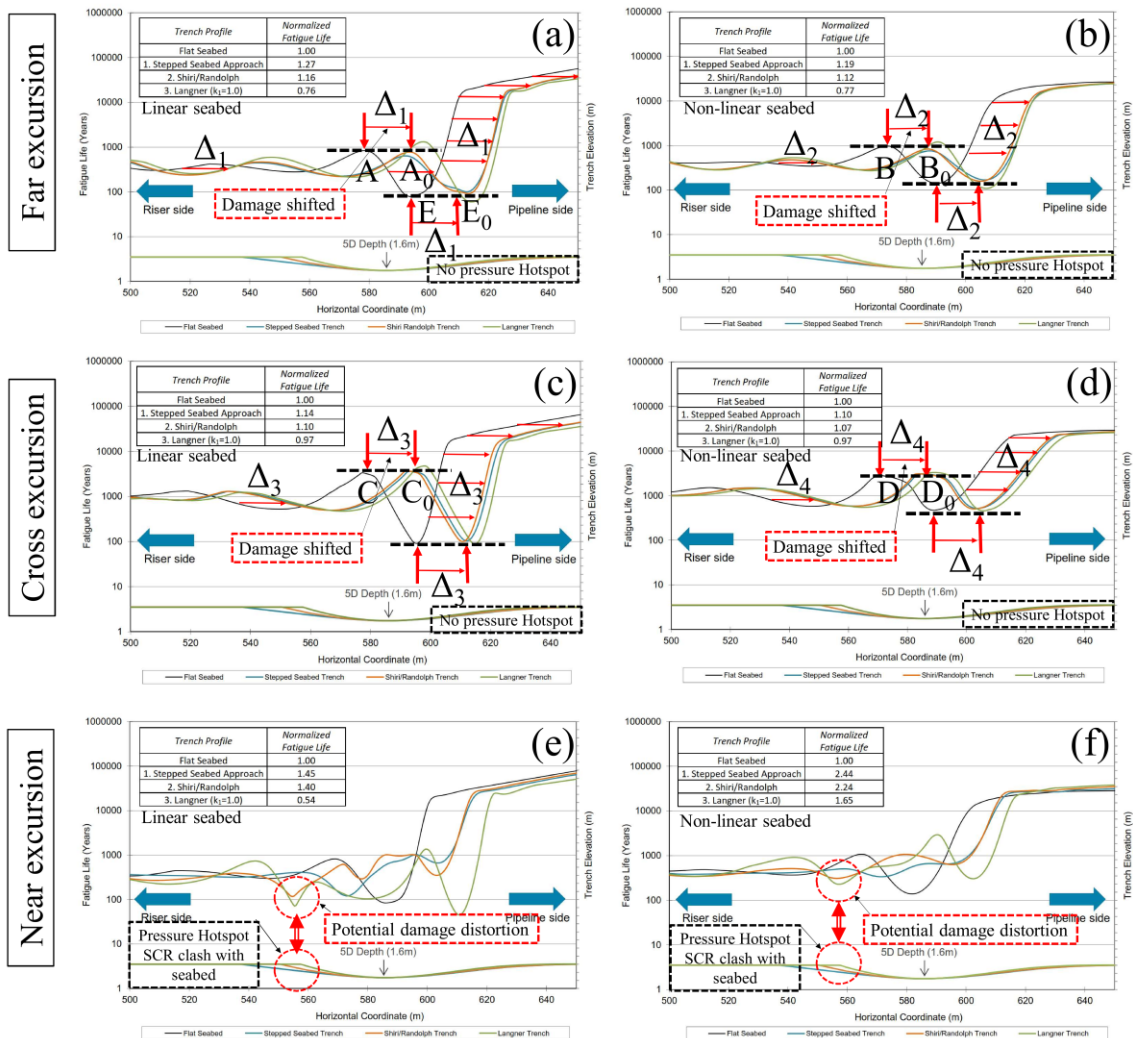


Figure 4-10. Assessment of test results published by Randolph et al. (2013)

A closer look at these series of plots shows an unexpected fatigue life fluctuation (circled by dashed red lines in Figure 4-10 (e) and (f)) that seems to be susceptible to potential pressure hot spots in the trench mouth. There is a sudden drop of damage distribution in green (Langner 2003) and orange (Shiri and Randolph 2010) lines right in the trench mouth. This sudden drop is not seen in blue line (Stepped method), but its overall profile is still largely different from the black line (Flat seabed). Overall, there is no coincidence or similar trends amongst different fatigue damage distribution profiles in the case of near vessel excursion. These results suggest care should be taken in assessing the near offset results. There might be a potential interference between the natural catenary shape and the artificially imposed trench profile at the trench mouth, while the vessel moves towards the near direction. This potential interference may have created a contact pressure hotspot and distorted the fatigue life distribution in the trench mouth and anywhere else, consequently. This unusual fluctuation is significantly limited in the “stepped trench” method because of its smart approach in defining the NOZ profile that has eliminated a sharp trench mouth. However, the stepped method proposed by Randolph et al. (2013) cannot guarantee and did not claim a perfect elimination of the potential pressure hot spots.

The automatic development of the trench profile by oscillation of the vessel seems to be less risky in terms of potential pressure hot spots compared with the artificial insertion of the trench. However, one may ask, why a similar problem has been observed by Randolph et al. (2013) using an automatically generated trench profile proposed by Shiri and Randolph (2010) (see orange line in Figure 4-10 (e) and (f)). The answer might be related to the way that Randolph et al. (2013) have generated the trench, i.e., initially using pure WF vessel motions for trench formation with no LF excursions. Hence, the created trench

might have not been able to accommodate the profile imposed by large near vessel offsets at the trench mouth resulting in a pressure hotspot. Relatively similar trends were observed by Randolph et al. (2013) in the case of Offshore Western Australia with some differences in the direction of the peak damage point relocation.

- **Sharma and Aubeny (2011)**

Sharma and Aubeny (2011) inserted a cubic polynomial trench with a profile fitted to the trench bottom point, and the near and far TDPs on the flat seabed. The authors obtained the trench depth from a decoupled analysis using a non-linear hysteretic seabed interaction model. They concluded that the trench is for the benefit of the SCR fatigue life. Figure 4-11 shows the results obtained by Sharma and Aubeny (2011) that has been further annotated for re-assessment purpose in this study. To facilitate reviewing of the plots, the key points in Figure 4-11 (b), (c), and (d), including the trench bottom and peak negative bending moment, were tried to be coincided between the horizontal axis of different plots, although an accurate coincidence is challenging because of the use of the arc length and in-plane distances in different plots. However, the overall coincidence is fairly accurate to perform the comparison. Figure 4-11 (d) shows a high potential of undesired pressure hot spots and the resultant distortion of the fatigue damage distribution in the NOZ (red line in Figure 4-11 (d)) due to the incompatibility of the riser and trench profile. A similar damage distortion is observed in Figure 4-11 (f), which is less severe than (e) due to a lower magnitude of significant wave height, less TDP oscillation amplitude, and consequently, a lower impact of the contact pressure hotspot.

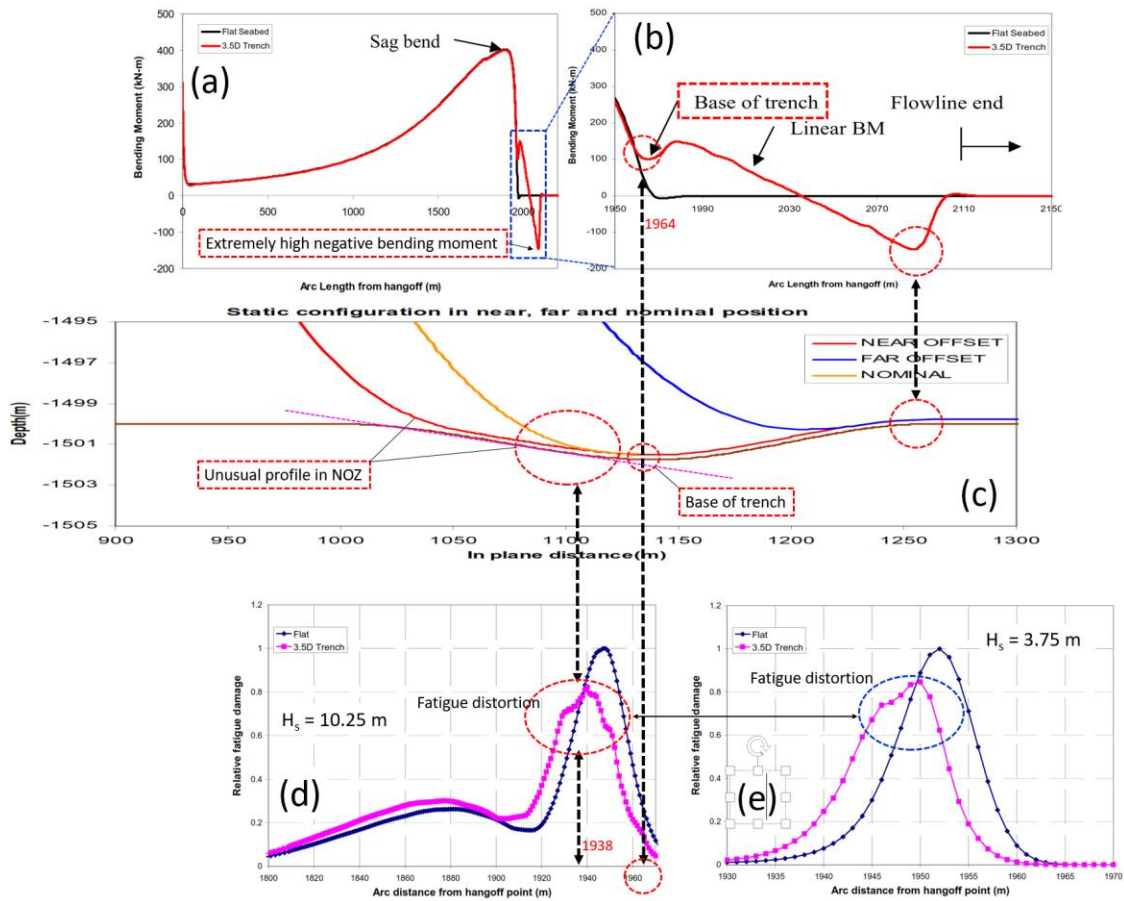


Figure 4-11. Potential fatigue distortion in Sharma and Aubeny (2011)

The undesired interference of the real catenary profile and the inserted trench profile (Figure 4-11 (c)) may have also affected the bending moment variation in Figure 4-11 (a), where a significant negative bending moment (about 35% of a positive peak bending moment) is observed in the trenched seabed, which seems unexpected.

The review of the studies No. 9, 13, and 17 from Table 4-3 shows similar aforementioned potential effects. Wang and Low (2016) fitted a surrogated trench curve to the results obtained from the non-linear hysteretic seabed interaction model. The surrogated model seems to reduce the overall length of the trench and push the trench mouth away from the vessel. This increases the potential risk of riser interference with the trench mouth and

distortion of fatigue results due to pressure hotspots. Clucky et al. (2007) used a relatively similar trench insertion approach and concluded that the trench is beneficial for improving fatigue life. However, the results published by Clucky et al. (2007) are not seemed to be in agreement with their later experimental studies, i.e., Elliott et al. (2013). As shown earlier in this paper, the results published by Elliott et al. (2013) indicates an increase and decrease of fatigue damage in different nodes on the riser in the TDZ, while Clucky et al. (2007) observed damage reduction almost in all of the nodes. The paper published by Langner (Langner 2003) does not provide sufficient data to re-assess the risk of the contact pressure hot spot between the riser and trench. However, this trench profile was used by Randolph et al. (2013) as reviewed earlier in this paper and showed a potential risk of unexpected interference between the riser and trench profile at the trench mouth.

4.4.2.1. Discussion

Combining the observations reviewed above and considering the potential impact of the interference between the natural catenary shape and the inserted trench profile at the trench mouth (i.e., the studies No. 9, 11, 12, 13, and 17 in Table 4-3), a coherent agreement was observed amongst the studies listed in Table 4-3. The trench presence was found less likely to be beneficial to the fatigue life, at least not as a robust and consistent conclusion. It was observed that the trench slightly increases the peak fatigue damage in the NOZ and slightly decreases in FOZ, which is in agreement with Shoghi and Shiri (2019) (see Table 4-1). Also, the trench causes a large shifting of the peak fatigue damage in the opposite direction of the vessel LF excursions.

It is noteworthy, the detrimental effect of the trench on fatigue may not be well aligned with engineering common sense, where reduced fatigue damage is expected due to the

progressive SCR relaxation by cyclic penetration into the seabed. However, there is no guarantee that such a common sense is true in every section of the SCR. Indeed, the catenary shape of the SCR and its interaction with the seabed is quite complex. In addition, the relaxation does not necessarily mean lower fatigue damage that is accumulated by cyclic stress variation and not the stationary magnitude of stress. In other words, the geometrical configuration of the structure can override the effect of soil stiffness. A sensible example of this phenomena is the difference between the influence of soil stiffness on the fatigue performance of SCRs and wellhead-conductors. It is widely accepted that the softer seabed reduces the peak fatigue damage in the TDZ of SCRs, while the trend is inverse in wellhead-conductors, where the harder the seabed, the lower the fatigue (Jeanjean 2009). The only difference between the SCRs and wellhead-conductors is the geometrical configuration of the structures that results in different trends in terms of the soil stiffness effect on fatigue.

Also, the cyclic soil stiffness degradation under the SCR is a two-way avenue, because the undrained shear strength is increased with penetration depth. In reality, it seems a complex equilibrium is gradually achieved between the cyclic soil stiffness degradation, the increasing of undrained shear strength because of the creation of the trench, and the catenary load applied by SCR oscillation under several environmental and operational loads. Furthermore, there are several other aspects affecting the riser-seabed interaction that has not been well explored, either solely, or interactive (see Figure 4-2).

Overall, an accurate estimation of the fatigue life of SCR in a real trench still seems to be extremely challenging and needs an extensive amount of the real trench shapes assessment accompanied by supporting field data such as vessel oscillation, stress/strain oscillation,

and seabed stiffness degradation histories. However, the observations of this study show that despite the effect of the trench on peak damage point migration, which can be quite significant, the variation of the peak fatigue damage magnitude in the TDZ due to trench effect is not significant.

4.5. Conclusions

A mathematical framework recently developed by Shoghi and Shiri (2019) was adopted to re-assess the effect of SCR “cyclic embedment” and “trench” on fatigue damage in the TDZ and achieve a more coherent agreement in the literature. The adopted framework utilizes the geometrical dominance of the TDP oscillation amplitude (Δ_{TDP}) to average shear force distribution (\tilde{V}) and the capability of their direct product ($\tilde{V} \times \Delta_{TDP}$) in mimicking the fatigue trends (2019) to assess the embedment effect on fatigue. This product (i.e., $\tilde{V} \times \Delta_{TDP}$) is neither equal to nor an approximation to the axial stress range or fatigue, but follows a variation trend similar to the axial stress range, and facilitates the re-assessment of the trench effect of fatigue. The proposed methodology was applied to re-assess the majority of the key publications in the literature. Some limitations were observed in having access to detailed information of some of the studies that make challenges against achieving a coherent agreement. A couple of examples being susceptible to distorted fatigue results by artificial insertion of mathematically expressed trenches were also observed. Taking into account the potential effect of existing inconsistencies, a more coherent agreement on trench effect on fatigue was observed that are summarized as follows:

- The WF vessel oscillations about a mean position result in a shallow “cyclic embedment” of the riser into the seabed by less than about one diameter (with the regular performance of the existing non-linear hysteretic riser-seabed interaction models). This cyclic penetration slightly increases the fatigue damage in the vessel side of the TDP (NOZ) and slightly decreases the damage in the anchor side (FOZ). The peak fatigue damage may slightly move towards the vessel or not move depending on the non-linear seabed model.
- The shallow “cyclic embedment” of the riser into the seabed is not necessarily the same as a deep “trench.” The existing non-linear hysteretic models are usually quickly stabilized by achieving a maximum penetration depth of less than one diameter, which is called a premature stabilization (Dong and Shiri 2018), while the real trenches observed in the field are in the range of several diameters deep (Bridge and Howells 2007). Also, there are still several important but less-explored contributors to the trench formation, either individually, or interactively. Therefore, care should be taken in generalizing the results obtained from “cyclic embedment” to “trench,” and further studies are required to see whether the ultimate trench profile is the scaled-up version of cyclic embedment profile.
- The LF vessel excursions with near, far, and out of plane offsets may have a significant influence on ultimate fatigue results. These excursions result in TDP migration towards the NOZ and FOZ of the trench that causes an increase and decreases in peak fatigue damage, respectively. Therefore, the results of the published studies, which have only

applied WF oscillations or the LF motions with no large excursions cannot be simply generalized to reality.

- The combined WF+LF motions on a trenched seabed were found to slightly increase the damage in near excursions (NOZ) and slightly decrease the damage in far excursions (FOZ). However, the peak fatigue damage is largely moved by tens of diameters (e.g., 50D) depending on the direction of excursions. In other words, in real life, where the environmental load spectra depend on geographical locations, scattered results may be obtained depending on the probability of the dominant TDP oscillations in NOZ or FOZ (as also observed by Randolph et al. (2013) for the Gulf of Mexico and Western Australia). This implies the case-dependence of trench effect on fatigue performance of SCR in the TDZ and emphasizes on the need for independent study of any individual project.
- The artificial insertion of a mathematical or pre-defined trench profile to study the trench effect on fatigue response is a risky approach. The fatigue results obtained by this approach are usually susceptible to potential distortion due to creating unexpected contact pressure hot spots at trench mouth. These pressure hotspots can be created as the result of a disagreement between the natural catenary profile of the SCR and the mathematical trench profile that alters the bending moment variation. This is less likely in reality since a fully developed trench is expected to accommodate the majority of oscillating SCR configurations that may happen during the operation life. There is only one study that has resolved this issue to some extent by proposing a “stepped trench” (Randolph et al. 2013). This method can be further developed to enhanced

performance. The automative trench creation using cyclic SCR perturbations and extreme seabed model parameters (Shiri 2014b) can be an appropriate approach to guarantee the prevention of having pressure hotspots. However, care shall be taken in the quickly scaled-up trench profiles that further develops towards the anchor end (Shiri 2014b).

The framework proposed by Shoghi and Shiri (2019) combined with rules established in this study can be further developed in the future for more quantitative fatigue damage assessment affected by trench formation in the TDZ. Developing new research programs with an extensive assessment of the real trench shapes accompanied by supporting field data such as vessel oscillations, SCR stress/strain oscillations, and seabed stiffness degradation histories can be significantly beneficial for obtaining robust and reliable solutions.

4.6. Acknowledgments

The authors gratefully acknowledge the financial support of this research by the Research and Development Corporation (RDC) (now InnovateNL) through the Ignite funding program, the Natural Sciences and Engineering Research Council of Canada through the Discovery funding program, and Memorial University of Newfoundland through VP start-up funding support.

References

- Bridge CD, Howells HA. Observation and modeling of steel catenary riser trenches. Proceedings of the 17th International Society of Offshore and Polar Engineers Conference ISOPE-I-07-321; 2007 July 1-6; Lisbon, Portugal. pp 803-813.
- Bridge C. Effect of seabed interaction on steel catenary risers. 2005; PhD thesis; University of Surrey, UK.

- Campbell M. The complexities of fatigue analysis for deepwater risers. Proceedings of the Deepwater Pipeline Technology Conference; 1999 March; New Orleans, USA.
- Clukey EC, Ghosh R, Mokarala P, Dixon M. Steel catenary riser (SCR) design issues at touchdown area. Proceedings of The 17th International Offshore and Polar Engineering Conference ISOPE-I-07-388; 2007 July 1-6; Lisbon, Portugal. <https://doi.org/10.4043/22557-MS>.
- Dong X, Shiri H. Performance of non-linear seabed interaction models for steel catenary riser, Part 1: nodal response. *Ocean Engineering*. 2018; (154) 153-166
- Draper S, Cheng L, White DJ. Scour and sedimentation of submarine pipelines: Closing the gap between laboratory experiments and field conditions. *Journal Scour and Erosion: Proceedings of the 8th International Conference on Scour and Erosion*. 2016 August. DOI: 10.1201/9781315375045-4.
- Elliott BJ, Zakeri A, Barrett J, Hawlader B, Li G, Clukey EC. Centrifuge modeling of steel catenary risers at touchdown zone Part II: assessment of centrifuge test results using kaolin clay. *Ocean Engineering*. 2013 March 1; 60, 208-218. <https://doi.org/10.1016/j.oceaneng.2012.11.013>.
- Elosta H, Huang S, Incecik A. Trenching effects on structural safety assessment of integrated riser/semisubmersible in cohesive soil. *Journal of Engineering Structures*; 2014; (77) 57-64.
- Fontaine E. SCR-soil interaction: effect on fatigue life and trenching. Proceedings of the International Society of Offshore and Polar Engineers Conference (ISOPE); 2006; 1-880653-66-4; May 28- June 02; California, USA.
- Fouzder, A., Zakeri, A., and Hawlader, B. (2012) "Steel catenary risers at touchdown zone - A fluid dynamics approach to understanding the water-riser-soil interaction", 9th International Pipeline Conference, Calgary, V4, 31-36.
- Giertsen E, Varley R, Schroder K. CARISIMA: a catenary riser/soil interaction model for global riser analysis. Proceedings of the 23rd International Conference on Offshore Mechanics and Arctic Engineering OMAE 2004-51345; 2004 June 20-25; Vancouver, Canada. doi:10.1115/OMAE2004-51345.
- Hodder M.S., Byrne B.W. 3D experiments investigating the interaction of a model SCR with the seabed. *Applied Ocean Research*; 2009; 32:145-157.
- Jeanjean P. Re-assessment of P-Y curves for soft clays from centrifuge testing and finite element modelling. 2009; Proceedings of the Offshore Technology Conference OTC-20158-MS; 2009 May 4-7; Texas, USA. <https://doi.org/10.4043/20158-MS>.

- Langner C. Fatigue life improvement of steel catenary risers due to self- trenching at the touchdown point. Proceedings of the Offshore Technology Conference OTC 15104; 2003 May 5-8; Texas, USA.
- Larsen CM, Halse KH. Comparison of models for vortex induced vibrations of slender marine structures. *Marine Structures* 1997 July; 10(6):413-441. [https://doi.org/10.1016/S0951-8339\(97\)00011-7](https://doi.org/10.1016/S0951-8339(97)00011-7).
- Leibniz. Solution to the problem of catenary, or funicular curve, proposed by M. Jacques Bernoulli in the Acta of June 1661. *Acta Eruditorum*. Leipzig, Germany.
- Leira BJ, Passano E, Karunakaran D, Farnes KA, Giertsen E. Analysis guidelines and application of a riser–soil interaction model including trench effects. Proceedings of the 23rd International Conference on Offshore Mechanics and Arctic Engineering OMAE 2004-51527; 2004 June 20-25; Vancouver, Canada. pp. 955-962, doi:10.1115/OMAE2004-5152.
- Martin CM, and White DJ. Limit analysis of the undrained capacity of offshore pipelines. *Géotechnique*, 2012, 62(9):847-863.
- Nakhaee A, Zhang J. Effects of the interaction with the seafloor on the fatigue life of a SCR. Proceedings of the 18th International Society of Offshore and Polar Engineers Conference ISOPE-I-08-397; 2008 July 6-11; Vancouver, Canada. pp 87-93.
- Oliphant J, Maconochie A, White DJ, Bolton MD. Trench interaction forces during lateral SCR movement in deepwater clays. Proceedings of Offshore Technology Conference, 2009 May, Houston, USA, paper OTC19944
- Pesce CP, Martins C, Silveira LM. Riser-Soil Interaction: Local Dynamics at TDP and a Discussion on the Eigenvalue and the VIV Problems. *Journal of Offshore Mechanical and Arctic Engineering*; 2006; 128(1), 39-55
- Pesce CP, Aranha JAP, Martins CA. The soil rigidity effect in the touchdown boundary layer of a catenary riser: Static problem. Proceedings of the International Society of Offshore and Polar Engineers Conference ISOPE-I-98-130; 1998 May 24-29; Montreal, Canada.
- Randolph MF, Bhat S, Mekha B. Modeling the touchdown zone trench and its impact on SCR fatigue life. Proceedings of the Offshore Technology Conference OTC-23975-MS; 2013 May 6-9; Texas, USA. <https://doi.org/10.4043/23975-MS>.
- Rezazadeh K, Shiri H, Zhang L, Bai Y. Fatigue generation mechanism in touchdown area of steel catenary risers in non-linear hysteretic seabed. *Research Journal of Applied Sciences, Engineering and Technology*. 2012; 4(24):5591-5601.

- Sharma PP, Aubeny CP. Advances in pipe-soil interaction methodology and application for SCR fatigue design. Proceedings of the Offshore Technology Conference OTC-21179-MS; 2011 May 2-5; Texas, USA. <https://doi.org/10.4043/21179-MS>.
- Shiri H. Response of steel catenary risers on hysteretic non-linear seabed. Applied Ocean Research, 2014a January; 44:20-28. <https://doi.org/10.1016/j.apor.2013.10.006>.
- Shiri H. Influence of seabed trench formation on fatigue performance of steel catenary risers in touchdown zone. Marine Structures. 2014b April; 36:1-20. <https://doi.org/10.1016/j.marstruc.2013.12.003>.
- Shiri H., Randolph MF. Influence of seabed response on fatigue performance of steel catenary risers in touchdown zone. Proceeding of the 29th International Conference on Ocean, Offshore and Arctic Engineering OMAE 2010-20051; 2010 June 6-11; Shanghai, China. pp. 63-72; doi:10.1115/OMAE2010-20051.
- Shoghi R, Shiri H. Modelling Touchdown Point Oscillation and Its Relationship with Fatigue Response of Steel Catenary Risers. 2019, Applied Ocean Research, 87 (2019) 142-154
- Timoshenko SP, Young DH. Theory of structures. McGraw-Hill Inc., US; 1968.
- Wang K, Xue H, Tang W. Time domain prediction approach for cross-flow VIV induced fatigue damage of steel catenary riser near touchdown point. Journal of Applied Ocean Research; 2013; (43) 166-174.
- Wang K, Low YM. Study of seabed trench induced by steel catenary riser and seabed interaction. Proceedings of the 35th International Conference on Ocean, Offshore and Arctic Engineering OMAE2016-54236; 2016 June 19-24; Busan: South Korea. doi:10.1115/OMAE2016-54236.
- Yuan F, White DJ and O'Loughlin CD. The evolution of seabed stiffness during cyclic movement in a riser touchdown zone on soft clay. Géotechnique, 2017, 67(2):127-137.
- Zargar, E. A new hysteretic seabed model for riser-soil interaction. PhD Thesis; 2017; University of Western Australia

Chapter 5

Influence of Trench Geometry on Fatigue Response of Steel Catenary Risers by Using a Boundary Layer Solution on a Sloped Seabed

Rahim Shoghi¹, Celso P. Pesce², Hodjat Shiri^{3,*}

1: Department of Civil Engineering
Memorial University of Newfoundland
e-mail: rshoghi@mun.ca

2: Department of Mechanical Engineering
University of São Paulo
e-mail: ceppesce@usp.br

3: Department of Civil Engineering
Memorial University of Newfoundland
e-mail: hshiri@mun.ca

This chapter was submitted as a journal paper to Ocean Engineering (Elsevier).

Abstract

Previous studies have shown that the geometry of the trench affects the fatigue response of steel catenary risers (SCR). Fatigue performance of SCR in the touchdown zone (TDZ) has been investigated in several studies, sometimes leading to contradictory results, with no coherent agreement regarding if the effect of the trench on fatigue performance of SCR would be beneficial or detrimental. This paper aims at developing a model based on the well-known boundary layer method (BLM) to capture the trench effect on the fatigue performance of SCR. Using analytical and numerical approaches, a meaningful relationship was observed between the slope of trench shoulders, the magnitude of the peak fatigue damage, and its location in the trench. It was also observed that the effect of trench formation on the fatigue performance of SCR could be predicted by using TDP oscillations on a sloped seabed. The study is now improved, leading to a coherent agreement about the trench effect on fatigue

Keywords: Steel catenary risers; Boundary layer method; Trench; Touchdown point; Fatigue response

5.1. Introduction

Steel catenary risers (SCRs) are welded steel pipes suspended from the vessel to the seabed. Due to environmental and operational loads, SCRs are continuously oscillating and thus are vulnerable to fatigue loads. The riser hang-off point and the touchdown zone (TDZ) are two important fatigue hot spots. However, the fatigue life assessment of the riser in TDZ is a significant challenge due to complex non-linear hysteretic riser seabed interaction. Several mechanisms contribute to the gradual formation of a trench underneath the SCR within a few years after installation. The influence of trench on fatigue response of SCR has been investigated in several studies, leading to contradictory results with no coherent agreement regarding its effect, if beneficial or detrimental. Some studies support the idea of beneficial trench effect (Langner, 2003; Wang and Low, 2016; Randolph et al., 2013), and some others oppose that (Shiri, 2014ab; Rezazadeh et al., 2012; Shiri, 2010). Finding a robust answer to this question is essential for a reliable and cost-effective SCR design. Shoghi and Shiri (2019) categorized the mechanisms involved in trench formation and mathematically proved that irrespective to the nature of the involved mechanism, the ultimate result appears in the form of two important factors: a) The average of peak shear force in the TDZ (\tilde{V}) that is related to seabed soil stiffness and b) The TDP oscillation amplitude (Δ_{TDP}) that is related to the trench geometry. The authors then showed that the direct product of these two fundamental parameters, i.e., $\tilde{V} \times \Delta_{TDP}$, mimics the same variation trend as axial stress ($\Delta\sigma$) or the fatigue damage. This product is neither equal to nor an approximation to the axial stress range. However, it is a sensible parameter that follows the variation trends identical to axial stress or fatigue damage. Also, the dominance of the TDP oscillation (Δ_{TDP}) was observed by Shoghi and Shiri (2019) through analytical and numerical studies. The

authors then developed a set of rules for qualitative assessment of the trench impact on fatigue. Shoghi and Shiri used the developed set of rules in 2019 to re-assess most of the key studies conducted on the trench effect of SCR fatigue. The study showed that depending on the dominance of the low-frequency vessel excursions that, in turn, depends on geographical location, the trench effect can be beneficial or detrimental to the ultimate fatigue life. Also, the authors showed the trench effect rather appears in the form of large relocation of peak fatigue damage. However, Shoghi and Shiri (2019) combined the conventional catenary equations, with a boundary layer solution that was previously developed for the flat seabed, by Pesce et al. (2006), while the trench inserts a sloped seabed within its shoulders in both, near and far direction. This could trigger some inaccuracies in terms of proper capturing the negative curvature right behind the TDP and consequently, the fatigue damage. In the current study, the static boundary layer solution proposed by Pesce et al., (1998), for elastic and horizontal seabeds, is further developed to account for the seabed slope in the TDZ aiming at better representing the shoulders of a real trench. Analytical and numerical analyses were conducted and compared with earlier studies. The study extended the validity of the methodology developed by Shoghi and Shiri (2019), and consequently supported the re-assessment results published by Shoghi and Shiri (2020).

5.2. Developing a Boundary Layer Model

The boundary layer solution proposed by Pesce et al. (1998) is further developed through the incorporation of the seabed slopes (clockwise and counter-clockwise) representing the trench shoulders. A numerical model is also constructed and results are compared with those obtained with the boundary layer analytical solution. Case studies are then conducted to further validate the developed model against the published data. The TDP was closely

monitored as a crucial point because: a) it is a non-material point of the SCR that sweeps the seabed surface, constrained to the trench profile or the seabed geometry, b) the maximum curvature occurs within a close neighborhood of the TDP towards the suspended part, c) the TDP position is directly affected by seabed soil stiffness, d) it has a pivotal rule in the continuity of shear force and bending moment distribution of the riser resting on a linear-elastic seabed, and e) the TDP is affected by cyclic loads and could represent the location of peak fatigue damage (fd_{max}), i.e., the point having the least fatigue life in the SCR. It was observed that the magnitude of peak fatigue damage and its location present a close relation with the oscillation of the TDP on the sloped seabed, which, in turn, is linked to the flexural response of SCR in TDZ.

Following the standard of the boundary layer techniques, the matching between inner and outer solutions, inside and outside the TDZ, is achieved by solving a system of linear equations obtained by enforcing continuity of the solution and its derivatives, up to fourth-order. First, the equations were obtained for the rigid sloped seabed, and then further extended to the sloped linear elastic seabed. Then, the response of the TDP, including oscillation amplitude and the relocation due to the seabed slope, was investigated.

5.2.1. Sloped Rigid Seabed

Depending on the dominant direction of sea states, the touchdown point (TDP) may move towards to or far from the offset zone (NOZ, FOZ). Figure 5-1 schematically shows these offset zones and the key parameters used for developing the boundary layer solution. The TDP relocation causes peak fatigue damage to relocate and affect the fatigue performance of SCR on trench shoulders. For developing the boundary layer solution, the FOZ and NOZ were simplified as straight sloped lines.

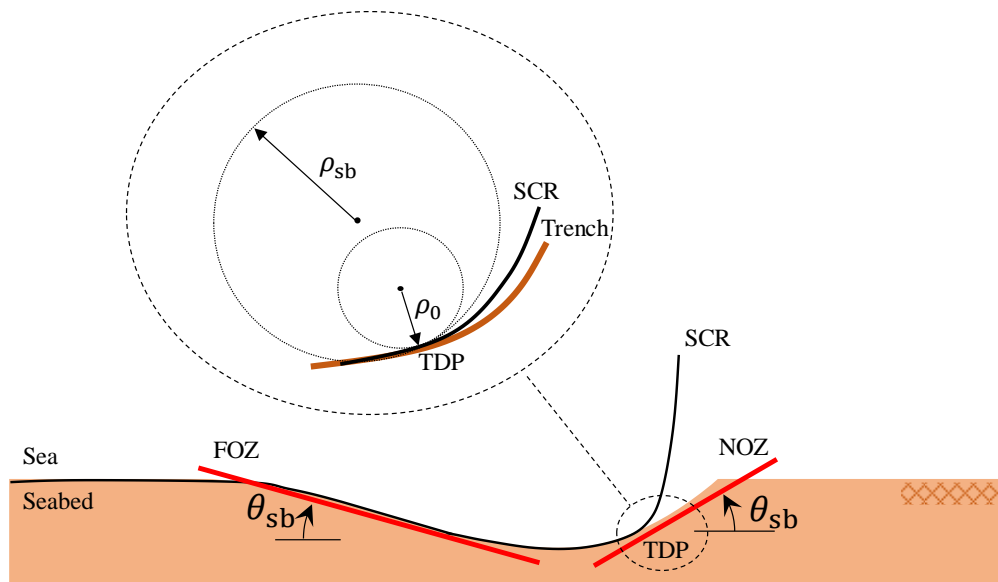


Figure 5-1. Schematic view of TDZ and trench slopes beneath the SCR

The realistic trench profile was also investigated in later stages. However, as shown by Shoghi and Shiri (2019), this kind of assumption has no negative impact on the objectives of the current study, which is to looking for the trends of the trench impact on fatigue.

Herein, the main steps of developing the model for sloped seabeds are explained. The reader is directed to Pesce et al. (1998) for derivations concerning the simpler linear elastic horizontal soil case and to the Appendix for some basic results on rigid soil, upon which both solutions are derived. Starting from the basics, it is well known that the solution to the problem of a *suspended cable* that touches a flat and rigid bed leads to a curvature discontinuity at the TDP (Pesce et al., 1998; Aranha et al. 1997; Pesce, 1997). In fact, the TDP curvature at the suspended side reaches a maximum value of $\chi_0 = 1/\rho_0 = q/T_0$, where χ_0 , ρ_0 , T_0 are respectively, curvature, radius of curvature and tension at TDP and q is the immersed weight of SCR per unit length, whereas, from the supported side, the curvature at TDP is null. If bending stiffness is considered included, the local solution for the curvature in the suspended part reads (Appendix, equation (A.9)):

$$\chi(s) = \chi_0 + c_1 e^{-(s-s_f)/\lambda} \quad (1)$$

where s_f is the new TDP arclength coordinate, herein named 'ideal' position, and λ is the flexural parameter that relates bending stiffness to geometrical rigidity effects. Let us now consider a curved seabed, and the following definitions: $\chi(s_f) = \chi_{sb}$ and $c_1 = (\chi_{sb} - \chi_0)$, which transforms equation (1) into the form:

$$\chi(s) = \chi_0 + (\chi_{sb} - \chi_0) e^{-(s-s_f)/\lambda} \quad (2)$$

where $\chi_{sb} = 1/\rho_{sb}$ is the seabed curvature at TDP, see Figure 5-1. Obviously, for a horizontal seabed, equation (2) recovers the results of Pesce et al. (1998). Following Pesce et al. (1998), this equation can once again be integrated over "s", to find the angle along the suspended part of the SCR:

$$\theta(s) = \chi_0 s - (\chi_{sb} - \chi_0)\lambda e^{-(s-s_f)/\lambda} + c_3 \quad (3)$$

Taking the flexural length λ as a length scale, in the far field, i.e., far enough from TDP, such that $(s - s_f)/\lambda \rightarrow \infty$, we can write $s \cong \rho_0 \theta(s)$. Therefore, $c_3 = 0$, (Pesce, 1997).

The matching equation $\theta(s_f) = \theta_{sb}$ gives the non-dimensional 'ideal' TDP position, s_f/λ .

The TDP relocation may be then obtained as a function of the flexural length parameter and the seabed slope as follow:

$$\frac{s_f}{\lambda} = -\left(1 - \frac{\chi_{sb}}{\chi_0} - \frac{\tan \theta_{sb}}{\lambda \chi_0}\right) = -(1 - R_\chi - R_\theta) \quad (4)$$

where $R_\chi = \chi_{sb}/\chi_0$ and $R_\theta = \tan \theta_{sb}/(\lambda \chi_0)$ are hereinafter called perturbation parameters of the seabed geometry with respect to curvature and slope of the seabed, which affect the riser solution around the seabed touching point. Likewise equation (2), equation (4) recovers the results of Pesce et al., (1998) for a horizontal seabed. Equation (4) shows

how the so-called ideal TDP is related to seabed geometric characteristics and may be relocated by considering the flexural stiffness of the riser around TDP. The non-dimensional TDP relocation equation (4) is assessed qualitatively for different seabed geometries in Table 5-1.

Table 5-1. Geometrical properties of rigid seabed.

	Straight rigid seabed property			Normalized TDP
	θ_{sb}	R_θ	R_χ	s_f/λ
Near seabed	> 0	> 0	0	> -1
Horizontal seabed	$= 0$	$= 0$	0	$= -1$
Far seabed	< 0	< 0	0	< -1
$y(s) = s \tan \theta_{sb}$	$\left(\frac{S_f}{\lambda}\right)_{\theta_{sb}>0} > \left(\frac{S_f}{\lambda}\right)_{\theta_{sb}=0} > \left(\frac{S_f}{\lambda}\right)_{\theta_{sb}<0}$ $\left \frac{S_f}{\lambda}\right _{\theta_{sb}<0} > \left \frac{S_f}{\lambda}\right _{\theta_{sb}=0} > \left \frac{S_f}{\lambda}\right _{\theta_{sb}>0}$			

The shear force at TDP on the suspended part, Q_0 , is then given by deriving equation (2) and taking $s \rightarrow s_f^+$ as:

$$Q_0 = q\lambda(1 - R_\chi - R_\theta) + T_0 \tan \theta_{sb} \quad (5)$$

On the supported part, the shear force at the TDP is zero if the seabed is rigid. Considering a sloped seabed, such that $\tan \theta_{sb} = \theta_{sb}$, and substituting R_θ in equation (5), the shear force at TDP reduces to $Q_0 = q\lambda$, in accordance with a result obtained in Pesce et al. (1998) for a horizontal seabed. It should be mentioned that the curvature is a continuous function, but there is a discontinuity in shear force distribution along the riser at TDP on the rigid seabed, which will be resolved in the next session for the linear elastic seabed. equation (3) can be integrated to find the SCR configuration, y , taking the origin at the known ideal TDP. Recalling that $c_3 = 0$, then:

$$y(s) = \chi_0 \left(\frac{s^2 - s_f^2}{2} \right) + (\chi_{sb} - \chi_0) \lambda^2 e^{-(s-s_f)/\lambda} + c_4 \quad (6)$$

Continuity of riser configuration, $y(s)$ at the ideal TDP shall be satisfied for both suspended and supported parts ($s \rightarrow s_f^\pm$). This will result in $c_4 = y_{sb}(s_f) - (\chi_{sb} - \chi_0) \lambda^2$.

Generalizing the results in Pesce et al. (1998), for a sloped seabed, the nondimensional forms of shear force, curvature, angle, and configuration functions around the ideal TDP are then given by the following equations:

$$\left| \frac{Q_0}{q\lambda} \right| = H \left(\frac{s}{\lambda} - \frac{s_f}{\lambda} \right) e^{-\left(\frac{s-s_f}{\lambda}\right)} \quad ; \quad s = s_f \quad (7)$$

$$\begin{cases} \frac{\chi(s)}{\chi_0} = \left(1 - e^{-\left(\frac{s-s_f}{\lambda}\right)} \right) & ; \quad \frac{s}{\lambda} \geq \frac{s_f}{\lambda} \\ \frac{\chi(s)}{\chi_0} = 0 & ; \quad \frac{s}{\lambda} < \frac{s_f}{\lambda} \end{cases} \quad (8)$$

$$\begin{cases} \frac{\theta(s)}{\lambda \chi_0} = \left(\frac{s}{\lambda} \right) + e^{-\left(\frac{s-s_f}{\lambda}\right)} & ; \quad \frac{s}{\lambda} \geq \frac{s_f}{\lambda} \\ \frac{\theta(s)}{\lambda \chi_0} = \frac{\theta_{sb}}{\lambda \chi_0} = R_\theta & ; \quad \frac{s}{\lambda} < \frac{s_f}{\lambda} \end{cases} \quad (9)$$

$$\begin{cases} \frac{y(s)}{\lambda^2 \chi_0 R_\theta} = \frac{\left(\frac{s}{\lambda}\right)^2 - \left(\frac{s_f}{\lambda}\right)^2}{2R_\theta} - \frac{e^{-\left(\frac{s-s_f}{\lambda}\right)}}{R_\theta} + \frac{R_\theta^2 - R_\theta + 1}{R_\theta} & ; \quad \frac{s}{\lambda} \geq \frac{s_f}{\lambda} \\ \frac{y(s)}{\lambda^2 \chi_0 R_\theta} = \frac{s}{\lambda} & ; \quad \frac{s}{\lambda} < \frac{s_f}{\lambda} \end{cases} \quad (10)$$

The local shear force distribution in TDZ, as well as the curvature, angle and configuration of the riser, for both, suspended and supported part on the straight sloped rigid seabed, were then obtained. These quantities are clearly affected by seabed geometry through the ‘ideal’ TDP position and the perturbation parameters.

5.2.2. Sloped Elastic Seabed

Continuity of shear force at TDP holds if the soil is considered to be deformable, (Pesce et al., 1998). It can also be shown that the flexural stiffness effect slightly alters the curvature diagram. The TDP moves towards the supported zone, causing an elastic inflection over the support. As in Pesca et al. (1998), a simplified model will be here considered, in which the soil reaction on the line is characterized only by a linear restoration coefficient k . Considering $y(s)$ as the elastic curve function, the static penetration of the riser into the soil, far enough from TDP is simply $y_{st} = -q/k$. For simplicity, it is assumed that the supported part of the riser on the seabed does not stand out from the ground if $s \leq s_f$, where s_f indicates the position of the contact or touchdown point. Equation (11) below, governs the static equilibrium of the riser on the supported elastic seabed. Notice that, in the contact region, within a second-order error in $\theta \cong dy/dx$, the following approximations are valid: $s \cong x$ and $\chi(s) \cong \chi(x) \cong d^2y/dx^2$, where x is horizontal coordinate. Therefore, the equation under consideration can be written as:

$$\frac{d^4y}{dx^4} - \frac{d}{dx} \left(\frac{1}{\lambda^2} y' \right) + \frac{k_s}{EI} y = \frac{k_s}{EI} y_{sb} - \frac{q}{EI} \quad (11)$$

In equation (11), y_{sb} is the seabed configuration function (straight line). In dimensionless form, with $\xi = x/\lambda$ and $\eta = y/\lambda$, equation (11) is written:

$$\eta^{(IV)} - \eta'' + K\eta = -\chi_0\lambda + K\eta_{sb} \quad (12)$$

where the dimensionless parameter of stiffness, K , is defined as $K = \lambda^4 k/EI = \lambda^2 k/T_0 = kEI/T_0$, Pesca et al., (1998). For usual applications, K is much larger than one ($K \gg 1$), so equation (12) can be approximated as follows:

$$\eta^{(IV)} + K\eta \cong -\chi_0\lambda + K\eta_{SB} \quad (13)$$

The solution to this equation shall satisfy the following conditions:

$$\lim_{\xi \rightarrow -\infty} \eta(\xi) \cong -\chi_0\lambda + \lim_{\xi \rightarrow -\infty} K\eta_{SB} \quad (14)$$

$$\lim_{\xi \rightarrow \xi_f} \eta(\xi) \cong \eta_{sb}(\xi_f) \quad (15)$$

For the linear elastic sloped seabed, equation (16) below, is considered as the first approximation for a general form of the seabed:

$$\eta_{sb}(\xi) = \tan \theta_{sb} \xi = m\xi \quad (16)$$

The solution on the supported part (measured relative to the static penetration due to the riser weight) and its derivatives take the following forms:

$$\eta(\xi) = c_1 e^{r(\xi - \xi_f)} \sin(r(\xi - \xi_f)) + m\xi \quad (17)$$

$$\eta'(\xi) = c_1 r e^{r(\xi - \xi_f)} (\sin r(\xi - \xi_f) + \cos r(\xi - \xi_f)) + m \quad (18)$$

$$\eta''(\xi) = 2c_1 r^2 e^{r(\xi - \xi_f)} \cos r(\xi - \xi_f) \quad (19)$$

$$\eta'''(\xi) = 2c_1 r^3 e^{r(\xi - \xi_f)} (\cos r(\xi - \xi_f) - \sin r(\xi - \xi_f)) \quad (20)$$

$$\eta^{(IV)}(\xi) = -4c_1 r^4 e^{r(\xi - \xi_f)} \sin r(\xi - \xi_f) \quad (21)$$

where $r = K^{0.25}/\sqrt{2}$. At the TDP, $\eta(\xi_f) = m\xi_f$; $\eta'(\xi_f) = c_1 r + m$; $\eta''(\xi_f) = 2c_1 r^2$; $\eta'''(\xi_f) = 2c_1 r^3$; $\eta^{(IV)}(\xi_f) = 0$.

On the other hand, the solution on the suspended part is:

$$\eta_{scr}(\xi) = \chi_0\lambda \frac{\xi^2 - \xi_f^2}{2} + (\chi_{sb} - \chi_0)\lambda e^{-(\xi - \xi_f)} + \frac{c_4}{\lambda} \quad (22)$$

$$\eta'_{scr}(\xi) = \chi_0\lambda\xi - (\chi_{sb} - \chi_0)\lambda e^{-(\xi - \xi_f)} \quad (23)$$

$$\eta''_{scr}(\xi) = \chi_0\lambda + (\chi_{sb} - \chi_0)\lambda e^{-(\xi - \xi_f)} \quad (24)$$

$$\eta'''_{scr}(\xi) = -(\chi_{sb} - \chi_0)\lambda e^{-(\xi - \xi_f)} \quad (25)$$

$$\eta^{(IV)}_{scr}(\xi) = (\chi_{sb} - \chi_0)\lambda e^{-(\xi - \xi_f)} \quad (26)$$

In equations (22) to (26), ξ_f is the *TDP relocation*, which is the sought unknown parameter.

Also,

$$\eta_{scr}(\xi_f) = (\chi_{sb} - \chi_0)\lambda + c_4/\lambda; \quad \eta'_{scr}(\xi_f) = \chi_0\lambda\xi_f - (\chi_{sb} - \chi_0)\lambda;$$

$$\eta''_{scr}(\xi_f) = \chi_0\lambda + (\chi_{sb} - \chi_0)\lambda; \quad \eta'''_{scr}(\xi_f) = -(\chi_{sb} - \chi_0)\lambda; \quad \eta^{(IV)}_{scr}(\xi_f) = (\chi_{sb} - \chi_0).$$

Moreover, equations (17) and (22) for the suspended and the supported parts, should both satisfy the seabed profile equation, at the ideal TDP.

$$\eta_{scr}(\xi_f) = \eta_{Support}(\xi_f) = \eta_{trench}(\xi_f) \quad (27)$$

Matching both sets of equations, for the suspended and the supported parts, at the ideal TDP, results in a linear system of equations as follows:

$$\begin{cases} (\chi_{sb} - \chi_0)\lambda + \frac{c_4}{\lambda} = m\xi_f \\ \chi_0\lambda\xi_f - (\chi_{sb} - \chi_0)\lambda = c_1r + m \\ \chi_0\lambda + (\chi_{sb} - \chi_0)\lambda = 2c_1r^2 \\ -(\chi_{sb} - \chi_0)\lambda = 2c_1r^3 \end{cases} \quad (28)$$

The solution of equation (28) gives then the non-dimensional TDP relocation, ξ_f , as a function of soil stiffness and seabed slope:

$$\xi_f = \frac{K^{-0.25} - K^{0.25}}{\sqrt{2} + K^{0.25}} + R_\theta \quad (29)$$

It should be mentioned that the geometric parameter R_θ , is a function of the seabed slope

and recovers asymptotically the known solution for a horizontal seabed, taking $\theta = 0$, (Pesce et al., 1998). Also, for the straight flat seabed, when $K \gg 1$ and $\theta = 0$, $\xi_f \rightarrow -1^+$, recovering the result in Pesce et al., (1998). The effect of soil deformability causes the contact point ('ideal' TDP) to move towards the vessel direction. However, at this new contact point, the line is not tangent to the seabed (for enough soft soils). The complete asymptotic solution around the new TDP, on elastic seabed, takes then the following form:

$$\begin{cases} \frac{y}{\lambda} = \eta(\xi) = \chi_0 \lambda \frac{\xi^2 - \xi_f^2}{2} + \frac{-\chi_0 \lambda K^{0.25}}{\sqrt{2} + K^{0.25}} e^{-(\xi - \xi_f)} + \bar{c}_{41} & ; \frac{s}{\lambda} \geq \frac{s_f}{\lambda} \\ \frac{y}{\lambda} = \eta(\xi) = \frac{\chi_0 \lambda \sqrt{\frac{2}{K}}}{\sqrt{2} + K^{0.25}} e^{r(\xi - \xi_f)} \sin(r(\xi - \xi_f)) + m\xi & ; \frac{s}{\lambda} < \frac{s_f}{\lambda} \end{cases} \quad (30)$$

$$\begin{cases} \theta(\xi) \cong \eta'(\xi) = \chi_0 \lambda \xi + \frac{\chi_0 \lambda K^{0.25}}{\sqrt{2} + K^{0.25}} e^{-(\xi - \xi_f)}; & \frac{s}{\lambda} \geq \frac{s_f}{\lambda} \\ \theta(\xi) \cong \eta'(\xi) = \frac{\chi_0 \lambda \sqrt{\frac{2}{K}} r e^{r(\xi - \xi_f)}}{\sqrt{2} + K^{0.25}} (\sin r(\xi - \xi_f) + \cos r(\xi - \xi_f)) + m; & \frac{s}{\lambda} < \frac{s_f}{\lambda} \end{cases} \quad (31)$$

$$\begin{cases} \chi(\xi) \cong \frac{\eta''(\xi)}{\lambda} = \chi_0 \left(1 - \frac{K^{0.25}}{\sqrt{2} + K^{0.25}} e^{-(\xi - \xi_f)} \right) & ; \frac{s}{\lambda} \geq \frac{s_f}{\lambda} \\ \chi(\xi) \cong \frac{\eta''(\xi)}{\lambda} = \frac{\chi_0 \sqrt{2}}{\sqrt{2} + K^{0.25}} e^{r(\xi - \xi_f)} \cos r(\xi - \xi_f) & ; \frac{s}{\lambda} < \frac{s_f}{\lambda} \end{cases} \quad (32)$$

$$\begin{cases} \frac{Q_0}{q\lambda} = \eta'''(\xi) = \frac{\lambda \chi_0 K^{0.25}}{\sqrt{2} + K^{0.25}} e^{-(\xi - \xi_f)} & ; \frac{s}{\lambda} \geq \frac{s_f}{\lambda} \\ \frac{Q_0}{q\lambda} = \eta'''(\xi) = \lambda \chi_0 \frac{K^{0.25}}{\sqrt{2} + K^{0.25}} e^{r(\xi - \xi_f)} (\cos r(\xi - \xi_f) - \sin r(\xi - \xi_f)); & \frac{s}{\lambda} < \frac{s_f}{\lambda} \end{cases} \quad (33)$$

in which $r = K^{0.25}/\sqrt{2}$. In the next section, the developed boundary layer solution will be used to investigate the influence of trench geometry on SCR response, by monitoring TDP relocation. The BLM solution will be compared with the numerical results obtained by using OrcaFlex® software.

5.3. Perturbation of the TDP on the sloped seabed

The effect of TDP relocation, on both sloped clockwise (FOZ) and counter-clockwise (NOZ) seabed is investigated by locally studying the static distribution of the riser angle, the shear force and the curvature. A numerical model was constructed in OrcaFlex® for a typical SCR, (Pesce et al. (2006)). Figure 5-2 shows the configuration of the numerical model with the main parameters given in Table 5-2.

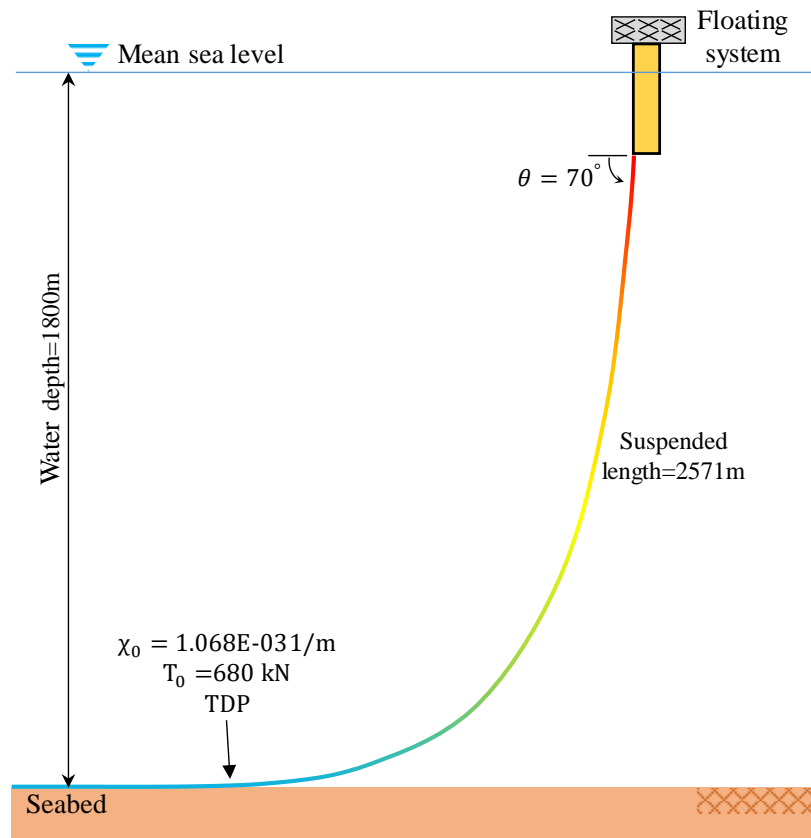


Figure 5-2. SCR configuration in numerical simulation

Table 5-2. Typical SCR data (Pesce et al., 2006).

Subject	Dimension	Value
Top angle	[deg]	70
Riser length (total)	[m]	5047
Depth	[m]	1800
Immersed weight per unit length	[N/m]	727
Bending stiffness	[Nm ²]	9.915E+06
Axial rigidity*	[N]	2.314E+09
TDP effective tension	[N]	6.80E+05
External diameter	[m]	0.2032
Suspended length	[m]	2571
Flexural length	[m]	3.82
Curvature Max	[1/m]	1.068E-03

*Axial rigidity, 2.314E+11, used in OrcaFlex® modelling.

A range of model parameters was considered to perform a sensitivity analysis and compare the results of the numerical model with the developed BLM solution.

5.3.1. Effect of Seabed Geometry and Soil Stiffness

The sensitivity of TDP location to different seabed slopes and soil stiffness is studied with both BLM and numerical analysis. Inextensibility of SCR in OrcaFlex® was enforced by considering the axial stiffness as hundred times the value of the real riser's in order to use inextensible Clebsh-Love formulation, (Love, 1927). The different seabed with positive slope (which represents a near shoulder, NOZ), negative slope (which represents a far shoulder, FOZ), and null slope (representing the ideal trench bottom) were considered. Figure 5-3 shows the non-dimensional results for horizontal, positive and negative seabed slopes obtained with the BLM analytical solution; where $\theta/\chi_0\lambda$ represents the non-dimensional angle with respect to the horizontal, χ/χ_0 the non-dimensional curvature, $Q/q\lambda$ the non-dimensional shear force and $\eta_{SCR}/\chi_0\lambda^2R_\theta$ the non-dimensional configuration of the SCR, whereas $\eta_{SCR}/\chi_0\lambda^2R_\theta$ represents the non-dimensional configuration of the seabed, respectively.

It should be taken into account that the vessel position is considered fixed for both analysed cases, positive and negative slope variations, and TDP relocations are obtained locally as a pure influence of seabed due to riser flexural stiffness in TDZ. Figure 5-3 shows that the non-dimensional slope of the riser is matched with the non-dimensional slope of the seabed for the supported part of the riser.

The curvature is matched with zero at TDP on the flat seabed. Also, it had already been observed, Pesce et al. (1998), that the typical matching length is about 4 to 5λ . This means that beyond this length along the riser, regardless the seabed configuration, results will merge smoothly. In other words, the trench geometry affects the fatigue performance of riser locally, and fatigue study should be investigated somewhere around or close to the TDP in TDZ, within a range of circa 5λ .

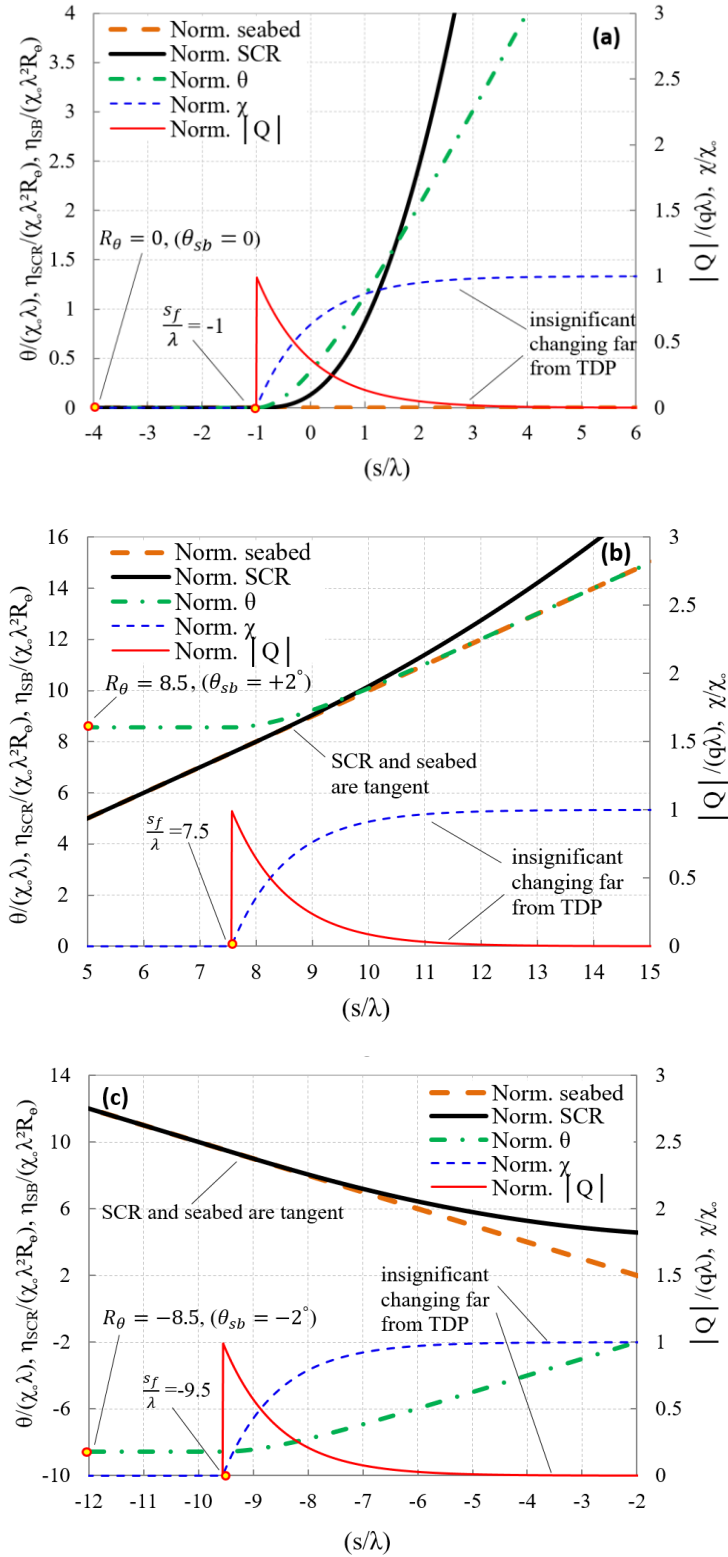


Figure 5-3. Non-dimensional BLM solutions around TDP for different seabed slopes, (a) horizontal seabed; (b) positive slope seabed (2 degrees), (c) negative slopes (2 degrees)

Figure 5-4 represents: the non-dimensional TDP position on the horizontal seabed, s_f/λ ; and the normalized TDP position, on positive and negative sloped seabeds, $s_f/(\lambda R_\theta)$; for a range of seabed soil stiffness.

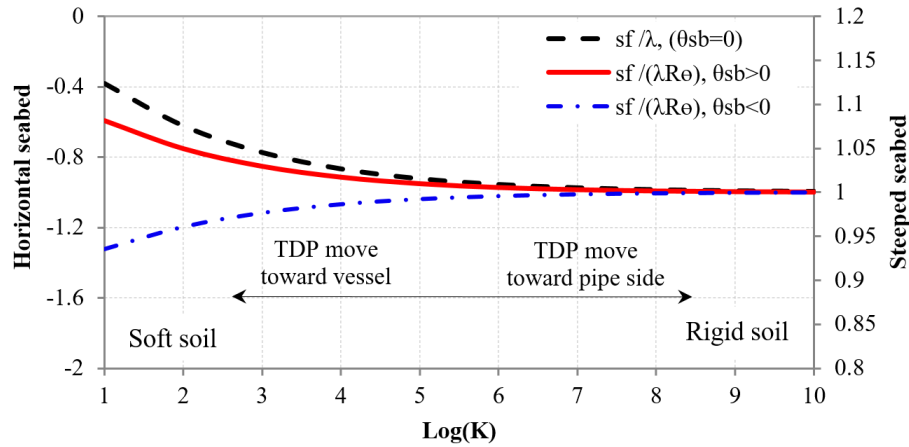


Figure 5-4. TDP relocation trend on the elastic seabed, obtained via BLM

It should be mentioned that in this figure, the non-dimensional TDP position on the horizontal seabed is related to the first term in equation (29) referring to the soil property in the horizontal seabed ($R_\theta = 0$), recovering results obtained in Pesce et al. (1998). When the soil is considered very rigid ($K \gg 1$), this term recovers the equation for infinitely rigid seabed, Pesce et al. (1998). In this case, for $K \rightarrow \infty$, $\frac{K^{-0.25} - K^{0.25}}{\sqrt{2} + K^{0.25}} \rightarrow -1$. For the sloped seabed ($\pm 2^\circ$), the TDP position is normalized by that on a rigid seabed; for these slopes, $R_\theta = \pm 8.56$. The TDP relocates towards the vessel in NOZ (positive slope seabed) and FOZ (negative slope seabed), as the soil gets softer. The non-dimensional results of the curvature, slope and shear force distributions around the TDP, obtained via BLM, are compared with OracFlex®, in Figure 5-5 to Figure 5-7.

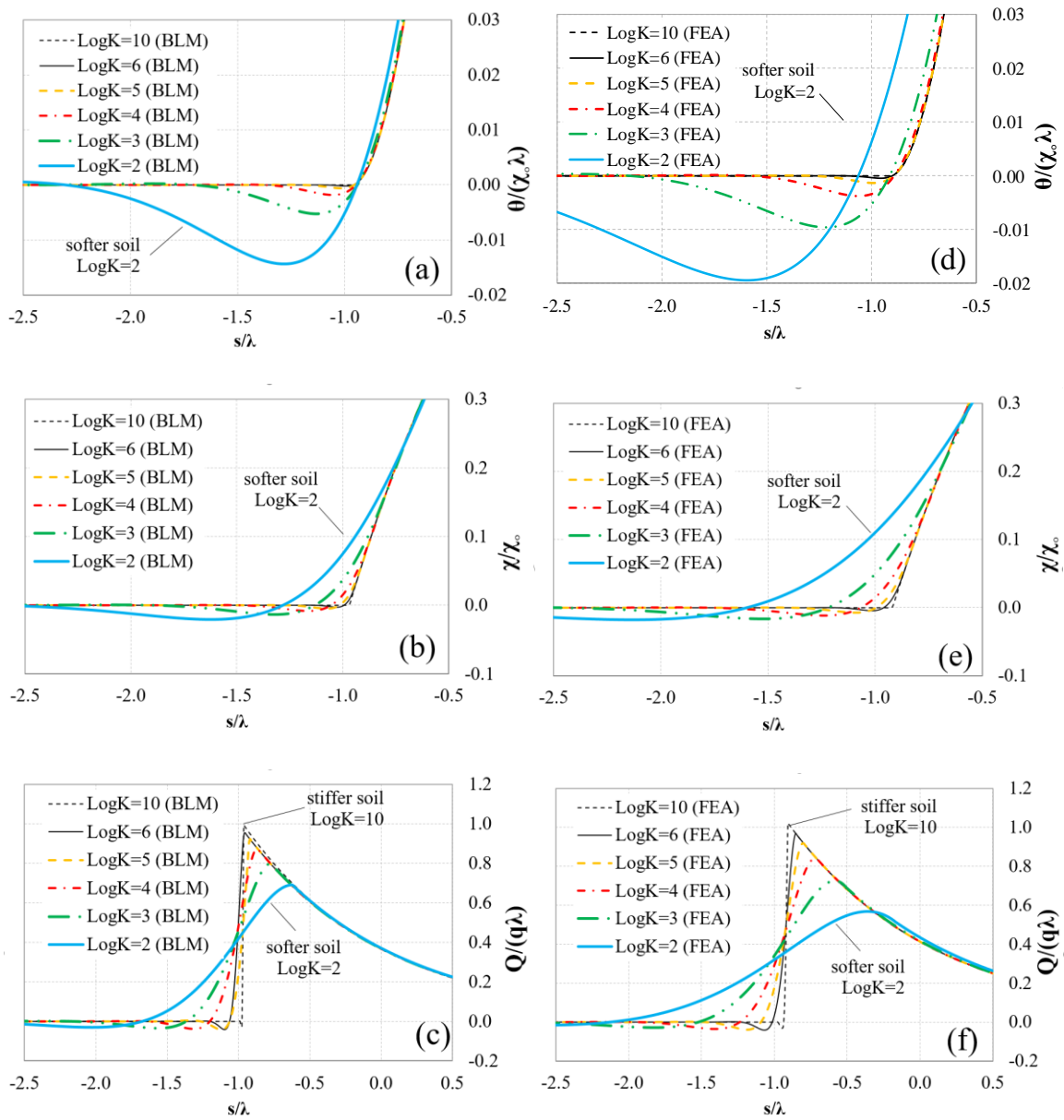


Figure 5-5. Inclination angle, curvature and shear force distribution. Non-dimensional results for a riser configuration close to the TDP on the horizontal seabed. Left: BLM; right: FEA

Figure 5-5 shows the non-dimensional results of BLM and OracFlex® on the flat seabed. The obtained non-dimensional real TDP location via BLM in Figure 5-3 (a), $s_f/\lambda = -1$,

is precise and close to the numerical result. Figure 5-5 (a) and (d) show the non-dimensional slope along the riser in the TDZ. The peak value of the negative slope in the riser and region of the negative slope increases for softer soils due to further riser penetration. Figure 5-5 (b) and (e) show a smooth distribution of the curvature variation around TDP; the softer the soil, the smoother is the curvature variation. As shown in Figure 5-5 (c) and (f), the maximum shear force occurs on the suspended part of the riser near to the TDP. This point further approaches the TDP as the soil stiffness increases. The results of BLM and finite element analysis are in an excellent agreement for higher values of seabed stiffness. However, the less agreement obtains as the seabed becomes very soft. This happens because of less adaptability of the elastic soil assumption on very soft soils, i.e., $s \cong x$ and $\chi(s) \cong \chi(x) \cong d^2y/dx^2$.

Figure 5-6 compares the non-dimensional results of BLM and OracFlex® on the positive sloped seabed (NOZ). The location of non-dimensional real TDP that was obtained by BLM in Figure 5-3 (b), $s_f/\lambda = 7.5$, is precise and close to the numerical result.

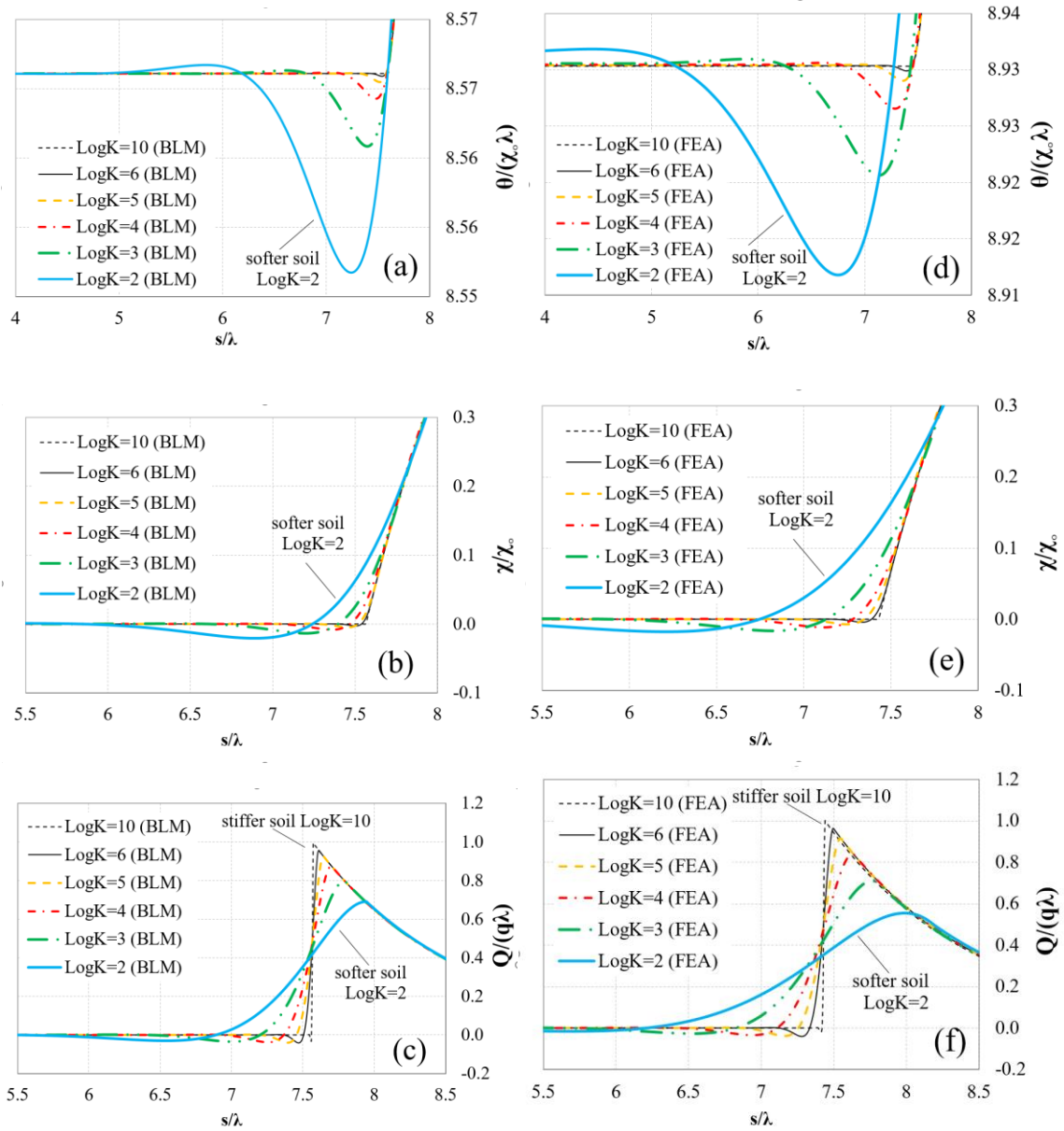


Figure 5-6. Inclination angle, curvature and shear force distribution. Non-dimensional results of riser configuration close to the TDP on NOZ shoulder (positive slope seabed).

Left: BLM; right: FEA

As shown in Figure 5-6 (a) and (d), the softer soil results in further riser penetration and a smoother curvature variation on the positive sloped seabed (NOZ). Also, the maximum shear force is still approaching the TDP on the stiffer seabed. Figure 5-7 shows the non-

dimensional results of BLM and OracFlex® on the negative sloped seabed (FOZ), where the location of non-dimensional real TDP obtained from BLM (Figure 5-3 (c)), $s_f/\lambda = -9.5$, is well close to the numerical result.

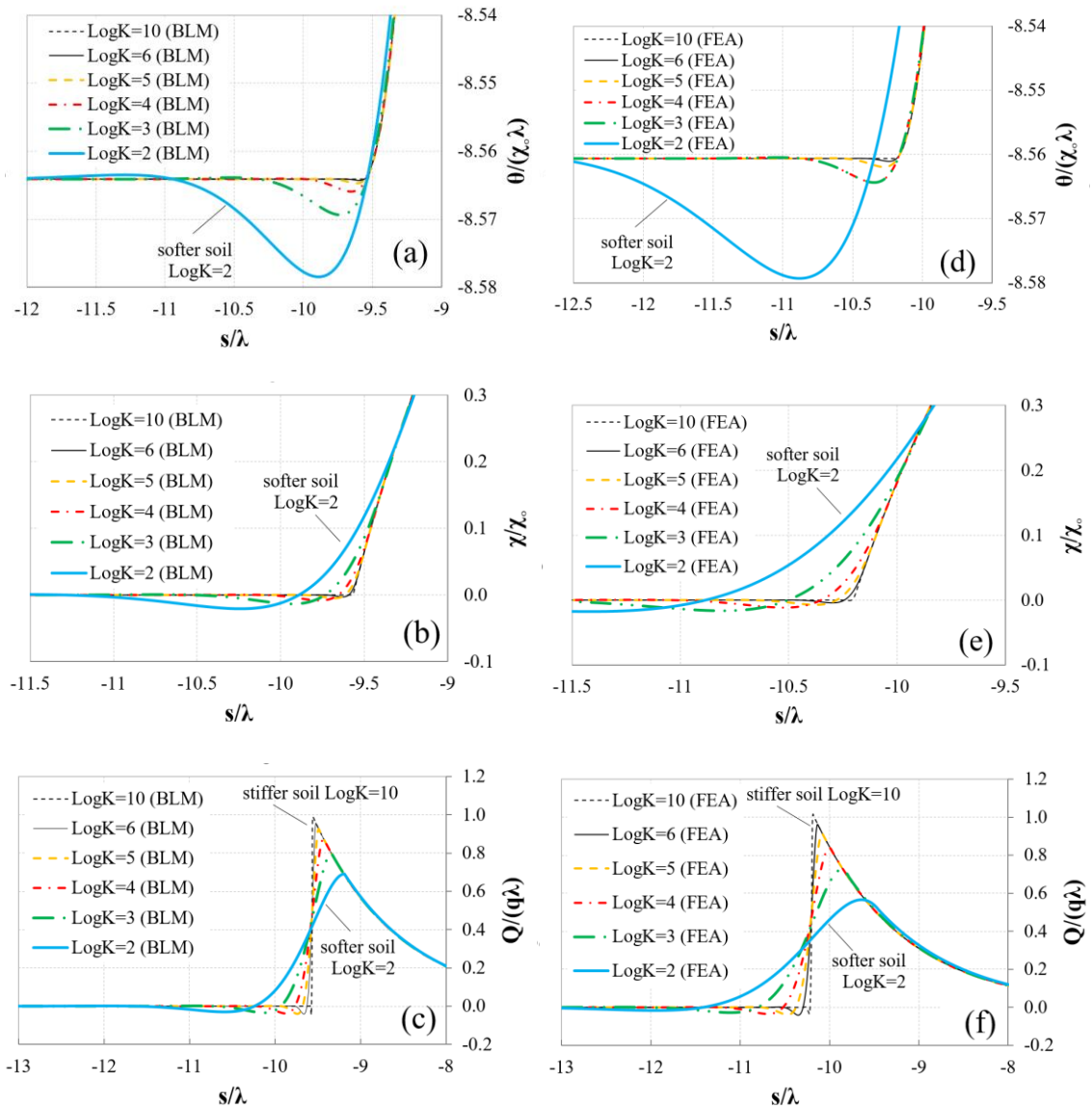


Figure 5-7. Inclination angle, curvature and shear force distribution. Non-dimensional results of riser configuration close to the TDP on FOZ shoulder (negative slope seabed).

Left: BLM; right: FEA

Similar trends were observed on the negative sloped seabed with a good agreement between the BLM analytical solution and FEA results. These validation results show that the developed BLM has sufficient accuracy to be used for qualitative assessment of the trench impact on fatigue, and even the fatigue life assessment of the riser in early design stages. However, an accurate assessment of the ultimate fatigue life needs performing numerical fatigue analysis.

5.3.2. Discussion on TDP Relocation on Sloped Seabed

The non-dimensional local TDP relocation obtained in equation (4) can be rewritten in terms of TDP effective tension as follow:

$$\frac{s_f}{\lambda} = - \left(1 - \frac{\tan \theta_{sb}}{q\sqrt{EI}} T_0^{1.5} \right) \quad (34)$$

Equation (34) shows that in the case of creating a NOZ shoulder ($\theta_{sb} > 0$), the TDP relocation will be positive, meaning that the TDP moves towards the vessel. On the other hand for FOZ shoulder ($\theta_{sb} < 0$), the TDP moves to the riser's anchored end. For the analytical investigation of TDP relocation, the magnitude of slope in the near side (NOZ) was considered approximately two times greater than the far side (FOZ) due to the general configuration of the proposed ladle shape trenches in the literature (see Figure 5-8).

Figure 5-8 shows that the proposed mathematical trenches may include a convex point, curvature, and different slopes in FOZ and NOZ. An analytical study was conducted to find TDP relocation (s_f/λ) trend on the created FOZ and NOZ seabed, for a typical SCR configuration shown in Figure 5-2. The three pairs of slopes were considered including 0.5, 1, and 1.5 degrees clockwise for creating FOZ; and 1, 2, and 3 degrees counter-clockwise for creating NOZ. It was assumed that the slope of NOZ shoulder is twice the FOZ one.

The TDP relocations for each of the created seabed were calculated using equation (34) and normalized by TDP relocation in FOZ. The obtained results are shown in Table 5-3 for each pair. Table 5-3 shows that the TDP relocation on FOZ is smaller than on NOZ. Also, an increase of the seabed slope results in a significant TDP relocation, which either migrates towards the vessel, on NOZ, or moves away from the vessel, on FOZ.

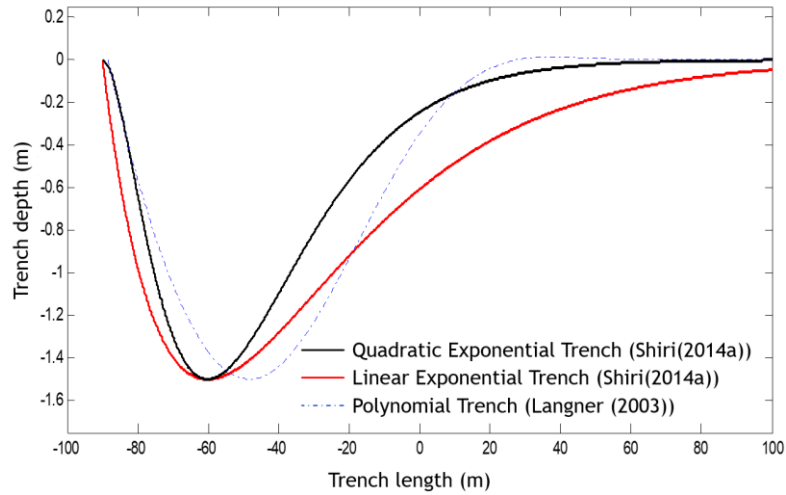


Figure 5-8. Comparison of different mathematical seabed geometry (Shoghi and Shiri, 2019)

Table 5-3. Normalized TDP relocation on the sloped seabed.

Shoulder	Slope (deg)	Tension at TDP (N)		λ (m)	$\left \frac{S_f}{\lambda} \right $	Normalized TDP relocation
Far	$\theta_{sb} = 0.5$	T_0	680000	3.82	3.14	1.00
Near	$\theta_{sb} = 1.0$	T_0	680000	3.82	3.28	1.05
Far	$\theta_{sb} = 1.0$	T_0	680000	3.82	5.28	1.00
Near	$\theta_{sb} = 2.0$	T_0	680000	3.82	7.55	1.43
Far	$\theta_{sb} = 1.5$	T_0	680000	3.82	7.41	1.00
Near	$\theta_{sb} = 3.0$	T_0	680000	3.82	11.84	1.60

The TDP relocation ratio of FOZ to NOZ as a function of seabed slope ($\theta_{sb} < 0$ for FOZ) was written as follows:

$$\frac{\left(\frac{S_f}{\lambda}\right)_{FOZ}}{\left(\frac{S_f}{\lambda}\right)_{NOZ}} = \frac{1 + \frac{\tan \theta_{sb}}{q\sqrt{EI}} T_0^{1.5}}{1 - \frac{\tan 2\theta_{sb}}{q\sqrt{EI}} T_0^{1.5}} \quad (35)$$

Figure 5-9 shows the analytical trend of the TDP relocation ratio, given by equation (35), versus a range of slopes.

The results show that the TDP relocation ratio given in equation (35) remains less than 1, for $0^\circ < \theta < 45^\circ$, which means the TDP relocation on FOZ is less than TDP relocation on NOZ. This is an interesting finding because the majority of distorted fatigue results in the literature have been reported to happen in the NOZ and trench mouth (Randolph et al., 2013; Sharma and Aubeny, 2011). These results show the significance of the methodology that is used to incorporate the trench effect in fatigue analysis. Simple incompatibilities between the trench profile and the riser profile in NOZ will result in non-reliable predictions because of unwanted pressure hot spots in the trench mouth (Shoghi and Shiri, 2019, 2020).

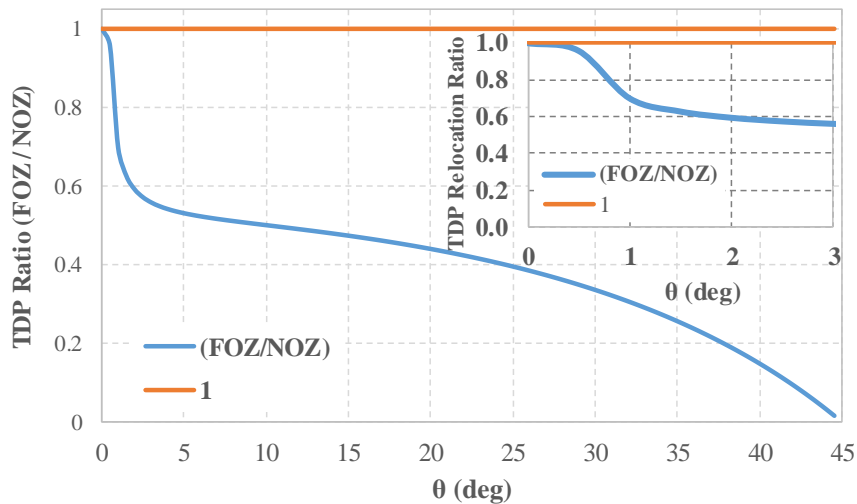


Figure 5-9. The magnitude of TDP relocation ratio

5.3.3. Discussion on TDP Oscillation Amplitude

The TDP oscillation amplitude (Δ_{TDP}) under the vessel motion towards the far and near offset was investigated analytically. Figure 5-10 and Figure 5-11 show a local view of the FOZ and NOZ shoulders both sloped in clockwise and counter-clockwise directions around the TDP. The TDP oscillation trends were investigated on the trench shoulders by using the developed BLM. Identical vessel motions were used to obtain the TDP oscillation amplitude in both FOZ and NOZ, quasi-statically (without applying low-frequency excursions).

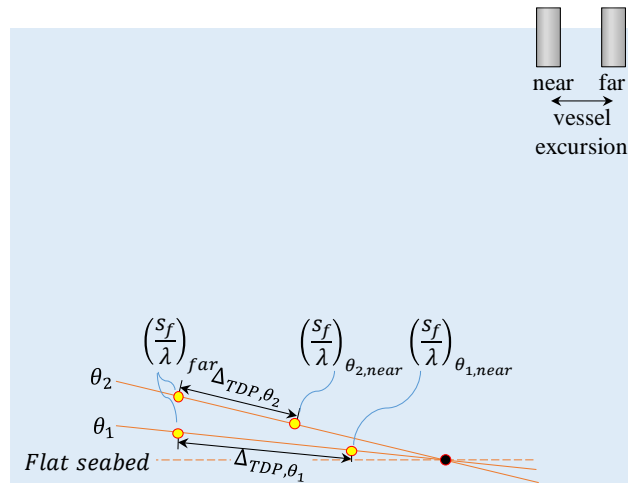


Figure 5-10. Schematic view of created FOZ shoulder respect to vessel positions

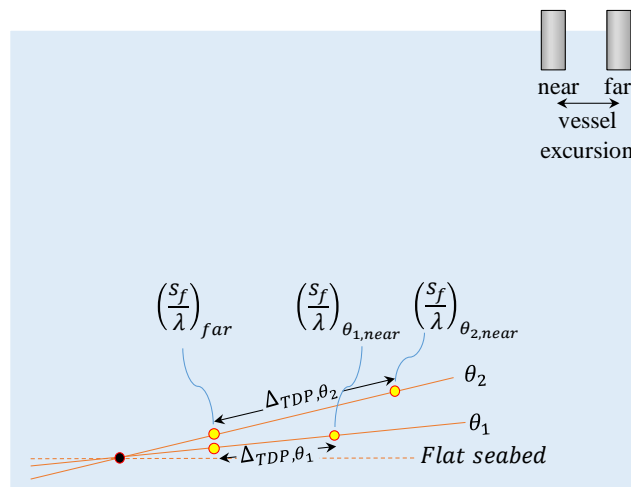


Figure 5-11. Schematic view of created NOZ shoulder respect to vessel positions

The study was conducted in two steps; first, the initial TDP relocation on the trench shoulder (sloped seabed) was found for the near vessel offset; second, A TDP was set for the far vessel position on sloped shoulders. The initial TDP location for far vessel excursions is assumed to be almost the same in the different sloped seabed because of its less significance. The primary influence of the seabed on TDP oscillation amplitude is on the initial TDP relocation. The TDP oscillation amplitude (Δ_{TDP}) was defined as the difference between the position of the TDP in both near and far vessel offsets as follow:

$$\Delta_{TDP,\theta_2} = \left(\frac{S_f}{\lambda}\right)_{\theta_2,near} - \left(\frac{S_f}{\lambda}\right)_{far} \quad (36)$$

$$\Delta_{TDP,\theta_1} = \left(\frac{S_f}{\lambda}\right)_{\theta_1,near} - \left(\frac{S_f}{\lambda}\right)_{far} \quad (37)$$

where the first and the second subscripts denote the sloped seabed and the vessel position; and $|\theta_2| > |\theta_1|$. Ignoring the slope effect on TDP position of the far vessel offset for NOZ or FOZ, the following equation was obtained:

$$\Delta_{TDP,\theta_2} - \Delta_{TDP,\theta_1} = \left(\frac{S_f}{\lambda}\right)_{\theta_2,near} - \left(\frac{S_f}{\lambda}\right)_{\theta_1,near} \quad (38)$$

Substituting equation (34) into equation (38), and rearranging, a meaningful relationship was obtained as follow:

$$\Delta_{TDP,\theta_2} - \Delta_{TDP,\theta_1} = \frac{T_0}{q\lambda} (\tan \theta_2 - \tan \theta_1) \quad (39)$$

A qualitative assessment of TDP oscillation amplitude on FOZ or NOZ, respecting the seabed slope on each zone, resulted in the following relations:

$$\begin{cases} \Delta_{TDP,\theta_2} < \Delta_{TDP,\theta_1} & ; \text{ in FOZ } (\theta_2 < \theta_1) \\ \Delta_{TDP,\theta_2} > \Delta_{TDP,\theta_1} & ; \text{ in NOZ } (\theta_2 > \theta_1) \end{cases} \quad (40)$$

Equation (40) shows that the absolute value of the seabed slope on NOZ or FOZ affects the TDP oscillation amplitude in each zone. Equation (40) also indicates that the TDP oscillation amplitude decreases with a steeper slope in FOZ, and increases with a steeper slope in NOZ, which is in a perfect agreement with the findings of Shoghi and Shiri (2019). In other words, as shown by Shoghi and Shiri (2019), the TDP oscillation amplitude (Δ_{TDP}) dominates the peak average shear force and properly mimics the overall variation trend of the axial stress range ($\Delta\sigma$) or the fatigue damage. This will be examined in the next section through FEA fatigue analysis and by reviewing a critical case study published in the literature, Randolph et al., 2013.

5.4. Numerical Fatigue Analysis and the Trench Effect

A series of finite element fatigue analysis was conducted using OrcaFlex®. The typical SCR model shown in Figure 5-2 was studied to verify the validity of analytical findings through a fatigue analysis instead of axial stress range variation ($\Delta\sigma$). The rigid seabed was taken and hinge boundaries were considered at both ends of the riser at the hang-off point and the anchored end. The hydrodynamic coefficients of drag, inertia, and added mass were taken as 1.2, 1.0, and 1.0, respectively. Three different seabed geometries were incorporated in the TDZ through relocating the seabed slope around the TDP by 0.5, 1, and 1.5 degrees clockwise (for creating FOZ) and 1, 2, and 3 degrees counter-clockwise (for creating NOZ), see Figure 5-12.

For simplicity, the vessel was excited by a single wave frequency motion (a wave of 6 m height and 7 s period). Figure 5-13 shows the results of the fatigue analysis and the corresponding local seabed slopes.

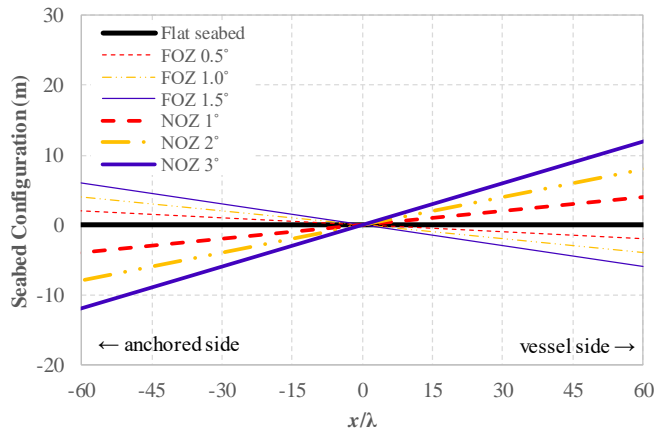


Figure 5-12. Incorporated seabed for NOZ and FOZ

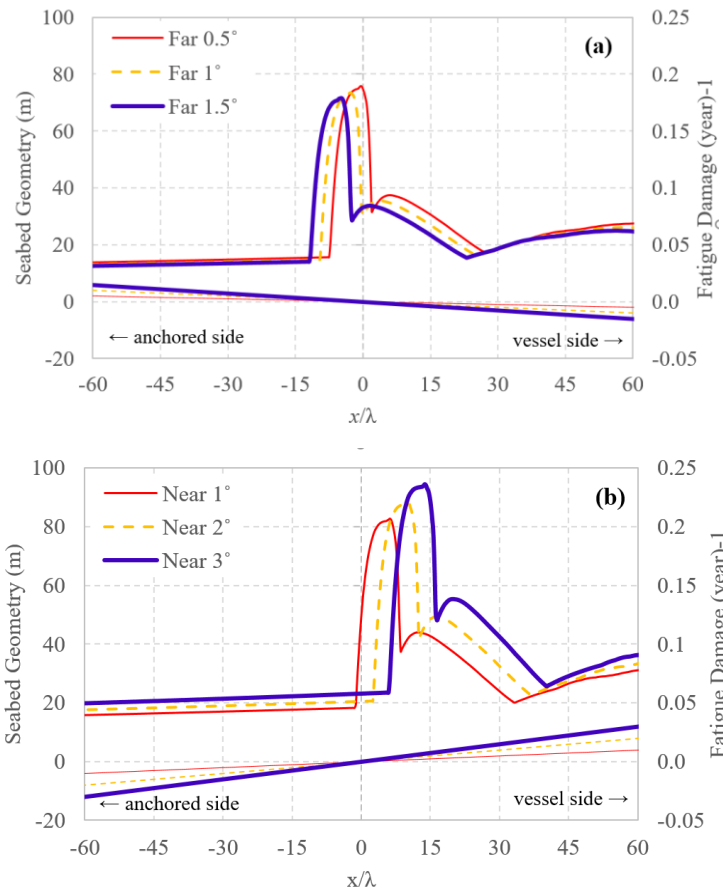


Figure 5-13. Fatigue damage distribution on SCR for different seabed configuration; (a) represents FOZ shoulder, (b) represents NOZ shoulder

Figure 5-13 shows that different local seabed configurations result in a different fatigue performance for an identical wave frequency vessel motion. The low-frequency vessel excursion was not considered in this analysis to obtain the pure influence of the seabed on fatigue. It was observed that the magnitude of the peak fatigue damage is less on FOZ compared to that NOZ. The peak fatigue damage (fd_{max}), which presents the least fatigue life, can be qualitatively expressed on a sloped seabed as follow:

$$\begin{cases} fd_1^\circ < fd_2^\circ < fd_3^\circ & ; \text{ for NOZ shoulder} \\ fd_{0.5^\circ} > fd_1^\circ > fd_{1.5^\circ} & ; \text{ for FOZ shoulder} \end{cases} \quad (41)$$

The location of the peak fatigue damage moves toward the vessel for the created local NOZ, as a result of the positive slope of shoulders. Results show that the steeper seabed causes more relocation (see strong solid line curve in Figure 5-13 (b)), which is in agreement with the analytical result in the previous section. The location of the peak fatigue damage moves away from the vessel for created local FOZ, as a result of the negative slope of the trench shoulders. In the FOZ case, the steeper seabed causes more relocation (see strong solid line curve in Figure 5-13 (a)). Figure 5-13 shows that the fatigue damages curves for SCR on FOZ are narrow and the relocation is less compared with NOZ. This is in agreement with the earlier observations (see Figure 5-9).

5.5. Re-assessing of a Case Study

In this section, a previously published study that has investigated the trench effect on SCR fatigue will be re-assessed using the findings of the current study (Randolph et al., 2013). Randolph et al. (2013) examined the effect of different trenches and various vessel oscillations, including combined WF + LF motions on SCR fatigue (see Figure 5-14). Randolph et al., (2013) studied cases in the Gulf of Mexico (GoM) and Western Australia

(WA), and assumed linear (a soil stiffness of 300 kPa for GoM and 1000 kPa for WA) and nonlinear seabed models. For LF excursions, predominant “far,” “near,” and cross directions were considered. For re-assessment, the Langner’s mathematical trench and the Stepped trench were considered. The variation of seabed slope throughout the trench was extracted and shown in Figure 5-15.

Figure 5-15 shows that the Langner’s trench is steeper in NOZ compared to the Stepped seabed. Although the Stepped seabed holds the minimum absolute value of slope throughout the trench, the locally different absolute values are observed for some areas in the FOZ (Figure 5-15). The fatigue life results of the study are shown in Figure 5-16 ((a) to (d) for the NOZ, and (e) to (h) for FOZ).

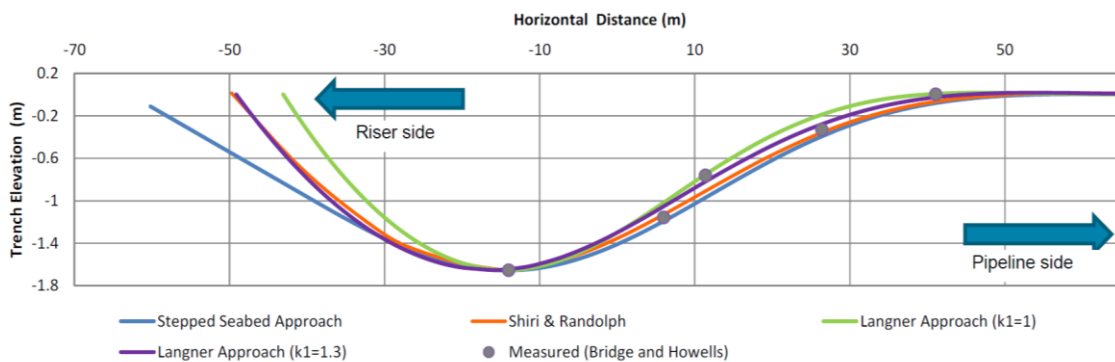


Figure 5-14. Different considered trench profiles, (Randolph et al., 2013)

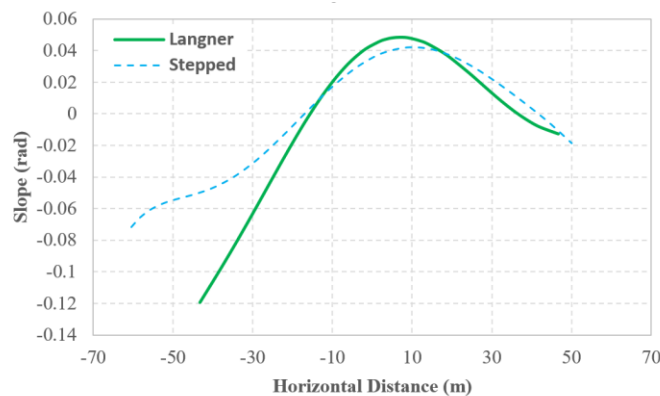


Figure 5-15. The slope of trench profile

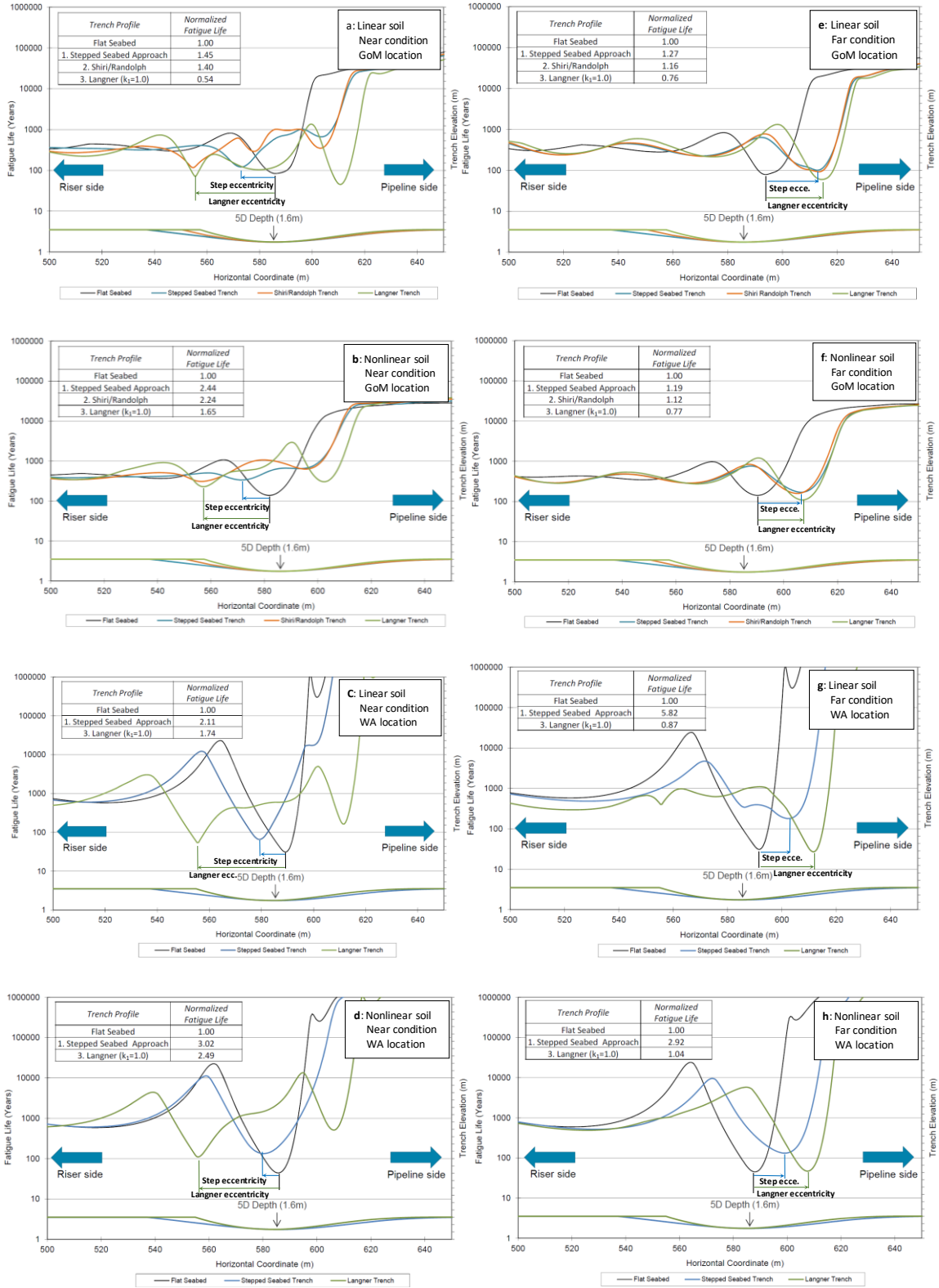


Figure 5-16. Fatigue life distribution over various trenches, (Randolph et al., 2013)

To facilitate the re-assessment, the key fatigue life data in Figure 5-16 was extracted and shown in Table 5-4 and Table 5-5. Also, the peak damage relocations (fd_{max}) were extracted and shown in Table 5-6.

Table 5-4. Fatigue damage peak coordination for GoM location, (Randolph et al., 2013).

Near				Far			
Elastic seabed (k=300 kPa)		Nonlinear seabed		Elastic seabed (k=300 kPa)		Nonlinear seabed	
(a)		(b)		(e)		(f)	
seabed	fd _{max} (m)	seabed	fd _{max} (m)	seabed	fd _{max} (m)	seabed	fd _{max} (m)
Langner	555	Langner	557	Langner	614	Langner	607
Stepped	573	Stepped	571	Stepped	612	Stepped	605
Horizontal	586	Horizontal	581	Horizontal	593	Horizontal	590

Table 5-5. Fatigue damage peak coordination for WA location, (Randolph et al., 2013).

Near				Far			
Elastic seabed (k=1000 kPa)		Nonlinear seabed		Elastic seabed (k=1000 kPa)		Nonlinear seabed	
(c)		(d)		(g)		(h)	
seabed	fd _{max} (m)	seabed	fd _{max} (m)	seabed	fd _{max} (m)	seabed	fd _{max} (m)
Langner	555	Langner	556	Langner	611	Langner	625
Stepped	579	Stepped	579	Stepped	602	Stepped	615
Horizontal	589	Horizontal	585	Horizontal	591	Horizontal	602

Table 5-6. Fatigue damage peak relocation of each trench respect to the horizontal seabed, (Randolph et al., 2013).

	Elastic seabed				Nonlinear seabed			
	Near		Far		Near		Far	
	seabed	fd _{max} (m)	seabed	fd _{max} (m)	seabed	fd _{max} (m)	seabed	fd _{max} (m)
GoM	Langner	31	Langner	21	Langner	24	Langner	17
	Stepped	13	Stepped	19	Stepped	10	Stepped	17
WA	Langner	34	Langner	20	Langner	29	Langner	23
	Stepped	10	Stepped	11	Stepped	6	Stepped	13

Moreover, the ratio of peak damage relocations was extracted and shown in Table 5-7.

Table 5-7. Normalized ratio of the peak damage relocation in Langner’s trench to the Stepped seabed, (Randolph et al., 2013).

Location	NOZ		FOZ	
	Elastic seabed	Nonlinear seabed	Elastic seabed	Nonlinear seabed
GoM	2.4	2.4	1.1	1
WA	3.4	4.8	1.8	1.8

The results in Table 5-7 show that as predicted by the BLM solution developed in the current study, the dominant peak damage relocation occurs in Langner’s trench, where the slopes of the trench shoulder are steeper in both NOZ and FOZ. The ratios for FOZ are in agreement with the absolute value of the trenches, but there is a sharp increase in the damage relocation at FOZ for the WA case. For the vessel excursion towards the near direction, and compared to the flat seabed, the points with the least fatigue life (fd_{max}) on NOZ shoulder are relocated toward the vessel, on both linear and nonlinear seabed (Figure 5-16 (a) to (d)). Also, Figure 5-16 (a) to (d) show that the maximum damage relocations for both linear and nonlinear seabed occur in the trench with the steeper shoulder in NOZ, which belongs to the Langner’s trench. Likewise, the minimum damage relocations correspond to the Stepped trench, which holds the minimum absolute value of slope in NOZ (see Figure 5-15). As expected, these damage relocations correlate with the slopes of the trench shoulders.

In the far vessel excursions (Figure 5-16 (e) and (h)), compared with the flat seabed, the points with the least fatigue life (fd_{max}) on FOZ shoulder move away from the vessel (towards the pipeline side). Figure 5-16 (e) and (f) show that the damage relocations are

not significant for the soft seabed (GoM) due to the overall similarity of the trenches in FOZ (see Figure 5-14). However, significant damage relocations were observed in the FOZ under the far vessel excursion in the stiff seabed (WA) (Figure 5-16 (g) and (h)). A closer look at the fatigue curves for Langner's trench in Figure 5-16 (a) to (d), shows potential pressure hotspots in FOZ due to incompatibility between the trench and riser profiles. The same is observed in all of the cases near the trench mouth when the vessel moves towards the near direction and the TDP moves to NOZ. The incompatibility between the trench and riser profiles could be due to the significance of riser flexural stiffness in the TDZ, which has been emphasized as an important factor in this paper. The unwanted pressure hotspots can exacerbate the local fatigue damage, particularly for the stiff soil. Overall, a steeper shoulder in NOZ compared to FOZ results in a larger peak damage relocation compared with the flat seabed. This happens due to the differences between the absolute value of the trench slopes in NOZ and FOZ, which was predicted by the developed BLM solution (see Figure 5-9).

The influence of the local trench slope on the magnitude of the fatigue life is interestingly observed in the results reported by Randolph et al., (2013). Table 5-8 and Table 5-9 show the normalized fatigue lives (by Stepped trench) on different trench shoulders in near and far vessel excursions that were extracted from Figure 5-16.

Table 5-8. Normalized fatigue lives of the trench shoulder, for GoM.

Trench model	GoM			
	NOZ		FOZ	
	Elastic seabed	Nonlinear seabed	Elastic seabed	Nonlinear seabed
Stepped	1.00	1.00	1.00	1.00
Langner	0.37	0.68	0.60	0.65

Table 5-9. Normalized fatigue lives of the trench shoulder, for WA.

Trench model	WA			
	NOZ		FOZ	
	Elastic seabed	Nonlinear seabed	Elastic seabed	Nonlinear seabed
Stepped	1.00	1.00	1.00	1.00
Langner	0.82	0.82	0.15	0.36

It was observed that in the NOZ shoulder, the magnitude of fatigue life is decreased for Langner’s trench (damage has increased) due to increasing the slope of NOZ, as predicted by BLM. Also, the magnitude of fatigue life is decreased for Langner’s trench on FOZ compared with the Stepped seabed. A closer look at Figure 5-15 shows that there is a change in the magnitude of the slope for inserted trenches in FOZ next to Langner’s peak. The local slope of the Langner’s trench has decreased at fd_{max} , which may explain the discrepancy in comparison with the Stepped seabed. Also, stress hotspots in the WA case are more significant because of the stiffer seabed compared to GoM. The re-assessment of this case study showed that, as predicted by the BLM analytical solution, the peak fatigue damage on the trench could be increased or decreased in both trench shoulders due to the difference of the local seabed slope, which affects the TDP oscillation amplitude. These findings denote the case-dependence of the trench effect on fatigue and are in agreement with the earlier study conducted by Shoghi and Shiri (2019 and 2020).

5.6. Conclusions

The beneficial or detrimental effect of the trench on SCR fatigue in the TDZ is still an open question, and there is no coherent agreement amongst the researchers in the literature. The recently developed methodologies for assessing this problem by using the boundary layer solutions are limited to the flat seabed. To examine the validity of the recent solutions in a more realistic trench with sloped shoulders, a boundary layer solution was developed to account for the seabed slope and resolve the discontinuity of the SCR profile on the trench. The model was validated by finite element analysis and re-assessing a well-known case study from the literature. The results supported the validity of the recently proposed analytical solutions for assessing the trench effect on riser fatigue.

It was observed that there is a direct relationship between the TDP oscillations on the trench with the magnitude and relocation of the peak fatigue damage of SCR in the TDZ. The study further supported the idea that the fatigue response of SCR is a case-dependent problem, heavily influenced by the dominant direction of fatigue sea states and the low-frequency vessel excursions. In any case, the slopes of trench shoulders play an important role, where steeper shoulder benefits fatigue life in FOZ and deteriorate in NOZ. It means, depending on the geographical location and the dominant direction of LF vessel excursions, the trench may increase or decrease the fatigue life.

Substituting $s_c = 0$, which represents the TDP, the $\chi_{0c} = q/T_{0c}$ is obtained as curvature at the TDP.

5.7. Appendix – some basics on the planar static problem at TDZ on horizontal and rigid seabed

For the reader easiness, this appendix brings a brief summary of a more detailed analysis that can be found in Pesce (1997) Chapter 3, in the manner previously presented in Pesce and Martins, (2005) sec 7.2.

The Clebsh-Love equations, see, e.g., Pesce and Martins (2005), governing the static equilibrium of slender curved bars in the vertical plane, under the hypothesis of large displacement, small strains and inextensibility, can be written:

$$\begin{aligned} \frac{dT}{ds} - Q \frac{d\theta}{ds} + f_t &= 0 \\ \frac{dQ}{ds} + T \frac{d\theta}{ds} + f_n &= 0 \\ EI \frac{d^2\theta}{ds^2} + Q &= 0 \end{aligned} \tag{A.1}$$

$T(s)$ is the effective tension, $Q(s)$ the shear force, EI is the 'equivalent' bending stiffness, $\theta(s)$ the angle with respect to the horizontal line, where s is the arch-length coordinate measured from TDP, and

$$\begin{aligned} f_n &= -q \cos \theta + h_n(s) \\ f_t &= -q \sin \theta + h_t(s) \end{aligned} \tag{A.2}$$

are the normal and tangential components of forces per unit length, with q the immersed weight of SCR per unit length and $h_n(s)$ and $h_t(s)$ the corresponding steady hydrodynamic forces due to the current action.

Following Love, art. 273A (Love, 1927), it is possible to eliminate $T(s)$ and $Q(s)$ from (A.1), resulting a single non-linear integral-differential equation in $\theta(s)$,

$$EI \frac{d^2\theta}{ds^2} \sec \theta + qs - \int_0^s \left(h_n \sec \theta + \sec^2 \theta \left(\frac{d\theta}{ds} \right) \int_0^\xi (h_n \sin \theta - h_t \cos \theta) d\xi \right) ds = \quad (\text{A.3})$$

$$= T_0 \tan \theta - Q_0$$

where $T_0 = T(0)$ and $Q_0 = Q(0)$ at TDP. Equation (A.3) shows explicitly that, as current forces are functions of $\theta(s)$, the solution must be found iteratively. In the absence of current action, in non-dimensional form

$$\varepsilon^2 \frac{d^2\theta}{d\hat{s}^2} \sec \theta + \hat{q}\hat{s} = \tan \theta + \hat{Q}_0 \quad (\text{A.4})$$

$$\lambda^2 = EI/T_0; \quad \varepsilon = \lambda/L; \quad \hat{s} = s/L; \quad \hat{q} = qL/T_0; \quad \hat{Q}_0 = Q_0/T_0$$

L being the suspended length and λ the flexural length-scale at TDP. The small nondimensional number $\varepsilon = \lambda/L$ gauges the small importance of flexural rigidity, in the global static problem, if compared to the geometric rigidity.

Note that if bending effects are neglected, the classical catenary equation is obtained (c is used for the ideal catenary, or inextensible cable solution),

$$\tan \theta_c(s_c) = \chi_{0c} s_c \quad (\text{A.5})$$

with $\chi_{0c} = q/T_{0c}$ the ideal catenary static curvature at TDP. The corresponding curvature and effective tension functions are:

$$\chi_c(s_c) = \frac{d\theta_c}{ds_c} = \chi_{0c} \cos^2 \theta_c(s_c) = \chi_{0c} \frac{1}{1 + (\chi_{0c} s_c)^2} \quad (\text{A.6})$$

$$T_c(s_c) = T_{0c} \sec \theta_c \quad (\text{A.7})$$

Let $s = s_f$ be the actual TDP, when the flexural rigidity effect is taken into account. It can be shown, Pesce (1997), that the hydrodynamic force (integral term) in equation (A.3) is locally (in the vicinity of the TDP) of order θ^2 ; $\theta \ll 1$. We can thus write, with an error of order θ^2 , with $\chi_0 = q/T_0$, the curvature at TDP:

$$\frac{d^2\chi}{ds^2} - \frac{1}{\lambda^2}\chi = -\frac{1}{\lambda^2}\chi_0; s > s_f \quad (\text{A.8})$$

where $Q_0 = EI \left. \frac{d^3\theta}{ds^3} \right|^{s=s_f^+}$ is the shear force at $s = s_f^+$, for which $\theta = 0$. It should be emphasized that the effect of the hydrodynamic forces all along the riser *is not neglectable*, being already embedded in T_0 , the tension at TDP, i.e., included in the geometric rigidity.

Assuming a rigid flat bottom and null curvature at the actual TDP, i.e., enforcing continuity for the curvature at $s = s_f$, such that $\chi(s_f^+) = 0$ and $\chi(s) \equiv 0; s \leq s_f$, equation (A.8) can be easily integrated, giving rise to a local solution of the form,

$$\chi(s) = \begin{cases} \chi_0(1 - e^{-(1+s/\lambda)}); & \text{if } s \geq -\lambda \\ 0 & ; \text{if } s < -\lambda \end{cases} \quad (\text{A.9})$$

$$\theta(s) = \begin{cases} \chi_0\lambda \left(\frac{s}{\lambda} + e^{-(1+s/\lambda)} \right); & \text{if } s \geq -\lambda \\ 0 & ; \text{if } s < -\lambda \end{cases} \quad (\text{A.10})$$

$$\frac{Q}{q\lambda} = H[(s - s_f)/\lambda]e^{-(1+s/\lambda)} \quad (\text{A.11})$$

As $\theta(s_f) = 0$, then $s_f = -\lambda$. In words, the flexural rigidity effect displaces the actual TDP to the left with respect to the ideal cable TDP, by an amount λ . From equation (A.4) we see that the shear force at the actual TDP, such that $s \rightarrow s_f^+ = -\lambda$, is given by, $Q_0 = -q\lambda$. This latter equation provides some new insight into the physical meaning for the λ parameter: it gives a measure for the order of magnitude of the length-scale within which the Euler-beam solution matches the cable solution, the shear force decaying exponentially to zero. Moreover, the length-scale λ gives a measure to properly define the meshing refinement at the TDP region, in the case of numerical analysis. The rigid-soil assumption and the condition $\chi(s) \equiv 0; s \leq s_f$ imply a discontinuity in the shear force, at the actual

TDP, represented by the Heaviside function in equation (A.11). Now, if a small slope is considered, and assuming that tension is not affected substantially at TDP, the following relation may be easily obtained:

$$\chi_0 \delta s = \delta \theta (1 + \tan^2 \theta) \rightarrow \frac{\delta \theta}{\delta s} = \chi_0 \cos^2 \theta(s) = \frac{\chi_0}{1 + (\chi_0 s)^2} \quad (\text{A.12})$$

This expression is valid for the cable case as well.

5.8. Acknowledgments

The authors gratefully acknowledge the financial support of this research by the Research and Development Corporation (RDC) (now TCII) through the Ignite funding program, the “Natural Science and Engineering Research Council of Canada (NSERC)” through Discovery program, and the Memorial University of Newfoundland through VP start-up funding support. The second author acknowledges a research grant from CNPq, the Brazilian National Council for Scientific Research, process 308230/2018-3 and the financial support by CAPES, the Coordination for the Improvement of Higher Education Personnel (CAPES) in Brazil, through the International Exchange Program PRInt-USP/2019.

References

- Aranha, JAP., Martins, C.A. and Pesce, C.P., 1997. Analytical Approximation for the Dynamic Bending Moment at the Touchdown Point of a Catenary Riser. *Int. Journal of Offshore and Polar Engineering*, Dec., vol. 7 (4), 293-300.
- Langner, C., 2003. Fatigue life improvement of steel catenary risers due to self-trenching at the touchdown point. *Proceedings of the Offshore Technology Conference OTC 15104*; May 5-8; Texas, USA.
- Love, AE. H., 1927. *A Treatise on the Mathematical Theory of Elasticity*. 4th edition., Dover Pub. Inc., N.Y., 1944, 643 pp.
- Pesce, C.P., Martins, C.A., Silveira, L.M., 2006. Riser-soil interaction: local dynamics at

- TDP and a discussion on the eigenvalue and the VIV problems, *J. Offshore Mech. Arctic Eng.* 128 (1) 39–55.
- Pesce, C.P., Aranha, J.A.P., Martins, C.A., 1998. The soil rigidity effect in the touchdown boundary layer of a catenary riser: Static problem. *Proceedings of the International Society of Offshore and Polar Engineers Conference ISOPE-I-98-130*; May 24-29; Montreal, Canada.
- Pesce, C.P., 1997. *Mechanics of Submerged Tubes and Cables in Catenary Configuration: analytical and experimental approaches.* (in Portuguese). Monograph, Livre Docencia, University of Sao Paulo, June, 350 pp.
- Pesce, C.P., Martins, C.A., 2005. Numerical Computational of Riser Dynamics. In: Subrata Chakrabarti. (Org.). *Numerical Models in Fluid-Structure Interaction.* 1st ed. Southampton: WIT Press, p. 253-309.
- Randolph M.F., Bhat S., Mekha B., 2013. Modeling the touchdown zone trench and its impact on SCR fatigue life, *Proceedings of the Offshore Technology Conference OTC-23975-MS*, <https://doi.org/10.4043/23975-MS> May 6-9.
- Rezazadeh, K., Shiri, H., Zhang, L., Bai, Y., 2012. Fatigue generation mechanism in touchdown area of steel catenary risers in non-linear hysteretic seabed. *Research Journal of Applied Sciences, Engineering and Technology*; 4(24):5591-5601.
- Shiri, H., 2014a. Response of steel catenary risers on hysteretic non-linear seabed. *Applied Ocean Research*, January; 44:20-28. <https://doi.org/10.1016/j.apor.2013.10.006>.
- Shiri, H., 2014b. Influence of seabed trench formation on fatigue performance of steel catenary risers in touchdown zone. *Marine Structures.* April; 36:1-20. <https://doi.org/10.1016/j.marstruc.2013.12.003>.
- Shiri, H., Randolph, M.F., 2010. Influence of seabed response on fatigue performance of steel catenary risers in touchdown zone. *Proceeding of the 29th International Conference on Ocean, Offshore and Arctic Engineering OMAE 2010-20051*; June 6-11; Shanghai, China. pp. 63-72; doi:10.1115/OMAE2010-20051.
- Shoghi, R., Shiri, H., 2019. Modelling Touchdown Point Oscillation and Its Relationship with Fatigue Response of Steel Catenary Risers. *Applied Ocean Research*, (87) 142-154.
- Shoghi, R., Shiri, H., 2020. Re-assessment of trench effect on fatigue performance of steel catenary risers in the touchdown zone. *Applied Ocean Research*, (94) 1-16.
- Sharma, P.P., Aubeny, C.P., 2011. Advances in pipe-soil interaction methodology and application for SCR fatigue design. *Proceedings of the Offshore Technology Conference OTC-21179-MS*; May 2-5; Texas, USA. <https://doi.org/10.4043/21179-MS>.
- Wang, K., Low, Y.M., 2016. Study of seabed trench induced by steel catenary riser and seabed interaction. *Proceedings of the 35th International Conference on Ocean, Offshore and Arctic Engineering OMAE2016-54236*; June 19-24; Busan: South Korea. doi:10.1115/OMAE2016-54236.

Chapter 6

Dynamic Curvature of a Steel Catenary Riser on Elastic Seabed Considering Trench Shoulder Effects: an Analytical Model

Rahim Shoghi¹, Hodjat Shiri^{2,*}, Celso P. Pesce³

1: Department of Civil Engineering
Memorial University of Newfoundland
e-mail: rshoghi@mun.ca

2: Department of Civil Engineering
Memorial University of Newfoundland
e-mail: hshiri@mun.ca

3: Department of Mechanical Engineering
University of São Paulo
e-mail: ceppesce@usp.br

This chapter was submitted as a journal paper to Engineering Structures (Elsevier).

Abstract

Prediction of the fatigue life of steel catenary risers (SCR) in the touchdown zone is a challenging engineering design aspect of these popular elements. It is publically accepted that the gradual trench formation underneath the SCR due to cyclic oscillations may affect the fatigue life of the riser. However, due to the complex nature of the several mechanisms involving three different domains of the riser, seabed soil, and seawater, there is still no strong agreement on the beneficial or detrimental effects of the trench on riser fatigue. Seabed soil stiffness and trench geometry play crucial roles in the accumulation of fatigue damage in the touchdown zone. There are several studies about the effect of seabed soil stiffness on fatigue. However, recent studies have proven the significance of trench geometry and identified the touchdown point oscillation amplitude as a key factor. In this study, a boundary layer solution, is used to obtain the dynamic curvature oscillation of the riser in the Touch Down Zone (TDZ), considering a certain range of seabed stiffness and a simplified trench geometry. It has been observed that the effect of soil stiffness is attributed to the curvature oscillation amplitude and to the minimum local curvature that SCR can take in the touchdown zone. The study further highlights the significance of trench geometry and shows that the seabed stiffness effect can also be assessed from the trench geometry perspective

Keywords: Steel catenary risers; Boundary layer method; Curvature dynamics; Touchdown point; Fatigue response

6.1. Introduction

Steel catenary risers (SCRs) are made of thin-wall steel pipes suspended from floating facilities to the seabed, in the form of a catenary. These attractive elements are common in offshore field developments for transferring gas and oil from the seabed to the floating systems or to convey water for some operational tasks. SCRs are subjected to cyclic and dynamic loads and are vulnerable to fatigue damage. Subsea surveys have shown that a trench is developed beneath the riser within a few years after installation, Bridge CD, Howells (2007), (see Fig. 6.1).

It is publically accepted that trench formation affects the fatigue life of the SCR in the touchdown zone (TDZ). However, there is still no coherent agreement on beneficial (Langned, 2003; Wang and Low, 2016; Randolph et al., 2013) or detrimental effects of the trench to fatigue damage (Shiri, 2014ab; Rezazadeh, 2012; Shiri and Randolph, 2010). The seabed soil stiffness and trench geometry have been identified as key influential factors in the accumulation of fatigue damage in the TDZ.

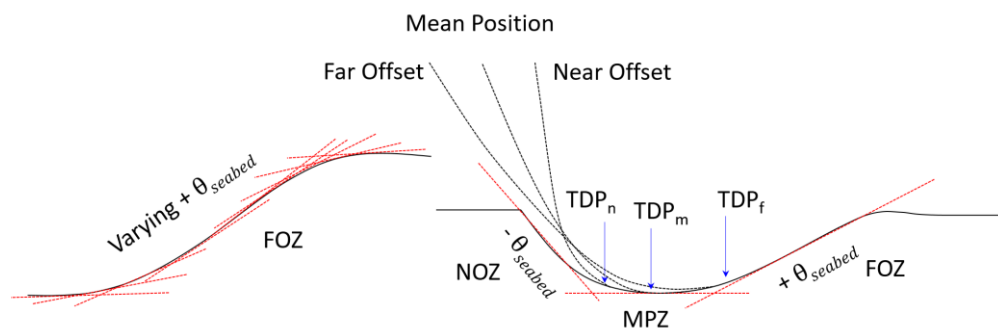


Figure 6-1. Dynamic curvature of SCR in TDZ (analytical results Schematic view of the simplified trench with linear sloped lines, Shoghi and Shiri (2019))

The effect of seabed soil stiffness on fatigue has widely investigated, showing that fatigue life is improved in softer seabed soils (Randolph et al., 2013; Campbell, 1999; Aubeny and Biscontin, 2008,2009; Clukey et al., 2009). However, recent studies have further focused on the significance of trench geometry and identified the touchdown point (TDP) oscillation amplitude as a key factor (Shoghi and Shiri, 2019; Wang and Low, 2016; Randolph et al., 2013; Shoghi and Shiri, 2020). As a matter of fact, in the simpler case of horizontal and flat (rigid or linear elastic) seabeds, the TDP excursion had already been shown to be a major contributor to fatigue damage, (Aranha et al., 1997; Pesce, 1997; Pesce et al., 1998a; Pesce et al., 2006). Indeed, the TDP, a point that separates the suspended from the supported part, i.e., a point of first contact (usually of tangency) with the soil, is, strictly speaking, a non-material one. Such a non-material point moves along the riser according to the motion of the structure, making the curvature at a given section to vary by large amounts as the pipe is, cyclically, suspended from and layed back on the soil. On the other hand, the soil stiffness governs the contact pressure between the riser and seabed; the contact pressure affects the magnitude of the shear force, which, in turn, is the gradient of the bending moment. As wellknown, bending moment has a direct relation with riser curvature. The oscillation of the bending moment is, by far, the main contributor to the occurrence of cyclic normal stress fields in TDZ, so a major factor for fatigue damage, as tension is usually low in this region.

In this study, expanding the work by Pesce et al. (2006), the dynamic equilibrium equations of a riser in the vertical plane is derived and matched to a the dynamic equation of a tensioned Euler-Bernoulli beam supported on a linear-elastic seabed, producing a local boundary layer solution, in TDZ, to obtain the curvature oscillation of the riser, within a

range of seabed stiffness. For that, a sloped seabed is considered as a simplified, however proper, representation of the trench shoulders. A series of finite element analyses (FEA) was conducted to validate the analytical model. It has been observed that the effect of soil stiffness is attributed to the dynamic curvature oscillation amplitude and to the minimum local curvature that SCR can take in the touchdown zone. The study further reveals the significance of trench geometry and shows that the seabed stiffness effect could also be assessed from a trench geometry perspective.

6.2. Boundary-Layer Solution in TDZ

The flexural stiffness of catenary-formed hanging elements has been widely investigated in the literature (Triantafyllou and Triantafyllou, 1991; Burgess, 1993; Dhotarad et al., 1978; Irvine, 1993). The planar problem of SCR with the absence of shock against the soil, which is called the sub-critical dynamic regime, was investigated by Aranha et al. using the boundary layer method (Aranha et al., 1997). The authors obtained the dynamic curvature as a function of the time histories of tension and TDP displacement. Further qualitative and quantitative assessments were conducted by Pesce and Pinto (1996) and Pesce et al. (1998b, 2006), by developing analytical solutions for the dynamic curvature of a SCR near the TDP. However, those studies were limited to the horizontal seabed, while the trench shoulders are sloped. In the current study, a local analytical quasi-static solution to the governing dynamic equilibrium equation for the suspended part of the riser is reassessed and matched to a general quasi-static solution for the governing equation of a tensioned Euler-Bernoulli beam supported on a linear-elastic sloped seabed. Different sloped seabeds, including those of ‘negative’ slopes (corresponding to the far vessel offset zone, FOZ) and positive slopes (corresponding to the near vessel offset zone, NOZ) are

considered (see Figure 6-2). When the vessel moves away from the riser (far offset), the TDP oscillates on the negative shoulder of the trench (FOZ). Likewise, when the vessel moves towards the SCR (near offset), the TDP oscillates on the positive shoulder of the trench (NOZ). In the manner of Aranha et al., (1997), and Pesce et al., (1998a), the effects of the vessel motions, due to incoming sea waves, is modelled through the corresponding variations in tension and in the TDP oscillations in the TDZ.

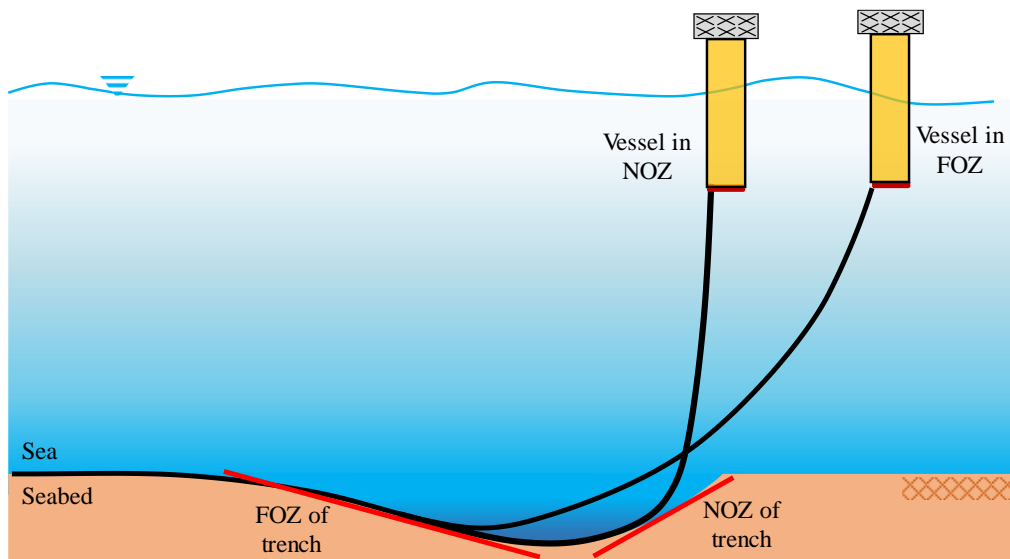


Figure 6-2. Schematic view of trench and vessel configuration

In order to obtain the riser-seabed interaction, first, the dynamic curvatures of the suspended and supported sections are formulated and, then, the results are matched at the TDP.

6.2.1. Planar Dynamic Equations for the Suspended Part of the SCR

Figure 6-3 shows the schematic riser dynamics around the static configuration. Only the planar problem is herein addressed. Small strains and linear constitutive equations are assumed throughout the whole derivation.

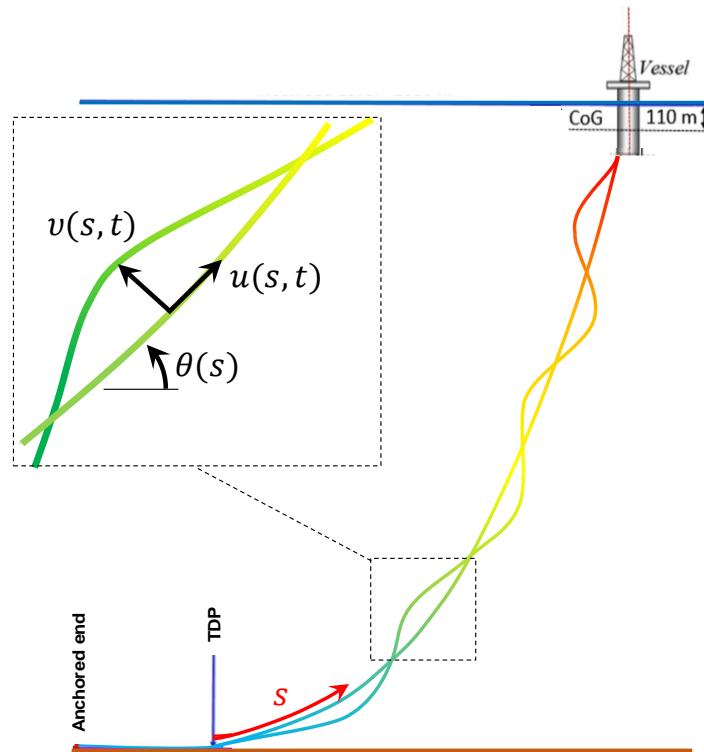
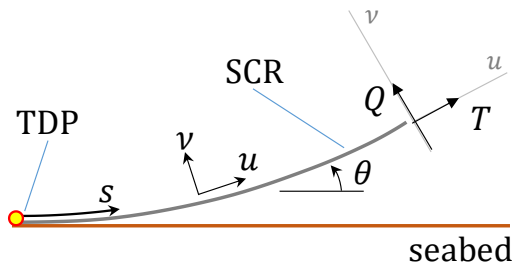


Figure 6-3. Schematic view of SCR configuration

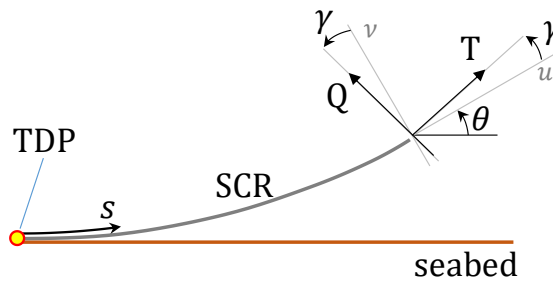
As worked out in the Appendix, based on Pesce (1997), let the planar static equilibrium configuration be expressed by three functions: $\theta(s)$, the angle of the center line of the SCR with respect to the horizontal and the fields $Q(s)$ and $T(s)$, the static shear force and effective tension, respectively, resulting from the immersed weight of SCR per unit length, q , and from the static component of the hydrodynamic loading. The curvilinear arch length coordinate s is measured from a static reference position taken as the TDP of a homologous cable problem. It is worth noting that the hydrodynamic load depends on the geometric configuration, which turns the procedure of finding the static equilibrium configuration a highly nonlinear problem that has to be solved iteratively, in advance.

The planar kinematics is defined around the supposedly known static equilibrium configuration (see Figure 6-4). The displacement fields $u(s, t)$ and $v(s, t)$ are considered small and in the tangential and normal directions of the center line of the SCR.

a) static configuration



b) dynamic configuration



c) shear forces and effective tensions

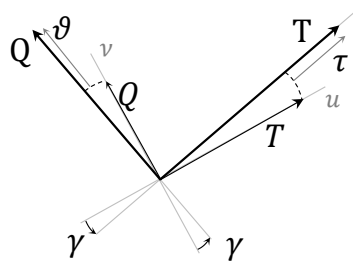


Figure 6-4. Static and dynamic configuration of SCR in the TDZ

The partial differential equations governing the dynamics of the riser around the static equilibrium configuration and projected onto the tangential and normal directions may then be written in the following form (see Appendix, equation (A.7)):

$$\begin{aligned} \frac{\partial T}{\partial s} - (T\gamma + Q) \frac{d\theta}{ds} - \frac{\partial}{\partial s}(Q\gamma) + h_u + \varpi_u - q \sin \theta &= m \frac{\partial^2 u}{\partial t^2} \\ \frac{\partial Q}{\partial s} + (T - Q\gamma) \frac{d\theta}{ds} + \frac{\partial}{\partial s}(T\gamma) + h_v + \varpi_v - q \cos \theta &= m \frac{\partial^2 v}{\partial t^2} \end{aligned} \quad (1)$$

In equation (1),

$$\begin{aligned} \Theta(s, t) &= \theta(s) + \gamma(s, t) \\ T(s, t) &= T(s) + \tau(s, t) \\ Q(s, t) &= Q(s) + \vartheta(s, t) \end{aligned} \quad (2)$$

are, respectively, the instantaneous angle of the line with the horizontal, the total effective tension and the shear force, being $\gamma(s, t)$, $\tau(s, t)$ and $\vartheta(s, t)$ their corresponding perturbed quantities around the static configuration, resulting from dynamic loads acting on the riser in the vertical plane. The terms $h_{u,v}(s)$ and $\varpi_{u,v}(s, t)$ are the components of the static and dynamic parcels of the hydrodynamic force, in the tangential and normal direction respectively. The last ones are due to the relative external water flow with respect to the riser, at section s , usually modeled through the well known Morison's formula.

To first order, the following well known linear kinematic relation is supposed valid, equation (A.2):

$$\gamma(s, t) = \frac{\partial v}{\partial s} + u \frac{d\theta}{ds} \quad (3)$$

and equation (1) may be alternatively written, equation (A.8):

$$\begin{aligned}
\frac{\partial T}{\partial s} - \left[T \left(\frac{\partial v}{\partial s} + u \frac{d\theta}{ds} \right) + Q \right] \frac{d\theta}{ds} - \frac{\partial}{\partial s} \left[Q \left(\frac{\partial v}{\partial s} + u \frac{d\theta}{ds} \right) \right] + h_u + \varpi_u - q \sin \theta \\
= m \frac{\partial^2 u}{\partial t^2} \\
\frac{\partial Q}{\partial s} + \left[T - Q \left(\frac{\partial v}{\partial s} + u \frac{d\theta}{ds} \right) \right] \frac{d\theta}{ds} + \frac{\partial}{\partial s} \left[T \left(\frac{\partial v}{\partial s} + u \frac{d\theta}{ds} \right) \right] + h_v + \varpi_v - q \cos \theta \\
= m \frac{\partial^2 v}{\partial t^2}
\end{aligned} \tag{4}$$

Notice, in equations (1) and (4), the coupling between the displacement field arising from the static curvature. These equations should be integrated numerically, for given boundary and initial conditions, to solve for the displacements $u(s, t)$ and $v(s, t)$ around the static configuration.

On the other hand, considering that no external distributed moment is applied to the line and consistently disregarding the effects of rotatory inertia due to the slenderness of the structure and by using the usual Kirschoff-Love hypotheses (Love, 1927), the following constitutive equation may be assumed valid, equation (A.16):

$$M(s, t) = EI \frac{\partial \Theta}{\partial s} = EI \chi(s, t) \tag{5}$$

where $M(s, t)$ is the bending moment, EI is the bending stiffness at section s , and $\chi(s, t)$ is the total curvature. Then, equation (1b) that governs the normal displacement, $v(s, t)$, may be put in the following form, with EI assumed a constant value along s (equation (A.20)):

$$-EI \frac{\partial^2 \chi}{\partial s^2} - \gamma EI \frac{d\theta}{ds} \frac{\partial \chi}{\partial s} + T \chi + \gamma \frac{\partial T}{\partial s} + h_v + \varpi_v - q \cos \theta = m \frac{\partial^2 v}{\partial t^2} \tag{6}$$

Equation (6) governs the dynamics of the suspended part of the riser in the normal direction, around the static configuration. Notice that equation (1a) could be discussed further, regarding axial dynamics and respective time scales, what enables one to gauge the

behaviour of the dynamic tension along the riser. A thorough and detailed analysis may be found in Pesce (1997), chapter 4, section 4.1, pages 191-203.

Close to TDP, it can be shown, Pesce (1997), that with an error of order $\sim O(\chi_0 \lambda \cdot \max\{\theta\gamma; \gamma^2; \theta^2\})$, where $\chi_0 = q/T_0$ is the curvature at TDP for a cable on a flat and rigid seabed and $\lambda = \sqrt{EI/T_0}$ is the length scale of the bending stiffness effect at TDP, Aranha et al. (1997) and Pesce et al. (1998b), that equation (6) reduces to:

$$-EI \frac{\partial^2 \chi}{\partial s^2} + T\chi + \gamma \frac{\partial T}{\partial s} + h_v + \varpi_v - q \cong m \frac{\partial^2 v}{\partial t^2} \quad (7)$$

Moreover, considering in this vicinity that, to first order, $\gamma(s, t) \approx \partial v / \partial s$, equation (7) may be approximated in the form:

$$-\lambda^2 \frac{\partial^2 \chi}{\partial s^2} + \frac{1}{T_0} \left(T\chi + \frac{\partial v}{\partial s} \frac{\partial T}{\partial s} + h_v + \varpi_v^V \right) - \chi_0 \cong \frac{1}{c_0^2} \frac{\partial^2 v}{\partial t^2} \quad (8)$$

where $c_0 = \sqrt{T_0/(m + m_a)}$ is the transversal wave celerity of a tensioned cable, a reference velocity scale for the problem, with m_a the cross-section added mass. Notice that, in equation (8), only the viscous hydrodynamic forces, $(h_v + \varpi_v^V)$, was left on the l.h.s, as the inertial parcel, proportional to the added mass and to the normal acceleration was brought to the r.h.s. It can be also shown, that at TDP vicinity the viscous hydrodynamic forces are locally of second order, hence not dominant governing terms, (Aranha et al., 1997; Pesce, 1997; Pesce et al., 1998b).

Moreover, it can be also shown, that, $\frac{\partial \tau}{\partial s} \frac{L}{EA} \approx O \left[v_0 \left(\frac{\omega}{\omega_u} \right)^2 \right]$, where $\omega_u = (\pi/L) \sqrt{EA/m}$ is a frequency scale for the axial vibration of the riser considering a total suspended length L , $v_0 = u_0/L$ is the typical nondimensional axial displacement amplitude and EA is the axial stiffness, Pesce (1997). For a typical 10"3/4 SCR in 1000m water depth, e.g., this value is

of order 10^{-5} . Also, from the catenary equation near TDP the static effective tension may be approximated as $T(s) \approx T_0 \sec \theta(s) \cong T_0(1 + O(\theta^2))$, such that its derivative with respect to s may be written, $T'(s) \cong T_0 \tan \theta(s) \sec \theta(s) \chi_0 \cong T_0 \chi_0 \theta(s) = q\theta(s)$. Therefore, in this neighborhood, the total effective tension can be well approximated by $T(s, t) \cong T_0 + \tau(0, t)$ and it is the only significant term that is left in the parenthesis of equation (8). Henceforth, the dynamic tension at TDP vicinity will be simply referred to as $\tau(0, t) = \tau(t)$. So, retaining only the dominant terms, equation (8) is written:

$$-\lambda^2 \frac{\partial^2 \chi}{\partial s^2} + \left(1 + \frac{\tau(t)}{T_0}\right) \chi - \chi_0 \cong \frac{1}{c_0^2} \frac{\partial^2 v}{\partial t^2} \quad (9)$$

Still, equation (9) is a dynamic equilibrium equation, since the inertial term appears explicitly in its r.h.s. However, as shown in Aranha et al. (1997), and discussed further in Pesce et al. (1998b), and in great detail in Pesce (1997), a quasi-static approximation to equation (9) may be constructed with an error of order $O(\mathcal{M}^2)$, where $\mathcal{M} = V_0/c_0$ is a nondimensional number formed by the ratio between the typical speed of the TDP (a non-material point), V_0 , and the transversal wave celerity of a cable, $c_0 = \sqrt{T_0/(m + m_a)}$. As a matter of fact, this number regulates the possible impact of a cable against the seabed. If $\mathcal{M} > 1$, i.e., if the TDP speed is larger than the cable transversal wave celerity, a shock will take place. Otherwise, if $\mathcal{M} < 1$, shock will not exist. It is like letting enough time to the cable to adjust its curvature, smoothly, at the tangency point (TDP) as it moves forwards or backwards. The first dynamic regime, $\mathcal{M} > 1$, is called supercritical. The second regime, $\mathcal{M} < 1$, is named subcritical. As pointed out in Pesce (1997) and Pesce et al. (2006), notice that $\mathcal{M} = V_0/c_0$ is physically analogous to the classic ‘Mach’ number in

compressible flows. In the subcritical regime the TDP can be viewed as an analogous of the instantaneous center of rotation of a ‘variable radius rigid disc’, that rolls without slipping on a smooth surface; Pesce et al. (1998a). This being said, it has been shown by Aranha et al. (1997), and discussed further in Pesce (1997), that the inertial term is of order:

$$\frac{\chi_0}{c_0^2} \frac{\partial^2 v}{\partial t^2} = O(\mathcal{M}^2) \quad (10)$$

Therefore, if a subcritical regime is assumed, such that $\mathcal{M}^2 \ll 1$, equation (9) may be written:

$$-\lambda^2 \frac{\partial^2 \chi}{\partial s^2} + \left(1 + \frac{\tau(t)}{T_0}\right) \chi = \chi_0 (1 + O(\mathcal{M}^2)) \quad (11)$$

or, correct to $O(\mathcal{M}^2)$, in a purely *quasi-static* form as,

$$-\lambda^2 \frac{\partial^2 \chi}{\partial s^2} + \left(1 + \frac{\tau(t)}{T_0}\right) \chi = \chi_0 \quad (12)$$

Equation (12) governs the total curvature of the suspended part of the riser, in the TDP region, once a subcritical dynamic regime is assumed to take place. Hereinafter, the quasi-static solution for this equation will be simply referred to as the ‘dynamic curvature’ along the suspended part of the riser in the TDZ.

The general solution for equation (12) is given by (see Pesce et al., 2006):

$$\begin{aligned} \chi(s, t) = & \frac{\chi_0}{1 + f(t)} + c_1(t) \exp - \left(\sqrt{1 + f(t)} \right) (s - s_K(t)) / \lambda \\ & + c_2(t) \exp \sqrt{1 + f(t)} (s - s_K(t)) / \lambda \end{aligned} \quad (13)$$

where, $f(t) = \frac{\tau(t)}{T_0}$ is the nondimensional dynamic tension at TDZ and $s_K(t)$ defines the still unknown actual TDP position; i.e, the instantaneous position of the point at which the riser touches the seabed. Assuming a finite solution in the far field, i.e., as $(s - s_K(t))/\lambda \rightarrow \infty$, it follows that $c_2(t) = 0$. Also, equation (13) should encompass the seabed curvature, χ_{sb} , at TDP, so that $c_1(t) = \left(\chi_{sb} - \frac{\chi_0}{1+f(t)}\right)$. Equation (13) can then be rewritten as the general ‘dynamic curvature’ of the suspended part of the riser in TDZ as follow:

$$\chi(s, t) = \frac{\chi_0}{1+f(t)} + \left(\chi_{sb} - \frac{\chi_0}{1+f(t)}\right) C_1(t) \exp\left(-\sqrt{1+f(t)}(s - s_K(t))/\lambda\right) \quad (14)$$

Local non-dimensional variables in the form of $\xi = x/\lambda$ and $\eta(\xi, t) = y(s, t)/\lambda$ are used to define position and the elastic line quota, as well as the non-dimensional curvature ($\eta'' = \lambda y'' \approx \lambda\chi$), related to bending moment, the third derivative (η'''), related to the shear force, and, by integration, the slope (η'), such that:

$$\eta''(\xi, t) = \frac{\lambda\chi_0}{1+f(t)} + \lambda \left(\chi_{sb} - \frac{\chi_0}{1+f(t)}\right) C_1(t) \exp\left(-\sqrt{1+f(t)}(\xi - \xi_K(t))\right) \quad (15)$$

$$\eta'''(\xi, t) = -\sqrt{1+f(t)}\lambda \left(\chi_{sb} - \frac{\chi_0}{1+f(t)}\right) C_1(t) \exp\left(-\sqrt{1+f(t)}(\xi - \xi_K(t))\right) \quad (16)$$

$$\eta'(\xi, t) = \frac{\lambda\chi_0(\xi - \xi_0(t))}{1+f(t)} - \frac{\lambda}{\sqrt{1+f(t)}} \left(\chi_{sb} - \frac{\chi_0}{1+f(t)}\right) C_1(t) \exp\left(-\sqrt{1+f(t)}(\xi - \xi_K(t))\right) \quad (17)$$

where $\xi_0(t) = x_0(t)/\lambda$, is a known (usually assumed cyclic) function, to consider the TDP oscillation of a homologous cable case, used as a local driving term, Pesce et al., (2006),

e.g., $x_0(t) = a_0 \cos(2\pi t/T_s + \varphi)$ being a_0 the cable case TDP oscillation amplitude and φ the phase, relative to the dynamic tension. Notice also that the non-dimensional boundary layer solution for the static problem is recovered through equations (15) to (17) by taking $f(t) = 0$ and $\xi_0(t) = 0, 0$.

Generally, the non-dimensional curvature solution for the suspended part in the TDZ can be expressed by substituting the still unknown function $\xi = \xi_K(t)$ in equations (15) - (17), leading to:

$$\eta'(\xi_K, t) = \frac{\lambda\chi_0}{1+f(t)} \left(\xi_K(t) - \xi_0(t) - \frac{C_1(t)}{\sqrt{1+f(t)}} \right) \quad (18)$$

$$\eta''(\xi, t) = \frac{\lambda\chi_0}{1+f(t)} (1 - C_1(t)) \quad (19)$$

$$\eta'''(\xi, t) = \frac{\lambda\chi_0}{\sqrt{1+f(t)}} C_1'(t) \quad (20)$$

Equations (18) - (20) are dependent on two unknown functions of time, $\xi_K(t)$ and $C_1(t)$, which will be found by a classical matching procedure with an analytical solution for the part of the riser supported on the seabed. In other words, the non-dimensional TDP relocation will be found as a function of soil stiffness, seabed slope, and time.

6.2.2. Dynamic Equations for the Supported Part of the SCR on the Seabed

The planar problem of riser dynamics on elastic soil is herein solved assuming known the static tension at TDP, T_0 and the functions $\tau(t)$ and $x_0(t)$ as two dynamic driving terms. Let y be the vertical coordinate for the SCR center line, measured from a certain reference position. The still unknown actual TDP position (i.e., the point where the riser touches the

seabed) has been defined as $s_K(t)$, such that $y(s_K(t)) = y_{sb}(s_K(t))$. For a flat and horizontal seabed this geometric condition is simply given by $y(s_K(t)) = 0$. For the part of the riser resting on the seabed, a non-separation restraining condition is assumed for $s < s_K(t)$. Taking a not too soft soil, the slope may be approximated by $\theta \approx dy/dx$, $s \approx x$, and the curvature by $\chi(s) \approx \chi(x) \approx d^2y/dx^2$. Then, assuming a linearly elastic seabed, the non-dimensional soil rigidity can be defined as follows 0:

$$K = \frac{kEI}{T_0^2} = \frac{k\lambda^2}{T_0} = \frac{k\lambda^4}{EI} = \chi_0\lambda \frac{k\lambda}{q} \quad (21)$$

In equation (32) K is the soil stiffness. The quasi-static equation of an Euler-Bernoulli beam supported on a linear-elastic soil, subjected to an applied dynamic tension, can be written in a non-dimensional form as follows, where the inertia term is disregarded for the subcritical regime with an error of order $(\lambda/L)^2$ (λ and L are boundary layer length and suspended riser length respectively), Pesce et al., (2006):

$$\frac{\partial^4 \eta}{\partial \xi^4} - \left(1 + \frac{\tau(t)}{T_0}\right) \frac{\partial^2 \eta}{\partial \xi^2} + K\eta = K\eta_{sb}; \quad \xi < \xi_K(t) \quad (22)$$

In equation (22), $\eta_{sb} = \xi \tan \theta_{sb}$ represents the seabed configuration, such that $\theta_{sb} = 0$ for the flat and horizontal seabed, $\theta_{sb} > 0$ for NOZ, and $\theta_{sb} < 0$ for FOZ. The following far-field boundary conditions are assumed to hold: $\lim_{\xi \rightarrow -\infty} \eta(\xi) \cong \lim_{\xi \rightarrow -\infty} K\eta_{sb}$, and $\lim_{\xi \rightarrow \xi_K} \eta(\xi) \cong \eta_{sb}(\xi_K(t))$. The solution of equation (22), and corresponding derivatives in space, can be written, for $\xi < \xi_K(t)$, i.e., for the part supported on the seabed, in the form of the following non-dimensional equations:

$$\eta(\xi, t) = C(t) \exp\left(\frac{K^{0.25}}{\sqrt{2}}(\xi - \xi_K(t))\right) \sin\left(\frac{K^{0.25}}{\sqrt{2}}(\xi - \xi_K(t))\right) + \xi \tan \theta_{sb} \quad (23)$$

$$\begin{aligned} \eta'(\xi, t) = \frac{K^{0.25}}{\sqrt{2}} C(t) \exp\left(\frac{K^{0.25}}{\sqrt{2}}(\xi - \xi_K(t))\right) & \left\{ \sin\left(\frac{K^{0.25}}{\sqrt{2}}(\xi - \xi_K(t))\right) \right. \\ & \left. + \cos\left(\frac{K^{0.25}}{\sqrt{2}}(\xi - \xi_K(t))\right) \right\} + \tan \theta_{sb} \end{aligned} \quad (24)$$

$$\eta''(\xi, t) = K^{0.5} C(t) \exp\left(\frac{K^{0.25}}{\sqrt{2}}(\xi - \xi_K(t))\right) \cos\left(\frac{K^{0.25}}{\sqrt{2}}(\xi - \xi_K(t))\right) \quad (25)$$

$$\begin{aligned} \eta'''(\xi, t) = \frac{K^{0.75}}{\sqrt{2}} C(t) \exp\left(\frac{K^{0.25}}{\sqrt{2}}(\xi - \xi_K(t))\right) & \left\{ \cos\left(\frac{K^{0.25}}{\sqrt{2}}(\xi - \xi_K(t))\right) \right. \\ & \left. - \sin\left(\frac{K^{0.25}}{\sqrt{2}}(\xi - \xi_K(t))\right) \right\} \end{aligned} \quad (26)$$

On the supported part, the values of the derivatives of the elastic line at the still unknown actual TDP (supposing the seabed represented locally by a constant slope) can be found by substituting $\xi = \xi_K(t)$ in equations (24) - (26). Therefore,

$$\eta'(\xi_K, t) = \frac{K^{0.25}}{\sqrt{2}} C(t) + \tan \theta_{sb} \quad (27)$$

$$\eta''(\xi, t) = K^{0.5} C(t) \quad (28)$$

$$\eta'''(\xi, t) = \frac{K^{0.75}}{\sqrt{2}} C(t) \quad (29)$$

Notice that a new unknown function of time, $C(t)$, appeared. Next, the above obtained solution, valid for the supported part will then be matched with the one valid for the suspended part to find the still unknown TDP relocation, as a function of soil stiffness, seabed slope, and time.

6.2.3. Matching Solutions at TDP

Matching both sets of equations, (18) - (20) and (27) - (29), leads to a system of three algebraic linear equations, for the three unknowns, $\xi_K(t)$, $C_1(t)$ and $C(t)$:

$$\begin{cases} \frac{\lambda\chi_0}{1+f(t)} \left(\xi_K(t) - \xi_0(t) - \frac{C_1(t)}{\sqrt{1+f(t)}} \right) = \frac{K^{0.25}}{\sqrt{2}} C(t) + \tan \theta_{sb} \\ \frac{\lambda\chi_0}{1+f(t)} (1 - C_1(t)) = K^{0.5} C(t) \\ \frac{\lambda\chi_0}{\sqrt{1+f(t)}} C_1(t) = \frac{K^{0.75}}{\sqrt{2}} C(t) \end{cases} \quad (30)$$

The solution of equation (30) gives, as the main result, the non-dimensional ideal TDP relocation, $\xi_K(t)$, written as an explicit function of soil stiffness, seabed slope and of the two dynamic driving terms:

$$\xi_K(t) = \xi_0(t) + \frac{(1+f(t))K^{-0.25} - K^{0.25}}{\sqrt{2}(1+f(t)) + \sqrt{(1+f(t))}K^{0.25}} + (1+f(t))R_\theta \quad (31)$$

$$C_1(t) = \frac{K^{0.25}}{\sqrt{2(1+f(t)) + K^{0.25}}} \quad (32)$$

$$C(t) = \frac{\lambda\chi_0}{(1+f(t))K^{0.5} + \sqrt{0.5 + \frac{f(t)}{2}}K^{0.75}} \quad (33)$$

In equation (31), $R_\theta = \tan \theta_{sb} / (\lambda\chi_0)$ is the normalized seabed slope. It should be mentioned that equations (23) - (26), with the use of equations (31) to (33), asymptotically recover the already known solution for the TDP relocation for the static SCR configuration on a horizontal seabed (for that, take $\theta = 0$, $f(t) = 0$ and $\xi_0(t) = 0$, Pesce et al., (1998a).

It also recovers the quasi-static solution for the case of a horizontal and linearly elastic soil, derived in Pesce et al., (2006), by taking $R_\theta = \frac{\tan \theta_{sb}}{(\lambda \chi_0)} = 0$. Now, the local non-dimensional dynamic curvature of the riser can be reconstructed from equation (15) (for the suspended part) and from equation (25) (for the supported part), in the form.

$$\begin{cases} \frac{\chi(\xi, \theta_{sb}, K, t)}{\chi_0} = \frac{1}{1+f(t)} \left(1 - \frac{K^{0.25} \exp(-\sqrt{1+f(t)}\beta(\xi, \theta_{sb}, t))}{\sqrt{2(1+f(t)) + K^{0.25}}} \right) ; \beta(\xi, \theta_{sb}, t) > 0 \\ \frac{\chi(\xi, \theta_{sb}, K, t)}{\chi_0} = \frac{K^{0.5} \exp\left(\frac{K^{0.25}}{\sqrt{2}}\beta(\xi, \theta_{sb}, t)\right) \cos\left(\frac{K^{0.25}}{\sqrt{2}}\beta(\xi, \theta_{sb}, t)\right)}{(1+f(t))K^{0.5} + \sqrt{0.5 + \frac{f(t)}{2}}K^{0.75}} ; \beta(\xi, \theta_{sb}, t) < 0 \end{cases} \quad (34)$$

where:

$$\beta(\xi, \theta_{sb}, K, t) = \xi - \xi_0(t) - \frac{-K^{0.25} + (1+f(t))K^{-0.25}}{\sqrt{2(1+f(t)) + \sqrt{1+f(t)}K^{0.25}}} - R_\theta(1+f(t)) \quad (35)$$

Equation (34) shows that the normalized dynamic curvature is a function of the TDP oscillation, $\xi_0(t)$; soil property, K ; and slope of the seabed, R_θ . It is worth recalling that the current study is targeted to the assessment of the dynamic curvature and fatigue performance of SCR in TDZ, for different soil stiffness and seabed slopes, topic that will be discussed in the coming sections.

6.3. Dynamic Curvature of SCR in TDZ

The dynamic curvature of an SCR due to vessel motion is investigated, for a typical and broad range of soil stiffness in the TDZ, by applying the obtained analytical solution. As it should be expected, the effects of both soil stiffness and TDP oscillation are found as very important factors. Also, a series of finite element analyses were conducted in OrcaFlex®

for a typical SCR to verify the analytical results. In the numerical simulations, linear springs were used to model the elastic seabed, and 0.1 m spacing was used between the nodes on the riser in the TDZ. Both ends of the riser at the top connection point and the anchored end were defined as simple hinge boundary conditions. The cross-sectional hydrodynamic coefficients for drag and added mass were considered as 1.2 and 1.0, respectively. Different slopes, including positive slope (which represents NOZ), negative slope (which represents FOZ), and null slope (which represents horizontal and flat seabed), were considered. Seabed slopes of $+2^\circ$ for NOZ and -1° for FOZ were used (see Figure 6-5). The numerical model constructed in OrcaFlex® took a typical SCR, Pesce et al., (2006), whose main properties are defined in Table 6-1. Figure 6-6 shows the configuration of the numerical model.

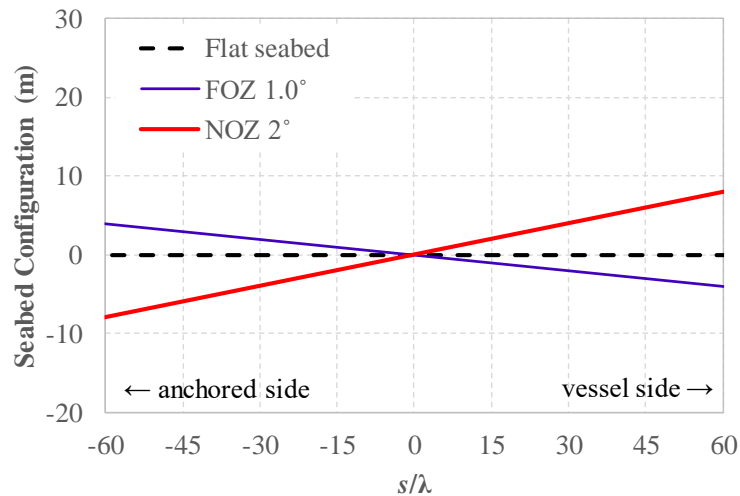


Figure 6-5. Considered seabeds, Flat: $\theta_{sb} = 0^\circ$, NOZ: $\theta_{sb} = +2^\circ$, and FOZ: $\theta_{sb} = -1^\circ$

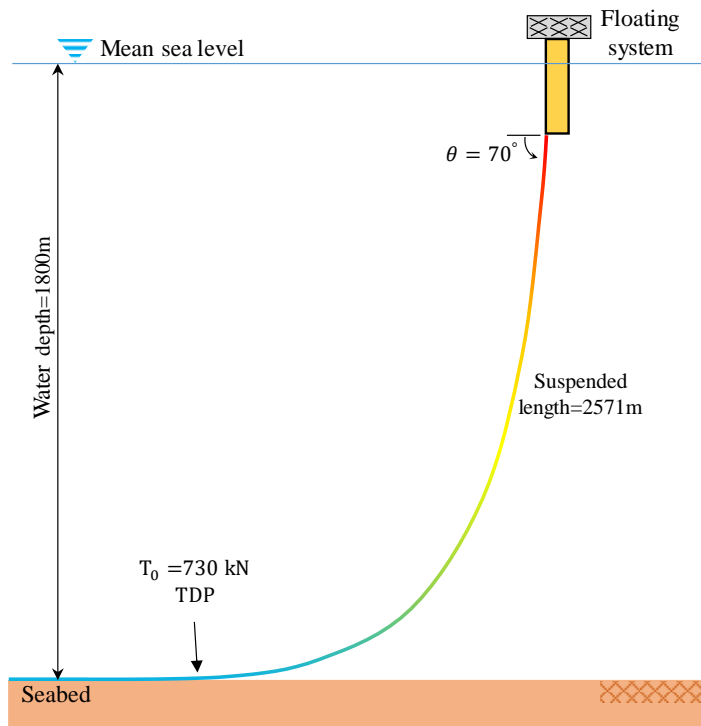


Figure 6-6. The SCR configuration in numerical simulation

Table 6-1. Typical SCR data, Pesce et al., (2006).

Subject	Dimension	Value
Top angle (w.r.t. horiz.)	[deg]	70
Riser length (total)	[m]	5047
Bending stiffness	[Nm ²]	9.915E+06
Axial rigidity*	[N]	2.314E+09
TDP tension	[N]	7.3E+05
External diameter	[m]	0.2032
Depth	[m]	1800
Typical soil stiffness	[kN/m/m]	53.3E+02 (K=2)

*Axial rigidity, 2.314E+11 was used in OrcaFlex® modelling, and immersed weight of SCR per unit length is 790 N/m.

Two scenarios were considered: first, a small TDP oscillation amplitude, resulting a dynamic tension amplitude of $\tau_0/T_0 = 0.01$; and second, a mild TDP oscillation amplitude, for which $\tau_0/T_0 = 0.03$. The tension oscillations were obtained from the

dynamic finite element analysis using OrcaFlex®. The TDP oscillation amplitudes ratio (a_0/λ), were observed as 0.27, 0.4, 0.6 for small oscillations, and 1.2, 1.3, 1.5 for large oscillations. Both the small and large TDP oscillation amplitudes are of the order of the boundary layer length scale (λ). A critical sector along the SCR, with a length of 2λ and a sharp increase of the curvature, was selected. A total number of 11 nodes were considered with a 0.2λ spacing; where $s/\lambda = -1$ corresponds to the TDP position on the rigid seabed ($K = 8$) (see Figure 6-7). The vessel excitation was considered by applying 0.8 m and 1.8 m horizontal surge motion amplitudes, to match identical dynamic tension ratios of $\tau_0/T_0 = 0.01$ (small oscillations) and $\tau_0/T_0 = 0.03$ (mild oscillations) with the analytical results. A sinusoidal motion with period of 15 s was considered, so providing subcritical regime conditions.

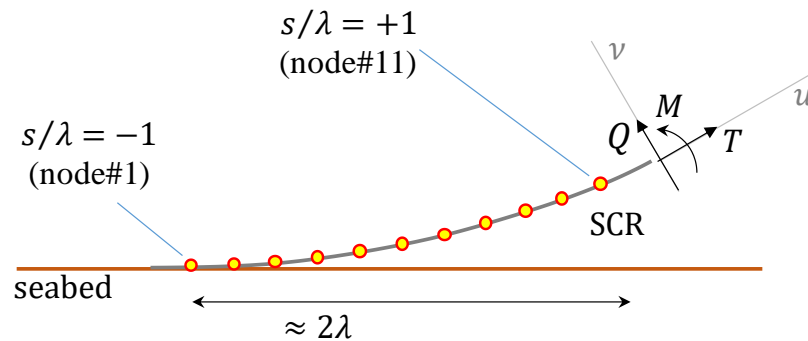


Figure 6-7. Schematic view of the critical zone of the SCR

Figure 6-8 and Figure 6-9 show the non-dimensional results of dynamic curvature oscillation for different seabed slopes, obtained from analytical and numerical analyses, respectively. Without losing generality, the results of curvature dynamics for a mildly rigid ($K = 8$) and soft soil ($K = 2$) were considered as stiffness states. Figure 6-8 illustrates two entire cycles of non-dimensional analytical results for the dynamic curvature oscillation on

FOZ, NOZ, and flat seabed, for small (a-f), and mild (g-l) TDP oscillation amplitudes. It was observed that regardless the soil stiffness, for the nodes near the TDP (node#1), the peak curvature increases in all cases by increasing the TDP oscillation amplitude. The larger TDP oscillation amplitudes cause more nodes on the suspended part to touch the rigid seabed and to experience the null curvature. Also, smoother curvatures were observed on the softer soil seabed.

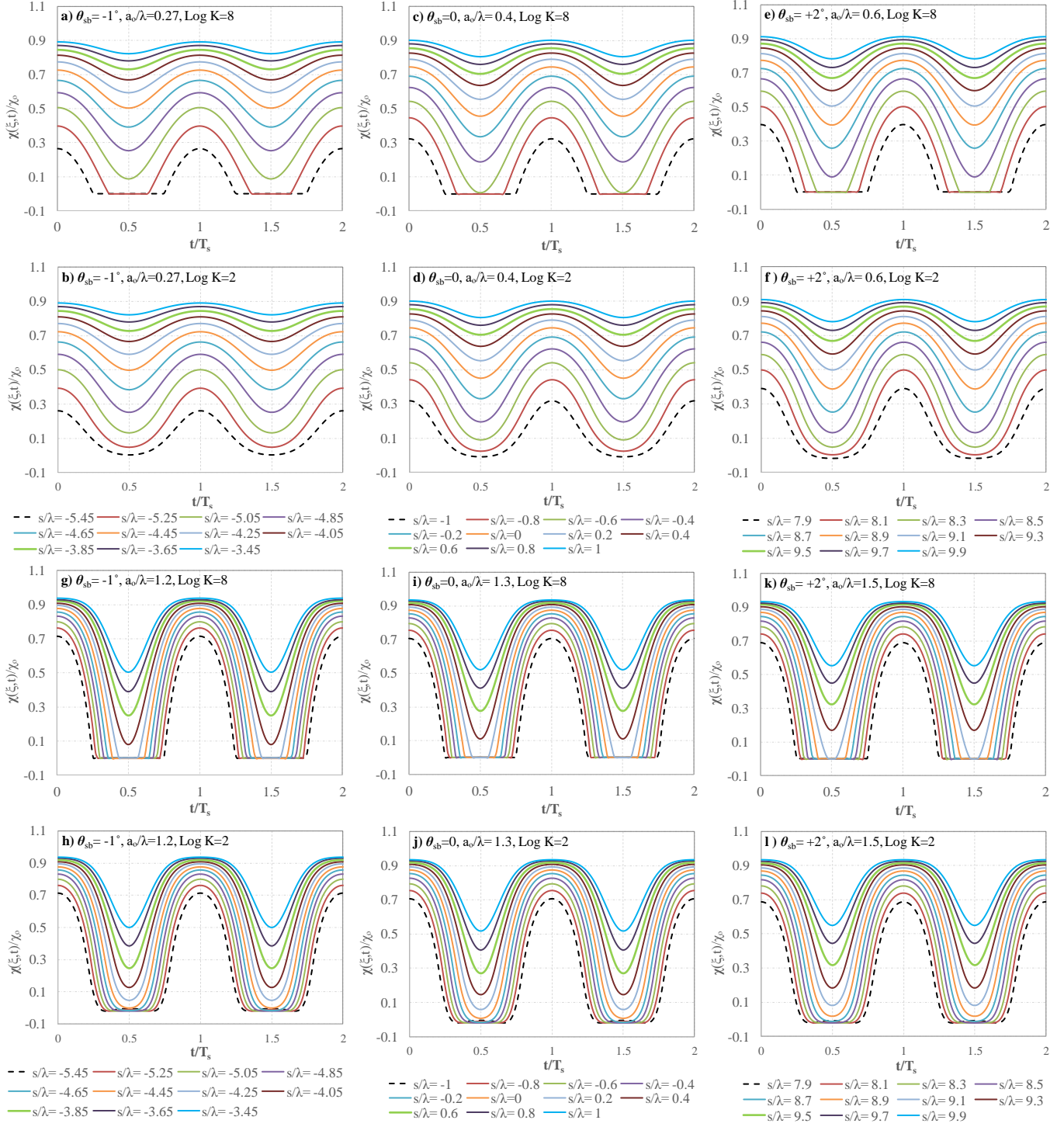


Figure 6-8. Nondimensional dynamic curvature of SCR in TDZ

(a-f): analytical solution for small TDP oscillation, $\tau_0/T_0 = 0.01$

(g-l): analytical solution for mild TDP oscillation, $\tau_0/T_0 = 0.03$

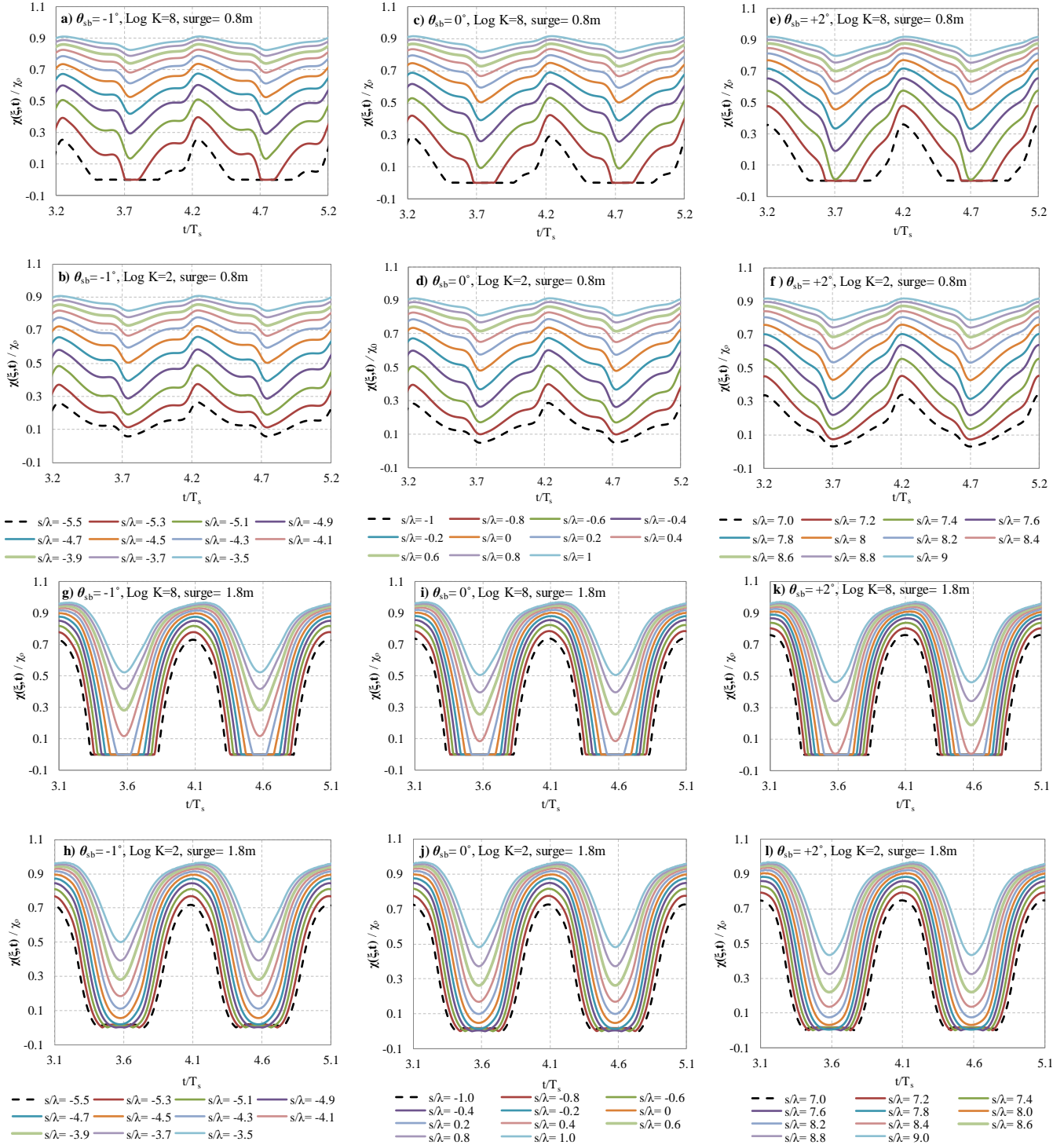


Figure 6-9. Nondimensional dynamic curvature of SCR in TDZ
 (a-f): numerical result for small vessel oscillation, $\tau_0/T_0 = 0.01$
 (g-l): numerical result for mild vessel oscillation, $\tau_0/T_0 = 0.03$

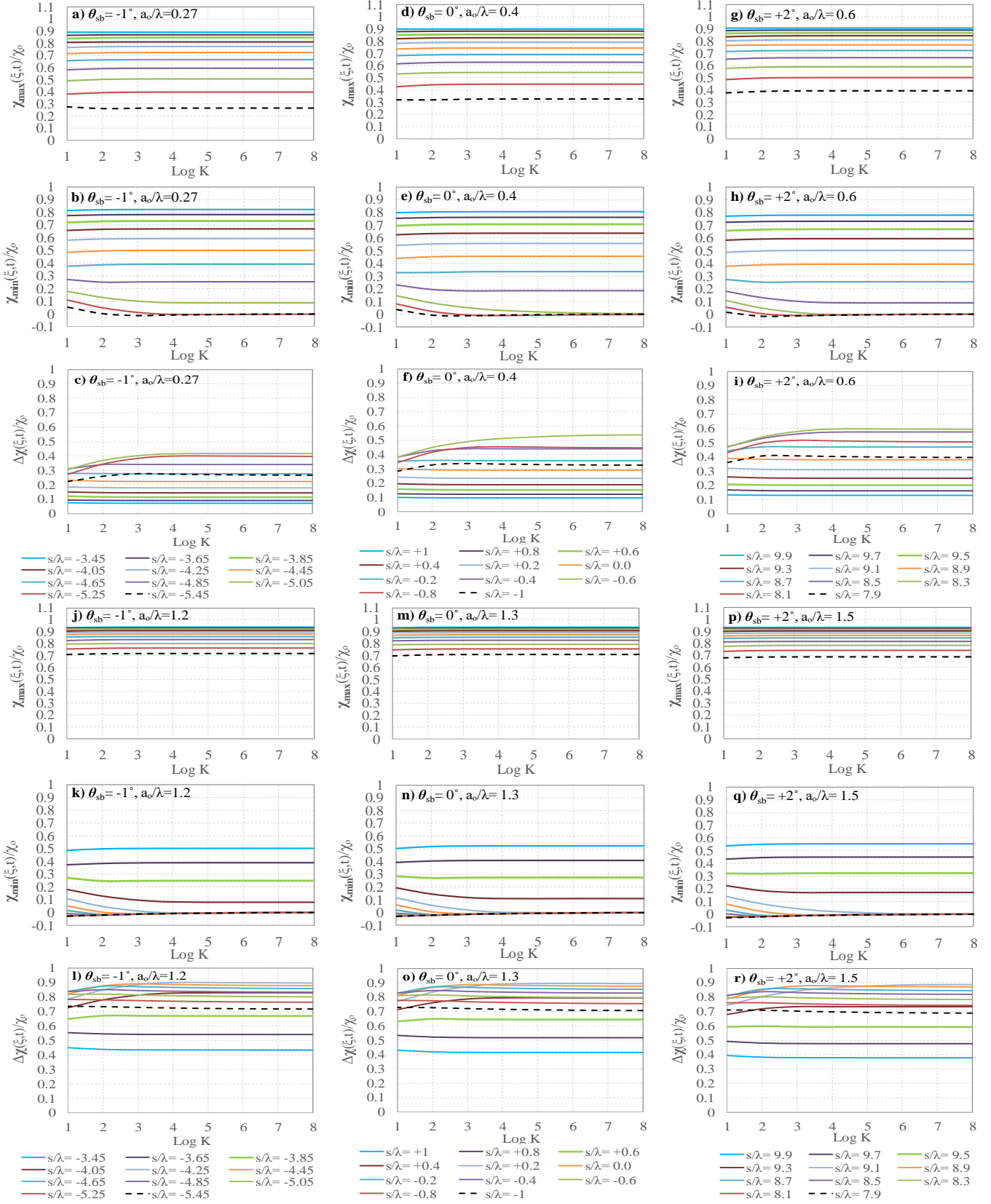


Figure 6-10. Nodal curvature sensitivity of SCR to seabed stiffness in TDZ. (a-i): analytical solution for small TDP oscillation, $\tau_0/T_0 = 0.01$; (j-r): analytical solution for mild TDP oscillation, $\tau_0/T_0 = 0.03$

The analytical sensitivity of each node to the seabed stiffness was then investigated, as shown in Figure 6-10 by comparing the non-dimensional values of maximum, minimum, and the curvature variation. It was observed that increasing the TDP oscillation amplitude causes the maximum curvature (χ_{max}) to increase in the nodes near the seabed. It means that the effect of TDP oscillation amplitude is insignificant in the nodes far away from the seabed (see Figure 6-10 a, j, d, m, g, and p). Also, this oscillation minimizes the least curvature (χ_{min}) for the nodes in TDZ, especially for the nodes far away from the TDP (see Figure 6-10 b, k, e, d, n, h, and q). The results in Figure 6-10 also show that the seabed stiffness variation has a remarkable impact on the minimum curvature (χ_{min}) due to the cyclic contact with the seabed, but almost no effect on maximum curvatures (χ_{max}). The mild vessel oscillations causes the location of seabed effect on minimum curvature to move towards the vessel (e.g., location $s/\lambda = -0.6$ (node 3) in Figure 6-10 (e) for small TDP oscillation amplitude, and $s/\lambda = +2$ (nodes 7) in Figure 6-10 (n) for mild TDP oscillation amplitude). The variation of curvature for each node is defined as the difference between the maximum and minimum curvature oscillations, $\Delta\chi$. The nodal changing of dynamic curvature magnitude can be attributed to the combination of the TDP oscillation amplitude effect on the maximum curvature, and the soil stiffness effect on the minimum curvature. The magnitude of $\Delta\chi$ is decreased due to the increasing in the minimum curvature in the soft soils, and invariant maximum curvature at nodes (see nodes 3 in Figure 6-10 (d) to (f) for small TDP oscillation and node 7 in Figure 6-10 (m) to (o) for large TDP oscillation). Figure 6-11 shows the curvature variations with different seabed stiffness for both analytical and numerical analyses.

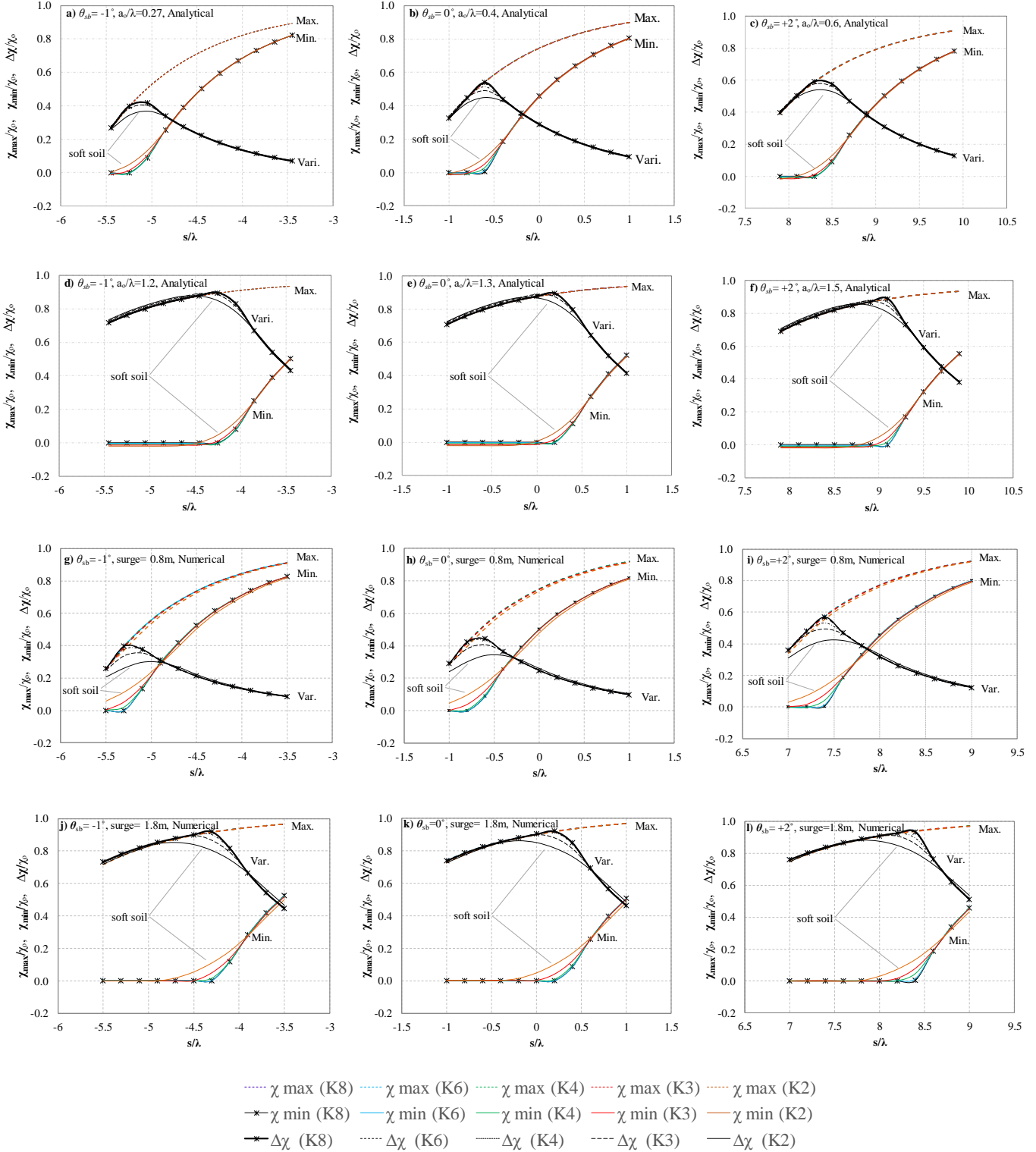


Figure 6-11. Nondimensional dynamic curvature of SCR in TDZ
(a, b, c): analytical solution for small TDP oscillation, $\tau_0/T_0 = 0.01$
(d, e, f): analytical solution for mild TDP oscillation, $\tau_0/T_0 = 0.03$
(g, h, i): numerical result for small vessel oscillation, $\tau_0/T_0 = 0.01$
(j, k, l): analytical result for mild vessel oscillation, $\tau_0/T_0 = 0.03$

Figure 6-11 shows that the softer soil provides a smaller amplitude of curvature oscillation in TDZ. The peak coordinates of curvature oscillations in both NOZ and FOZ are in a good agreement, considering the numerical and the analytical results. The maximum curvature has a direct relationship with the TDP oscillation amplitude near the TDP (see maximum curvatures at a few of first nodes in Figure 6-11 (b), (e), (h), and (k)). However, this effect is reduced for the nodes far away from TDP (see maximum curvatures at $s/\lambda = 1$ (node 11)). Also, the soft seabed increases the minimum curvature around the TDP, with no significant effect on nodes far away. This reduces the curvature amplitude (see black lines of curvature variation in Figure 6-11 (b), (e), (h), and (k)). In all cases, the peak dynamic curvature is related to seabed stiffness and the TDP oscillation amplitude. The results of numerical and analytical analyses bear a close resemblance in terms of the soil stiffness effect on curvature dynamics in the TDZ.

6.4. Fatigue Response of SCR

A series of simplified fatigue analyses were conducted using vessel motion in surge direction to investigate the effect of seabed soil stiffness in the sloped seabed and its relationship with dynamic curvature oscillation. Recall that the analytical formulation is valid only for subcritical regimes, when the maximum speed of the TDP does not exceed the local transversal wave celerity of a homologous cable. Amplitudes of 1.6m and 3.2m in a horizontal direction and a period equal to 15s was then considered, satisfying the quasi-static motion assumption for the TDP oscillation, so not violating the subcritical regime hypothesis. The DNV E class, $SCF = 1.15$, $m = 3$, and $\text{Log } a = 11.61$, according to DNV-RP-F204 S-N curve, in seawater, was considered. Figure 6-12 shows the results of the fatigue analysis with the corresponding dynamic curvature oscillation presented in Figure

6-13. It was observed that the softer soil results in a greater minimum curvature. Also, the TDP oscillation amplitude in the TDZ has a direct impact on the maximum dynamic curvature as the result of vessel excitation. Increasing the amplitude of oscillation enlarges its magnitude and relocates it toward the vessel.

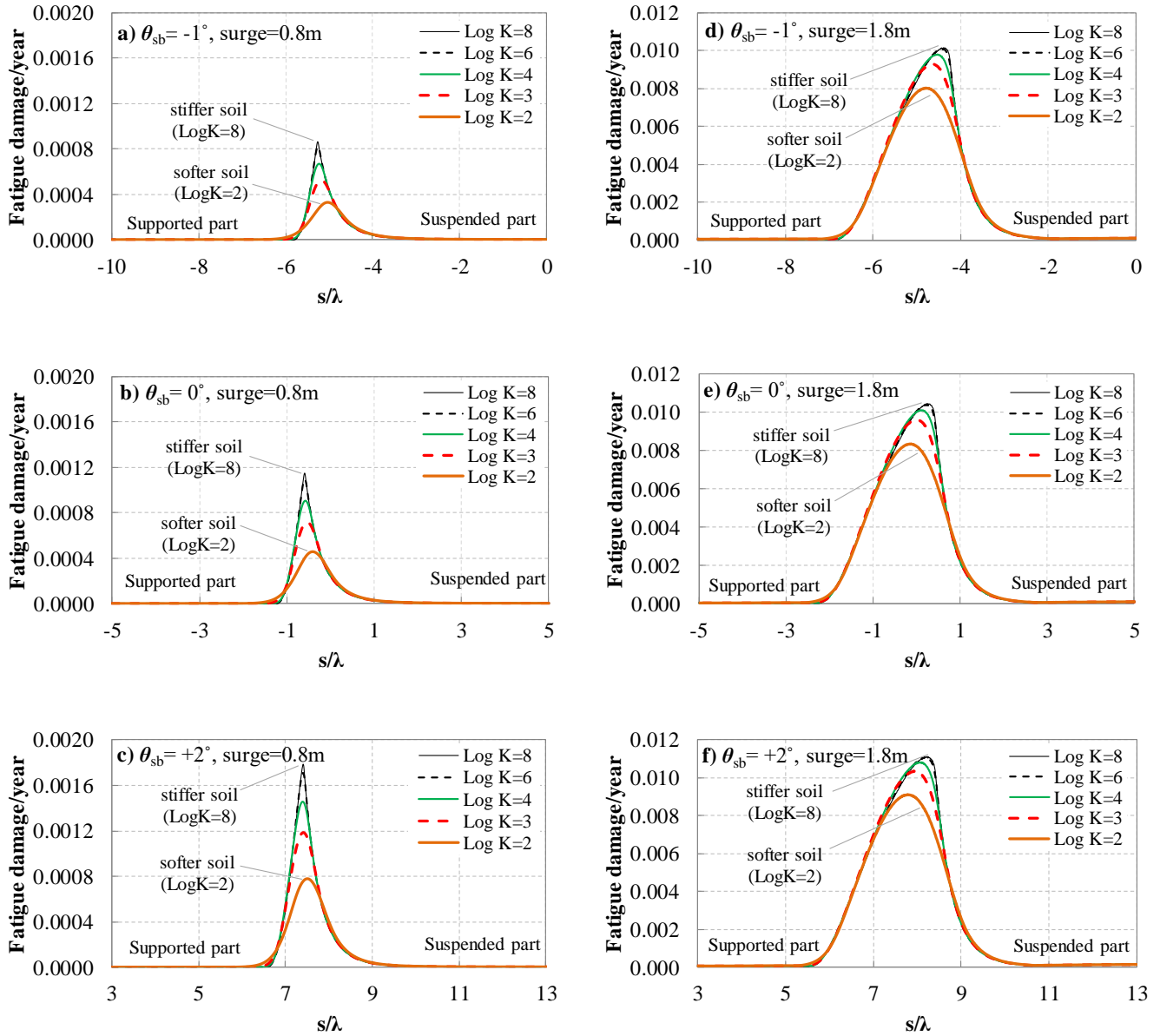


Figure 6-12. Fatigue damage distribution on SCR in TDZ

(a, b, c): result for small vessel oscillation, $\tau_0/T_0 = 0.01$

(d, e, f): result for mild vessel oscillation, $\tau_0/T_0 = 0.03$

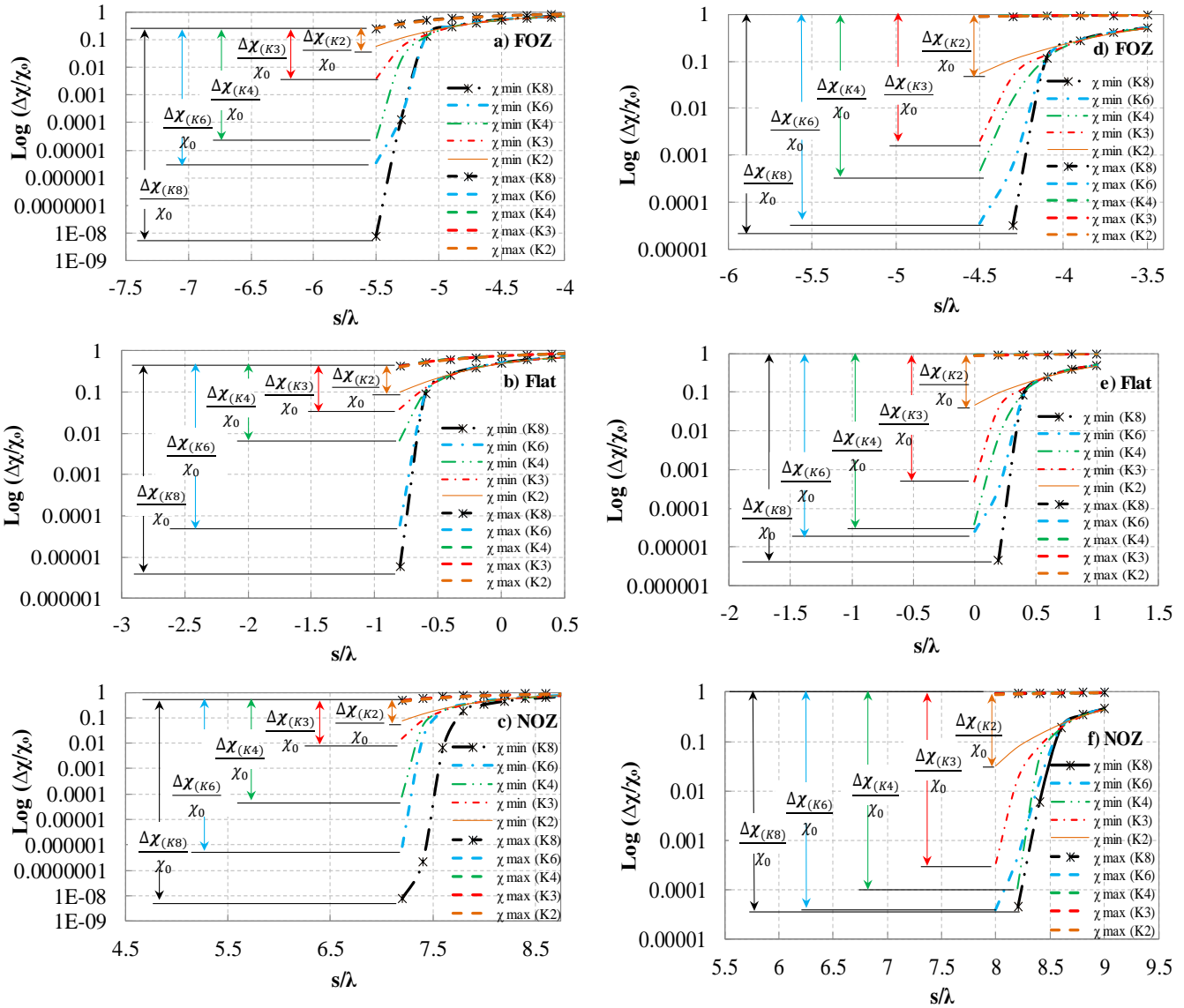


Figure 6-13. Nondimensional dynamic curvature of SCR in TDZ

(a, b, c): result for small vessel oscillation, $\tau_0/T_0 = 0.01$

(d, e, f): result for mild vessel oscillation, $\frac{\tau_0}{T_0} = 0.03$

The fatigue analysis results, on FOZ, NOZ and on flat seabed, show the influence of the TDP motion and soil stiffness. Figure 6-12 shows that increasing the seabed stiffness and the TDP oscillation amplitude results in increasing the magnitude of damage, regardless the seabed slope.

As concluded in the previous section, by tuning the TDP oscillation amplitude in the analytical investigation, the fatigue life is improved in the FOZ and deteriorated in the NOZ. It means that the trench may have a beneficial or detrimental effect on fatigue life due to different trends of TDP oscillation amplitude on the trench shoulder. This may justify some of the contradictory predictions found in the literature that have used different environmental loads and seabed properties. The results of numerical fatigue analysis show that there is a close resemblance between the magnitude and the location of the peak dynamic curvature (Figure 6-11) and fatigue damage (Figure 6-12). The study further revealed the significance of soil stiffness on the minimum curvature of the riser and the TDP oscillation amplitude that in turn, is related to the vessel excitation and trench geometry.

6.5. Conclusions

The dynamic curvature oscillation of a typical SCR in TDZ was investigated by deriving a comprehensive analytical model, generalizing a previous one by Pesce et al. (1998a, 2006) by including trench geometry effects considering different seabed slopes. The analytical model was validated by finite element analysis using a commercial software. A range of seabed stiffness was examined and the corresponding fatigue responses were compared. The study showed that even the effect of the seabed stiffness could be attributed to the geometrical effects of the trench in the TDZ, a factor that has been recently highlighted in

the literature. The study showed that the seabed stiffness has a local effect on SCR and the main contribution of linear soil property (soil stiffness) can be attributed to increasing the local minimum curvature of the SCR, and reducing the dynamic curvature oscillation amplitude. The study further supports the idea of the case-dependence of the trench effect on fatigue. Depending on the dominant direction of fatigue sea states and low-frequency vessel excursions, the TDP may migrate to FOZ or NOZ of the trench, while oscillating under wave-frequency motions. This, in turn, would result in reduced or increased fatigue life.

6.6. APPENDIX – Dynamic equilibrium equations for the planar problem of a catenary riser

This Appendix brings a derivation that can be found in a more detailed analysis in Pesce (1997), Chapter 4, section 4.1. It is however essential for the understanding of the local analysis close to TDP, carried out through the Boundary-Layer technique, in the main core of the text. Consider a planar problem of a riser suspended from a floating unity, whose static configuration is characterized by the functions $\theta(s)$, $T(s)$ and $Q(s)$, respectively the angle of the line with respect to the horizontal, the effective tension and the shear force at a given section s . Let their dynamic counterparts be written as,

$$\begin{aligned}
 \Theta(s, t) &= \theta(s) + \gamma(s, t) \\
 T(s, t) &= T(s) + \tau(s, t) \\
 Q(s, t) &= Q(s) + \vartheta(s, t)
 \end{aligned}
 \tag{A.1}$$

where $\gamma(s, t)$, $\tau(s, t)$ and $\vartheta(s, t)$ are the corresponding perturbed values, resulting from dynamic loads acting on the riser in the vertical plane. Let also $u(s, t)$ and $v(s, t)$ be small displacements around the static equilibrium configuration in their tangential and normal

directions, respectively. To first order, the following well known kinematic relation can be promptly derived.

$$\gamma(s, t) = \frac{\partial v}{\partial s} + u \frac{d\theta}{ds} \quad (\text{A.2})$$

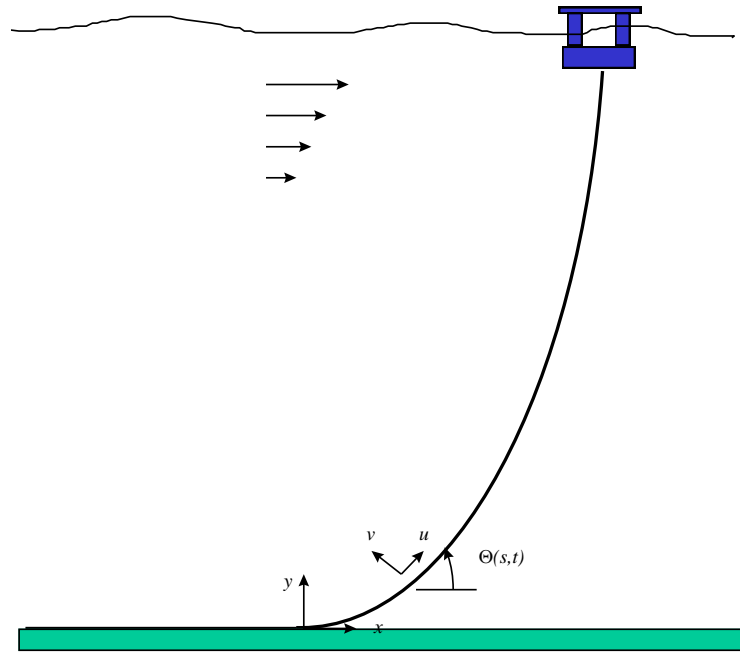


Figure 6-14. The planar problem; Pesce (1997)

Taking a small segment Δs , the resultant of effective tension and shear force projected onto the tangential and normal directions of the static configuration are readily obtained in the form:

$$\begin{aligned} \Delta F_u &= T(s + \Delta s, t) \cos(\Delta\theta + \gamma(s + \Delta s, t)) - T(s, t) \cos \gamma(s, t) - \\ &\quad - (Q(s + \Delta s, t) \sin(\Delta\theta + \gamma(s + \Delta s, t)) - Q(s) \sin \gamma(s, t)) \\ \Delta F_v &= Q(s + \Delta s, t) \cos(\Delta\theta + \gamma(s + \Delta s, t)) - Q(s) \cos \gamma(s, t) + \\ &\quad + (T(s + \Delta s, t) \sin(\Delta\theta + \gamma(s + \Delta s, t)) - T(s, t) \sin \gamma(s, t)) \end{aligned} \quad (\text{A.3})$$

If only first order terms in $\Delta\theta$ and γ are retained, equation (A.3) reduces to

$$\begin{aligned}
\Delta F_u &\cong T(s + \Delta s, t) - T(s, t) \gamma(s, t) - \\
&\quad - (Q(s + \Delta s, t)\Delta\theta + Q(s + \Delta s, t)\gamma(s + \Delta s, t) - Q(s)\gamma(s, t)) \\
\Delta F_v &\cong Q(s + \Delta s, t) - Q(s) + \\
&\quad + (T(s + \Delta s, t)\Delta\theta + T(s + \Delta s, t)\gamma(s + \Delta s, t) - T(s, t)\gamma(s, t))
\end{aligned} \tag{A.4}$$

The dynamic equilibrium equation of the segment Δs then reads

$$\begin{aligned}
\Delta F_u + h_u \Delta s - q \sin \theta \Delta s &= m \frac{\partial^2 u}{\partial t^2} \Delta s \\
\Delta F_v + h_v \Delta s - q \cos \theta \Delta s &= m \frac{\partial^2 v}{\partial t^2} \Delta s
\end{aligned} \tag{A.5}$$

where,

$$\begin{aligned}
h_u(s, t) &= h_u(s) + \varpi_u(s, t) \\
h_v(s, t) &= h_v(s) + \varpi_v(s, t)
\end{aligned} \tag{A.5}$$

refer to the hydrodynamic forces, q is the immersed weight of SCR per unit length and m is the mass of the structure, all per unit length. The terms $h_{u,v}(s)$ and $\varpi_{u,v}(s, t)$ are the components of the static and dynamic parcels of the hydrodynamic force in the tangential and normal direction, regarding the static configuration. The last ones are due to the relative external water flow with respect to the riser, at section s , usually modeled through the well known Morison's formula. Equations (A.5) transform into partial differential ones, by the usual process of taking the limit when $\Delta s \rightarrow 0$, in the following form

$$\begin{aligned}
\frac{\partial T}{\partial s} - (T\gamma + Q) \frac{d\theta}{ds} - \frac{\partial}{\partial s} (Q\gamma) + h_u + \varpi_u - q \sin \theta &= m \frac{\partial^2 u}{\partial t^2} \\
\frac{\partial Q}{\partial s} + (T - Q\gamma) \frac{d\theta}{ds} + \frac{\partial}{\partial s} (T\gamma) + h_v + \varpi_v - q \cos \theta &= m \frac{\partial^2 v}{\partial t^2}
\end{aligned} \tag{A.7}$$

Alternatively, equations (A.9) may be written with the use of the kinematic relation (A.2)

as,

$$\begin{aligned} \frac{\partial T}{\partial s} - \left[T \left(\frac{\partial v}{\partial s} + u \frac{d\theta}{ds} \right) + Q \right] \frac{d\theta}{ds} - \frac{\partial}{\partial s} \left[Q \left(\frac{\partial v}{\partial s} + u \frac{d\theta}{ds} \right) \right] + h_u + \varpi_u - q \sin \theta &= m \frac{\partial^2 u}{\partial t^2} \\ \frac{\partial Q}{\partial s} + \left[T - Q \left(\frac{\partial v}{\partial s} + u \frac{d\theta}{ds} \right) \right] \frac{d\theta}{ds} + \frac{\partial}{\partial s} \left[T \left(\frac{\partial v}{\partial s} + u \frac{d\theta}{ds} \right) \right] + h_v + \varpi_v - q \cos \theta &= m \frac{\partial^2 v}{\partial t^2} \end{aligned} \quad (\text{A.8})$$

Notice that, by using equations (A.1-b,c), equations (A.7) may be also rewritten as,

$$\begin{aligned} \left\{ \frac{\partial T}{\partial s} - Q \frac{d\theta}{ds} + h_u - q \sin \theta \right\} + \left\{ \frac{\partial \tau}{\partial s} - (T\gamma + \vartheta) \frac{d\theta}{ds} - \frac{\partial}{\partial s} (Q\gamma) + \varpi_u \right\} &= m \frac{\partial^2 u}{\partial t^2} \\ \left\{ \frac{\partial Q}{\partial s} + T \frac{d\theta}{ds} + h_v - q \cos \theta \right\} + \left\{ \frac{\partial \vartheta}{\partial s} + (\tau - Q\gamma) \frac{d\theta}{ds} + \frac{\partial}{\partial s} (T\gamma) + \varpi_v \right\} &= m \frac{\partial^2 v}{\partial t^2} \end{aligned} \quad (\text{A.9})^1$$

or, from (A.8),

$$\begin{aligned} &\left\{ \frac{\partial T}{\partial s} - Q \frac{d\theta}{ds} + h_u - q \sin \theta \right\} \\ &\quad + \left\{ \frac{\partial \tau}{\partial s} - \left(T \left(\frac{\partial v}{\partial s} + u \frac{d\theta}{ds} \right) + \vartheta \right) \frac{d\theta}{ds} - \frac{\partial}{\partial s} \left(Q \left(\frac{\partial v}{\partial s} + u \frac{d\theta}{ds} \right) \right) + \varpi_u \right\} \\ &= m \frac{\partial^2 u}{\partial t^2} \\ &\left\{ \frac{\partial Q}{\partial s} + T \frac{d\theta}{ds} + h_v - q \cos \theta \right\} \\ &\quad + \left\{ \frac{\partial \vartheta}{\partial s} + \left(\tau - Q \left(\frac{\partial v}{\partial s} + u \frac{d\theta}{ds} \right) \right) \frac{d\theta}{ds} + \frac{\partial}{\partial s} \left(T \left(\frac{\partial v}{\partial s} + u \frac{d\theta}{ds} \right) \right) + \varpi_v \right\} \\ &= m \frac{\partial^2 v}{\partial t^2} \end{aligned} \quad (\text{A.10})$$

The first terms in brackets, either in equations (A.9) or (A.10) are, in fact, Love's equations for the static equilibrium of curved bars on the plane. Therefore, they are identically null.

¹ Naturally, these dynamic equilibrium equations may be also derived from variational principles, by applying, for instance the extended Hamilton's Principle, see Hamilton (1834). This is left for a further work.

The (perturbed) dynamic variables are, therefore, governed by the following coupled nonlinear partial differential equations:

$$\begin{aligned}\frac{\partial \tau}{\partial s} - ((T + \tau)\gamma + \vartheta) \frac{d\theta}{ds} - \frac{\partial}{\partial s}((Q + \vartheta)\gamma) + \varpi_u &= m \frac{\partial^2 u}{\partial t^2} \\ \frac{\partial \vartheta}{\partial s} + (\tau - (Q + \vartheta)\gamma) \frac{d\theta}{ds} + \frac{\partial}{\partial s}((T + \tau)\gamma) + \varpi_v &= m \frac{\partial^2 v}{\partial t^2}\end{aligned}\tag{A.11}$$

or, given just in terms of the displacements $u(s, t)$ and $v(s, t)$,

$$\begin{aligned}\frac{\partial \tau}{\partial s} - \left((T + \tau) \left(\frac{\partial v}{\partial s} + u \frac{d\theta}{ds} \right) + \vartheta \right) \frac{d\theta}{ds} - \frac{\partial}{\partial s} \left((Q + \vartheta) \left(\frac{\partial v}{\partial s} + u \frac{d\theta}{ds} \right) \right) + \varpi_u &= m \frac{\partial^2 u}{\partial t^2} \\ \frac{\partial \vartheta}{\partial s} + \left(\tau - (Q + \vartheta) \left(\frac{\partial v}{\partial s} + u \frac{d\theta}{ds} \right) \right) \frac{d\theta}{ds} + \frac{\partial}{\partial s} \left((T + \tau) \left(\frac{\partial v}{\partial s} + u \frac{d\theta}{ds} \right) \right) + \varpi_v &= m \frac{\partial^2 v}{\partial t^2}\end{aligned}\tag{A.12}$$

On the other hand, the third planar static Love's equation, that relates bending moment and shear force may be written, in the absence of any external applied moment per unit length as,

$$\frac{\partial M}{\partial s} + Q = 0\tag{A.13}$$

Consistently with the kinematic relation (A.2), and considering that the slenderness of the structure makes the effect of the rotatory inertia neglectable, the corresponding dynamic equation regarding the rotation would be written:

$$\frac{\partial \mu}{\partial s} + \vartheta = 0\tag{A.14}$$

where $\mu(s, t)$ is the dynamic parcel of the bending moment. In fact this is a quasi-static approximation.

Therefore, bending moment and shear may be said to be simply related by

$$\frac{\partial M}{\partial s} + Q = 0 \quad (\text{A.15})$$

On the other hand, from the three basic and usual hypotheses: (i) small strains; (ii) linear relations between stresses and strains; (iii) Kirschoff's 'plane sections remain plane after deformation', the following constitutive equation may be assumed valid:

$$M(s, t) = EI \frac{\partial \Theta}{\partial s} = EI \chi(s, t) \quad (\text{A.16})$$

where EI is the bending stiffness at section s , and $\chi(s, t)$ is the total curvature. The following relations, regarding the static and dynamic parcels, are then promptly derived:

$$M(s) = EI \frac{d\theta}{ds}$$

$$\mu(s, t) = EI \frac{\partial \gamma}{\partial s} \cong EI \left[\frac{\partial^2 v}{\partial s^2} + \frac{\partial}{\partial s} \left(u \frac{d\theta}{ds} \right) \right] \quad (\text{A.17})$$

From (A.13) and (A.14), it follows that,

$$Q(s) = -\frac{\partial}{\partial s} \left(EI \frac{d\theta}{ds} \right)$$

$$\vartheta(s, t) = -\frac{\partial}{\partial s} \left(EI \frac{\partial^2 v}{\partial s^2} + EI \frac{\partial}{\partial s} \left(u \frac{d\theta}{ds} \right) \right) \quad (\text{A.18})$$

Also, using (A.16) in (A.15) and then substituting the result in equation (A.7,b) it follows that,

$$-\frac{\partial^2}{\partial s^2} (EI\chi) + \left(T - \frac{\partial}{\partial s} (EI\chi)\gamma \right) \frac{d\theta}{ds} + \frac{\partial}{\partial s} (T\gamma) + h_v + \varpi_v - q \cos \theta = m \frac{\partial^2 v}{\partial t^2} \quad (\text{A.19})$$

In the common case in which the bending stiffness is assumed constant along the line, equation (A.19) reduces to

$$-EI \frac{\partial^2 \chi}{\partial s^2} - \gamma EI \frac{d\theta}{ds} \frac{\partial \chi}{\partial s} + T\chi + \gamma \frac{\partial T}{\partial s} + h_v + \varpi_v - q \cos \theta = m \frac{\partial^2 v}{\partial t^2} \quad (\text{A.20})$$

Equation (A.20) is a fundamental result to be used in the local analysis, close to TDP, via the Boundary-Layer technique. It can be used in the vicinity of the hang-off point as well; see Pesce (1997).

6.7. Acknowledgments

The authors gratefully acknowledge the financial support of this research by the Research and Development Corporation (RDC) (now Innovate NL) through the Ignite funding program, the “Natural Science and Engineering Research Council of Canada (NSERC)” through Discovery program, and the Memorial University of Newfoundland through VP start-up funding support. The third author acknowledges a research grant from CNPq, the Brazilian National Council for Scientific Research, process 308230/2018-3 and the financial support by CAPES, the Coordination for the Improvement of Higher Education Personnel (CAPES) in Brazil, through the International Exchange Program PRInt-USP/2019.

References

- Aranha, JAP., Martins, CA, Pesce, CP (1997). Analytical Approximation for the Dynamic Bending Moment at the Touchdown Point of a Catenary Riser. *Int Journal of Offshore and Polar Engineering*, vol. 7 (4): 241-249.
- Aubeny, C., and Biscontin, G., (2008). Interaction model for Steel Compliant Riser on Soft Seabed. OTC194193, Houston, TX.
- Aubeny, C., and Biscontin, G., (2009). Seafloor-Riser Interaction Model. *International Journal of Geomechanics* 9(3), 133–141.
- Bridge CD, Howells HA (2007). Observation and modeling of steel catenary riser trenches. *Proceedings of the 17th International Society of Offshore and Polar Engineers Conference ISOPE-I-07-321*; July 1-6; Lisbon, Portugal. pp 803-813.
- Burgess JJ (1993). Bending stiffness in a simulation of undersea cable deployment. *International Journal of Offshore and Polar Engineering* 3(3): 197–204.
- Campbell, M. (1999), "The Complexities of Fatigue Analysis for Deepwater Risers." *Deepwater Pipeline Conference*, New Orleans, USA.

- Clukey, E. C., Young, A. G., Dobias, J. R., and Garmon, G. R. (2008), "Soil response and stiffness laboratory measurements of SCR pipe/soil interaction." *Offshore Technology Conference*, Houston, USA, OTC 19303.
- Dhotarad MS, Ganesan N and Rao BVA (1978). Transmission line vibration with 4R dampers. *Journal of Sound and Vibration* 60(4): 604–606.
- Hamilton WR (1834) On a general method in dynamics. *Philosophical Transaction of the Royal Society Part II*: 247–308.
- Irvine M. (1993). Local bending stresses in cables. *International Journal of Offshore and Polar Engineering* 3(3): 172–175.
- Langner C (2003). Fatigue life improvement of steel catenary risers due to self- trenching at the touchdown point. *Proceedings of the Offshore Technology Conference OTC 15104*; May 5-8; Texas, USA.
- Love AEH. *A Treatise on the Mathematical Theory of Elasticity*. 4th (1927) edition., Dover Pub. Inc., N.Y., 1944, 643 pp.
- Pesce, CP, Pinto, MMO, (1996). First-order Dynamic Variation of Curvature and tension in Catenary Risers. 6th International Offshore & Polar Engineering Conference, Los Angeles, May 26-31, *Proceedings*, vol. 2, pp 163-175.
- Pesce CP, Aranha JAP, Martins CA (1998a). The soil rigidity effect in the touchdown boundary layer of a catenary riser: Static problem. *Proceedings of the International Society of Offshore and Polar Engineers Conference ISOPE-I-98-130*; May 24-29; Montreal, Canada.
- Pesce CP, Aranha JAP, Martins CA, Ricardo OGS and Silva S (1998b), Dynamic Curvature in Catenary risers at the Touch Down Point: an experimental study and the analytical boundary layer solution. *International Journal of Offshore and Polar Engineering, USA*, 8(3): 302-310.
- Pesce, CP, (1997). *Mechanics of cables and tubes in catenary configuration: an analytical and experimental approach*. ‘Livre-Docência’ Thesis, (in Portuguese). University of São Paulo.
- Pesce CP, Martins C, Silveira LM, (2006). Riser-soil interaction: local dynamics at TDP and a discussion on the eigenvalue and the VIV problems, *J. Offshore Mech. Arctic Eng.* 128 (1) 39–55.
- Randolph MF, Bhat S, Mekha B, (2013). Modeling the touchdown zone trench and its impact on SCR fatigue life, *Proceedings of the Offshore Technology Conference OTC-23975-MS*, <https://doi.org/10.4043/23975-MS> May 6-9.
- Rezazadeh K, Shiri H, Zhang L, Bai Y (2012). Fatigue generation mechanism in touchdown area of steel catenary risers in non-linear hysteretic seabed. *Research Journal of Applied Sciences, Engineering and Technology*; 4(24):5591-5601.
- Shiri H (2014a). Response of steel catenary risers on hysteretic non-linear seabed. *Applied Ocean Research*, January; 44:20-28. <https://doi.org/10.1016/j.apor.2013.10.006>.

- Shiri H (2014b). Influence of seabed trench formation on fatigue performance of steel catenary risers in touchdown zone. *Marine Structures*. April; 36:1-20. <https://doi.org/10.1016/j.marstruc.2013.12.003>.
- Shiri H., Randolph MF, (2010). Influence of seabed response on fatigue performance of steel catenary risers in touchdown zone. *Proceeding of the 29th International Conference on Ocean, Offshore and Arctic Engineering OMAE 2010-20051*; June 6-11; Shanghai, China. pp. 63-72; doi:10.1115/OMAE2010-20051.
- Shoghi R, Shiri H., (2019). Modelling Touchdown Point Oscillation and Its Relationship with Fatigue Response of Steel Catenary Risers. *Applied Ocean Research*, 87 142-154.
- Shoghi R, Shiri H., (2020). Re-assessment of trench effect on fatigue performance of steel catenary risers in the touchdown zone. *Applied Ocean Research*, 94 1-16.
- Triantafyllou MS and Triantafyllou GS (1991). The paradox of the hanging string an: explanation using singular perturbation. *Journal of Sound and Vibration* 148(2): 343–351.
- Wang K, Low YM, (2016). Study of seabed trench induced by steel catenary riser and seabed interaction. *Proceedings of the 35th International Conference on Ocean, Offshore and Arctic Engineering OMAE2016-54236*; June 19-24; Busan: South Korea. doi:10.1115/OMAE2016-54236.

Chapter 7

Conclusions and Recommendations

7.1. Conclusions

The current study collectively resulted in several important observations and conclusions that are considered significant contributions to the research topic. The key findings of the study are summarized as follows:

- The WF vessel oscillations about a mean position result in a shallow “cyclic embedment” of the riser into the seabed by less than about one diameter (with the regular performance of the existing non-linear hysteretic riser-seabed interaction models). This cyclic penetration slightly increases the fatigue damage in the vessel side of the TDP (NOZ) and slightly decreases the damage in the anchor side (FOZ). The peak fatigue damage may slightly move towards the vessel or not move depending on the non-linear seabed model.
- The shallow “cyclic embedment” of the riser into the seabed is not necessarily the same as a deep “trench.” The existing non-linear hysteretic models are usually quickly stabilized by achieving a maximum penetration depth of less than one diameter, which is called a premature stabilization, while the real trenches observed in the field are in the range of several diameters deep. Also, there are still several important but less-explored contributors to the trench formation, either individually, or interactively. Therefore, care should be taken in generalizing the results obtained from “cyclic

embedment” to “trench,” and further studies are required to see whether the ultimate trench profile is the scaled-up version of cyclic embedment profile.

- The LF vessel excursions with near, far, and out of plane offsets may have a significant influence on ultimate fatigue results. These excursions result in TDP migration towards the NOZ and FOZ of the trench that causes an increase and decreases in peak fatigue damage, respectively. Therefore, the results of the published studies, which have only applied WF oscillations or the LF motions with no large excursions cannot be simply generalized to reality.
- The combined WF+LF motions on a trenched seabed were found to slightly increase the damage in near excursions (NOZ) and slightly decrease the damage in far excursions (FOZ). However, the peak fatigue damage is largely moved by tens of diameters (e.g., 50D) depending on the direction of excursions. In other words, in real life, where the environmental load spectra depend on geographical locations, scattered results may be obtained depending on the probability of the dominant TDP oscillations in NOZ or FOZ. This implies the case-dependence of the trench effect on fatigue performance of SCR in the TDZ and emphasizes on the need for independent study of any individual project.
- The artificial insertion of a mathematical or pre-defined trench profile to study the trench effect on fatigue response is a risky approach. The fatigue results obtained by this approach are usually susceptible to potential distortion due to creating unexpected contact pressure hot spots at trench mouth. These pressure hotspots can be created as

the result of a disagreement between the natural catenary profile of the SCR and the mathematical trench profile that alters the bending moment variation. This is less likely in reality since a fully developed trench is expected to accommodate the majority of oscillating SCR configurations that may happen during the operation life. There is only one study that has resolved this issue to some extent by proposing a “stepped trench.” This method can be further developed to enhanced performance. The automative trench creation using cyclic SCR perturbations and extreme seabed model parameters can be an appropriate approach to guarantee the prevention of having pressure hotspots. However, care shall be taken in the quickly scaled-up trench profiles that further develops towards the anchor end.

- Fatigue performance of SCR is engaged with behaviour of TDP motion, which is affected by seabed geometry. In both far and near zones of the trench, the slope plays a fundamental rule. According to this view, fatigue performance of SCR on the trench can result from beneficial to detrimental effects, in a way steeper seabed has a beneficial effect in FOZ and a detrimental effect in NOZ on fatigue performance of riser. It should be taking into account that fatigue performance of SCR in the presence of inserted trench is result-oriented in most of the studies, which each of the components such as soil parameters, trench geometry, vessel excitations, vessel position, and so many more parameters could alter the result or obtained damage for a specific case study respect to the flat seabed or other trench geometries. Then, fatigue performance of the SCR project in a given geographical location with its specific environmental loads and seabed conditions should be assessed individually.

- Assessments of the fatigue performance of SCR demonstrate that fatigue damage of SCR is related to both TDP motion and seabed stiffness, which are known as critical parameters of SCR fatigue performance. TDP motion is linked to trench geometry and vessel excitation, and seabed stiffness is linked to seabed soil. Seabed stiffness has a local effect on SCR fatigue performance and can be attributed to altering the riser vibration in TDZ. The linear soil mechanism reduces the dynamic SCR oscillation amplitude in softer soils. The trench geometry influences the fatigue damage by its shoulder slopes. However, the soil stiffness shows almost a uniform effect on the fatigue damage, where the fatigue life is improved for the softer seabed.

7.2. Recommendations for Future Study

Riser-seabed interaction is a complex phenomenon with a range of less or non-explored aspects that need deep investigations. The following research works are recommended for future studies:

- Developing new research programs providing access to the real trench shapes accompanied by supporting field data such as vessel oscillations, SCR stress/strain oscillations, and seabed stiffness degradation histories. These data can be significantly beneficial for obtaining robust and reliable solutions to predict and mitigate the fatigue damage in the TDZ.
- Improving the simplified trench geometries to consider the curvature of trench shoulders, particularly in NOZ, where the fatigue results are usually distorted because of pressure hot spots between the SCR and the trench profiles. It is also important to investigate whether the real fully developed trench profile accommodates all riser

configurations during the lifetime oscillation without creation any pressure hot spots in NOZ, particularly in the trench mouth? The answer to this question needs subsea surveys and is crucial for reliable assessment of the trench effect on fatigue in the TDZ.

- Investigating the proper relationship between the average shear force, TDP oscillation, and the axial stress range. This can result in quantitative fatigue assessment using analytical solutions, which will be of significant importance in the early stages of riser engineering design.
- There are still several important but less-explored contributors to the trench formation, either individually, or interactively. Therefore, care should be taken in generalizing the results obtained from “cyclic embedment” to “trench,” and further studies are required to see whether the ultimate trench profile is the scaled-up version of cyclic embedment profile.
- As the fatigue performance of SCR in the TDZ is case-dependent, comprehensive studies, including different metocean data, are needed to categorize the fatigue study for different excitations.

Bibliography

- API-STD-2RD. (2013). "Standard for riser systems that are part of a floating production system (FPS)." American Petroleum Institute, Washington, DC, USA.
- API-RP-16Q. (2017). "Recommended practice for design, selection, operation and maintenance of drilling riser system." American Petroleum Institute, Washington, DC, USA.
- API-RP-17A. (2017). "Design and operation of subsea production systems." American Petroleum Institute, Washington, DC, USA.
- API-RP-17B. (2014). "Design and operation of subsea production systems." American Petroleum Institute, Washington, DC, USA.
- API-RP-17C. (2003). "Recommended practice for TFL (Through Flowline) systems." American Petroleum Institute, Washington, DC, USA.
- Aranha JAP, Martins CA & Pesce CP. (1997) Analytical Approximation for the Dynamic Bending Moment at the Touchdown Point of a Catenary Riser. *Int. Journal of Offshore and Polar Engineering*, Dec., 1997, vol. 7 (4), 293-300.
- Aranha, J.A.P., Martins, C.A. & Pesce, C.P. Dynamic Bending Moment at the Touch Down Point of a Steel Catenary Riser; 1995; Original Manuscript.
- Aranha, J. A. P., Pesce, C. P., Martins, C. A., & Andrade, B. L. R. Mechanics of Submerged Cables: Asymptotic Solution And Dynamic Tension. 3rd International Society of Offshore and Polar Engineers Conference, Singapore, Jun 6-11, 1993. Vol 2, pp. 345-356.
- Aubeny, C., and Biscontin, G., 2008. Interaction model for Steel Compliant Riser on Soft Seabed. OTC194193, Houston, TX.
- Aubeny, C., and Biscontin, G., 2009. Seafloor-Riser Interaction Model. *International Journal of Geomechanics* 9(3), 133–141.
- Aubeny CP, Biscontin G. Seafloor interaction with steel catenary risers. Offshore Technology Research Center. Texas A&M University, College Station, Houston, Final Project Report to Minerals Management Service 2006, OTRC Library Number 9/06A173.
- Aubeny CP, Gaudin C, Randolph MF. Cyclic tests of model pipe in kaolin. Proceedings of the Offshore Technology Conference OTC 2008-19494-MS; 2008 May 5-8; Texas, USA. <https://doi.org/10.4043/19494-MS>.

- Aubeny, C. P., Shi, H., and Murff, J. D. (2005). "Collapse loads for a cylinder embedded in trench in cohesive soil." *International Journal of Geomechanics, ASCE*, 5(4),320–325.
- Bridge CD, Howells HA. Observation and modeling of steel catenary riser trenches. *Proceedings of the 17th International Society of Offshore and Polar Engineers Conference ISOPE-I-07-321*; 2007 July 1-6; Lisbon, Portugal. pp 803-813.
- Bai, Y. (2001). *Pipelines and risers*, Elsevier Science.
- Bridge C. Effect of seabed interaction on steel catenary risers. 2005; PhD thesis; University of Surrey, UK.
- Bridge, C., Laver, K., Clukey, E., and Evans, T. (2004), "Steel Catenary Riser Touchdown Point Vertical Interaction Models." *Offshore Technology Conference*, Houston,Texas, USA, OTC16628.
- Bridge, C., and Willis, N. (2002), "Steel Catenary Risers—Results and Conclusions from Large Scale Simulations of Seabed Interaction". *14th Annual Conference Deep Offshore Technology*, Cape Town, South Africa, 40-60.
- Bruton, D., Carr, M., & White, D. J. (2007, January 1). The Influence Of Pipe-Soil Interaction On Lateral Buckling And Walking of Pipelines- *The SAFEBUCK JIP. Society of Underwater Technology*.
- Burgess JJ (1993). Bending stiffness in a simulation of undersea cable deployment. *International Journal of Offshore and Polar Engineering* 3(3): 197–204.
- Campbell, M. (1999), "The Complexities of Fatigue Analysis for Deepwater Risers." *Deepwater Pipeline Conference*, New Orleans, USA.
- Cathie, D. N., Jaeck, C., Ballard, J. C., and Wintgens, J. F. (2005), "Pipeline geotechnics—State of the Art." *Proceedings of the international symposium on frontiers in offshore geotechnics*, Perth, Australia, 95–114.
- CARISIMA - Catenary Riser Soil Interaction Model for global riser Analysis - JIP Proposal T99-70.003 March 1999, Marintek. Trondheim, Norway.
- Champneys, A. R., Van der Heijden, G. H. M., and Thompson, J. M. T. (1997). "Spatially complex localization after one-twist-per-wave equilibria in twisted circular rods with initial curvature." *Philosophical Transactions: Mathematical, Physical and Engineering Sciences*, 2151-2174.
- Cheuk, C. Y., and White, D. J. (2008), "Centrifuge modelling of pipe penetration due to dynamic lay effects." *Proceedings of the 27th International Conference on Offshore Mechanics and Arctic Engineering*, Estoril, Portugal, 15–20.

- Clukey EC, Aubeny CP, Zakeri A, Randolph MF, Sharma PP, White DJ, Sanico R, Cerkovnic M. A perspective on the state of knowledge regarding soil-pile interaction for SCR fatigue assessments. Proceedings of the Offshore Technology Conference OTC 27564-MS; 2017 May 1-4; Texas, USA
- Clukey EC, Ghosh R, Mokalala P, Dixon M. Steel catenary riser (SCR) design issues at touchdown area. Proceedings of The 17th International Offshore and Polar Engineering Conference ISOPE-I-07-388; 2007 July 1-6; Lisbon, Portugal. <https://doi.org/10.4043/22557-MS>.
- Clukey E, Jacobs P, Sharma PP. (2008) "Investigation of riser seafloor interaction using explicit finite element methods", *Offshore Technology Conference*, Houston, Texas, OTC19432-MS.
- Clukey, E. C., Young, A. G., Dobias, J. R., and Garmon, G. R. (2008), "Soil response and stiffness laboratory measurements of SCR pipe/soil interaction." *Offshore Technology Conference*, Houston, USA, OTC 19303.
- Dhotarad MS, Ganesan N and Rao BVA (1978). Transmission line vibration with 4R dampers. *Journal of Sound and Vibration* 60(4): 604–606.
- Dixon, D. A., and Rutledge, D. R. (1968). "Stiffened catenary calculations in pipeline laying problem." *ASME J. Engng. Indust*, 90, 153–160.
- Dixon M (2009). "Modelling advances enhance riser fatigue prediction accuracy." *Online Oil & Gas Engineer Magazine-Exploration Drilling*, London, UK.
- DNV-OS-C101 (2018). "Design of offshore steel structures, general- LRFD method." Det Norske Veritas, Hovik, Norway.
- DNV. (1996). "Rules for submarine pipeline systems." Det Norske Veritas, Hovik, Norway.
- Dong X, Shiri H. Performance of non-linear seabed interaction models for steel catenary riser, Part 1: nodal response. *Ocean Engineering*. 2018; (154) 153-166
- Dong X, Shiri H. Performance of non-linear seabed interaction models for steel catenary riser, Part 1: global response. *Ocean Engineering*. 2019; (82) 158-174
- Draper S, Cheng L, White DJ. Scour and sedimentation of submarine pipelines: Closing the gap between laboratory experiments and field conditions. *Journal Scour and Erosion: Proceedings of the 8th International Conference on Scour and Erosion*. 2016 August. DOI: 10.1201/9781315375045-4.
- Elliott BJ, Zakeri A, Barrett J, Macneill A, Phillips R, Clukey EC, and Li G. Centrifuge modeling of steel catenary risers at touchdown zone Part I: Development of novel centrifuge experimental apparatus. *Ocean Engineering*. 2013 March 1; 60, 200-

207. <https://doi.org/10.1016/j.oceaneng.2012.11.012>.

- Elliott BJ, Zakeri A, Barrett J, Hawlader B, Li G, Clukey EC. Centrifuge modeling of steel catenary risers at touchdown zone Part II: Assessment of centrifuge test results using kaolin clay. *Ocean Engineering*. 2013 March 1; 60, 208-218. <https://doi.org/10.1016/j.oceaneng.2012.11.013>.
- Elosta H, Huang S, Incecik A. Trenching effects on structural safety assessment of integrated riser/semisubmersible in cohesive soil. *Journal of Engineering Structures*; 2014; (77) 57-64.
- Fontaine, E. "SCR-Soil Interaction: Effect on Fatigue Life and Trenching. (2006), *Proceedings of the Sixteenth (2006) International Offshore and Polar Engineering Conference*, San Francisco, CA, USA, 2.
- Fouzder, A., Zakeri, A., and Hawlader, B. (2012) "Steel catenary risers at touchdown zone - A fluid dynamics approach to understanding the water-riser-soil interaction", 9th International Pipeline Conference, Calgary, V4, 31-36.
- Giertsen E, Varley R, Schroder K. CARISIMA: a catenary riser/soil interaction model for global riser analysis. *Proceedings of the 23rd International Conference on Offshore Mechanics and Arctic Engineering OMAE 2004-51345*; 2004 June 20-25; Vancouver, Canada. doi:10.1115/OMAE2004-51345.
- Guarracino, F., and Mallardo, V. (1999). "A refined analytical analysis of submerged pipelines in seabed laying." *Applied Ocean Research*, 21(6), 281-293.
- Hamilton WR (1834) On a general method in dynamics. *Philosophical Transaction of the Royal Society Part II*: 247–308.
- Hasselmann, K., Barnett, T. P., Bouws, E., Carlson, H., Cartwright, D. E., Enke, K., Ewing, J. A., Gienapp, H., Hasselmann, D. E., and Kruseman, P. (1973). "Measurements of wind-wave growth and swell decay during the Joint North Sea Wave Project (JONSWAP)." *Dtsch. Hydrogr. Z. Suppl. A*, 8(12), 289–300.
- Hatton, S. A., and Willis, N. (1998), "Steel catenary risers for deepwater environments." *Offshore Technology Conference*, Houston, TX, USA, OTC8607.
- Hodder, M.S. and Byrne, B.W. (2009) "3D experiments investigating the interaction of a model SCR with the seabed", *Applied Ocean Research*, 32:145-157.
- Howells H. (1995). *Advances in Steel Catenary Riser Design*. 2H OffShore Engineering Ltd, Surrey.
- Irvine M. (1993). Local bending stresses in cables. *International Journal of Offshore and Polar Engineering* 3(3): 172–175.

- Jeanjean P. Re-assessment of P-Y curves for soft clays from centrifuge testing and finite element modelling. 2009; Proceedings of the Offshore Technology Conference OTC-20158-MS; 2009 May 4-7; Texas, USA. <https://doi.org/10.4043/20158-MS>.
- Karayaka, M., and Xu, L. "Catenary Equations for Top Tension Riser Systems." *Proceedings of the International Offshore and Polar Engineering Conference 2003*, Honolulu, HI, United States, 638-644.
- Konuk, I. (1980). "Higher-order approximations in stress analysis of submarine pipelines." *J. Energy Resour. Technol.*, 102(4), 190-196.
- Langner, C. G. (2003), "Fatigue Life Improvement of Steel Catenary Risers due to Self-Trenching at the Touchdown Point." *Offshore Technology Conference*, Houston, Texas, USA, OTC15104.
- Larsen CM, Halse KH. Comparison of models for vortex-induced vibrations of slender marine structures. *Marine Structures 1997 July*; 10(6):413-441. [https://doi.org/10.1016/S0951-8339\(97\)00011-7](https://doi.org/10.1016/S0951-8339(97)00011-7).
- Leibniz. (1691). "Solutions to the Problem of the Catenary, or Funicular Curve, Proposed by M. Jacques Bernoulli in the Acta of June 1691." *Acta Eruditorum, Leipzig, Germany*.
- Leira BJ, Passano E, Karunakaran D, Farnes KA, Giertsen E. Analysis guidelines and application of a riser-soil interaction model including trench effects. Proceedings of the 23rd International Conference on Offshore Mechanics and Arctic Engineering OMAE 2004-51527; 2004 June 20-25; Vancouver, Canada. pp. 955-962, doi:10.1115/OMAE2004-5152.
- Lim F, Gauld S. (2003). Riser Solutions for Ultra-Deep Water Developments. *Proceedings of 10th Annual India Oil & Gas Symposium*, Mumbai, India.
- Love AE H. A Treatise on the Mathematical Theory of Elasticity. 4th (1927) edition., Dover Pub. Inc., N.Y., 1944,643 pp.
- Martin CM, and White DJ. Limit analysis of the undrained capacity of offshore pipelines. *Géotechnique*, 2012, 62(9):847-863.
- Maclure D, Walters D. (2007). Freestanding Risers in the Gulf Of Mexico — A Unique Solution For Challenging Field Development Configurations. *2H Offshore Engineering Ltd*, Surrey.
- MCS. (1994). *User Manual for FLEXCOM3D, a taylor-made finite element programme for non-linear time domain analysis of offshore structures*, MCS Advanced Subsea Engineering, Galway, Ireland.

- Miner, M. A. (1945). "Cumulative damage in fatigue." *Journal of applied mechanics*, 12(3), 159-164.
- Nakhaee A, Zhang J. Effects of the interaction with the seafloor on the fatigue life of a SCR. *Proceedings of the 18th International Society of Offshore and Polar Engineers Conference ISOPE-I-08-397*; 2008 July 6-11; Vancouver, Canada. pp 87-93.
- Nakhaee, A., and Zhang, J., (2010). Trenching effects on dynamic behavior of a steel catenary riser. *Ocean Engineering*. 37. 277–288.
- Oliphant J, Maconochie A, White DJ, Bolton MD. Trench interaction forces during lateral SCR movement in deepwater clays. *Proceedings of Offshore Technology Conference, 2009 May, Houston, USA, paper OTC19944*
- Orcina Ltd. (1986). "Orcaflex User Manual." Cumbria, UK.
- Palmer, A., Hutchinson, G., and Ells, J. (1974). "Configuration of Submarine Pipelines during Laying Operation." *ASME J. Engng. Industry* (96), 1112-1118.
- Palmgren, A. G. (1924). "Die Lebensdauer von Kugellagern (Life Length of Roller Bearings. In German)." *Zeitschrift des Vereines Deutscher Ingenieure (VDI Zeitschrift)*, 68(14), 339-341.
- Pesce C.P. Mechanics of Submerged Tubes and Cables in Catenary Configuration: analytical and experimental approaches. 'Livre-Docência' Thesis (in Portuguese), University of Sao Paulo, June, 1997, 350 pp.
- Pesce, C. P., Aranha, J. A. P., and Martins, C. A. (1998), "The Soil Rigidity Effect in the Touchdown Boundary-Layer of a Catenary Riser: Static Problem." *Eighth International Offshore and Polar Engineering Conference ISOPE-I-98-130*; 1998 May 24-29; Montreal, Canada, 207-213.
- Pesce CP, Aranha JAP, Martins CA, Ricardo OGS and Silva S. Dynamic Curvature in Catenary risers at the Touch Down Point: an experimental study and the analytical boundary layer solution. *7th Int. Offshore and Polar Engineering Conference, ISOPE'97*; Honolulu, May, 1997. *Proceedings vol II*, 656-665.
- Pesce CP, Martins C, Silveira LM. Riser-Soil Interaction: Local Dynamics at TDP and a Discussion on the Eigenvalue and the VIV Problems. *Journal of Offshore Mechanical and Arctic Engineering*; 2006; 128(1), 39-55
- Pesce, C. P., and Martins, C. A., 2005, "Numerical Computation of Riser Dynamics," *Numerical Modelling in Fluid-Structure Interaction, Advances in Fluid Mechanics Series*, S. Chakrabarti ed., WIT Press, Southampton, UK, Chap. 7, pp. 253–309.

- Pesce, C.P., & Pinto, M.M.O. First-order Dynamic Variation of Curvature and tension in Catenary Risers. 6th International Offshore & Polar Engineering Conference, Los Angeles, May 26-31, 1996, Proceedings, vol. 2, pp 163-175.
- Phifer, E. H., Frans, K., Swanson, R. C., Allen, D. W., and Langner, C. G. (1994), "Design And Installation Of Auger Steel Catenary Risers." *Offshore Technology Conference*, Houston, Texas, USA, OTC7620.
- Pierson Jr, W. J., and Moskowitz, L. (1964). "A proposed spectral form for fully developed wind seas based on the similarity theory of SA Kitaigorodskii." *Journal of Geophysical Research*, 69(24), 5181–5190.
- Plunkett, R. (1967). "Static bending stresses in catenaries and drill strings." *Journal of Engineering for Industry, Transactions of the ASME*, 89(1), 31–36.
- Randolph MF, Bhat S, Mekha B. Modeling the touchdown zone trench and its impact on SCR fatigue life. *Proceedings of the Offshore Technology Conference OTC-23975-MS*; 2013 May 6-9; Texas, USA. <https://doi.org/10.4043/23975-MS>.
- Randolph, M. F., and Quiggin, P. (2009), "Non-linear hysteretic seabed model for catenary pipeline contact" *28th International Conference on Ocean, Offshore and Arctic Engineering OMAE 2009*, Honolulu, Hawaii, USA, 79259.
- Randolph, M. F., and White, D. J. (2008) "Pipeline embedment in deep water: processes and quantitative assessment." *Offshore Technology Conf.*, Houston, USA, OTC 19128.
- Rezazadeh K, Shiri H, Zhang L, Bai Y. Fatigue generation mechanism in touchdown area of steel catenary risers in non-linear hysteretic seabed. *Research Journal of Applied Sciences, Engineering and Technology*. 2012; 4(24):5591-5601.
- SACS. (2009). "The manual of Structural Analysis Computer system program (SACS)." *Engineering Dynamic Inc*, Release 5, Rev 3.
- Sheehan, J. M., Grealish, F. W., Smith, R. J., and Harte, A. M. (2005). "Characterization of the Wave Environment in the Fatigue Analysis of Flexible Risers." *Proceedings of OMAE2005, Paper*, 67507.
- Sharma PP, Aubeny CP. Advances in pipe-soil interaction methodology and application for SCR fatigue design. *Proceedings of the Offshore Technology Conference OTC-21179-MS*; 2011 May 2-5; Texas, USA. <https://doi.org/10.4043/21179-MS>.
- Shiri H., *Influence of seabed response on fatigue performance of steel catenary risers in touchdown zone*. PhD Thesis; (2010); University of Western Australia
- Shiri H. Response of steel catenary risers on hysteretic non-linear seabed. *Applied Ocean Research*, 2014 January; 44:20-28. <https://doi.org/10.1016/j.apor.2013.10.006>.

- Shiri H. Influence of seabed trench formation on fatigue performance of steel catenary risers in touchdown zone. *Marine Structures*. 2014 April; 36:1-20. <https://doi.org/10.1016/j.marstruc.2013.12.003>.
- Shiri H., Randolph MF. Influence of seabed response on fatigue performance of steel catenary risers in touchdown zone. *Proceeding of the 29th International Conference on Ocean, Offshore and Arctic Engineering OMAE 2010-20051*; 2010 June 6-11; Shanghai, China. pp. 63-72; [doi:10.1115/OMAE2010-20051](https://doi.org/10.1115/OMAE2010-20051).
- Shoghi R, Shiri H. Modelling Touchdown Point Oscillation and Its Relationship with Fatigue Response of Steel Catenary Risers. 2019, *Applied Ocean Research*, 87 (2019) 142-154.
- Timoshenko SP, Young DH. *Theory of structures*. McGraw-Hill Inc., US; 1968.
- Triantafyllou MS and Triantafyllou GS (1991). The paradox of the hanging string an: explanation using singular perturbation. *Journal of Sound and Vibration* 148(2): 343–351.
- Vughts, J. H., and Kinra, R. K. (1976), "Probabilistic fatigue analysis of fixed offshore structures." *Offshore Technology Conference*, Dallas, Texas, OTC2608.
- Wang K., Xue H., and Tang W., Time domain prediction approach for cross-flow VIV induced fatigue damage of steel catenary riser near touchdown point. *Applied Ocean Research*, (2013) October, Vol 43, Pages 166-174.
- Wang K, Low YM. Study of seabed trench induced by steel catenary riser and seabed interaction. *Proceedings of the 35th International Conference on Ocean, Offshore and Arctic Engineering OMAE2016-54236*; 2016 June 19-24; Busan: South Korea. [doi:10.1115/OMAE2016-54236](https://doi.org/10.1115/OMAE2016-54236).
- Yuan F, White DJ and O'Loughlin CD. The evolution of seabed stiffness during cyclic movement in a riser touchdown zone on soft clay. *Géotechnique*, 2017, 67(2):127-137.
- Zargar, E. A new hysteretic seabed model for riser-soil interaction. PhD Thesis; 2017; University of Western Australia.

APPENDIX

Appendix A

The Geometrical Significance of Seabed Trench in Fatigue Performance of Steel Catenary Risers in the Touchdown Zone

Hodjat Shiri¹, Rahim Shoghi²

1: Department of Civil Engineering
Memorial University of Newfoundland
e-mail: hshiri@mun.ca

2: Department of Civil
Engineering, Memorial University of Newfoundland
e-mail: rshoghi@mun.ca

This paper was submitted to 4th International Symposium on Frontiers in Offshore Geotechnics (ISFOG) 2020 and it is summery of chapter 3 and chapter 4.

Abstract

The cyclic contact of the SCR with the seabed soil causes progressive remoulding and degradation of the seabed soil stiffness. This process results in gradual embedment of the SCR into the seabed and developing a trench several diameters deep underneath the riser. The oscillating SCR tries to progressively achieve an equilibrium between the trench geometrical profile and the seabed soil stiffness evolution in the touchdown zone through a complex process. Several studies have used different trench modeling approaches to investigate the trench effect on fatigue. However, contradictory observations have been reported with no coherent agreement on the beneficial or detrimental effect of the trench on fatigue. In this study, the significance of trench geometry in fatigue damage evaluation was investigated against the seabed stiffness degradation effect. It was observed that the geometrical riser profile dominates the effect of seabed stiffness degradation on many occasions. This strengthened the probability of the case dependency of the peak damage accumulation and its significant dependence on the direction of the low-frequency vessel excursions.

Keywords: Steel catenary risers; Riser-seabed interaction; Touchdown point; Trench profile; Fatigue response

A.1. Introduction

Steel catenary risers (SCRs) are made of thin-wall steel pipes suspended from floating facilities to the seabed in the form of a catenary. These popular elements are usually used in offshore field developments for transferring hydrocarbon from the seabed to the floating systems. SCRs are subjected to dynamic and cyclic loads and are vulnerable to fatigue loads. One of the most fatigue prone parts of the SCR is the touchdown zone (TDZ), where it continuously experiences cyclic contact with the seabed around the touchdown point (TDP). Subsea surveys have proven a trench formation under the SCR several diameters deep (see Figure A-1) (Bridge 2005).

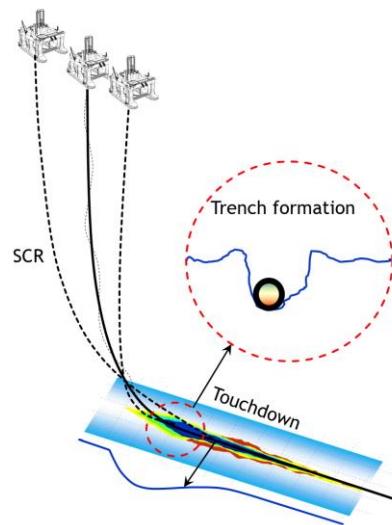


Figure A-1. Cyclic trench development in the TDZ of SCR

Previous studies that have investigated the influence of trench formation on fatigue life have reported contradictory observations. Some of the studies have concluded that the trench formation benefits fatigue life because of the gradual relaxation of the SCR by penetrating into the seabed (e.g., Wang and Low 2016, Elliott et al. 2013, Randolph et al. 2013, Nakhaee and Zhang 2010, Clukey et al. 2007, Langner 2003). Other studies have

observed the detrimental effect of the trench on fatigue performance (Zargar 2017, Shiri 2014a,b, Rezazadeh et al. 2012, Shiri and Randolph 2010, and Giertsen et al. 2004). Different methodologies have been used to incorporate the trench in the TDZ, such as the artificial insertion of mathematically expressed trenches or the automatic development of trenches using advanced non-linear hysteretic riser-seabed interaction models. However, there remains no coherent agreement amongst researchers on the trench effect on fatigue. Obtaining a robust answer for this question is significant for developing a reliable and cost-effective design of SCRs.

A mathematical basis and a set of geometrical rules were proposed to facilitate the qualitative prediction of the trench effect on the fatigue performance of SCR in the TDZ. The proposed basis was developed using the existing mathematical solutions and validated through performing advanced numerical analysis and comparing with published experimental and numerical studies. The impact of trench geometry on the fatigue response of SCR in the TDZ was investigated through analytical and numerical approaches. Wave-frequency (WF) vessel motions and its combination with low-frequency (LF) vessel excursions towards different directions were considered. Meaningful relationships were observed between the seabed slope in different zones of the trench and peak fatigue damage. The direct product of the TDP oscillation amplitude (Δ_{TDP}) and average shear force distribution (\tilde{V}) was found to have an overall variation trend similar to the axial stress variation range ($\Delta\sigma$) (or fatigue damage). This product ($\tilde{V} \times \Delta_{TDP}$) is neither equal to nor an approximation of von Mises stress range or fatigue, and there seems to be a complex relationship between them. However, it is a sensible parameter that mimics the axial stress variation and facilitates the evaluation of the overall trench effect on fatigue.

These observations led to the development of a set of rules used for qualitative assessment of the overall trend of the trench effect on fatigue. It was observed that the direction of predominant fatigue sea states and the LF vessel excursions in a given geographical location influenced the peak fatigue damage, which might be increased towards the near offset zone (NOZ) or decreased towards the far offset zone (FOZ) of the trench. This could explain the contradictions in the previously published studies. The observation implied that the fatigue damage variation due to the trench effect is case dependent. Also, the results obtained from studies with purely WF oscillations cannot be generalized to the real SCR response.

A.2. Conceptual Basis

Several complex and interactive mechanisms may contribute to trench formation underneath the SCR and fatigue performance. This has made challenges against achieving a coherent agreement about the trench effect on fatigue, and identifying the sources of contradiction in the published results. However, a qualitative assessment of various mechanisms shows that regardless of the source of the contribution, it may ultimately affect only the soil stiffness degradation and/or the variation of TDP oscillation path on the sea bottom (Shoghi and Shiri 2019). A boundary layer solution (BLM) proposed by Pesce et al. (2006) and the catenary equations solved by Leibniz (1691) were combined and manipulated to mathematically prove the dependency of the fatigue damage on average shear force (\tilde{V}) and TDP oscillation amplitude (Δ_{TDP}). For an arbitrary SCR configuration, the circular cross-sectional axial stress can be written as follows for a given vessel position:

$$\sigma_{axial} = \frac{T}{A} + \frac{M}{S} \quad (37)$$

where T , T , A , and S are tension force, bending moment, cross-section area, and the section modulus of the riser, respectively. Fatigue damage in SCR is accumulated by cyclic oscillation of the stress defined in equation (1) through the far and near vessel offsets. Using the equation (1), the cyclic stress change which is the governing factor in the calculation of fatigue damage could be written as follows:

$$\begin{aligned} \Delta\sigma_{axial} = \sigma_{v-far} - \sigma_{v-near} &= \frac{\Delta T}{A} + \frac{\Delta M \times C}{I} \\ &= \frac{1}{A}(T_{x,f} - T_{x,n}) + \frac{C}{I}(M_{x,f} - M_{x,n}) \end{aligned} \quad (38)$$

The subscripts n and f correspond to the near and far vessel offsets. Using the conventional catenary equations and expanding some mathematical works, the axial stress variation was shown to depend on average shear force and TDP oscillation amplitude:

$$\Delta\sigma \approx f(\tilde{V}, \Delta_{TDP}) \quad (39)$$

The details of the mathematical development of the above equation can be found in Shoghi and Shiri (2019). The equation (3) shows that the ultimate fatigue damage can be expressed in terms of the average shear force (\tilde{V}), and the TDP migration amplitude (Δ_{TDP}). As shown in Figure A-2 the WF vessel motions on a flat seabed about the mean vessel position causes the TDP to oscillates around its mean position (see Figure A-2 (a)) (called “mean position zone” (MPZ) from now on (dashed SCRs in Figure A-2 (b,c,and d))).

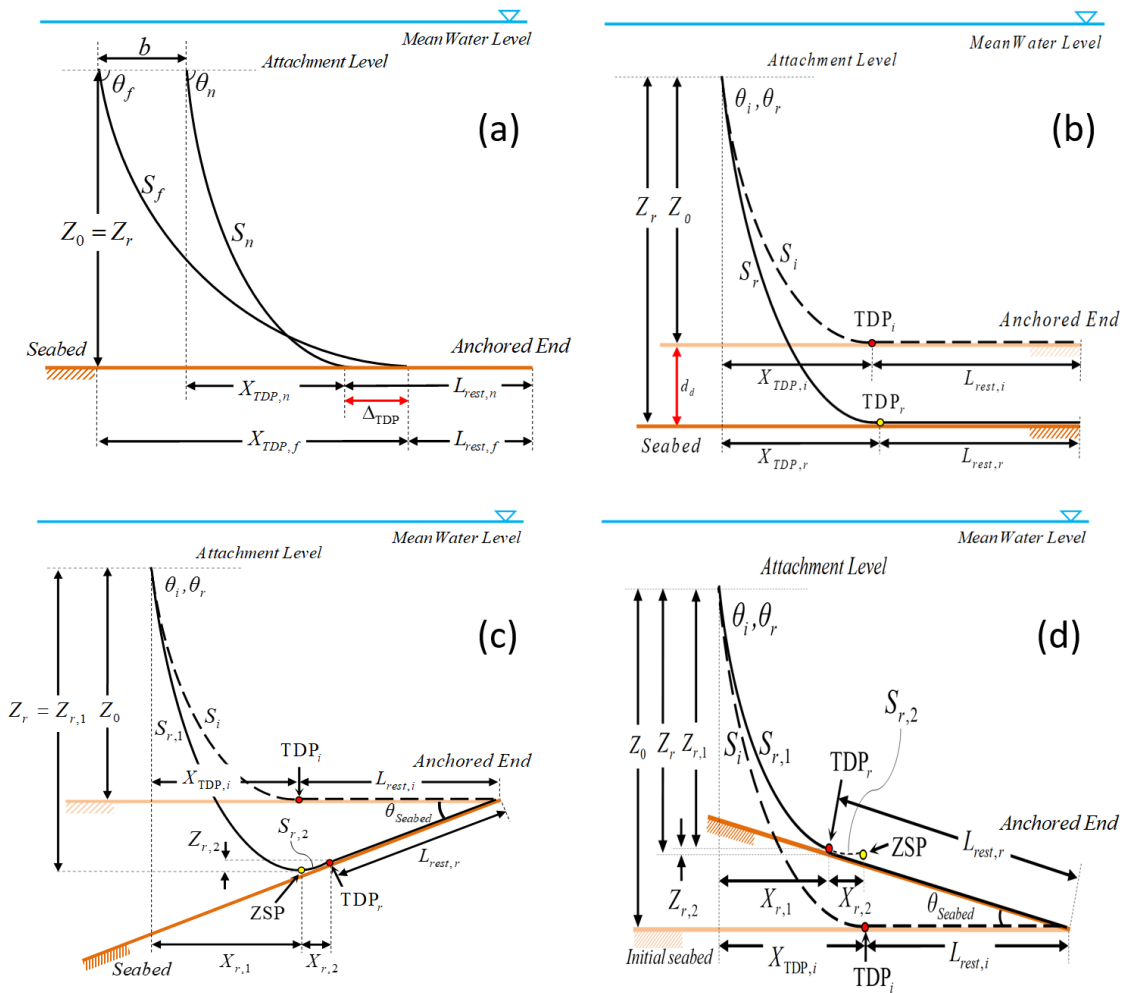


Figure A-2. Different scenarios of TDP oscillation on the seabed (Shoghi and Shiri 2019)

While the trench is developed, the trench bottom point is shifted downward. Therefore, The MPZ area can be simply mimicked by the downward shifting of the flat seabed by a given maximum embedment depth (see Figure A-2 (b)). While the vessel oscillates about the mean position due to WF motions, depending on the type of vessel and the system configuration, the LF excursions may also largely relocate the vessel (e.g., up to 5% of the water depth (Bridge and Howells 2007)). An LF excursion moving the vessel away from the anchored end (“far offset”) causes the TDP to relocate towards the far end of the trench

with a positive slope ($+\theta_{\text{seabed}}$) (called “far offset zone” (FOZ)). This curved area can be simplified by a positive-sloped straight line (see Figure A-2 (c)). Inversely, the “near offset” of the vessel due to the LF vessel excursions shifts the TDP towards the vessel side of the trench with a negative slope ($-\theta_{\text{seabed}}$) (called “near offset zone” (NOZ)). For simplification, this curved area can also be replaced by a negative-sloped strength line (see Figure A-2 (d)). It was assumed that the TDP might oscillate in one of these three different idealized zones depending on the combined effects of the WF vessel motions and the LF excursions (See Figure A-2). The TDP oscillation amplitude (Δ_{TDP}) can be analytically expressed for all of these scenarios only by developing the compatibility equations, and the Timoshenko solutions for catenary equations. The details of the obtained equations can be found in Shoghi and Shiri (2019).

Performing various case studies showed that the product of these two key parameters ($\tilde{V} \times \Delta_{\text{TDP}}$) has the same variation trend as the axial stress range ($\Delta\sigma$) or fatigue damage. In addition, the TDP oscillation amplitude dominates the average shear force in their proposed product. Although, the mathematical relationship between the fatigue damage and these two key parameters can be a complicated explicit equation. However, the advantage of this dependency was used in this study to assess the overall trend of the trench effect on fatigue life, i.e., the improvement or deterioration, without a quantitative assessment. It is noteworthy that the product of the average shear force and the TDP migration amplitude ($\tilde{V} \times \Delta_{\text{TDP}}$) is neither equal to nor an approximation to von Mises stress range or fatigue. However, it is a sensible parameter that mimics the same variation trends in the axial stress

range. Table A-1 has summarized these findings. The details of the analyses can be found in Shoghi and Shiri (2019):

Table A-1. Variation trends of key parameters relative to the non-trenched virgin seabed.

parameter	FOZ	MPZ	NOZ
\tilde{V}	Decrease	Decrease	Decrease
Δ_{TDP}	Decrease	Increase	Increase
$\tilde{V} \times \Delta_{TDP}$	Decrease	Slightly increase	Increase
$\Delta\sigma$	Decrease	Slightly increase	Increase

The content of Table A-1 was verified by various numerical and experimental studies. Figure A-3 shows a sample of experimental studies conducted by Hodder and Byrne (2009). In their experiments, the pipe was placed on a bed of sand for benchmarking purposes for the riser structural responses and trench formation. Figure A-3 shows the variation of the bending moment (or fatigue) in three key locations selected from NOZ, NOZ near TDP, and FOZ (i.e., BM1, BM3, and BM4) to facilitate the comparison of the trends with the finding of the current study. The variation of the bending moment (or fatigue damage) shows a good agreement with the findings of the current study (summarized in Table A-1). Bridge (2005) also reported results for fatigue damage variation in the sloped seabed with positive and negative gradient, which are in perfect agreement with Table A-1.

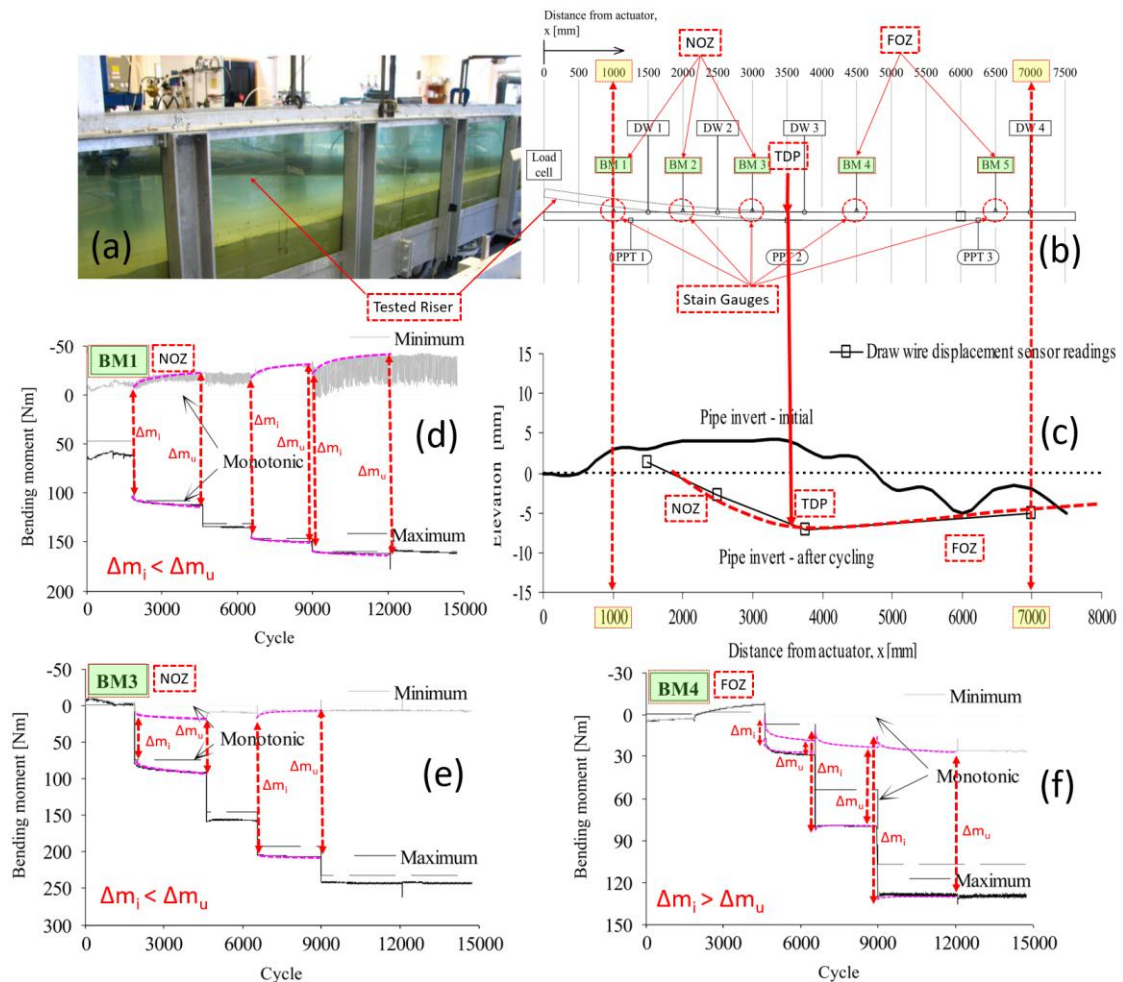


Figure A-3. Assessment of test results published by Hodder and Byrne (2009)

The observations summarized in Table A-1 resulted in four geometrical rules (Shoghi and Shiri 2019) for qualitative assessment of the trench effect on SCR fatigue performance in the TDZ.

A.3. Re-assessment of Previous Studies

The effect of “cyclic embedment” and “trench” on fatigue damage and their classification based on the proposed rules were re-assessed for most of the studies published in the literature. The details of this re-assessment process can be found in Shoghi and Shiri

(2020). A widely coherent agreement was achieved amongst most of the studies. However, few exceptions were observed that would be shortly reviewed in this section.

- *Elliott et al. (2013)*

The authors conducted experimental studies and observed a cyclic reduction of peak bending moment variation near the TDP and concluded that the “trench” is for the benefit of fatigue life. This conclusion seems to disagree with the results in Table A-1 in the NOZ. The embedment profile observed by Elliott et al. (2013) seems to be opposed to mathematical fundamentals (e.g., Pesce et al. 2006), the published numerical and experimental studies, and also the full-scale tests on a riser in the harbour (e.g., Bridge 2005), where the mouth of ladle-shape embedment profile in the TDZ is inversely towards the vessel. The pin support may have caused the truncated riser model not to match the target realistic catenary shape perfectly. Technically, it is quite challenging to develop a semi-flexible truncated riser connection to the actuator in order to update the bending moment or the hang-off angle with riser oscillations. This usually causes the researchers to use the pin connection between the riser and the actuator. However, researchers usually combine three different remedial approaches to ensure that the truncation will not prevent the catenary action, which plays a significant role in the riser-seabed interaction. These remedial solutions may include a) lower SCR bending stiffness (e.g., using polyethylene pipes by Wang et al. (2013), and Hodder and Byrne (2009)), b) heavier pipe weight (e.g., adding metal ballast wires inside the pipe by Hodder and Byrne (2009)), and/or c) selection of a far enough truncation point (e.g., 363D actuator to TDP, 57D actuator height from seabed by Bridge and Howells (2007)), all of which are seemed to be limitations when

using centrifuge testing. By using the pin-roller support at the end of the riser, which is quite close to the TDP, the bending moment in Elliott et al. (2013) has been forced to become zero exactly in the location that SCR undergoes the highest bending moment oscillations (see Figure A-4 with a schematic and exaggerated representation of the sectional pipe testing issue (bottom-right)). In addition, it seems that the short length of the truncation (about 106D from the actuator to TDP, and 9.5D actuator height from seabed) combined with the high bending stiffness of the model riser and the low submerged weight have prevented the desired catenary shape to form resulting in a TDZ curvature that is much larger than expected. This enlarged curvature has interfered with the NOZ and imposed a straight line seabed profile instead of a steeply sloped curve. The lower bending moment variation and consequently, less fatigue accumulation (see Figure A-4) have caused the authors to conclude that the “trench” effect is beneficial for improving the fatigue life. A comparison of global SCR with a sectional SCR used in centrifuge tests was presented by Bhattacharyya et al. (2011) supporting the approach. The study showed a good agreement of the fatigue life between the global and sectional models in the pipeline part of the SCR. However, the horizontal distance between the cut-off point and the TDP, the location of catenary bottom point, and the riser profile in the touchdown zone were not provided. Also, the study did not discuss the 25 ft. relocation of the peak fatigue point between the global and sectional riser and its potential impact on centrifuge tests. This area is exactly same as the affected zone shown in Figure A-4.

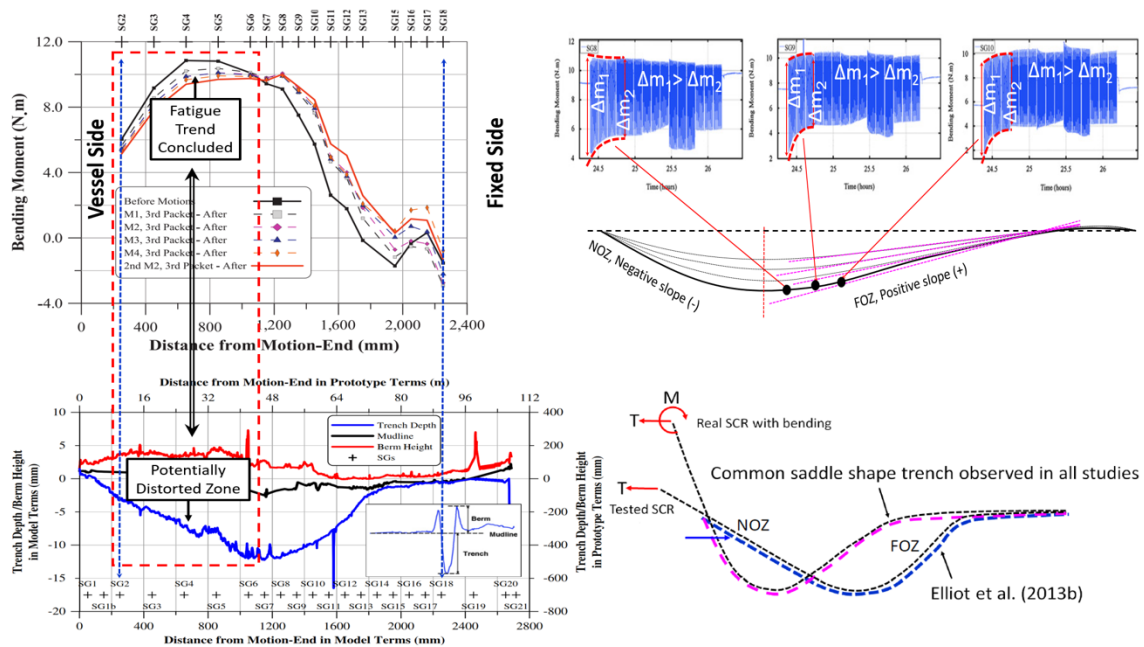


Figure A-4. Assessment of profile vs. bending moment obtained by Elliott et al. (2013)

The sample nodes presented in Figure A-4 with bending moment variation through the first episode of vessel motions (M1) shows that the results produced by Elliott et al. could be potentially in agreement with the findings of the current study if the desired riser curvature in the TDZ was properly achieved.

- *Randolph et al. (2013)*

Randolph et al. (2013) examined three different approaches for modeling the trench and evaluating its impact on fatigue in two different geographical locations, the Gulf of Mexico and Offshore Western Australia. The authors considered low-frequency vessel excursions towards the far, cross, and near directions and investigated the analytical trench proposed by Langner (2003), the cyclically created trench proposed by Shiri and Randolph (2010), and a new approach called the “stepped method.” Randolph et al. (2013) concluded that in

most of the cases, the trench is for the benefit of fatigue life in the TDZ. However, the authors also observed some exceptional cases with increased fatigue damage due to the trench effect. Figure A-5 shows some of the key results obtained by Randolph et al. (2013) that have been further annotated to highlight the findings of the current re-assessment study.

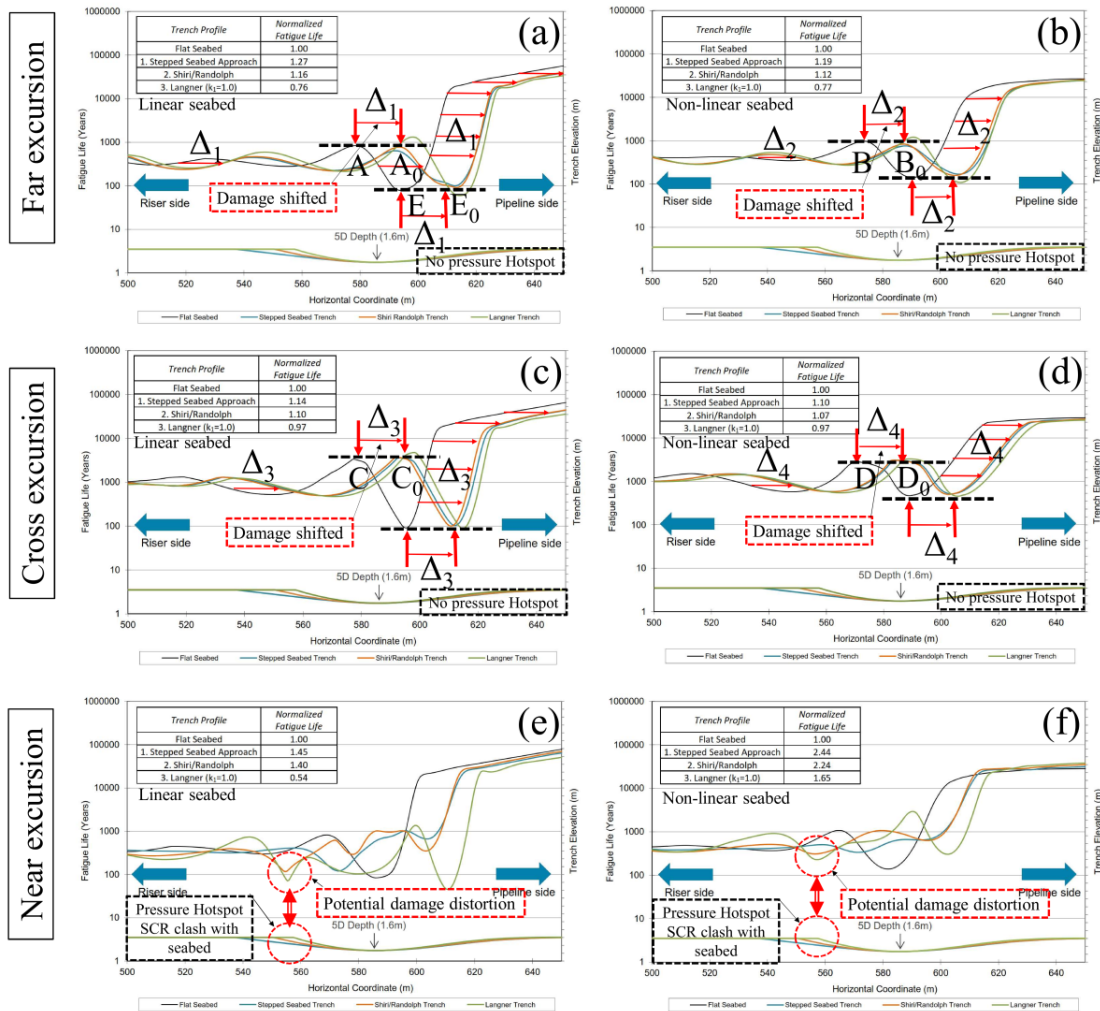


Figure A-5. Assessment of test results published by Randolph et al. (2013)

For far and cross vessel excursions, Randolph et al. (2013) compared the fatigue lives on the flat and trenched seabed at points A0, B0, C0, and D0 (near the TDP, Figure A-5 (a),

(b), (c), and (d)) and concluded that the fatigue life is modestly improved near the TDP of trrenched seabed (12% to 27% for far offset, and 7% to 14% for cross offset in case of Gulf of Mexico). This conclusion is completely true and in agreement with Elliot et al. (2013) but it seems to be only a part of the scenario. A closer look at Figure A-5 (a) to (d) shows that the insertion of the trench has not remarkably changed the fatigue life but shifted the life distribution towards the pipeline end (by $\Delta 1$, $\Delta 2$, $\Delta 3$, and $\Delta 4$). Points A, B, C, and D on the flat seabed have been transferred to corresponding points A0, B0, C0, and D0 on the trrenched seabed. In other words, while the fatigue life is increased at the point A0, the point E0 experiences an inverse trend or a decreased fatigue life. Therefore, a more consistent conclusion of the study can be improvement of the fatigue life in the TDP (e.g., point A0) and reduction of the fatigue life in the TDZ (e.g., point E0), which is well in agreement with the findings of Shoghi and Shiri (2019) summarized in Table A-1. This seems to be an appropriate approach since the industry is mainly looking for the effect of the trench on peak fatigue damage in the TDZ, not the TDP alone. In near offset analyses, Randolph et al. (2013) observed a significant improvement of fatigue life in the case of the Gulf of Mexico (40% to 144%, see Figure A-5 (e) and (f)). A closer look at these series of plots shows an unexpected fatigue life fluctuation (circled by dashed red lines in Figure A-5 (e) and (f)) that seems to be susceptible to potential pressure hot spots in the trench mouth. There is a sudden drop in damage distribution in green and orange lines right in the trench mouth. This sudden drop is not seen in the blue line (Stepped method), but its overall profile is still largely different from the black line (Flat seabed). Overall, there is no coincidence or similar trends amongst different fatigue damage distribution profiles in the case of near vessel excursion. These results suggest care should be taken in assessing the near offset

results. There might be a potential interference between the natural catenary shape and the artificially imposed trench profile at the trench mouth, while the vessel moves towards the near direction. This potential interference may have created a contact pressure hotspot and distorted the fatigue life distribution in the trench mouth and anywhere else, consequently. This unusual fluctuation is significantly limited in the “stepped trench” method because of its smart approach in defining the NOZ profile that has eliminated a sharp trench mouth. However, the stepped method proposed by Randolph et al. (2013) cannot guarantee and did not claim a perfect elimination of the potential pressure hot spots. The same scenario has exactly happened in Sharma and Aubeny (2011) where the different curvature of the SCR and trench in NOZ has caused distortion of the results. The details of discussion about these studies can be found in Shoghi and Shiri (2020).

A.4. Conclusions

A mathematical framework recently was developed to re-assess the effect of SCR “cyclic embedment” and “trench” on fatigue damage in the TDZ and achieve a more coherent agreement in the literature. The adopted framework utilizes the geometrical dominance of the TDP oscillation amplitude (Δ_{TDP}) to average shear force distribution (\tilde{V}) and the capability of their direct product ($\tilde{V} \times \Delta_{TDP}$) in mimicking the fatigue trends to assess the embedment effect on fatigue. This product (i.e., $\tilde{V} \times \Delta_{TDP}$) is neither equal to nor an approximation to the axial stress range or fatigue, but follows a variation trend similar to the axial stress range, and facilitates the re-assessment of the trench effect of fatigue. The proposed methodology was applied to re-assess the majority of the key publications in the literature. Some limitations were observed in having access to detailed information of some of the studies that make challenges against achieving a coherent agreement. A couple of

examples being susceptible to distorted fatigue results by artificial insertion of mathematically expressed trenches were also discussed. Taking into account the potential effect of existing inconsistencies, a more coherent agreement on trench effect on fatigue was observed that are summarized as follows:

- The WF vessel oscillations about a mean position result in a shallow “cyclic embedment” of the riser into the seabed by less than about one diameter (with the regular performance of the existing non-linear hysteretic riser-seabed interaction models). This cyclic penetration slightly increases the fatigue damage in the vessel side of the TDP (NOZ) and slightly decreases the damage in the anchor side (FOZ). The peak fatigue damage may slightly move towards the vessel or not move depending on the non-linear seabed model.
- The shallow “cyclic embedment” of the riser into the seabed is not necessarily the same as a deep “trench.” The existing non-linear hysteretic models are usually quickly stabilized by achieving a maximum penetration depth of less than one diameter, which is called a premature stabilization, while the real trenches observed in the field are in the range of several diameters deep. Also, there are still several important but less-explored contributors to the trench formation, either individually, or interactively. Therefore, care should be taken in generalizing the results obtained from “cyclic embedment” to “trench,” and further studies are required to see whether the ultimate trench profile is the scaled-up version of cyclic embedment profile.
- The LF vessel excursions with near, far, and out of plane offsets may have a significant influence on ultimate fatigue results. These excursions result in TDP migration towards

the NOZ and FOZ of the trench that causes an increase and decreases in peak fatigue damage, respectively. Therefore, the results of the published studies, which have only applied WF oscillations or the LF motions with no large excursions cannot be simply generalized to reality.

- The combined WF+LF motions on a trenched seabed were found to slightly increase the damage in near excursions (NOZ) and slightly decrease the damage in far excursions (FOZ). However, the peak fatigue damage is largely moved by tens of diameters (e.g., 50D) depending on the direction of excursions. In other words, in real life, case-dependent scattered results may be obtained depending on the probability of the dominant TDP oscillations in NOZ or FOZ. In any case, the trench effect seems to be significant in terms of relocation of peak damage location, but minor in terms of peak damage magnitude.
- The artificial insertion of a mathematical or pre-defined trench profile to study the trench effect on fatigue response is a risky approach. The fatigue results obtained by this approach are usually susceptible to potential distortion due to creating unexpected contact pressure hot spots at trench mouth. These pressure hotspots can be created as the result of a disagreement between the natural catenary profile of the SCR and the mathematical trench profile that alters the bending moment variation. This is less likely in reality since a fully developed trench is expected to accommodate the majority of oscillating SCR configurations that may happen during the operation life. There is only one study that has resolved this issue to some extent by proposing a “stepped trench” (Randolph et al. 2013). The automative trench creation using cyclic SCR perturbations and extreme seabed model parameters (Shiri and Randolph 2010) can be an appropriate

approach to guarantee the prevention of having pressure hotspots. However, care shall be taken in the quickly scaled-up trench profiles that further develops towards the anchor end.

The proposed framework can be further developed in the future for more quantitative fatigue damage assessment affected by trench formation in the TDZ. Developing new research programs with an extensive assessment of the real trench shapes accompanied by supporting field data such as vessel oscillations, SCR stress/strain oscillations, and seabed stiffness degradation histories can be significantly beneficial for obtaining robust and reliable solutions.

A.5. Acknowledgments

The authors acknowledge the financial support of InnovateNL through the Ignite program, the Natural Sciences and Engineering Research Council of Canada through the Discovery funding program, and the Memorial University of Newfoundland through VP start-up funding support.

References

- Bhattacharyya A, Tognarelli MA, Li G, Ghosh R, Clukey EC, Sun Q. Simulation of SCR behavior at touchdown zone - Part I: numerical analysis of global SCR model vs. sectional SCR model, *Offshore technology Conference*; 2011; Brasil, Rio de Janeiro, Brazil.
- Bridge C. Effect of seabed interaction on steel catenary risers. 2005; PhD thesis; Uni. of Surrey, UK.
- Bridge CD, Howells HA. Observation and modeling of steel catenary riser trenches. *Proceedings of the 17th International Society of Offshore and Polar Engineers Conference ISOPE-I-07-321*; 2007 July 1-6; Lisbon, Portugal. pp 803-813.

- Clukey EC, Ghosh R, Mocarala P, Dixon M. Steel catenary riser (SCR) design issues at touchdown area. *Proceedings of The 17th International Offshore and Polar Engineering Conference ISOPE-I-07-388*; 2007 July 1-6; Lisbon, Portugal.
- Elliott BJ, Zakeri A, Barrett J, Hawlader B, Li G, Clukey EC. Centrifuge modeling of steel catenary risers at touchdown zone Part II: assessment of centrifuge test results using kaolin clay. *Ocean Engineering*. 2013 March 1; 60, 208-218. <https://doi.org/10.1016/j.oceaneng.2012.11.013>.
- Giertsen E, Varley R, Schroder K. CARISIMA: a catenary riser/soil interaction model for global riser analysis. *Proceedings of the 23rd International Conference on Offshore Mechanics and Arctic Engineering OMAE 2004-51345*; 2004 June 20-25; Vancouver, Canada.
- Hodder, M.S. and Byrne, B.W. (2009) "3D experiments investigating the interaction of a model SCR with the seabed", *Applied Ocean Research*, 32:145-157.
- Langner C. Fatigue life improvement of steel catenary risers due to self-trenching at the touchdown point. *Proceedings of the Offshore Tech. Conf. OTC 15104*; 2003 May 5-8; Texas, USA.
- Leibniz. Solution to the problem of catenary, or funicular curve, proposed by M. Jacques Bernoulli in the Acta of June 1691. *Acta Eruditorum*. Leipzig, Germany.
- Nakhaee A, Zhang J. Effects of the interaction with the seafloor on the fatigue life of a SCR. *Proceedings of the 18th International Society of Offshore and Polar Engineers Conference ISOPE-I-08-397*; 2008 July 6-11; Vancouver, Canada. pp 87-93.
- Pesce CP, Martins C, Silveira LM. Riser-Soil Interaction: Local Dynamics at TDP and a Discussion on the Eigenvalue and the VIV Problems. *J. of Offsh. Mech. and Arctic Eng.*; 2006; 128(1), 39-55.
- Randolph MF, Bhat S, Mekha B. Modeling the touchdown zone trench and its impact on SCR fatigue life. *Proceedings of the Offshore Technology Conference OTC-23975-MS*; 2013 May 6-9; Texas, USA. <https://doi.org/10.4043/23975-MS>.
- Rezazadeh K, Shiri H, Zhang L, Bai Y. Fatigue generation mechanism in touchdown area of steel catenary risers in non-linear hysteretic seabed. *Research Journal of Applied Sciences, Engineering and Technology*. 2012; 4(24):5591-5601.
- Sharma PP, Aubeny CP. Advances in pipe-soil interaction methodology and application for SCR fatigue design. *Proceedings of the Offshore Technology Conference OTC-21179-MS*; 2011 May 2-5; Texas, USA. <https://doi.org/10.4043/21179-MS>.

- Shiri H., Randolph MF. Influence of seabed response on fatigue performance of steel catenary risers in touchdown zone. *Proceeding of the 29th Int. Conf. on Ocean, Offsh. and Arctic Eng.* OMAE 2010-20051; 2010 June 6-11; Shanghai, China. pp. 63-72; doi:10.1115/OMAE2010-20051.
- Shiri H. Response of steel catenary risers on hysteretic non-linear seabed. *Applied Ocean Research*, 2014 January; 44:20-28.
- Shiri H. Influence of seabed trench formation on fatigue performance of steel catenary risers in touchdown zone. *Marine Structures*. 2014 April; 36:1-20.
- Shoghi R. and Shiri H. Modeling Touchdown Point Oscillation and Its Relationship with Fatigue Response of Steel Catenary Risers, *Applied Ocean Research* 2019, (87) 142-154.
- Shoghi R. and Shiri H. Re-assessment of Trench Effect on Fatigue Performance of Steel Catenary Risers in the Touchdown Zone, *Applied Ocean Research* 2020, (94) 101989.
- Wang K, Low YM. Study of seabed trench induced by steel catenary riser and seabed interaction. *Proceedings of the 35th International Conference on Ocean, Offshore and Arctic Engineering* OMAE2016-54236; 2016 June 19-24; Busan: South Korea. doi:10.1115/OMAE2016-54236.
- Zargar, E. E new hysteretic seabed model for riser-soil interaction. PhD Thesis; 2017; University of Western Australia.